

1-1-1976

Small-angle x-ray and small-angle light scattering studies of the morphology of polymer blends.

Farrokh Burjor Khambatta
University of Massachusetts Amherst

Follow this and additional works at: https://scholarworks.umass.edu/dissertations_1

Recommended Citation

Khambatta, Farrokh Burjor, "Small-angle x-ray and small-angle light scattering studies of the morphology of polymer blends." (1976). *Doctoral Dissertations 1896 - February 2014*. 622.
<https://doi.org/10.7275/hs6n-sp26> https://scholarworks.umass.edu/dissertations_1/622

This Open Access Dissertation is brought to you for free and open access by ScholarWorks@UMass Amherst. It has been accepted for inclusion in Doctoral Dissertations 1896 - February 2014 by an authorized administrator of ScholarWorks@UMass Amherst. For more information, please contact scholarworks@library.umass.edu.

SMALL-ANGLE X-RAY AND SMALL-ANGLE LIGHT SCATTERING
STUDIES OF THE MORPHOLOGY OF POLYMER BLENDS

A Dissertation Presented

By

FARROKH B. KHAMBATTA

Submitted to the Graduate School of the
University of Massachusetts
in partial fulfillment of the requirements
for the degree of

DOCTOR OF PHILOSOPHY

May 1976

Polymer Science and Engineering

(c) Farrokh B. Khambatta 1976

All Rights Reserved

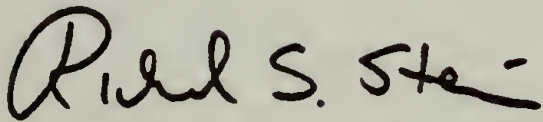
SMALL-ANGLE X-RAY AND SMALL-ANGLE LIGHT SCATTERING
STUDIES OF THE MORPHOLOGY OF POLYMER BLENDS

A Dissertation

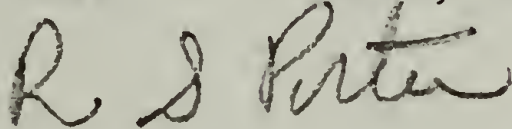
By

FARROKH KHAMBATTA

Approved as to style and content by:



Professor R. S. Stein, Chairman of Committee

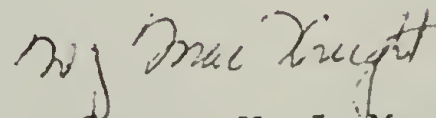
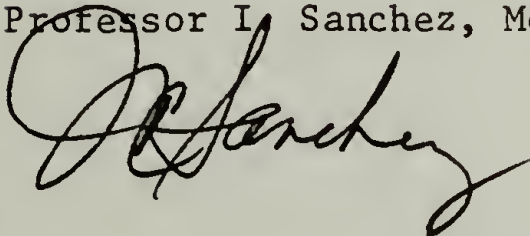


Professor R. S. Porter, Member



Professor F. E. Karasz, Member

Professor I. Sanchez, Member



Professor W. J. MacKnight
Head of Department
Polymer Science & Engineering

May 1976

DEDICATED TO
MY WIFE MAHARUKH AND MY PARENTS

ACKNOWLEDGEMENTS

This modest research effort has been a source of tremendous personal fulfillment but only because of the cooperation and assistance of several persons which made it all possible.

The author is indebted in a very special way to his thesis director Professor Richard S. Stein for not only his inspiration and invaluable guidance during this work, but also his inexhaustible patience throughout.

Many thanks are due to the committee members for their helpful comments and criticisms at various stages of this work and for accommodating the author in many ways towards the end of his stay at the University of Massachusetts.

Samples of both polymers were provided by Dr. J. Koleske of Union Carbide Corp. and a standard Lupolen sample was kindly provided by Professor O. Kratky of the University of Graz. Their generousities are appreciated very much.

Thanks are also due to members of the research group for their valuable suggestions during the course of several presentations, particularly to continued stimulating discussions with Drs. Prud'homme, Misra and Natarajan, especially with regards to small-angle light scattering studies. The many interesting discussions with Drs. Wenig and Waisiak regarding small-angle x-ray scattering are also appreciated.

ABSTRACT

The morphology of polymer blends using poly- ϵ -caprolactone (PCL)/poly(vinyl chloride) (PVC) as a model system has been studied by small-angle x-ray scattering (SAXS) and small-angle light scattering (SALS).

Previous research efforts had concluded from the observance of a single glass transition that blends of PCL/PVC were compatible for all compositions inspite of one of the components (PCL) crystallizing up to a composition of 50/50* (PCL/PVC). It had also been established that the addition of PVC to PCL progressively impeded the crystallization of the ester and for compositions rich enough in PVC, crystallization did not occur.

Results of SAXS and SALS studies are consistent with the above observations regarding the trend and have moreover served to establish the morphological details on a more quantitative basis.

Compositions rich in PCL crystallize in volume-filling spherulitic morphologies thus incorporating the PVC within the spherulites. While the lamellae continue to be exclusively PCL as shown by wide-angle x-ray diffraction (WAXD) the interlamellar region is a partially mixed amorphous phase of PVC and uncrystallized PCL from analysis of absolute intensity measurements and comparison with independent measures of volume crystal-

*All compositions are in weight-percent unless otherwise specified.

linities. The crystallinity of the spherulites and consequently the system begins to drop resulting in coarser spherulites with more open structures as shown by the corresponding increase in the long period. On the basis of a one dimensional sandwich model of alternating crystalline and amorphous layers, the one dimensional crystallinity is in good agreement with the volume crystallinities measured by the density gradient column and differential scanning calorimetry. Simultaneously the drop in the crystallinity of PCL itself is not so marked. The same trend is seen in SALS experiments where the intensity of H_v scattering (absolute units) shows a steady drop proportional to that of PCL's crystallinity. The crystallite size seems almost independent of composition.

With more PVC saturating the spherulites, the excess of it forms a matrix by virtue of its high concentration in the amorphous phase and the system now crystallizes as a non-volume-filling one in which the spherulites are partially truncated. The long period is difficult to estimate accurately for such a system and the one dimensional crystallinity is also overestimated. The SALS intensity shows a drop simultaneous to that in the crystallinity of PCL itself and can be accounted for on that basis.

Higher concentrations of PVC result in amorphous morphologies which seem to show the presence of domains that vary in their average size with the blend composition and have diffuse transition zones whose dimensions are proportional to the domain sizes. The domain sizes are reasonable in magnitude and trend and the same is true for the transition zone thick-

nesses when it is considered that the PCL/PVC system is an exceptionally compatible one with respect to the more widespread incompatibility between polymers.

Also, on the basis of absolute intensity analysis it is concluded that the compatibility is not segmental throughout the morphology but that domains of mixed compositions exist with distributions in their size and compositions and that the electron density is smeared out across broad transition zones within the system.

When one considers the fineness of the dispersion from the specific surface values it is not surprising that the system exhibits single but not sharp glass transitions.

The techniques of SAXS and SALS have been suitably complemented with other measurements viz. WAXD, optical microscopy, SEM, DSC, etc., as and when necessary.

The ideas and efforts of previous workers have also been complemented and extended towards a deeper understanding of the system's morphology and it has simultaneously been demonstrated that SAXS and SALS used judiciously can be powerful characterization tools in the hands of a polymer scientist.

TABLE OF CONTENTS

	<u>Page</u>
<u>Acknowledgements</u>	v
<u>Abstract</u>	vii
<u>Chapter</u>	
I. Introduction	1
II. Historical Survey	10
A. Compatibility	10
B. Small-Angle X-Ray Scattering	25
C. Small-Angle Light Scattering	37
III. Theoretical Background	42
A. Scattering and Diffraction	42
B. Small-Angle X-Ray Scattering	44
C. Small-Angle Light Scattering	69
IV. Experimental Techniques	77
A. Sample Preparation	77
B. Small-Angle X-Ray Scattering	84
C. Small-Angle Light Scattering	98
V. Results and Discussion	110
A. Semi-Crystalline Morphologies	110
B. Amorphous Morphologies	135
VI. Summary and Conclusions	158
VII. Suggestions for Further Studies	164

TABLE OF CONTENTS (cont.)

	<u>Page</u>
<u>Appendix</u>	168
<u>Bibliography</u>	227
<u>List of Figures</u>	240

C H A P T E R I

INTRODUCTION

The virtues of combining materials of differing individual properties in order to obtain superior performance has been known for quite some time. Alloys, cermets, composites, etc., are all too familiar to the traditional "materials engineer". Synthetic polymers are relative latecomers to the materials discipline and blends of different polymers are even more recent. Though the advantages of blending polymers have always been realized, a systematic effort to investigate their morphologies and subsequent correlation with their properties has been undertaken only a little over a decade ago.

The literature on polyblends abounds in industrial patents¹ which is one indicator of their commercial and technological importance. The most obvious and outstanding advantage of blending different polymers is that it provides a relatively facile means to manipulate and control physical properties.^{1,2} Thus the potential for circumventing expensive synthetic techniques which would otherwise be needed to make special polymers for specific applications is considerable. A growing number of symposia on multicomponent polymeric systems is another measure of their importance.

A polymer molecule, on account of its long chain nature, is capable of coiling and intertwining with itself as well as with other such molecules of the same species. In fact for a sufficiently long molecule,

it would not know its own tail from that of a segment of a neighboring molecule. In the words of Tobolsky³ a mass of polymer molecules can be appropriately likened to a "bowl of cooked spaghetti". However, when two different polymeric species are mixed, the story is not quite the same. Under such circumstances inter-molecular interactions come into play and the level at which mixing can occur now becomes a complex function of the environment in which a given molecule finds itself. The word species as used above, is both in the sense of a chemically different polymer and physically different in tacticity, molecular weight, etc.

Experience has shown that in the case of blends, incompatibility is more the rule and compatibility the exception.⁴ In other words, molecular mixing at the segmental level between different polymeric species is a rare occurrence. Also, the general consensus is that even in seemingly compatible systems the equilibrium of the system is "pseudo" at best.⁵ Thus with time, the components of even a well-mixed system will tend to separate into their original pure phases. This is thermodynamically favored, as demixing results in a lowering of the system's free energy.

On the other hand, such demixing of intertwined molecules involves the slipping of chains past each other. At the very high viscosities especially in the bulk state, such motion is severely impeded resulting in infinitesimal diffusion rates.⁶ Thus the tendency to phase separate is kinetically unfavorable. The actual state of affairs in "real-time" will therefore depend on the nature of the equilibrium between the two

opposing tendencies. Such a situation would be quasi-static and hence the term "pseudo equilibrium".

In the light of the above phenomenological argument, one can thus conceive of a situation in which neither complete separation nor complete mixing will occur; but rather partial demixing at various dimensional levels could produce a microheterogeneous frozen-in morphology. Such a morphology will not be in thermodynamic equilibrium but would continue to approach it at an infinitesimal rate.

It was against this background that Koleske and Lundberg⁷ announced the remarkable compatibility characteristics of poly- ϵ -caprolactone (PCL) with a spectrum of several different polymers^{8,9} over wide compositional ranges. The compatibility is especially intriguing in the light of the fact that PCL has a high tendency to crystallize and crystallization is inherently a phase separation phenomenon.

It was further noticed by Koleske and Lundberg⁷ that when PCL was blended with poly(vinyl chloride) (PVC) the blends showed single glass transitions intermediate between the glass transition temperatures of the two homopolymers. This combined with the optical homogeneity of the films, were their criteria for compatibility which covered the entire compositional range. The blends richer in PCL continued to crystallize resulting in semi-crystalline spherulitic morphologies that were volume-filling. Those richer in PVC possessed little or no crystallinity and were transparent. Intermediate compositions showed non-volume-filling spherulitic morphologies.

Price and Ong¹⁰ also studied the compatibility characteristics of the same system but from the point of view of crystallization kinetics.

Since PVC did not show any noticeable crystallinity, its effect on the crystallization of PCL was essentially that of a high molecular weight diluent and of considerable interest in the study of kinetics.

The crystallinity of commercial atactic PVC has been estimated by a number of workers¹¹⁻¹⁵ to be of the order of 10% or less. Even though the chemical structure of PVC is rather regular, its stereochemistry is not. The main cause of the low values of crystallinity is very irregular chain packing. Calorimetric^{12,13} and wide angle x-ray¹¹ studies have been the most commonly used characterization techniques for PVC crystallinity. Absence of any diffraction rings in a WAXD photograph and a pronounced diffuse halo instead should give a first indication of low crystallinity.

Keith and Padden^{16,17} have studied the crystallization of blended systems to analyze the effect of the diluent on the perfection of the crystalline component and coarseness of the texture using their own phenomenological theory¹⁸ of fractionation and impurity segregation during crystallization.

According to the observations of Price and Ong, while crystallization did occur up to almost 40/60 of PCL/PVC (all compositions are in weight percent unless otherwise specified) the crystallization rates were severely impeded as the concentration of PVC built up. Thus the PCL/PVC system presented an interesting challenge to the understanding of compatibility by other independent techniques.

It is a truism that the properties of a system are a consequence of its structure.¹⁹ Blends can possess a combination of morphologies resulting in complex structures at a spectrum of dimensions. Their

characterization has been attempted by various experimental methods such as heat of mixing,^{6,20-23} thermal transitions,²⁴⁻³⁰ dynamic mechanical analysis,^{7,31-36} optical microscopy,^{10,17,18,27,28,38} electron microscopy^{10,27,38} and miscellaneous,³⁹⁻⁴⁴ all with a view to learning about the level of phase separation and its effect on properties.

In spite of considerable work on blends the phenomenon of compatibility defies a unique definition and it is possible that no unique definition may exist. This is partly due to the complexity of the situation but also due to the differing sensitivities of different experimental techniques to different levels of morphologies. Thus the criteria of compatibility as established by one technique may not always suffice for another.³⁵ It becomes immediately apparent that any one technique will not suffice in general and a multi-pronged approach using several widely differing methods of characterization is necessary.

Optical characterization by a variety of methods and correlation of their results with those of other independent methods could be one such alternative. Among the many standard methods available, light microscopy (LM) is the most commonly used. It explores gross morphologies such as fibrillar and spherulitic structures with an upper limit of resolution in the neighborhood of one micron or better ($1\mu = 10,000 \text{ \AA}$). For very fine structural details at the atomic and molecular levels wide-angle x-ray diffraction (WAXD), infrared and Raman spectroscopy, and NMR are used. These techniques can elucidate morphologies from a few Angstroms to a few tens of Angstroms. Structures of intermediate sizes viz. several tens of thousands of Angstroms can be studied by electron microscopy (EM). EM however has its limitations in that it is a selected

area analysis and is more representative of surface structure than bulk morphology. Also its interpretation is often subjective and hence ambiguous in the absence of good resolution or poor contrast, which is usually the case for polymers.

Information in the electron microscopy range is conveniently obtainable by the technique of small-angle x-ray scattering (SAXS). A rough application of Bragg's law viz. $\lambda = 2d\sin\theta$ where λ is the wavelength of x-rays ($\lambda = 1.542 \text{ \AA}$ for CuK_{α} radiation), d is some measure of periodicity in the scattering system, and θ is half the scattering angle, shows the reciprocity between d and θ at constant λ . Thus for d in the range of 100 \AA to several thousand Angstroms, the scattering angles (2θ) will be $\leq 1^{\circ}$ and experimentally quite accessible. In most SAXS instruments the upper limit of resolution is in the vicinity of $\sim 5000 \text{ \AA}$, as 2θ cannot be lowered indefinitely.*

Any experimental technique is less reliable at the limits of its capabilities and the range from approximately 5000 \AA (0.5μ) to $100,000 \text{ \AA}$ (10μ) is very suitably explored by small-angle light scattering (SALS) using visible light ($\lambda \approx 0.5\mu$) as the incident radiation. Thus SALS overlaps SAXS and LM on either side and can be further complemented by scanning electron microscopy (SEM). In fact SALS complements LM by providing a statistical evaluation of the sizes and shapes of the scattering entities. Such evaluation is often difficult from micrographs where the morphology is not well defined.

* Kratky claims resolution up to as high as $20,000 \text{ \AA}$ but this is under the best experimental conditions which are seldom realized and very demanding on equipment.

Thus the application of a variety of optical techniques is a potentially powerful method of unravelling the morphologies at various dimensional levels particularly in the case of polymer blends where a variety of heterogeneities could exist in a given system.

Coming back to the PCL/PVC system, it was observed by Ong¹⁰ and the author from WAXD studies that the crystalline phase in the blend was exclusively PCL. LM and SALS showed clear evidence of a spherulitic morphology whenever crystallization occurred. Hence the lamellae of the spherulites were comprised of PCL while the amorphous and interlamellar material should be some kind of mixture of PVC and uncrystallized PCL, for volume-filling morphologies.

It is possible for interlamellar material to undergo secondary crystallization with the passage of time. The crystallites so formed would be smaller and probably have different morphological features. Nevertheless they would contribute to the total crystallinity of the system. In the case of blends, the interlamellar PCL would have to demix from the PVC (all of which is considered interlamellar for volume-filling systems) in order to undergo secondary crystallization. This point could be substantiated by comparing crystallinities from the various conventional techniques which measure the overall crystallinity, to the one dimensional crystallinity as estimated by SAXS. Reasonably good agreement would support the idea that such secondary crystallization would not occur to any appreciable extent, as this feature is not included in the SAXS model.

In a sense then, as the crystallites formed, demixing of some of the PCL took place at the micro-level giving micro-heterogeneities of

the dimensions of crystallites. These often tend to be of the order of $\sim 100 \text{ \AA}$ as experience has shown for polymer systems that do crystallize.

While all this and the rest of Ong's observations formed a consistent picture kinetically, very little could be said quantitatively about the morphological details. The laborious EM experiments of Ong could at best show a trend for reasons already mentioned.

Small angle x-ray scattering is essentially the quantitative arm of electron microscopy in that it statistically averages the morphology with much less ambiguity. In this respect SAXS complements EM like a "hand and glove fit"⁴⁵ much like SALS complements LM.¹⁴

When crystallization occurs in lamellar morphology the average distance between centers of adjacent crystallites also called the "long period" (Fig. 10) becomes some kind of a periodicity in a macrolattice, the lattice points being the centers of the crystallites themselves. Such long periods tend to be of dimensions ranging from 100-200 \AA to several hundred Angstroms, i.e., quite within the domain of sensitivity of SAXS. Besides, SAXS is sensitive to local differences in electron densities and the microheterogeneities due to domain formation in blends provide just that. Thus such heterogeneities whether due to crystallization or otherwise can be studied very efficiently by SAXS.

A detailed morphological knowhow in turn becomes indispensable towards understanding the physical properties of blends and the correlation of experimental findings from other techniques.

It was with this in mind that SAXS studies of the PCL/PVC system were undertaken so as to be able to both complement and extend the works of Koleske and coworkers, and Price and Ong. It would simultaneously

serve to establish the feasibility and uniqueness of the technique towards the quantitative study of other multicomponent systems.

In this study SAXS was adopted as the major experimental technique and suitably supplemented by SALS, WAXD, LM, SEM, thermal measurements and density measurements as and when necessary. Among these SALS was the major supplementary technique.

C H A P T E R I I

HISTORICAL SURVEY

This chapter is divided into three main sections in order to give an individual historical perspective to compatibility and its current understanding, the evolution of small-angle x-ray scattering as a valuable tool in macromolecular research and the development of small-angle light scattering as an indispensable technique particularly in the understanding of the morphology of semi-crystalline polymeric systems.

Compatibility

The phenomenon of polymer compatibility has interested workers for almost three decades now and theoretical attempts to predict and explain it were made almost about the same time as interesting experimental observations were published. Among the first experimental observations on solutions of polymers were performed by Dorby and Boyer-Kawenoki⁴⁶ while Scott⁴⁷ and Tompa⁴⁸ were the first to apply the Flory^{49,50} - Huggins^{51,52} theory of polymer solutions to mixtures of polymers with and without added solvent.

Theoretical aspects. For a binary system of two polymers A and B, i.e., (no solvent), Scott obtained essentially the following expression for the Gibbs' free energy of mixing:⁴⁷

$$\Delta F_{\text{MIX}} = \frac{RTV}{V_r} \left[\frac{\phi_A}{x_A} \ln \phi_A + \frac{\phi_B}{x_B} \ln \phi_B + \chi_{AB} \phi_A \phi_B \right] \quad (1)$$

where:

V = total volume of the mixture

V_r = reference volume, which is taken as close to the molar volume of the smallest polymer repeat unit as possible

ϕ = volume fraction of polymer

x = degree of polymerization of polymer in terms of the reference volume V_r

χ_{AB} = interaction parameter between the two polymers.

The assumptions inherent in equation (1) are that:

1. the solution can be treated as a "lattice" with each lattice being occupied by one segment of the polymer molecule or one solvent molecule.
2. all lattice cells have the same volume
3. there is no volume change on mixing
4. χ_{AB} is based on the Hildebrand solubility parameter δ as

$$\chi_{AB} = \frac{V_r}{RT} (\delta_A - \delta_B)^2 \quad (2)$$

For dilute solutions of polymers, the Flory-Huggins treatment is not a good approximation as ideally speaking there cannot be uniform mixing, because due to the long chain nature of the polymer molecule the concentration in its vicinity will not be the average value but higher. However when the mixture is that of two polymers only, their individual segments more or less have the same segmental volume and at moderate concentrations the uniform mixing approximation is not in serious error.

χ_{AB} as given in equation (2) is also not rigorously expressed but when the two species are of comparable size, the expression is valid. This is so for blends of two polymers in the absence of any solvent. However for mixtures of molecules of very different sizes, χ_{AB} cannot be associated just with the energies of interaction between molecules but as Huggins⁵² noted, must also include an entropic contribution in its definition. This aspect is discussed shortly.

For a binary system the critical conditions as represented by the critical point on the phase diagram are easily calculable and by the criteria:

$$\frac{\partial^2 \Delta F_{MIX}}{\partial \phi_A^2} = \frac{\partial^3 \Delta F_{MIX}}{\partial \phi_A^3} = 0 \quad (3)$$

Scott found that

$$(\chi_{AB})_{cr} = \frac{1}{2} \left[\frac{1}{\sqrt{x_A}} + \frac{1}{\sqrt{x_B}} \right]^2 \quad (4)$$

This represents one of the conditions under which a binary system will just begin to separate into two phases, i.e., the limits of compatibility. This shows that critical conditions are reached very quickly for two polymers having appreciable degrees of polymerization and by this line of reasoning, Scott concluded that "unless their heat of mixing is virtually zero or negative, two high polymers are always immiscible in the absence of a solvent."

Scott also extended his thermodynamic analysis of a ternary system of one polymer and two liquids⁴⁷ to two polymers and one solvent and

concluded that the presence of the solvent served only to diminish the "effective" interaction parameter $\chi_{AB}(1-\phi_s)$ where ϕ_s is the volume fraction of the solvent. When there is a large amount of solvent present, i.e., when $\phi_s \approx 1$, the effective interaction parameter approaches zero and the whole system forms a single phase. In other words, if a solvent which dissolves both polymers exists, no matter how incompatible the two polymers may be, it is always possible to make a very dilute solution containing both polymers.^{47,53}

Three-component systems and their phase diagrams are more complex than binary systems and it is usually not possible to discuss them in terms of a single parameter such as the critical point. Tompa⁵⁴ has discussed the thermodynamics of such polymer mixtures at length.

The treatment of Scott was further extended by Krause⁵³ to "predict" compatibility between pairs of polymers in an extensive review article. Krause's approach involves the theoretical calculation of χ_{AB} and comparing it with $(\chi_{AB})_{cr}$ using Scott's equation.

χ_{AB} can be calculated for molecules of comparable size in terms of the Hildebrand^{55,56} solubility parameter δ using equation (2) which for $V_r = 100$ cc/mole, the gas constant $R = 1.987$ cal/(deg mole) and $T = 298^\circ\text{K}$ reduces to a convenient form

$$\chi_{AB} \approx \frac{(\delta_A - \delta_B)^2}{6} \quad (5)$$

Equation (2) involves the assumption of neglect of an entropic contribution on mixing such as no association of molecules due to specific interactions between them; for example, polarity effects, hydrogen

bonding, etc. The only interactions allowed are the energetic ones represented by $\Delta\epsilon$

$$\Delta\epsilon = ZA \left[\frac{\epsilon_{AA}}{2} + \frac{\epsilon_{BB}}{2} - \epsilon_{AB} \right] \quad (6)$$

where:

$-\epsilon_{AA}$ and $-\epsilon_{BB}$ = potential energy of contacts with the same species

$-\epsilon_{AB}$ = potential energy of cross-contacts

Z = lattice coordination number

A = Avogadro's Number

In the absence of any specific interactions it is valid to say that

$$\epsilon_{AB} \approx \sqrt{\epsilon_{AA}\epsilon_{BB}} \quad (7)$$

This expression of cross-contact energetics being equal to the geometric mean of like-contacts follows from the London theory of "dispersion forces". It leads to

$$\begin{aligned} \Delta\epsilon &= \frac{ZA}{2} \left[\sqrt{\epsilon_{AA}} - \sqrt{\epsilon_{BB}} \right]^2 \\ &= \left[\sqrt{a_A} - \sqrt{a_B} \right]^2 \\ &= (\delta_A - \delta_B)^2 \end{aligned} \quad (8)$$

where a = cohesive energy density (CED)

and δ = the solubility parameter = \sqrt{a}

At constant pressure the heat of mixing is given by

$$\Delta H_m = \Delta E_m + P\Delta V_m \quad (9)$$

and since the lattice model assumes no volume change on mixing $\Delta V_m = 0$ giving $\Delta H_m = \Delta E_m$

$$\Delta E_m = (\Delta \epsilon) n_A \phi_B \quad (10)$$

where n_A = moles of species A

ϕ_B = volume fraction of species B

$$\Delta H_m = RT \chi_{AB} n_A \phi_B / V_r \quad (11)$$

This leads to

$$\chi_{AB} = (\Delta \epsilon) V_r / RT \quad (12)$$

and eventually to

$$\chi_{AB} = \frac{V_r}{RT} (\delta_A - \delta_B)^2 \quad (13)$$

Subject to the above assumptions, equation (13) is the same as equation (2).

Solubility parameter values if unavailable can be estimated⁵³ to a satisfactory degree of precision using tabulated values of group molar attraction constants of Small⁵⁷ as revised by Hoy.⁵⁸ According to Krause they are more reliable than experimental values.

If $\chi_{AB} > (\chi_{AB})_{cr}$, incompatibility at some percentage composition is predicted. Also, the greater the value of $|\chi_{AB} - (\chi_{AB})_{cr}|$ the smaller the compositional range for compatibility. This implies that for compatibility over as wide a range as possible, χ_{AB} should be as small and as close to $(\chi_{AB})_{cr}$ as possible. Also the lower the value

of χ_{AB} the more closely the values of δ_A and δ_B must be matched. The above approach must however be used with care and is not guaranteed as universally true. Bohn⁵⁹ has listed several polymer pairs where anomalous behavior occurs. This is probably due to some kind of intermolecular interactions between polymer molecules, such as hydrogen bonding, polar attractions, etc.

Another approach commonly used in compatibility literature is the prediction of the free energy from enthalpic and entropic considerations. For any spontaneous mixing to occur between any species, their overall free energy of mixing ΔF_m , must be negative.^{1,4,39} Thus, one can write

$$\Delta F_m = \Delta H_m - T\Delta S_m \quad (14)$$

ΔS_m is a measure of randomness and is positive for a mixing process. ΔH_m is a measure of the affinity of molecules to their environment, a negative ΔH_m indicating a preference for mixing and a positive value reflecting preference for their own kind. However the entropy to be gained on intermixing polymer molecules, i.e., the magnitude of the term ΔS_m , is very small owing to the small number of molecules involved.⁴ Gee⁶⁰ has given values of the $T\Delta S_m$ term to give an order of magnitude feeling of the unfavorable entropic effect.

<u>MIXTURE</u>	<u>$T\Delta S_m$</u>	(T = 25°C)
(1 ml of each is mixed)	(cal.)	
Two liquids	8.30	
Liquid plus polymer	4.15	
Two polymers	0.0083	

Molal volume of liquids = 100 ml.

Molal volume of polymers = 100,000 ml.

All this underlines Scott's predictions⁴⁷ that almost a trivially unfavorable heat of mixing (i.e., $\Delta H_m > 0$) will suffice to cause phase separation by making $\Delta F_m > 0$. Hence knowledge of the sign and magnitude of ΔH_m could provide a facile way of predicting compatibility through the measurement of a convenient experimental parameter. In fact Brodsky²¹ has suggested a "degree of compatibility" concept on the basis of the magnitude as well as the sign of ΔF_m which for polymers is dominated by ΔH_m .

Gee⁶¹ has shown that the swelling of a crosslinked rubber is maximum in solvents having the same cohesive energy density (CED) as that of the rubber. The same idea could be paraphrased for blends to say that polymers having the same CED values will be compatible. The solubility parameter δ is defined as the square-root of CED and more commonly used. For two amorphous polymers at constant volume and constant pressure one can approximate ΔH_m by ΔE_m the internal energy change of mixing. Thus

$$\Delta H_m = \phi_A \phi_B (\delta_A - \delta_B)^2 \quad (\text{cal/cc of solution}) \quad (15)$$

Though the above equation always predicts a positive value for ΔH_m it is useful. It indicates that unless the δ values are almost perfectly matched true mutual solubility will not occur as the $T\Delta S_m$ term is itself of a very small magnitude.

Pazonyi and Dimitrov²⁰ have proposed in their theoretical treatment, that if the difference between the CED values of two components is

smaller than 0.016 cal/cc there exists the possibility of mutual solubility, whatever the sign of ΔH_m turns out to be.

Using the approach suggested by Gee,⁶¹ Schneier²³ has derived an expression for ΔH_m which indicates compatibility within the range of 0.001 cal to 0.010 cal for values of the heat of mixing. Gee's value of $T\Delta S_m$ as mentioned previously for two polymers on an average was 0.0083 cal, which is quite consistent considering all the various approximations involved.

Thus to summarize the theoretical predictions, compatibility is favored for lower molecular weights so that critical conditions are not reached rapidly, lower concentrations in a common solvent so that the effective interaction parameter is further diminished, higher temperatures so that the magnitude of $T\Delta S_m$ is raised to offset ΔH_m , closely matched solubility parameters which lower both ΔH_m and χ_{AB} and any other conditions that will favor these criteria.

Hydrogen bonding and other intermolecular forces will further enhance compatibility. All this is meant to be only a rough guide and odd instances of compatibility can be expected.

Experimental observations. Compared to theoretical work on compatibility a vast amount of experimental findings are reported in the literature on a myriad of systems examined in a variety of ways. It is not possible to do justice to, nor is it the objective of this work to comprehensively report such work. Excellent review articles have dealt with the subject more completely.^{1,53,59} Rather, the main objective is to point out the various methods used to study phase separation, the

criteria that was adopted to define compatibility, the limitations of each method and their comparison with theoretical predictions.

As early as 1947 Dorby and Boyer-Kawenoki,⁴⁶ investigating the compatibility between solutions of polymers in a variety of differing solvents, observed that even when polymers could be codissolved in a common solvent, phase separation occurred at low to moderate concentrations. This led them to conclude that incompatibility was the general phenomenon. Though their observations were macroscopic in nature, they noted that "one can conceive of microphase separation in which a mixture would become microheterogeneous". This is not unreasonable if one considers that nonequilibria can be kinetically frozen into a metastable morphology such as when the matrix is glassy and does not allow diffusional mobility to the blend's species. Their observations found a general but not detailed agreement with Scott's later predictions.⁴⁷

Further work on polymer/polymer/solvent systems was done by Kern⁶²⁻⁶⁴ and Bristow⁶⁵ who also observed that polymers tend to separate into phases even in a common solvent, when allowed to stand. These phases could be either pure with sharp partitioning indicating incompatibility or could be rich in one component and lean in the other indicating partial compatibility.

In extending his study on the compatibility of conventional low molecular weight plasticizers with polymers to that of high molecular weight plasticizers, Boyer⁶⁶ observed that they were difficult to incorporate into the parent polymer and tended to phase separate.

In general the experimental observations support the prediction that compatibility is not an oft observed phenomena and classification

birefringence using an ordinary microscope with polarized light. Phase contrast microscopy has also been used successfully.^{27,28,37,70}

Transition phenomena: The most interesting transitions for polymers are commonly the thermal and mechanical ones. Though melting points are characteristic thermal and mechanical transitions, one needs to have a crystalline phase for that and polymer blends are by and large amorphous. The glass transition temperature (T_g) is the one most frequently monitored and this can be done by a variety of experimental techniques both thermal and mechanical. Differential scanning calorimetry (DSC), differential thermal analysis (DTA), dynamic mechanical testing, e.g., using a torsion pendulum or a rheovibron, etc., are conveniently used.

A reliable criteria of compatibility is that if two polymers can mix at a fine enough level they ought to lose their characteristic transitions and respond with just one transition temperature intermediate between those of the original homopolymers. The position of this should depend on the composition of the blend and the width of this transition should be a measure of the fineness of the dispersion.

The Fox equation⁷¹ for the glass transition temperature of copolymers (T_{g12}) given by

$$\frac{1}{T_{g12}} = \frac{w_1}{T_{g1}} + \frac{w_2}{T_{g2}} \quad (16)$$

is based on additive properties (w = weight fraction) of the monomeric units and should serve equally well for blends. Another equation due to Gordon and Taylor⁷² is

thus lowering the glass transition even further. The O/V parameter can conveniently be estimated by SAXS as will be shown later and the Tg's measured conventionally by DSC and dynamic mechanical methods could be used to test the above hypothesis.

Buchdahl and Nielson³¹⁻³³ were the first to apply the method of dynamic mechanical testing to polymer blends followed by Wolff and co-workers^{74,75} and Jenckel.⁷⁶ Nielson³² demonstrated dramatically the compatibility of the now almost classic system of PVC and nitrile rubber containing 30-35% acrylonitrile. The more recent data of Takayanagi³⁴ on the same system shows only one transition for all compositions with the homopolymers exhibiting a more abrupt drop in E' (the real part of Young's Modulus) than the blends, indicating a range of compatibility depending on composition. In fact Takayanagi's comparison of the viscoelastic data on real systems versus the viscoelastic data on model systems (i.e., both are experimental quantities) is able to give a much more detailed insight into the mechanical behavior of blends and their degree of compatibility.

The very system that forms the central point of this thesis viz. PCL/PVC was discovered to be compatible by Koleske and Lundberg⁷ using the glass transition criteria by dynamic mechanical testing with a torsion-pendulum.

Stoelting et. al.,³⁵ in their studies on PPO/PS blends, came across an interesting phenomenon viz. that their system showed partial compatibility by the dynamic mechanical method indicating a PPO rich phase and a PS rich phase but exhibited a single broad transition by DSC indicating compatibility. This confirms the phenomenological

prediction that depending on the molecular process involved and its sensitivity to a given method of testing, a system could be characterized either as compatible, partially so or incompatible. In the above case, whatever the domain sizes involved, they were small enough to escape thermal detection but not quite so small as to prevent discriminating them by mechanical spectroscopy.

Another instance of a compatible system when one of the components (PVF_2) has a pronounced tendency to crystallize was discovered by Noland et al.²⁶ on the PVF_2/PMMA and PVF_2/PEMA systems and confirmed by Paul and Altamirano.²⁹ They measured the T_g 's by the method of DTA.

Using a variety of techniques, Hickman and Ikeda²⁸ and Hammer³⁶ have found other compatible systems of PVC with other polymers. MacKnight, Stoelting and Karasz have also demonstrated the use of dielectric dispersions to study phase separation.²⁵

Thermodynamic changes on mixing: Two of the thermodynamic parameters that indirectly influence mixing are ΔH_m , the heat of mixing, and χ_{AB} , the interaction parameter. Relatively few measurements of these quantities have been reported. As has already been said before, the true solubility ΔH_m must either be negative (exothermic) or very close to zero and similarly χ_{AB} must be very small in magnitude.

Slonimskii⁶ has established ΔH_m values for polymer pairs using Hess' law of the independence of heat effects on the particular path chosen for the mixing process. Their observations can be summarized as: in all cases where the experimental value of ΔH was > 0 (i.e., endothermic) phase separation occurred and even when ΔH was < 0 a single phase is

not always observed. They explained this in terms of a volume change on mixing.

More recently Ichihara et al.²² used the method of Hess' law to estimate the enthalpy of mixing for PMMA and PVAc, and showed how they could discriminate by heat effects between the morphologies of the blends prepared by solvent casting and freeze drying.

Very few studies have estimated the χ_{AB} the interaction parameter between two polymers A and B during the course of compatibility studies by other techniques. For the rubber/PMMA system, Bristow⁶⁵ estimated $\chi_{AB} \approx 0.038$, for PB/PS system known to be incompatible, Paston⁴⁰ gave values of 0.072 and 0.112 for two different series and more for a mixture of low molecular weight polypropylene oxide and polyethylene oxide, both of which are capable of crystallizing. Booth and Pickles⁷⁷ estimated $\chi_{AB} \approx -0.063$ to 0.067 indicating partial miscibility.

Miscellaneous: Several miscellaneous criteria have been proposed to define compatibility⁷⁸ such as intrinsic viscosity,^{37,38} rheological models^{41,42} and dynamic viscosity.⁴³

Small Angle X-Ray Scattering

General comments. The very first experimental studies of the general phenomenon of small angle x-ray scattering were done in the early 1930's⁷⁹ and followed by theoretical attempts of Guinier⁸⁰ and Kratky.⁸¹ Historically, SAXS studies commonly done at angles less than 2° off the undeviated incident beam, have lagged behind those of WAXD done at the "normal" Bragg angles of 10° to 40° .⁸² This is understandable when one considers that, 1) the experimental requirements for obtaining SAXS

information are stringent, and 2) the exact interpretations of SAXS data were not easily understood. Today SAXS has come into its own and is more widely used as a tool of research. A recent international conference* devoted solely to the phenomena of SAXS is a measure of its current popularity.

However, certain aspects of interpreting SAXS data on polymeric systems continue to be ambiguous and are often debated. The growing volume of literature on SAXS allows one to follow trends and derive general parameters with sufficient confidence but the understanding of finer details is somewhat obscured. As one case in point, the broad but discrete maximum often observed for semicrystalline polymers at non-zero scattering angles that previously could not be correlated with electron microscopic observations, is now accepted to be due to a macro-periodicity or "long-period" as it is so often called. The average distance between centers of adjacent crystallites is believed responsible for this periodicity. Semi-crystalline polymers have an amorphous component which resides between the crystallites and so the long period on an average is the sum of the average thicknesses of crystalline and amorphous layers. For a stack of single crystal mats where there is little or no amorphous material between the crystals, the long period is directly the average size of the crystals. However, for semi-crystalline polymers where discrete scattering occurs, the estimation of crystallite sizes, the nature and influence of their size-distribution, the magnitude and shape of the

* Third International Conference on Small-angle scattering, Grenoble, France, 4-8 September 1973; proceedings in J. Appl. Cryst., Vol. 7, Part 2 (1974).

transition-zone profile between the crystalline and amorphous components, the origin of the sometimes observed second order maximum at higher angles, etc., still continue to be discussed.

Among the contributors to the theoretical understanding of SAXS the works of Guinier⁸³ and Porod^{84,85} deserve special mention, while on the experimental side, the contributions of Kratky and coworkers⁸⁶ stand out clearly. Extensive review articles^{82,87-89} and texts^{83,90-92} do justice to the subject.

The scattering of x-rays by matter is the result of fluctuations in the electron density of the material. If a material was completely homogeneous in its electron density, no scattering would occur. Most materials have some kind of heterogeneity or a range of kinds. If they occur on a macro level, i.e., 50 Å to 5000 Å, SAXS can be used to investigate such a morphology. Typical systems studied by SAXS are those composed of discrete particles such as colloidal suspensions; dilute solutions of macromolecules; and phase separated systems such as polymer blends, semi-crystalline polymers, microvoids in homogeneous solids (catalysts, fibers), metallic alloys, etc.

Polymers exhibit two types of x-ray effects at small angles: diffuse scattering and discrete diffraction. It is important to recognize the distinctions between these effects as there may be no relation at all between them.⁷⁵ They are caused by different aspects of aggregation of the macromolecules.

Diffuse scattering can be obtained from polymers either in solid or liquid states. There is no scattering maximum at non-zero angles and the intensity drops continuously with increasing angle. Diffuse

scattering when due to solutions (dilute systems) is much more amenable to definitive theoretical interpretation⁹² and the well known Guinier plot is one example of this. Solid and molten polymers (densely packed systems) also give diffuse scattering but interparticle interference effects complicate their analysis. Solid polymers upon deformation can develop voids which also produce diffuse scattering. Air or solvent swollen natural fibers also cause diffuse effects and in both these instances the assumption of "diluteness" can be valid enough for application of the theory of scattering by dilute systems.⁹² In general, in interpreting diffuse scattering from dense systems, interparticle effects cannot be neglected.

Discrete diffraction effects can be obtained from many polymers but always from the solid state and never from materials which appear amorphous in a wide-angle x-ray pattern, according to Statton.⁸² Most commonly, a single broad maximum at non-zero scattering angles corresponding to long-periods of 100 Å to 200 Å is observed. The usual pattern is a complex combination of the discrete diffraction which is superposed on a diffuse background of some sort.

In certain cases, under special conditions, there can be diffuse scattering with an intensity maximum at non-zero angles. This effect is not the same as the maxima due to discrete diffraction but probably related to it. The analysis of this feature is attempted by Guinier⁹³ and Porod.⁸⁵

The theoretical treatment is relatively simple for systems in which large discrete molecules (such as proteins) can be dispersed essentially monomolecularly in suitable solvents. In the analysis of these systems, the intensities due to individual scattering particles are

additive and interference effects are negligible. The character of the scattering curve is determined by the variability in size and shape of the particles but even in dilute systems there are limitations to interpretations. Experimental parameters free of any ambiguity can be derived from SAXS patterns only if all the particles in the system are identical in size and shape (monodisperse) and sufficiently diluted to eliminate interference effects between them. Even if such ideality is possible experimentally, the particle shape must be known if the size is to be specified unequivocally, and vice versa.⁹² Where polydispersity exists only average effective parameters can be deduced.

This points out an important truth in the analysis of SAXS data, viz. that in the absence of other information about a system, or assumptions as to the nature of inhomogeneities of the system, the only factor which can be obtained, without ambiguity, is the "mean-square fluctuation" of the electron density also called the "scattering power" of the system as a whole, and denoted by $\langle \eta^2 \rangle$.^{83,94} Another general parameter that can be obtained unambiguously from SAXS but cannot be interpreted so, is the Debye correlation function $\gamma(r)$.^{95,96} This is obtained by Fourier inversion of the experimental data but it needs some kind of model to interpret its physical significance.

The need for other independent experiments becomes obvious as far as supplementary data goes and model building becomes necessary for meaningful assumptions to be made. Both these aspects are dealt with in more detail later on.

The treatment of densely packed systems is far more complicated and a general treatment is difficult. The importance of interference

effects was pointed out by Kratky^{81,97} and three particular cases of dense systems are given by Kratky and Porod.⁹⁸ Porod⁸⁴ has further shown how significant quantitative parameters can be obtained for two-phase systems from an analysis of the tail of the scattering curve which has come to be known as "Porod's Law" and also⁸⁵ dealt with the very complex analysis of discrete interference effects in the absence of any diffraction from closely packed systems.

Since this work is devoted to the study of polymer blends and blends are densely packed systems, dilute systems are not discussed any further. Some historical comments on dense systems, particularly those possessing a semi-crystalline morphology are in order. This will provide a continuous link to some of the more specific discussions in the succeeding chapters.

Discrete diffraction. The occurrence of discrete maxima may be regarded as the manifestation of a periodic or at least a quasi-periodic order. More than one order of such reflections have been observed, e.g., for collagen⁹⁹ which is an exception.

Recently Kawai and coworkers¹⁰⁰ were able to obtain as many as eight orders of SAXS reflections for solvent cast films of styrene-isoprene block copolymers which are believed to possess a very ordered lamellar morphology. It is generally difficult to record beyond the second order¹⁰¹⁻¹⁰³ which itself is not easily observed. Even the first order reflection is quite broad and has a diffuse character to it. It is more like a statistical interference phenomenon and has been so treated in the literature.

A statistical phenomena can best be treated in terms of distortions and distribution functions of progressively complex kind. Distortions of the first kind represent a fluctuation about some fixed value or position such as the points of a lattice. Those of the second kind are represented by a "paracrystalline lattice", i.e., the location or position of a point oscillates with respect to its neighbors instead of a fixed lattice point. Therefore, the absolute deviations from positions corresponding to strict periodicity increase with increasing distance from any reference point. This concept of the paracrystal was developed and has been used extensively by Hosemann.⁹⁰

Zernicke and Prins¹⁰⁴ and Kratky¹⁰⁵ have developed theories with distortions of the second-kind to explain the structure of liquids in the approximation of a unidimensional, quasi-periodical arrangement of particles. For diffraction from such a linear lattice, J. J. Hermans¹⁰⁶ has reported a mathematical solution of general applicability. More specific models have been treated by Hosemann¹⁰⁷ and by Porod.^{84,85,108} These calculations predict diffuse maxima which are only approximately related in their position to the mean period according to the Bragg equation. Also the predictions include progressively broader, higher order reflections which will coalesce and if statistical variations in excess of approximately 25% occur, they are washed out with only the first order being detectable. According to Porod¹⁰⁸ if the linear lattice consists of lamellar shaped particles which are ordered with respect to their thickness (which is what one sees in spherulitic growth by electron microscopy) then the maxima ought to be further reduced as a result of

the Lorentz factor (Appendix I). It follows that for sufficiently large variations even the first order reflections can be lost.

Among the first SAXS experiments showing discrete effects were those of Hess and Kiessig¹⁰⁹ on synthetic polyamide and polyester fibers. Hess and Kiessig developed the "bundle or string model" (Fig. 1) to explain their results and, according to them, the long-period is related to the average distances between centers of adjacent crystallites. Similar reflections were observed by other workers on a variety of polymers. The model incorporated the correct basic ideas about alternating crystalline and amorphous regions but the concept of chain folding did not exist then.

The model, however, was found to be inconsistent with the dependence of the long-period on the various after-treatments of the polymers, unless a complete rearrangement of the structure was assumed.¹¹⁰ This would involve irreversible changes, whereas Zahn's¹¹¹ results indicated that reversible changes could occur. Also, the four point pattern indicated the presence of diagonal lattice planes with respect to the fiber axis and the question has been discussed in detail by Statton.^{112,113} In the same publication, Statton also showed that the "crystallite size", as estimated by WAXD using the Scherrer equation, was always less than the long period and had a fairly linear relationship with it. The difference was accounted as the intercrystalline amorphous regions and these results were, at that time, considered a strong support for the Hess-Kiessig model.

With the advent of polymer single crystals and the concept of chain folding,¹¹⁴⁻¹¹⁶ the above model has been substantially modified due to a drastically altered thinking about polymer morphology. Single

crystal units of PE produced SAXS patterns with a series of strong, well-defined maxima which would be related to each other through the Bragg equation and to the microscopically observed lamellar thickness.¹¹⁷ Further, micrographs of free surfaces and fracture surfaces of many well-crystallized materials reveal a lamellar structure reminiscent of the solution crystallized material.¹¹⁸

Suffice it to say that due to the contributions and efforts of many workers¹¹⁹⁻¹²⁵ in this relatively new field, it is now accepted almost universally that in the case of semi-crystalline polymers possessing a lamellar kind of morphology, the first order discrete maximum observed at non-zero angles, is related to the average dimensions of the periodicity of a macrolattice within the material and that this periodicity which is termed the "long period", is equal to the average dimensions of one crystalline lamella and one interlamellar amorphous layer.

When more than one maximum is observed, there is as yet no definite agreement as to whether it is a higher order reflection of the first or due to a different morphological aspect.¹²⁶ In two recent review articles,^{127,128} Crist has tried to show how higher order reflections can be used to understand the distribution functions of the size of crystallites and the amorphous layers according to the criteria of the ratio of their positions being > 2 . Crist has also compared several existing models and noted that while each has its merits and deficiencies, the choice of a model could easily depend on the nature of the system examined. This implies that no unique model is as yet available to explain discrete SAXS patterns of semi-crystalline polymers.

Among the models compared by Crist are those representing a restricted as well as the general paracrystalline model of Hosemann,⁹⁰ the skewed or assymmetric distribution function model of Reinhold et al.,¹²⁹ the symmetric but Gaussian distribution function model of Blundell,¹³⁰ the transition zone model of Tsvankin with distribution functions of two kinds^{131,132} and the Tsvankin model as modified by Buchanan.¹³³ Wenig and Kilian¹³⁴ have formulated their own paracrystalline model which they claim has more advanced features.

It was remarked earlier that the analysis of SAXS data needs other independent information and the assumption of size or shape parameters. The observation of lamellar type of morphology by electron microscopy in bulk and solution crystallized polymers is established¹¹⁸ well enough to consider the model of alternating crystalline and amorphous layers as valid. Nevertheless, there could be infinite combinations of various model parameters and it quickly becomes apparent that model building can become an extensive undertaking. Also for reasons of mathematical tractability and limitations in computing time, some of the more realistic but complex features of the model have very often sacrificed. No matter how realistic a model, when interpreting SAXS data one must remember that in spite of the most reliable experimental data, the derived parameters are only as good as the model is. In this respect, especially for densely packed systems one would do well to heed Porod's advice⁸⁹ and "abstain from an attempt to derive an exhaustive description of the system and confine oneself to certain parameters or characteristic quantities which can be derived from small-angle scattering". Such quantities are the

"scattering power" and "specific surface". They are dealt with in detail in Chapter III.

Another interesting method to characterize dense systems is the correlation function approach of Vonk^{122,123} which will also be discussed in Chapter III. Suffice it to say that it also involves the use of a model and gives equivalent results.¹³³ This approach has its origins in the more general treatment of diffuse scattering by Debye^{95,96} and Porod.^{84,85} Ruland¹³⁵ and Strobl¹³⁶ have also proposed methods for the analysis of SAXS from dense systems. It should be mentioned that in the method of Vonk, i.e., using the correlation function approach, interparticle interference effects are implicitly considered in its derivation.

Diffuse scattering. Diffuse scattering in densely packed systems is normally the result of a randomly arranged morphology, i.e., one in which neither the shape nor the position nor the orientation of particles has any particular definition. The situation is thus one of the degree of randomness. However, it is not as hopeless as it looks and some interesting general parameters can be derived as mentioned earlier by the correlation function approach. Both Debye⁹⁶ and Porod⁸⁴ have derived relations that give a meaningful interpretation of such morphologies.

Again even for diffuse scattering, interparticle interference must be expected for a dense system. According to Statton,⁸² it can take three forms: 1) limited penetration, in which two particles are closer to each other than the distance of their diameters causing a blurred interference effect; 2) association, in which particles aggregate into large group or clusters and cause the scattering curve to rise steeply at very small angles; and 3) ordering, in which strong forces act between

particles, and build up a certain periodicity in the electron density of the system. Ordering of a close packed system can result in a maximum as mentioned previously and the extent could depend upon the monodispersity.

Transition zone. When two phases of different densities coexist, the nature of the phase boundary separating them could vary in its character from sharp to diffuse depending upon the constituents of the phases, the conditions under which their separation came about, the nature of the existing equilibrium, etc.

In two phase polymeric systems, whether they be semi-crystalline polymers or blends of polymers, the nature of the boundary or transition-zone as it is often called is important to know for a variety of reasons. For example, a very sharp boundary in polymer blends is a strong indication of incompatibility as opposed to a diffuse one which would indicate some kind of compatibility. Very diffuse boundaries between crystallites and the amorphous medium indicate poor quality crystallites which can be linked to the kinetics of crystallization of the system, etc.

In all of Porod's and Debye's general work, the assumption of sharp boundaries was implicit. Thus, their systems were ideal in this respect which is seldom the case in practice. Most boundaries between two polymeric species tend to have finite dimensions.

Tsvankin^{131,132} was the first to introduce this concept with a linear density profile in his lamellar model and the width of the transition zone was one of the model's adjustable parameters. Blundell¹³⁷ also included a linear transition zone in his one dimensional Gaussian distribution SAXS model.

Ruland¹³⁵ and Strobl and Muller¹³⁸ considered the presence of transition zones as deviations from Porod's model and showed how such deviations could be handled. Ruland also showed how, in the course of testing the identity of the system against Porod's Law, the width of the transition zone could also be estimated. Vonk's¹³⁹ rigorous treatment of the same model as Tsvankin proposed allows the estimation of the width and volume fraction of the material in the transition zone using the correlation function approach of Debye et al.. Stein and Khambatta¹⁴⁰, also using the general theory of Debye but with a much simpler derivation, have proposed a method to calculate the volume fraction of the transition zone in a system of non-lamellar amorphous blends. It is interesting to note that while Vonk's derivation (like those of the preceeding works) was meant to apply to a lamellar morphology, it is identical in its final form to the Stein-Khambatta equation.

In two recent publications, Bonart^{141,142} has proposed a very elegant method for estimating the width of the transition zone along with other interesting parameters and this will be discussed later in more detail.

Helfand and Tagami^{143,144} and Meier¹⁴⁵ have proposed theoretical methods using statistical mechanics to estimate the width of transition zones from the point of understanding interface behavior between polymeric domains in blended systems and experimental values will be compared with their theories.

Small-Angle Light Scattering (SALS)

As mentioned previously, SALS is a very handy and convenient technique to study heterogeneities in the range of 0.5 to 50 microns and

complements both SAXS and LM on either side of this range. The use of SALS for the study of polymers has been largely pioneered in the laboratories of the University of Massachusetts under the leadership of Professor Stein.

While work has been done on several different aspects of light scattering from a myriad of systems such as two and three dimensional spherulites, two and three dimensional rod structures, static and dynamic modes, oriented and unoriented systems, etc., a comprehensive survey of all the published literature is not feasible, especially since SALS was not the major technique of this thesis. Excellent review articles on SALS exist.^{19,146-150}

The author has thus restricted the discussion to the photographic and photometric techniques in both the H_V and V_V modes under static conditions for semi-crystalline systems having a spherulitic morphology; with passing references to other aspects wherever necessary.

The general theoretical framework of SALS is essentially the same as that of SAXS^{19,95,151} in the sense that while SAXS is sensitive to changes in local electron densities, SALS is sensitive to changes in refractive indices, i.e., fluctuations in densities as well as anisotropy of course at relatively macro levels. SAXS is insensitive to anisotropy fluctuations since it involves inner electrons of atoms which are not influenced by chemical bonding which is the source of anisotropy.¹⁹

Polymers scatter light because they contain heterogeneous entities of dimensions comparable to the wavelength of light. As in SAXS, the angular dependence of scattered light is characteristic of the size, shape and distribution of the scattering particles.

In semi-crystalline polymer films, three sources of heterogeneities could occur, 1) density fluctuations due to crystallinity, areas of differing density due to statistical fluctuations or voids; 2) orientation fluctuations due to anisotropy; and 3) anisotropy fluctuations due to areas of differing anisotropy. By selecting the proper mode of polarization, one can discriminate between the various fluctuations. In the H_V mode, the polarizer and analyzer are crossed with respect to their polarization directions while in the V_V mode they are parallel. H_V scattering is insensitive to density fluctuations.

The interpretation of SALS results can be done either by the statistical approach or by the model approach. Debye and Bueche⁹⁵ were the first to propose a general theoretical treatment of SALS from polymer films. Theirs is the well known correlation function approach in which they considered only density fluctuations. According to their theory, the intensity of scattered light from a density heterogeneous system is proportional to the mean squared fluctuations in the refractive indices and also to a density correlation function. The latter is a measure of the degree of correlation between fluctuations a certain distance apart. The above treatment was generalized by Goldstein and Michalik¹⁵² to include both density and orientation fluctuations but its overall complexity has discouraged its application.

The Stein-Wilson¹⁵³ treatment is a special case of random orientation fluctuations of anisotropic elements and assumed that the probability of having two optic axes with correlated orientations depends only upon their distance of separation and not on the angle these axes make with the separating vector. This gave azimuthally independent results which

is not the usual case experimentally. The above treatment was extended by Stein et al.¹⁵⁴ to include nonrandom orientation fluctuations in which the angular dependence of the optic axes and the separating vector is considered. This predicts an azimuthal dependence as seen experimentally. The above treatments were two dimensional. The three dimensional calculations were done by van Aartsen¹⁵⁵ and applications to oriented systems were done by Stein and coworkers.¹⁵⁶⁻¹⁵⁸

All the above treatments are very general due to their statistical nature and consequently difficult to interpret in terms of the structural features of the scattering systems. Also, the more random the system's morphology, the more meaningful is the statistical approach because for random morphology, the structural features are difficult to define. However, such theories are a poor approximation for describing any organized or well ordered morphology such as spherulitic structures. The model approach is better suited to this.

Stein and Rhodes^{159,160} proposed a three dimensional model of homogeneous anisotropic spheres with the optic axes either along or normal to the sphere's radius. The shapes of the corresponding H_v and V_v patterns as predicted by the model agreed very well with many experimental observations^{159,161} but the absolute intensities of scattering could not be reconciled between the two.^{162,163} For example, the excess H_v intensities at small and large angles on either side of the intensity maximum could not be accounted for theoretically. The angle of maximum scattered intensity is very simply related to the size of the spherulite.¹⁵⁹ Small angles represent scattering from larger structures such

as spherulites while as the angles get progressively larger, small structures such as intraspherulitic details begin to contribute.

The discrepancy between theory and experiment was thought to be due to the relatively idealistic nature of the models. The model assumes scattering from an isolated single spherulite which is particulate scattering just as mentioned for SAXS.

In crystalline polymer films, microscopic observations show that the structure is quite densely packed and, moreover, seldom spherical or circular. The dense packing must result in interspherulitic interference effects and the impingement of spherulites result in polygonic spherulites. Moreover, the spherulites due to random truncations are polydisperse in sizes. These effects can be considered as forms of "external disorder" and treated by Stein and coworkers^{164,166-170,172} and Kawai.^{165,171}

Another kind of disorder that could occur within the spherulites and hence termed as "internal disorder" could be due to the deviation of the optic axis orientation from its ideal position.^{162,173-176}

In addition to the above factors, Stein and Keane¹⁷⁷ have shown how the experimental data may be corrected for reflection, refraction and secondary scattering. A more refined multiple scattering theory has been recently proposed.^{178,179} The consideration of all the various disorders and necessary experimental corrections have resulted in much better agreement between theory and practice.¹⁸⁰

C H A P T E R III

THEORETICAL BACKGROUND

Since the major emphasis of this work is on the techniques of small-angle x-ray scattering and small-angle light-scattering, a few words on the meaning of the terms "scattering" and "diffraction" are in order.

Scattering and Diffraction

When any form of radiation interacts with matter, it is scattered. The manner in which this scattering occurs depends on the internal distribution of "scattering entities", i.e., heterogeneities, their size and shape and the wavelength of the incident radiation.

Ordinarily, the wavelength is kept constant during an experiment and the scattered intensity is simply monitored in a convenient way, as a function of the scattering angle. This gives the "scattering envelope" or curve, the shape of which is representative of the morphology of the scattering system. In fact, every point of the scattering curve is indicative in some way of some features of the system's morphology, viz. whether there is randomness or an ordered arrangement, whether the system is isotropic or has preferred orientation (texture), whether the heterogeneities are micro or macro on an average, the degree of heterogeneity or homogeneity, the nature and degree of correlation between the various

scattering entities, etc. It is thus apparent that "scattering" as such is a very general phenomenon.

Nevertheless, there are basically two main kinds of scattering viz. "diffuse scattering", often simply termed as "scattering"; and "discrete scattering" which is synonymous with "diffraction".

When the scattering entities are arranged in a regular geometrical array such that their physical positions within a material's morphology can be described by some lattice, by virtue of such geometry the scattering vectors reinforce each other at preferential angles of scattering. This is the same as saying that the amplitude of scattering goes through a maximum, the sharpness of which depends on the regularity with which the heterogeneities conforms to a given lattice. Such discrete effects are termed "diffraction" and are more common in low molecular weight materials where a larger freedom for ordered packing exists. Polymers, by virtue of their high molecular weight, are restricted in this respect due to kinetic considerations. Their heterogeneities often conform to a disordered geometry which broadens the maxima if any and even washes them out when the disorder is large enough. This leads to the diffuseness in scattering. Diffraction is thus a special case of the more general phenomenon of scattering.

By and large, at least for x-rays, the diffraction effects occur in the wide-angle region and scattering in the small-angle region. Hence, the often used acronyms of WAXD and SAXS. This does not in any way restrict each phenomenon to certain angular ranges but merely that conventionally WAXS and SAXD are seldom used symbols even when justified.

Small-Angle X-Ray Scattering

The general theory of SAXS has been well worked out, particularly by Guinier⁸³ in the case of dilute systems and by Porod,^{84,85} Debye^{95,96} and Hosemann⁹⁰ for dense systems. As mentioned in Chapter II, excellent review articles^{82,87-89} and texts^{83,90-92} are available that do justice to both.

Since this work is concerned with polymer blends in the solid-state, theory only pertinent to dense systems is discussed.

General. One of the most useful quantities obtained from SAXS experiments is the total integrated scattered intensity, also called the INVARIANT by Porod.⁸⁴ It is a characteristic property of the system and denoted by Q . In general:

$$Q = \int_0^{\infty} x^2 \cdot I(x) \, dx \quad (20)$$

where x is any convenient angular parameter. x can be represented by a variety of alternate symbols such as s , m , etc. as defined below.

$$s = \frac{2 \sin \theta}{\lambda} \quad (21)$$

$$m = 2a \sin \theta \quad (22)$$

where λ = wavelength of x-rays ($\lambda_{\text{CuK}\alpha} = 1.542 \text{ \AA}$)

a = distance between sample plane and detector plane

2θ = scattering angle (Fig. 2)

s is also called the "scattering vector" and in the terminology of the

"reciprocal lattice"⁹²

$$s = |\rho_{hkl}| = \frac{1}{d_{hkl}} \quad (23)$$

where $|\rho_{hkl}|$ is the magnitude of the reciprocal vector and d_{hkl} is the distance between planes of (hkl) indices. For small angles, i.e., $2\theta < 1^\circ$, the following approximations are quite valid:

$$s = 2\theta/\lambda$$

and $m = (2\theta)a$

For purely arbitrary reasons, m has been adopted as the working parameter* throughout this thesis. Thus,

$$Q_m = \int_0^\infty m^2 \cdot I(m) dm \quad (24)$$

The above equation, however, assumes ideal collimation, i.e., an infinitely small pinhole as the source of x-ray radiation. Such a source is not feasible in practice as it results in very low intensities and unreasonably high counting times for quantitative data accumulation. One can build up the intensity by having a fine line shaped beam instead, whose length to breadth ratio is very large. As will be explained in the next chapter, the intensity with such a beam is distorted due to smearing effects and such intensities are denoted as \tilde{I} (i.e., with a tilde).

Hence, according to Porod's theory⁸⁴

* i.e., for all computational purposes in the reduction of experimental data.

$$\tilde{Q}_m = \int_0^{\infty} m \cdot \tilde{I}(m) \, dm = 2Q_m \quad (25)$$

The various conversions between Q_m , Q_s , Q_θ , etc. have been tabulated by Alexander.¹⁸¹

The importance of the INVARIANT lies in the fact that it allows the evaluation of some of the most general parameters such as the mean squared fluctuation in electron density $\langle \eta^2 \rangle$ and the internal or specific surface (O/V).

In any heterogeneous material, the point to point electron density $\rho(x)$ fluctuates about a mean value $\bar{\rho}$. If the fluctuation is denoted by η , then for a point x one can write

$$\eta(x) = (\bar{\rho} - \rho(x)) \quad (26)$$

The square of this is given by $\eta^2(x)$ and the mean of all the squared fluctuations over all points in space is denoted by $\langle \eta^2 \rangle$. It is an overall measure of all the density fluctuations in any system and an indirect measure of heterogeneity. $\langle \eta^2 \rangle$ is also called the "scattering power of the system"^{94,175,183} and is a fundamentally important quantity in SAXS.

$$\langle \eta^2 \rangle = \left(\frac{2\pi}{i_e N^2} \right) \frac{1}{d \lambda^3} \int_0^{\infty} m \cdot \tilde{I}_n(m) \, dm \quad (27)$$

where $i_e = 7.9 \times 10^{-26}$ (Thompson scattering constant of a free electron)

$N = 6.023 \times 10^{23} \text{ mole}^{-1}$ (Avogadro's Number)

d = sample thickness (appropriate units)

\tilde{I}_n = smeared intensity in absolute (electron) units

The evaluation of \tilde{I}_n is routine and straightforward if the intensity of the primary incident beam is known, and this is most conveniently done with the aid of a calibrated sample (Lupolen) kindly provided by Professor O. Kratky.

Equation (27) can be condensed for $\lambda = 1.542 \text{ \AA}$ to the form

$$\langle \eta^2 \rangle = \frac{60}{da} \tilde{Q}_n(m) \quad (28)$$

$\tilde{Q}_n(m)$ is merely the absolute smeared invariant and is experimentally more convenient to work with than its desmeared analog. This statement needs qualification and the reasons are given below:

1. There exist more than one unique technique by which desmearing is done as will be elaborated in Appendix II, and as yet it is difficult to discriminate amongst them regarding quality and ambiguities. Thus, different techniques could potentially give relatively different results and this can be avoided by processing smeared data which is not only straightforward but for which an equally exact theoretical framework exists.
2. Desmearing, again depending on the method used, is sensitive to errors in the experimental data and thus involves a certain degree of curve smoothening which should be considered also. Quantitative x-ray data due to its statistical nature, always has some statistical-noise in it, especially in the case of SAXS.

For an ideal system of two phases, each being uniform and isotropic in its electron density and separated by sharp boundaries^{83,84,184} (see Appendix III for derivation)

$$\langle \eta^2 \rangle = (\rho_1 - \rho_2)^2 \phi_1 \phi_2 \quad (29)$$

where ρ = electron density of the phase

and ϕ = volume fraction of the phase.

If three pure phases coexist, one can analogously write¹⁸⁵

$$\langle \eta^2 \rangle = (\rho_1 - \rho_2)^2 \phi_1 \phi_2 + (\rho_2 - \rho_3)^2 \phi_2 \phi_3 + (\rho_3 - \rho_1)^2 \phi_3 \phi_1 \quad (30)$$

By matching the experimental and theoretical scattering powers, one can thus test the validity of an assumed model which, as was mentioned earlier, is necessary to interpret SAXS data. In the estimation of the theoretical value of $\langle \eta^2 \rangle$ enough independent information about the volume fractions and the densities of the phases is necessary. If only ϕ_1 is known since $\phi_1 + \phi_2 = 1$, $(\rho_1 - \rho_2)^2$ can be estimated and ρ_1, ρ_2 cannot be resolved by SAXS alone. Also, due to the Babinet principle of reciprocity in optics⁸⁴ one cannot identify which is the dispersed phase and which is the continuous one as the same value of $\langle \eta^2 \rangle$ is obtained by the interchanging of phases. A third ambiguity is with regards to the shape and size of the particles as two systems can be "scattering equivalent" and yet have different morphologies.

Porod's law. According to Porod⁸⁴ for an ideal two phase system, i.e., phases with uniform densities separated by sharp boundaries, the scattered intensity should fall off as m^{-3} if it is smeared (slit-collimated) and m^{-4} if it is desmeared (pin-hole collimated) in the tail end of the scattering curve. This important and general principle is known as POROD's LAW and written as:

$$\tilde{I}(m) = k_1 / m^3 \quad (31)$$

where k_1 is a constant. This is experimentally verifiable most readily for granular systems but for platelike particles (e.g., lamellae), conformance to the law recedes into the extreme end of the tail of the curve where the intensity is weak and commonly distorted by other background factors causing deviations.¹⁸⁶

The estimation of the invariant requires experimental data at both very small and large angles. The former is difficult due to the incident beam itself and can be circumvented by a linear extrapolation.¹⁸⁴ The latter is also difficult because of very low intensities and consequently poor counting statistics. However, the constant term k_1 can be used to synthesize the curve at large angles and get a reasonable overlap with the original experimental one.

For the ideal two phase model, the estimation of the invariant enables the calculation of another interesting parameter called the "internal surface" by Porod.⁸⁴

$$\frac{O}{V} = \frac{\text{area of phase interface}}{\text{volume of the system}} = \frac{8\pi}{a\lambda} \phi_1 \phi_2 \frac{k_1}{\tilde{Q}} \text{ \AA}^{-1} \quad (32)$$

All the terms have been already defined. According to Kratky,¹⁸⁴ the "internal surface" is a correct measure of the fineness of a system's heterogeneity.

The above analysis, true to Porod's style, is of a very general nature and can be applied to a system of random or ordered geometry as long as the phases are homogeneous and the phase boundary is sharp. For

well ordered systems such as the lamellae within a spherulite, as will be discussed later, the "model approach" or the "correlation function" approach can be applied. For a completely random distribution of phases such as in Fig. 3, the "correlation function" approach is the only meaningful one.

Debye⁹⁶ and Porod^{84,85} working independently, proposed a very powerful theoretical framework to describe dense two-phase systems with a chaotic distribution of phases much like a piece of sponge with cavities.

The scattering of such a system can be described by the Debye-Bueche theory⁹⁵ for spherically symmetric systems as:

$$I(h) = K_1 \langle \eta^2 \rangle \int_0^{\infty} \gamma(r) \frac{\sin hr}{hr} r^2 dr \quad (33)$$

where K_1 = constant

$\langle \eta^2 \rangle$ = scattering power

$h = (4\pi/\lambda) \sin \theta$

$\gamma(r)$ = correlation function

r = a scalar quantity

$\gamma(r)$ is further defined as

$$\gamma(r) = \frac{\langle \eta(x) \cdot \eta(x+r) \rangle_r}{\langle \eta^2 \rangle} \quad (34)$$

where, as mentioned before, $\eta(x)$ represents the fluctuation in electron density at a point x within the material and the symbol $\langle \rangle_r$ designates

an average over all pairs of volume elements separated by a constant scalar distance, r . $\gamma(r)$ decays from unity at $r = 0$ toward zero as r approaches infinity in a manner that is characteristic of the structure of the system.

$$\text{for } r = 0 \quad \gamma(r) = \frac{\langle \eta^2(x) \rangle}{\langle \eta^2 \rangle} = 1 \quad (\text{complete correlation})$$

$$\text{for } r = \infty \quad \gamma(r) = \frac{0}{\langle \eta^2 \rangle} = 0 \quad (\text{no correlation})$$

The correlation function $\gamma(r)$ also called the "characteristic" by Porod may be obtained from Fourier inversion of $I(h)$. For specific model systems $\gamma(r)$ can be calculated theoretically, e.g., for a dilute dispersion of spheres of radius R ,

$$\gamma(r) = 1 - \frac{3}{4} \left(\frac{r}{R}\right) + \frac{1}{16} \left(\frac{r}{R}\right)^3 \quad (35)$$

and serves as a measure of the size of the sphere.¹⁸⁷ For systems with no clearly defined structure, $\gamma(r)$ often decreases monotonically with r (Fig. 4) and can often be simply represented by an empirical equation such as (95)

$$\gamma(r) = \exp(-r/\bar{\ell}_c) \quad (36)$$

where $\bar{\ell}_c$ is defined as the "correlation distance" and is a measure of the size of the heterogeneity. For dilute discrete particles, $\bar{\ell}_c$ is related to the particle size, e.g., for spheres of radius R , $\bar{\ell}_c \approx (4R/3)$. For more concentrated systems, $\bar{\ell}_c$ cannot be easily related to any structural unit as it depends on both inter and intra particle distances. It thus

becomes difficult to interpret $\bar{\ell}_c$ directly in a physical sense. It could be considered as an average wavelength of the fluctuation $\eta(x)$, with $\langle \eta^2 \rangle$ as the average squared amplitude (Fig. 5).

On substituting $\gamma(r) = \exp(-r/\bar{\ell}_c)$ in equation (33), one gets

$$I(h) = K_2 \langle \eta^2 \rangle (\bar{\ell}_c)^3 / [1 + h^2 (\bar{\ell}_c)^2]^2 \quad (37)$$

where K_2 is another constant term. On rearranging, this gives:

$$I(h)^{-1/2} = [1 + h^2 (\bar{\ell}_c)^2] / [K_2 \langle \eta^2 \rangle (\bar{\ell}_c)^3]^{1/2} \quad (38)$$

showing that a plot of $I(h)^{-1/2}$ against h^2 should give a straight line with a slope to intercept ratio of $(\bar{\ell}_c)^2$.

For SAXS the angles are small enough to validate the equivalence $\sin \theta = \theta$. Thus

$$h = \frac{4\pi}{\lambda} \sin \theta = \frac{4\pi\theta}{\lambda} \quad (39)$$

which when substituted in equation (38) gives

$$\begin{aligned} I(\theta)^{-1/2} &= [K_2 \langle \eta^2 \rangle (\bar{\ell}_c)^3]^{-1/2} \left[1 + \frac{16\pi^2 \theta^2}{\lambda^2} (\bar{\ell}_c)^2 \right] \\ &= K_2 [\langle \eta^2 \rangle (\bar{\ell}_c)^3]^{-1/2} + [K_2 \langle \eta^2 \rangle (\bar{\ell}_c)^3]^{-1/2} \frac{16\pi^2}{\lambda^2} (\bar{\ell}_c)^2 \theta^2 \end{aligned} \quad (40)$$

Thus if a plot of $I(\theta)^{-1/2}$ against θ^2 is made,⁹⁶ the ratio

$$\frac{\text{SLOPE}}{\text{INTERCEPT}} = \frac{16\pi^2}{\lambda^2} (\bar{\ell}_c)^2 \quad (41)$$

which gives

$$\bar{\ell}_c = \frac{\lambda}{2\pi} \sqrt{\frac{\text{SLOPE}}{\text{INTERCEPT}}} \quad (42)$$

Also conformance to such a straight line is an indication of the appropriateness of the empirical form (eqn. (36)) used. Other assumed forms of $\gamma(r)$ such as gaussian, or those with higher order terms have also been proposed¹⁸⁸ and alternative testing procedures may be applied.

It may be added that $\bar{\ell}_c$ is the integral breadth of $\gamma(r)$. Porod and associates refer to $\bar{\ell}_c$ as the "reduced inhomogeneity length".

Debye, Anderson and Brumberger⁹⁶ have also shown that for an ideal two phase model:

$$\frac{O}{V} = \frac{4\phi_1\phi_2}{\bar{\ell}_c} \quad (43)$$

where all the terms have been previously defined.

Somewhat more easy to comprehend are what Porod has termed the "average chord lengths" or "transversals", $\bar{\ell}_1$ and $\bar{\ell}_2$.^{184,185}

$$\bar{\ell}_1 = \frac{4\phi_1}{O/V} \quad \text{and} \quad \bar{\ell}_2 = \frac{4\phi_2}{O/V} \quad (44)$$

If one can visualize a randomly arranged morphology to be pierced in all random directions by arrows, as shown in Fig. 3, then the mean length of all the line segments intercepted by each phase is represented by the "transversals".

Combining equations (43) and (44) it is easy to see that:

$$\frac{1}{\bar{\ell}_c} = \frac{1}{\bar{\ell}_1} + \frac{1}{\bar{\ell}_2} \quad (45)$$

$$\text{and } \bar{\ell}_1 = \frac{\bar{\ell}_c}{\phi_2} \quad \text{and} \quad \bar{\ell}_2 = \frac{\bar{\ell}_c}{\phi_1} \quad (45)$$

Thus, as was said before, $\bar{\ell}_c$ is a weighted average of inter and intra phase dimensions $\bar{\ell}_1$ and $\bar{\ell}_2$.

Deviations from Porod's Law. If Porod's law is obeyed as expressed in equation (31), then $m^3 \cdot \tilde{I}(m)$ should be a constant and independent of the scattering angle. Luzzati and coworkers¹⁸⁹ found such conformance in the case of dilute silane solutions of lysozyme, but no known cases for dense systems exists. The reasons for non-conformity are varied and lumped under the common name of "deviations".

Basically two main kinds of deviations could occur viz., 1) inhomogeneity of electron density within the phases and 2) diffuse boundaries between the phases across which the electron density varies continuously and not abruptly. Superimposed on these, incoherent thermal fluctuations^{135,190} across the entire system should also be included. All these are molecular to atomic effects and it is therefore not surprising that they affect the tail intensities of the scattering curve which is precisely the domain of applicability of Porod's law.

Inhomogeneity within the phases can be due to trapped impurities in general; crystalline imperfections such as kinks, line and point defects, etc. (Fig. 6)¹⁹¹ nonuniformity of the amorphous phase; interpenetration of each phase by chemical constituents of the other as can happen for frozen-in morphologies in blends,^{141,142} etc. The degree to which phases are inhomogeneous is difficult to determine experimentally in a multiphase system in the solid state.

On the other hand, experimental evidence^{142,192} and some theoretical treatments^{143-145,193} both favor the existence of a finite transition zone between phases across which the density varies continuously. Electron microscopy indicates that in a semicrystalline system the transition zone thickness is a function of the system's history and for blends it is more complex. Helfand and Tagami^{143,144} and Meier^{145,194} estimate thicknesses of the order of 10 to 20 Å for blends such as those of PS/PMMA commonly classified as incompatible.⁵³

Luzzati and coworkers¹⁸⁹ were the first to suggest that all kinds of deviations from the ideal two phase model would contribute a constant excess intensity due to incoherent scattering and represented this by k_2 . On combining this with Porod's law, one can write:

$$\tilde{I}(m) = \frac{k_1}{m^3} + k_2 \quad (47)$$

which on rearranging gives:

$$m^3 \cdot \tilde{I}(m) = k_1 + k_2 m^3 \quad (48)$$

According to this a plot of $m^3 \cdot \tilde{I}(m)$ against m^3 should result in a straight line of slope k_2 and intercept k_1 . Thus the excess intensity k_2 could be estimated and consequently the corrected intensity $\tilde{I}(m)$, after subtracting k_2 , i.e., $(\tilde{I}(m) - k_2)$ be used for estimating a more precise value of the invariants.

Perret and Ruland¹⁹⁵ from their SAXS study on solution precipitated and bulk-crystallized polyethylene, have shown that if after correcting for k_2 , the plot of $\tilde{I}(m) \cdot m^3$ vs m^3 is linear at large angles, then the

perturbation due to a transition zone is negligible or that the interface can be considered to be relatively sharp. Kim¹⁹⁶ has substantiated this line of reasoning in his study on the SAXS of S-B-S block copolymers and so have Roe and Gieniewski¹⁹⁷ on melt crystallized chlorinated polyethylene.

In another publication, using the convolution procedure of Hosemann and Bagchi,⁹⁰ Ruland¹³⁵ has shown how the effects due to density deviations may be separated from those of a transition zone using appropriate intensity plots. According to Ruland,¹³⁵ when density fluctuations predominate, the Luzzati method¹⁸⁹ is best suited, but when the phase boundary is diffuse equation (47) is modified to

$$\tilde{I}(m) = \frac{k_1}{m^3} + \frac{k_2'}{m} \quad (49)$$

On rearranging it gives:

$$\tilde{I}(m) \cdot m^3 = k_1 + k_2' m^2 \quad (50)$$

which indicates that for the case of diffuse boundaries a plot of $\tilde{I}(m) \cdot m^3$ against m^2 rather than m^3 should give a straight line. It must be pointed out that these discrimination methods need extremely accurate data in order to resolve such differences within experimental error and systems with both kinds of deviations cannot be handled easily. According to him, the former produce positive deviations while the latter give rise to negative deviations and partial to total compensation is conceivable in exceptional cases. In this respect, the Bonart method as explained later is more elegant and enlightening.

Vonk¹³⁹ has proposed another method to estimate the width of the transition zone by estimating the slope of a one dimensional correlation function at the origin, i.e., $(d\gamma(r)/dr)r = 0$ (as originally proposed by Debye et al.⁹⁶ for estimation of the "internal surface") and combining this with other expressions. Vonk's results for the transition zone are in good agreement with those calculated by Ruland's¹³⁵ method and in accord with electron microscopy evidence the solvent-crystallized samples show sharper boundaries than melt-crystallized samples.

Blundell¹³⁷ and Strobl¹³⁸ have also considered the effect of a transition zone in their efforts to test the validity of Porod's law for semi-crystalline systems.

Stein and Khambatta¹⁴⁰ have proposed a more simplistic but very general theory for estimating the volume fraction of material in the transition zone with a linear density profile from an estimation of the scattering power of the system. If the theory is applied to an assumed model, the fractional thickness of the transition zone can also be estimated. The theory is derived in the following section but a few words about a very elegant method recently proposed by Bonart¹⁴¹ are in order.

Bonart's Theory.^{141,142} According to Bonart it is not enough to correct the intensity (smeared) for a constant background k_2 as was discussed previously and check for conformation for a linear $\tilde{I}(m) m^3$ vs m^3 plot to estimate the correct parameters. He has shown experimentally that intercept values (k_1) from such linear plots are very small in magnitude and give unreasonable values for the "internal surface".

Referring to Fig. (7a) subtraction of k_2 cleans up the data for statistical fluctuations within the phases resulting in $\langle \eta^2 \rangle'$ as shown in

Fig. (7b) and further reduction of the system to eliminate the transition zone results in a "comparison system" which, according to Bonart, can then be compared to the ideal two phase system of Porod. He proposes that Porod's Law be further modified by a damping factor $D^2(m)$ to account for deviations caused by the transition zone which can be assumed to be Gaussian. Thus

$$\tilde{I}(m) \xrightarrow{m \rightarrow \infty} D^2(m) \frac{k_1}{m^3} + k_2 \quad (51)$$

and estimation of $D^2(m)$ (Appendix IV) should give the correspondingly corrected invariant $\tilde{Q}_B(m)$ as

$$\tilde{Q}_B(m) = \int_0^{\infty} \frac{(I(m) - k_2)}{D^2(m)} m \, dm \quad (52)$$

$\tilde{Q}_B(m)$ in turn is used to estimate the scattering power of the "comparison system" as shown in Fig. (7c) and denoted by $\langle \eta^2 \rangle'$. According to Bonart, this should result in more realistic values of the internal or specific surface (O/V).

$$\left(\frac{O}{V}\right)_B = \frac{8\pi}{\lambda a} \phi_1 \phi_2 \frac{k_1}{\tilde{Q}_B(m)} \quad (53)$$

As a result of his analysis, one can also estimate the width of the transition zone (B) and the fraction of sharp boundaries (Appendix IV)

$$B = 0.605 (\lambda a) \left[\frac{\Delta \log \{m^3 [\tilde{I}(m) - k_2] - k_{\infty}\}}{\Delta m^2} \right]^{1/2} \quad (54)$$

where k_∞ is the intercept of $\tilde{I}(m) \cdot m^3$ plot (i.e., same as k_1) but for $m \rightarrow \infty$.

Stein-Khambatta theory.¹⁴⁰ Consider two homogeneous phases to be separated by a gradual phase boundary across which a linear electron density gradient exists as shown in Fig. 8, and represented by

$$\rho_3(x) = \rho_1 + (\rho_2 - \rho_1) (x/\epsilon) \quad (55)$$

where ϵ is the "thickness of the boundary". If ϕ_1 and ϕ_2 are the initial volume fractions of the two phases (i.e., components) mixed together and ϕ_3 is the volume fraction occupied by the boundary regions, then for a linear gradient, the remaining parts of the two components occurring as pure phases are

$$\phi_1' = \phi_1 - (\phi_3/2) \quad (56)$$

and

$$* \quad \phi_2' = \phi_2 - (\phi_3/2) \quad (57)$$

as shown in Fig. 9. It is assumed that the dispersed phase (phase 2) is sufficiently dilute so that overlap of the boundary regions may be neglected.

In this case the average electron density of the system is given, as in the sharp boundary case as

$$\bar{\rho} = \phi_1 \rho_1 + \phi_2 \rho_2 \quad (58)$$

* since $\phi_1' + \phi_2' + \phi_3 = \phi_1 + \phi_2 = 1$

while the value of $\langle \eta^2 \rangle$ is given by

$$\langle \eta^2 \rangle = \phi_1' (\rho_1 - \bar{\rho})^2 + \phi_2' (\rho_2 - \bar{\rho})^2 = \phi_3 \overline{[\rho_3(x) - \bar{\rho}]^2} \quad (59)$$

Using equations (55) and (58)

$$\begin{aligned} \rho_3(x) - \bar{\rho} &= \rho_1 + (\rho_2 - \rho_1) (x/\epsilon) - \phi_1 \rho_1 - \phi_2 \rho_2 \\ &= (\rho_2 - \rho_1) [(x/\epsilon) - \phi_2] \end{aligned} \quad (60)$$

Then

$$\begin{aligned} \overline{[\rho_3(x) - \bar{\rho}]^2} &= \frac{1}{\epsilon} \int_0^\epsilon [\rho_3(x) - \bar{\rho}]^2 dx \\ &= \frac{(\rho_2 - \rho_1)^2}{\epsilon} \int_0^\epsilon [(x/\epsilon) - \phi_2]^2 dx \\ &= (\rho_2 - \rho_1)^2 \left[\frac{1}{3} - \phi_1 \phi_2 \right] \end{aligned} \quad (61)$$

Upon resubstituting into equation (59) one gets

$$\begin{aligned} \langle \eta^2 \rangle &= (\rho_2 - \rho_1)^2 \left\{ \phi_1 \phi_2 - \frac{\phi_3 (\phi_1^2 + \phi_2^2)}{2} + \phi_3 \left[\frac{1}{3} - \phi_1 \phi_2 \right] \right\} \\ &= (\rho_2 - \rho_1)^2 \left\{ \phi_1 \phi_2 - \frac{\phi_3}{2} [(\phi_1 + \phi_2)^2 - \frac{1}{3}] \right\} \\ &= (\rho_2 - \rho_1)^2 \left[\phi_1 \phi_2 - \frac{\phi_3}{6} \right] \end{aligned} \quad (62)$$

Thus, the effect of a finite transition zone is to lower the scattering power of the system by one-sixth of its volume fraction.

Equation (62) is consistent with the ideal two phase model since for $\phi_3 = 0$, $\langle \eta^2 \rangle = (\rho_2 - \rho_1)^2 \phi_1 \phi_2$ which is equation (29).

Also it is important to mention that using an altogether different approach, Vonk¹³⁹ derived an expression identical to equation (62) in

terms of the internal or specific surface O/V and the thickness of the transition zone ϵ . According to Vonk¹³⁹

$$\langle \eta^2 \rangle = (\rho_2 - \rho_1)^2 \left[\phi_1 \phi_2 - \frac{\epsilon(O/V)}{6} \right] \quad (63)$$

$\epsilon(O/V)$ is the volume fraction of the transition zone. An equivalent expression was also proposed by Blundell.¹³⁷

The result of equation (62) is general and independent of the sizes and the distribution of the dispersed phases so long as the density gradient is linear.

In the sharp boundary case $\langle \eta^2 \rangle$ will be symmetrical in ϕ_1 and ϕ_2 and pass through a maximum when $\phi_1 = \phi_2 = 0.5$. In the diffuse boundary case, the symmetry is lost. Also as ϕ_2 approaches 0.5, the assumption of non-overlap of boundaries becomes less valid and phase inversion is likely to occur. Then equation (62) becomes a poor approximation.

If the application of equation (62) is to be more specific, it requires the assumption of some kind of a model which can relate ϕ_3 to ϕ_1 and ϕ_2 in terms of structural parameters. The simplest case is that of spherical domains of phase 2 in a continuous medium of phase 1, with a number density of N spheres/cm³ each of radius R . Then

$$\phi_2' = N \cdot \left(\frac{4}{3} \pi R^3 \right) \quad (64)$$

and

$$\begin{aligned} \phi_3 &= N \cdot \left(\frac{4\pi}{3} \right) [(R + \epsilon)^3 - R^3] \\ &= N \frac{4\pi}{3} [\epsilon^3 + 3R\epsilon^2 + 3R^2\epsilon] \end{aligned} \quad (65)$$

If the boundary region is thin as compared to the radius of the sphere, i.e., $\epsilon \ll R$, then the first and second terms can be neglected and

$$\phi_3 \approx N \cdot 4\pi R^2 \epsilon \approx (3\epsilon/R) \phi_2' \quad (66)$$

This can be written more conveniently as

$$\phi_3 = \frac{3(\epsilon/R)}{1 + (3\epsilon/2R)} \phi_2 \quad (67)$$

which, on substituting into equation (12), gives

$$\begin{aligned} \langle \eta^2 \rangle &= (\rho_2 - \rho_1)^2 \left[\phi_1 \phi_2 - \frac{1}{6} \frac{3(\epsilon/R)}{1 + (3\epsilon/2R)} \phi_2 \right] \\ &= (\rho_2 - \rho_1)^2 \left[(1 - \phi_2) \phi_2 - \left(\frac{\epsilon/2R}{1 + 3\epsilon/2R} \right) \phi_2 \right] \\ &= (\rho_2 - \rho_1)^2 \left[\phi_2 - \phi_2^2 - \left(\frac{\epsilon/2R}{1 + 3\epsilon/2R} \right) \phi_2 \right] \end{aligned} \quad (68)$$

Thus

$$\frac{K_2 \langle \eta^2 \rangle}{\phi_2} = K_2 (\rho_2 - \rho_1)^2 \left\{ \left[1 - \left(\frac{\epsilon/2R}{1 + (3\epsilon/2R)} \right) \right] - \phi_2 \right\} \quad (69)$$

where $K_2 \langle \eta^2 \rangle$ can be obtained from the intercept of the Debye-Bueche plot according to equation (40). For the case where the fractional thickness $f = \epsilon/R$ is independent of the composition of the system, a plot of

$\frac{K_2 \langle \eta^2 \rangle}{\phi_2}$ versus the volume fraction of the dispersed phase ϕ_2 , should

give a straight line of negative slope with a ratio of intercept to slope denoted by δ as

$$\begin{aligned}\delta &= \left[\frac{(\epsilon/2R)}{1 + (3\epsilon/2R)} - 1 \right] \\ &= \left[\frac{(f/2)}{1 + (3f/2)} - 1 \right]\end{aligned}\tag{70}$$

On rearranging, we have

$$f = \frac{2(1 + \delta)}{1 - 3(1 + \delta)}\tag{71}$$

Thus, if f varies with ϕ_2 the above plot will not conform to a straight line. In such a case, curves could be fitted using alternate hypotheses such as constancy of ϵ , etc. and R could be calculated from \bar{l}_c through an assumed model.

Tsvankin Model. To explain small-angle x-ray scattering of semi-crystalline polymers, Tsvankin¹³¹ proposed a microfibril (disordered infinite one dimensional lattice) consisting of alternating crystalline and amorphous layers as shown in Fig. (10). The amorphous thicknesses obey an exponential distribution (most probable) function while the crystalline thickness distribution is rectangular and symmetric. The choice of the exponential form was based on the earlier work of Zernicke and Prins¹⁰⁴ and the rectangular form was assumed for mathematical convenience. Tsvankin also included in his model a transition zone of thickness δ^* over which the electron density varied linearly from the amorphous to the crystalline region. Such a transition zone was superimposed on each end of a crystallite of thickness a^{**} , resulting in a trapezoidal density profile along the lattice. Fig. (10).

* The δ parameter of Tsvankin has the same meaning as ϵ (Stein-Khambatta), B (Bonart), E (Vonk, Ruland), etc.

** a is not to be confused with the sample to detector distance used to define the reduced angle m .

The attractiveness of this particular model, or any system in which the thickness distribution of one phase is symmetric and that of the other is asymmetric, is that for any set of values for the symmetric width parameter and the transition zone thickness, both the width of the scattering peak (a measure of the total disorder) and the position of the scattering maximum (a measure of the asymmetry of the overall distribution) are uniquely related to the crystallinity of the sample. Thus, one only need measure the reduced half-width of the peak in addition to the scattering peak angle to obtain the true long period as well as the average thickness of both the crystalline and amorphous phases.¹²⁷

In general, the diffracted intensity from a system of N crystals of different lengths (i.e., with different structure amplitudes F , where F is the Fourier transform of the electron density distribution within a crystal) is given by

$$I \propto N (|\bar{F}^2| - |\bar{F}|^2) + |\bar{F}|^2 (N + \sum_{i \neq k}^N \sum \exp \{iS \cdot z_{ik}\}) \quad (72)$$

where $|S| = 4\pi \sin\theta/\lambda$ is the diffraction vector and z_{ik} is the vector from the center of the i^{th} crystal to that of the k^{th} crystal.

The first term $(|\bar{F}^2| - |\bar{F}|^2)$ arises from differences in the scattering power among individual crystals and was assumed to be constant by Tsvankin and neglected in his analysis. Buchanan¹³³ showed that Tsvankin's assumption was in error and that the continuous scattering from the assembly of crystals must be taken into account. In doing so, he modified Tsvankin's expressions for $|\bar{F}^2|$ and $|\bar{F}|^2$ to those more suited to his analysis.

The general expression for F as given by Buchanan is

$$F = \int_0^{\epsilon x} (z/\delta) \exp \{i y z / l\} dz + \int_{\epsilon x}^{(1-\epsilon)x} \exp \{i y z / l\} dz + \int_{(1-\epsilon)x}^x [(a - z)/\delta] \exp \{i y z / l\} dz \quad (73)$$

where $\epsilon = \delta/x$ is a measure of the sharpness of the transition zone

(Fig. 10)

$$y = S\ell = 2\pi\ell \sin 2\theta/\lambda$$

ℓ = mean amorphous length

a = mean crystallite length with limits of $a \pm \Delta$

c = long period = $\ell + a$

z is the direction perpendicular to the alternating layers.

$$\bar{F} = \frac{1}{2\Delta} \int_{a-\Delta}^{a+\Delta} F(x) dx \quad (74)$$

$$|\bar{F}|^2 = |\bar{F}| \cdot |\bar{F}^*| \quad (75)$$

$$\text{also } F^2 = F \cdot F^* \quad (76)$$

$$\text{and } |\bar{F}^2| = \frac{1}{2\Delta} \int_{a-\Delta}^{a+\Delta} F^2(x) dx \quad (77)$$

The expression for $|\bar{F}|^2$ and $|\bar{F}^2|$ as obtained by Buchanan, are

given below:

$$\begin{aligned}
|\bar{F}|^2 = & \frac{a^2}{\varepsilon^2(\alpha y)^4} \left\{ \left[\frac{\sin(1 - \varepsilon)\beta y}{(1 - \varepsilon)\beta y} \cos(1 - \varepsilon)\alpha y + \frac{\sin\varepsilon\beta y}{\varepsilon\beta y} \cos\varepsilon\alpha y \right. \right. \\
& - \left. \frac{\sin\beta y}{\beta y} \cos\alpha y - 1 \right]^2 + \left[\frac{\sin(1 - \varepsilon)\beta y}{(1 - \varepsilon)\beta y} \sin(1 - \varepsilon)\alpha y + \frac{\sin\varepsilon\beta y}{\varepsilon\beta y} \sin\varepsilon\alpha y \right. \\
& \left. \left. - \frac{\sin\beta y}{\beta y} \sin\alpha y \right]^2 \right\} \quad (78)
\end{aligned}$$

$$\begin{aligned}
|\bar{F}^2| = & \frac{\alpha^2}{\varepsilon^2(\alpha y)^4} \left[4 + 2 \frac{\sin(1 - 2\varepsilon)\beta y}{(1 - 2\varepsilon)\beta y} \cos(1 - 2\varepsilon)\alpha y - 4 \frac{\sin(1 - \varepsilon)\beta y}{(1 - \varepsilon)\beta y} \right. \\
& \left. \times \cos(1 - \varepsilon)\alpha y - 4 \frac{\sin\varepsilon\beta y}{\varepsilon\beta y} \cos\varepsilon\alpha y + 2 \frac{\sin\beta y}{\beta y} \cos\alpha y \right] \quad (79)
\end{aligned}$$

The parameters α and β/α are defined as follows:

$\alpha = \frac{a}{\ell}$ and is a measure of the crystal packing density

$\frac{\beta}{\alpha} = \frac{\Delta}{a}$ and is a measure of the crystallite size dispersion about its mean value of a , where $\beta = \Delta/\ell$.

The second term of Tsvankin's expression describes the scattering from the lattice of crystalline and amorphous regions and is responsible for the occurrence of maxima in the scattering pattern at scattering angles other than zero.

Tsvankin showed that this second term can be represented by

$\bar{F}^2 I_1$ where

$$I_1 = (N + \sum_{i \neq k}^N \sum \exp \{iS \cdot z_{ik}\}) \quad (80)$$

$$\begin{aligned}
&= (\beta^2 y^2 + \beta^2 y^4 - \sin^2 \beta y) / (\sin^2 \beta y + \beta^2 y^2 + \beta^2 y^4 \\
&\quad - 2\beta y \cos \alpha y \sin \beta y + 2\beta y^2 \sin \alpha y \sin \beta y)
\end{aligned} \tag{81}$$

Using the above expressions, theoretical scattering curves can thus be computed¹³³ as functions of y for variations of parameters α , β/α and ϵ . From these theoretical curves, "calibration curves" are established so as to facilitate comparison of experimental SAXS curves with the theoretically predicted ones, an example of which is shown in Fig. 11. For this, a priori values of ϵ and β/α must be chosen. The curves are not very sensitive to the choice of ϵ the transition zone sharpness as long as $\epsilon > 0$ and electron microscopy work indicates $\epsilon = 0.2$ to be a reasonable choice. β/α on the other hand is varied from 0.2 to 0.5 which indicates a 20% to 50% fluctuation in the crystallite size thickness and is reasonable for semi-crystalline polymers from WAXD and electron microscopy experiments.¹⁹⁸⁻²⁰⁰ The final choice is generally arbitrary.¹³³

The details are available in Buchanan's paper but a brief outline of the procedure to estimate the true long period and related parameters is given in Appendix (V).

The Buchanan modified Tsvankin analysis is by no means the last word in SAXS analysis of semi-crystalline polymers and admittedly has its deficiencies.^{127,128} Nevertheless, it provides a deeper insight into the system's morphology than is gotten from a superficial application of Bragg's law to the intensity maxima. It is especially useful and convenient to follow a trend on a routine basis and is amongst the most direct method available. A simple application of the Bragg's law to the

first maximum is both hazardous^{83,84} and wasteful of all other information in the scattering envelope.

An alternate method is that proposed by Vonk and Kortleve^{122,123} on a model similar to Tsvankin's but without a transition zone. Instead of a rectangular crystal-length distribution, they assume identical assymetric log normal distributions for both phases again on grounds of mathematical tractability. The Vonk method involves Fourier transformation of the experimental curve to obtain a one dimensional correlation function which is compared with a correlation function obtained by the self-convolution of a theoretical model. The two are then compared in terms of model parameters to obtain morphological information. According to Buchanan,¹³³ in the case of polyethylene the two methods yield substantial equivalent results.

A third approach is that of Hosemann⁹⁰ using paracrystallinity theory and various symmetric and assymetric distribution functions as proposed, e.g., by Rheinhold et al.¹²⁹ This has been reviewed in detail by Crist.^{127,128} Blundell^{130,137} has carried out calculations for Gaussian distribution functions of an alternating layer model and also tested the effect of a transition zone. In fact, there is no end to such exercise as semi-crystalline polymers may never really be possible to interpret by any one kind of unique model due to the statistical nature of their morphologies. This points to an important truth in the interpretation of SAXS data viz. it must be used in conjunction with data obtained from other independent techniques in order to interpret its results in the most meaningful manner.

Small Angle Light-Scattering

It was mentioned in Chapter II that the general theoretical framework for SALS was pioneered by Debye and Bueche⁹⁵ and generalized later even more by Goldstein and Michalik.¹⁵² In the theoretical section on SAXS, the work of Debye^{95,96} was again elaborated and similarities were drawn with the general contributions of Porod.^{84,85} This is for the very simple reason that in the classical sense, the phenomena of SALS and SAXS are similar though not alike. Whereas SAXS is sensitive to differences in electron density, SALS is in general responsive to differences in refractive index which are due to differences in densities as well as anisotropy. Of course, since the wavelengths used are different by orders of magnitude, so are the dimensions of the heterogeneities investigated. However, high resolution SAXS experiments could potentially be made to overlap into the range of SALS studies.

The SALS of semi-crystalline polymers possessing spherulitic morphology has largely been pioneered by Stein and coworkers¹⁴⁷⁻¹⁴⁹ in this laboratory and extended to polymers with other kinds of morphologies. The first attempts were photographic, using both H_v and V_v modes where H_v refers to vertically polarized light that is horizontally analyzed and V_v to vertically polarized light that is vertically analyzed. The vertical direction is arbitrary for undeformed isotropic systems, but parallel to the stretching direction for oriented samples. Thus, for unoriented systems, the terms H_v and V_v simply denote cross and parallel polarizations.

The scattered intensities for three-dimensional isolated spherulites in the H_v and V_v modes respectively are:

$$I_{H_v} = AV^2 \left(\frac{3}{U}\right)^2 [(\alpha_t - \alpha_r) \cos^2\left(\frac{\theta}{2}\right) \sin\mu \cos\mu (4 \sin U - U \cos U - 3 \text{Si}U)]^2 \quad (82)$$

and

$$I_{V_v} = AV^2 \left(\frac{3}{U}\right)^2 [(\alpha_t - \alpha_s)(2 \sin U - U \cos U - \text{Si}U) + (\alpha_r - \alpha_s)(\text{Si}U - \sin U) - (\alpha_t - \alpha_r) \cos^2\left(\frac{\theta}{2}\right) \cos\mu (4 \sin U - U \sin U - 3 \text{Si}U)]^2 \quad (83)$$

where the terms are defined below:

A = constant of proportionality

V = volume of the spherulite

U = $(4\pi R_s / \lambda) \sin(\theta/2)$

R_s = radius of the spherulite

λ = wavelength of light in the scattering medium

θ = scattering angle (Fig. 12) (also in the scattering medium)

μ = azimuthal angle (Fig. 12)

α_t = tangential polarizability of the spherulite

α_r = radial polarizability of the spherulite

α_s = polarizability of the medium surrounding the spherulite

$$\text{Si} = \int_0^U (\sin x)/x \, dx$$

Photographically, spherulitic samples give a four-leaf clover pattern in the H_v mode and a dumbell shaped pattern in the V_v mode, as shown in Fig. 21. The above equations could give qualitative agreement with experimental results but quantitative agreement was lacking. For

example, the shape of the theoretical patterns were similar to the ones seen photographically, but for I_{H_v} the theory predicted zero intensities at $\theta = 0^\circ$ and a rapid fall off at higher angles, whereas photometric measurements give non-zero intensities at $\theta = 0^\circ$ and excess intensity at higher angles.

The discrepancy is believed to lie in the idealistic assumptions of the theoretical model which does not duplicate the real situation and these will be discussed shortly. Nevertheless, it is instructive to compare equations (82) and (83) qualitatively to gain some insight into their predictions.

The assumptions of the Stein-Rhodes model are that the spherulites are isolated, homogeneous, three-dimensional, anisotropic spheres with no disorder in the orientation of the optic axis that lies at fixed angles to the radius of the spherulite.

The equations show that I_{H_v} is proportional to $(\alpha_t - \alpha_r)^2$, i.e., the anisotropy of the spherulite, while I_{V_v} is in addition also to $(\alpha_t - \alpha_s)^2, (\alpha_r - \alpha_s)^2$, i.e., to the difference in polarizabilities of the spherulite and the surrounding medium. Thus, for a volume filling case, α_s will represent the average polarizability of the spherulites but for a non volume filling case, α_s could be quite different depending on the composition of the medium. One can see therefore that in the latter case I_{V_v} will be more intense than I_{H_v} due to the higher contributions of the terms $(\alpha_t - \alpha_s)^2$ and $(\alpha_r - \alpha_s)^2$. I_{V_v} will also lose its dumbbell shaped identity, becoming a more circular pattern.

Thus a preliminary photographic check between I_{H_v} and I_{V_v} could be revealing about the volume filling aspect of the morphology for

spherulitic polymers, which can be confirmed microscopically. I_{V_v} can be used accordingly to study systems where α_s is changing with time, sample treatment, composition, etc.

For spherulites, the H_v four leaf clover pattern varies both with μ and θ . Along the θ direction, the intensity goes through a maximum, the position of which is inversely proportional to the average size of the spherulites given by the radius R . Thus, for the angle of maximum intensity, the reduced angle U can be written using equation (84) as

$$U_{\max} = \frac{4\pi R_s}{\lambda} \sin\left(\frac{\theta_{\max}}{2}\right) = 4.1 \quad (85)$$

Using this, one can get the average dimensions of the spherulites again as a function of any convenient experimental parameter such as time, temperature, composition, etc.

In reality, λ and θ are both quantities that should be measured within the medium of scattering. At small angles where $\sin \theta \approx \theta$, the angle of scattering within the medium can be corrected as θ/n where n is the refractive index of the scattering medium. Also since $\lambda = \lambda_0/n$ where λ_0 is the wavelength in vacuum, the two correlations compensate each other. So for larger spherulites, the error is negligible.

The parameter $(\alpha_t - \alpha_r)_{cr}$ which represents the anisotropy due to the crystalline part of the spherulite is the difference between the tangential and radial polarizabilities of the spherulite. α_j has units of polarizability per unit volume and is defined as

$$\alpha_j = N_s P_j \quad (86)$$

where P_j is the polarizability per segment along a particular crystallographic axis j such as a , b or c and N_s is the number of segments per unit volume. P_j can be estimated using the relation

$$P_j = \sum_i P_i = \sum_i [(b_L - b_T)_i \cos^2 \theta_i + (b_T)_i] \quad (87)$$

where P_i is the polarizability of the i^{th} bond which is oriented at an angle θ to any particular direction j and b_L and b_T represent bond polarizabilities along and normal to the bond respectively. Thus, from a knowledge of bond polarizability values and their orientation, one can estimate ρ_a , ρ_b and ρ_c along the crystallographic axes and in turn calculate $(\alpha_t - \alpha_s)_{\text{cr}}$ as shown below.

$$\alpha_t = \frac{\alpha_a + \alpha_c}{2} = N_s \frac{(P_a + P_c)}{2} \quad (88)$$

and $\alpha_r = \alpha_b = N_s P_b$

$$(\alpha_t - \alpha_r)_{\text{cr}} = N_s \left(\frac{P_a + P_c}{2} - P_b \right) \quad (89)$$

This is so because, like polyethylene, PCL has its optic axis c and its other axis a in a helicoidal twist about the b axis which is oriented in the direction of the radius. In fact, PCL and polyethylene also have quite similar unit cell structures^{201,202} except that the PCL unit cell is more anisotropic along the c direction as shown below.

	a(Å)	b(Å)	c(Å)
PCL (orthorhombic)	7.496	4.974	17.297
PE (orthorhombic)	7.400	4.930	2.534

For the bond polarizability values, those of Bunn and Daubenny²⁰³ are used even though their work on n-paraffins could include contributions due to "internal field" effects. Denbigh's²⁰⁴ values from work on gaseous molecules should be more accurate, however, the choice will be justified and numerically substantiated in Chapter V.

The implicit assumption all along has been that the anisotropy of the spherulite is determined by that of the crystalline phase only, i.e., the second and third terms in equation (90) below do not contribute appreciably to it.

$$\begin{aligned}
 (\alpha_t - \alpha_r)_{\text{spherulite}} = & X_{\text{CR}} (\alpha_t - \alpha_r)_{\text{CR}} f_{\text{CR,SP}} \\
 & + \\
 & (1 - X_{\text{CR}}) (\alpha_t - \alpha_r)_{\text{AM}} f_{\text{AM,SP}} \\
 & + \\
 & (\Delta\alpha)_F
 \end{aligned} \tag{90}$$

In the above equation X_{CR} is the volume fraction crystallinity of the spherulite and $(\Delta\alpha)_F$ is the form anisotropy due to the crystalline-amorphous boundary. For a volume filling morphology X_{CR} is the same as the overall crystallinity but otherwise it has to be accounted for in some way. More will be said about this later.

The above discussion was with regards to the I_{H_v} and I_{V_v} expressions in equations (82) and (83). However, the reconciliation of

experimental observations with scattering theory necessitates that both be expressed in "absolute units" which in light-scattering terminology is called the "Rayleigh ratio" denoted by R and defined in the next section. The Rayleigh ratio in SALS is analogous to $\langle \eta^2 \rangle$ the scattering power in SAXS.

Rayleigh ratio. The Rayleigh ratio " R " is the expression of light scattering intensities in "absolute units" and inclusive of all the factors that affect the measurement of such intensities. In the general sense, R could be defined as

$$R(\theta, \mu) = \frac{I(\theta, \mu)}{I_0} \times \frac{F_c}{V} \times k \quad (91)$$

where $I(\theta, \mu)$ = the experimentally measured intensities

I_0 = the incident beam intensity

V = scattering volume (i.e., volume irradiated)

F_c = product of all the necessary correction factors

k = instrument calibration constant

The procedure for the estimation of k has been outlined²⁰⁹ and will not be repeated here except to say that should any experimental conditions change, k will change proportionately. It is estimated using a system whose scattering power is known theoretically such as benzene, and which can also be measured experimentally.

It was remarked in the preceeding section that the assumptions in the Stein-Rhodes model were idealistic which was responsible, at least in part, for the discrepancy with experimental observations. Real

systems are often densely packed, truncated, polydisperse and imperfect in their optic axis orientation. Each of these factors affects the scattering curve in some measure and must be corrected for. The way in which they affect is explained more fully in the section on "corrections" in the next chapter.

CHAPTER IV

EXPERIMENTAL TECHNIQUES

This chapter basically deals with the setting up of sound experimental techniques for the accumulation of reproducible experimental data and their routine analysis starting with the preparation of samples and extending up to the various corrections used, to reduce the raw data to an interpretable form. At every step, the necessary details are explained with appropriate appendices and, where a multiplicity in choice exists, the particular route chosen is explained and justified. Where a choice does not exist, the limitations are pointed out.

Experimental data as obtained directly from equipment is seldom useful for direct interpretation and must be processed through a series of corrections. This is particularly true in the case of both SAXS and SALS. Each correction step has its own philosophy and influences the final result depending on its importance. Some of the corrections seem superficially trivial but must nevertheless be executed if consistency is to be maintained.

Sample Preparation

Blends can be prepared in a variety of ways and amongst the most common methods used are:⁵⁹

1. Solvent casting (if a common solvent can be found)
2. Coprecipitating with a non-solvent after codissolving

3. Melt blending by using e.g. a Brabender plasticorder
4. Freeze drying followed by solvent sublimation under vacuum
5. Copolymerizing either in blocks of each component or by grafting one component to the parent polymeric chain.

Except for the last technique, which is rather involved, the others can be used for mixing two homopolymers quite conveniently. Melt blending requires special equipment if meaningful mixing is to be achieved and coprecipitating is potentially capable of fractionation due to differences in the rate of precipitation for the blended components. For the same reason, one component could be preferentially precipitated which alters the composition of the blend and elemental analysis then becomes imperative. Freeze drying has been advocated to give essentially molecularly mixed blends as it freezes the components when the mixing is maximized. This technique is, however, cumbersome though routinely adaptable.

Solvent casting with slow evaporation of the solvent is very convenient and is known to give homogeneous films if the evaporation is done carefully. An inherent drawback of this technique is that as the solvent evaporates, the concentration of the solution changes. This must affect chain mobility as a function of time which in turn must affect the kinetics of domain formation. In fact, during the early stages of casting due to the diluteness of the solution, the mixing ought to be optimum, whereas during the final stages, having gone past the critical concentration, precipitation must dominate. If this is relatively uniform so will be the morphology.

The PCL/PVC system, as first studied by Koleske and Lundberg, was with melt-blended samples. Price and Ong used solvent cast samples followed by bulk crystallization in some instances. Due to lack of facility for melt blending, it was considered most feasible to solvent cast so as to justify comparison of final results with the crystallization studies of Ong.

Not only is the morphology of a blend sensitive to the method of preparation, but also to the history of sample preparation even for the same technique. Even though the solvent is evaporated slowly nevertheless fluctuations in room temperatures, etc., give an ill-defined history especially since one of the components, viz. PCL, shows a pronounced tendency to crystallize. Thus it was decided to follow solution casting by isothermal crystallization so that at least meaningful comparisons between various compositions could be made, by normalizing their crystallization history.

Also, in order to allow comparison of results with those of Koleske and Ong, the polymers used were identical in all respect to theirs and very kindly provided by Dr. J. Koleske of Union Carbide Corporation. Their description and molecular weights are outlined in Table I. The compositions studied were varied at intervals of 10% by weight across the entire spectrum from PCL to PVC inclusive of the pure homopolymers. The notation PCL/PVC always in percentage by weight will be used to denote the compositions and volume fractions will be specified where used.

The sample preparation procedure is outlined below sequentially.

TABLE I[†]

Molecular Weight Determined by GPC

Sample	\bar{A}_w^+	\bar{A}_n^+	\bar{A}_w/\bar{A}_n	\bar{M}_w	\bar{M}_n
PCL	1,017	570	1.94	23,600	12,200++
				25,400	13,100*
PVC	3,119	1,542	2.02	66,200	32,800++
				78,000	38,600**

+ Chain length in Angstroms based on polystyrene standards

++ Molecular weight calculated using a simplified universal calibration.

* Molecular weight based on a Q factor of 23, received from Cellomer Associates for PCL

** Molecular weight based on a Q factor of 25 for PVC

† Data of J. Ong, Table I, ref. (10).

1. Dilute solutions of 2% (WT.) concentration were made in THF with continuous stirring for at least 6 hours to ensure complete dissolution of the components. PCL is relatively easy to dissolve and the choice of THF was made due to it being classified as a good solvent for PVC. No heating of the solution was attempted.
2. Specially made pyrex petri dishes with very flat and even surfaces were used to cast the films. A predetermined amount of solution was cast each time so as to obtain films 2 to 3 mils thick on the average. This was done so as to facilitate residual solvent removal which would be relatively difficult from thick films, while thinner ones would result in surface tension forces and not be representative of bulk samples. Small-angle x-ray work in particular demands high sample purity with respect to residual solvent as well as microvoids since they contribute a spuriously high electron density "difference" with the polymers. Also, at room temperature, PVC is below its glass transition temperature which causes it to be very viscous as it forms a film and traps some of the solvent. Lastly, as shown in Table II, the optimum thicknesses of the samples rich in PVC were not as high as those rich in PCL due to their higher chlorine content.* Since a composite sandwich of several films can be made for x-ray studies, 2 to 3 mil films were considered adequate.

* This statement is further qualified in Chapter IV.

TABLE II

Optimum Thickness for SAXS for Different Compositions

Blend Composition WT. % PCL	Optimum Thickness t_m (MIL)
100	56
90	26
80	17
70	13
60	10
50	8
40	7
30	6
20	6
10	5
PVC	4

The petri dishes were covered with a finely holed Al foil and a large beaker was inverted over this assembly which was kept for several hours (overnight) inside a laboratory hood with a modest draft.

Slow evaporation gave excellent homogeneity, no bubbles, minimum shrinkage and good mechanical integrity.

3. The majority of the residual solvent was at first removed under vacuum at room temperature in excess of 48 hours until no further weight loss was noticed.
4. The samples were then isothermally crystallized by raising their temperature very slowly at approximately 5°C per hour to 70°C at ambient pressure in a large oven, and then immediately transferring them to another oven that was equilibrated at $30^{\circ}\text{C} \pm 1^{\circ}\text{C}$.
 - (i) Slow heating is necessary to avoid any microtraces of residual solvent from flashing and thereby causing voids. Also, it insures complete melting of PCL ($T_m \approx 63^{\circ}\text{C}$).
 - (ii) The T_g of PVC is approximately 85 to 90°C which, if approached or exceeded, would allow diffusion over long times and complicate the morphology. Hence 70°C was chosen as the optimum temperature.
 - (iii) The samples were kept at 70°C for 30 minutes before quenching to 30°C , to ensure complete melting of PCL.
 - (iv) All samples were transferred simultaneously so as to affect them identically.

(v) All experiments on scattering, etc., were done at room temperature which fluctuates. Hence 30°C was chosen as the temperature for isothermal crystallization so that crystallization could be done at temperatures close to ambient and the samples would yet have a well defined history. The crystallization was allowed to proceed for times in excess of five times the half times of crystallization for each composition as determined by Ong.¹⁰

For light scattering experiments it is necessary to have the samples between glass slides with continuous glass to sample interface. One way is to have the sample fused to the glass and this was done by sandwiching the sample between two coverslips and using two equilibrated silicone oil baths at $70^{\circ}\text{C} \pm 0.5^{\circ}\text{C}$ and $30^{\circ}\text{C} \pm 0.5^{\circ}\text{C}$ in a manner identical to the two ovens. The samples were slowly heated in the oven at first to 70°C , then immersed for 30 minutes in the first oil bath and immediately transferred to the other one for the necessary period of time to complete crystallization.

Small-Angle X-Ray Scattering

As mentioned in the introduction, the basic emphasis in any scattering experiment is to obtain the "scattering envelope", i.e., the variation of scattered intensity with the scattering angle. This can be done both photographically and photometrically, the former being the more qualitative of the two and more suited to a routine check rather than detailed analysis.

Photographic SAXS experiments can best be done using cameras developed by Hess and Keisig²⁰⁵ or what is commonly called the Warhus camera²⁰⁶ designed by Statton. The advantage of this technique is that it integrates the intensity with time which causes any instrumental fluctuations to affect the envelope simultaneously at all angles and since pinhole collimation can be used, the pattern is not as distorted or smeared if their diameters are kept small. Thus stability and de-smearing are circumvented. The disadvantages are many and quite serious for quantitative data accumulation, most critical of them being the extraction of numerical data with a densitometer which, if fitted with a slit shaped window on the detector, can cause smearing and ambiguity in normalizing the intensities to an absolute scale. Besides photographic SAXS experiments need exposures commonly in excess of 24 hours. All experiments in this work were done photometrically as explained below.

In the case of photometric SAXS, the pattern is step-scanned, i.e.,
the intensity is monitored at each angle before advancing to the next
angular increment. The detector thus advances in an arc on the goniometer arm and counting of the x-ray photons is done either for a fixed number of counts or a preset time interval. The angular increment is determined by the shape of the curve, i.e., the slope of the intensity profile while the time or counts is determined by counting statistics.

If there is any kind of instability in the instrument depending on whether it is random or systematic, the data will correspondingly be affected in a complex manner which in turn will distort the intensity profile. This is so because the curve will be affected differently at

different angles. Professor Kratky has developed a monitoring device which keeps track of the incident beam intensity fluctuations²⁰⁷ to circumvent this problem. In the absence of such a device, as was the case in this work, other indirect methods can be used to lessen the effect of instability although not eliminate it and this will be discussed shortly. Another drawback of the photometric method is that it is a very slow technique and this is inherent on account of low x-ray intensities on account of fine-collimation, the requirements for which are rather stringent. This can be partly compensated by having a high intensity rotating-anode x-ray source or by the novel technique of Energy Dispersive SAXS which, incidentally, also circumvents the stability requirements. However, the latter is still in an embryonic state, but the potential for its use exists. The once tedious problem of de-smearing slit-collimated data is a more routine exercise today and more will be said about this aspect later. In spite of these difficulties, photometric data is more accurate.

Apparatus. The apparatus used was a Rigaku-Denki type 2022 small-angle x-ray goniometer (schematic Fig. 14). It was adopted for automatic step scanning and data acquisition by interfacing with a PDP-8E minicomputer which was hooked to an ARS-33 teletype terminal. Initial instructions at the start of each run were given through the teletype which then printed the final data and simultaneously punched in on paper-tape throughout the run. The paper-tape data was then processed using the CDC-3600 computer at the University of Massachusetts. The schematic of the entire set up is shown in Fig. 13. The computer programs used for data reduction are given in Appendix 7.

The x-ray source was a fine focus Copper target tube of the type Ca8-F/Cu made by General Electric. The tube was operated at 12 mA and 40KV by a General Electric x-ray generator and was water cooled at a constant flow rate of 1 gal/min. using water filtered by a series of FRAM-CW1RO filters. There was no provision for regulating the water temperature. The x-ray generator was connected to a line voltage stabilizer, Stabiline Model IES9206B, which regulated the incoming line voltage to $\pm 1\%$ approximately. The goniometer table was mounted on four shock absorbing pads and weighed down by large steel blocks to minimize the effect of spurious vibrations on the alignment of the goniometer. The entire goniometer was enclosed in a fiber-glass insulated hood which maintained a more uniform temperature within it, than the ambient. The hood itself was mounted on a foam lining and had a front window for access to the equipment.

The heart of a SAXS goniometer is its collimation system. The ideal collimation system is a series of well aligned pin-holes but, as has been already discussed, it is not the most feasible for quantitative measurements. It is common practice in SAXS to use a slit-shaped beam instead and sacrifice some of the resolution for a corresponding gain in intensity. A series of fine slits are aligned as shown in Fig. 14 to produce a beam with a profile shown in Fig. 15. The alignment procedure is described in sufficient detail in the manual.²⁰⁸ For aligning the instrument, the very finest slit combination available is normally used but the choice of slit system for any particular experiment is determined by the accuracy desired and the system studied. If the information of interest is close to the incident beam then the slit width is

correspondingly reduced to obtain better resolution. Resolution is commonly defined as the full-width at half-maximum intensity (FWHM) of the incident beam profile. Table III outlines the slit combinations used and the corresponding FWHM values from the profile shown in Fig. 15.

The fabled Kratky camera is designed with essentially infinite slits (i.e., very high length to width ratios ~ 5000). The Rigaku-Denki camera uses slits of finite length, with length to width ratios ~ 100 .

One of the main disadvantages of using a slit collimated beam is that the data so obtained is smeared or distorted. It is easy to see how this comes about, if one considers a fine slit as a linear array of equally fine pin holes. Each pinhole produces a ring shaped pattern (i.e., for unoriented isotropic samples) and these patterns overlap in a complex manner thus smearing out each others details and thereby distorting the real profile. Thus the slit data has somehow to be desmeared and advantage is taken of the fact that the distorted and ideal profiles are related through a Fourier Transformation. Several numerical methods exist and modern computers can handle the desmearing routinely. Various methods of desmearing slit data exist.²⁰⁹ The technique used in this work is that of Schmidt²¹⁰ for finite slits. The distortion of the profile is more serious at smaller angles than at larger ones and this is suitably handled by a weighting function which depends solely on the instrument geometry. The method of Hendricks and Schmidt²¹¹ was used to estimate the weighting factor and for this the computer program of Buchanan and Hendricks²¹² for numerical evaluation was utilized. The computer programs for both the estimation of the weighting factor using

TABLE III
Collimation Slit Dimensions

Slit No.	Slit Dimensions (MM) for	
	Alignment	Experimental
1	10 x .05	10 x .10
2	10 x .05	10 x .10
3	10 x .12	10 x .18
4	10 x .05	10 x .10
5	10 x .02	10 x .05
FWHM* (MIN)	4	6
Resolution (\AA)	1100	800

*FWHM represents full width at half maximum intensity of the beam profile.

a Gaussian weighting function and that for the actual desmearing operation are listed in Appendix II.

Another important aspect of the experimental procedure is the spectral purity of the incident beam. There are various ways of accomplishing this,^{82,92} but for SAXS work a combination of Ni filtered Cu radiation with pulse height discrimination is considered sufficient in the majority of cases. The setting up of a pulse height analyzer (PHA) is well covered in the literature²¹³⁻²¹⁵ and suffice it to say that this simple and direct method of electronic discrimination of unwanted wavelengths is done by imposing an energy barrier in the form of a baseline to incoming radiation. Since the wavelength is a manifestation of a photon's energy, all the unwanted wavelengths can thus be eliminated along with any electronic noise by setting an appropriate baseline. Further discrimination is done by allowing an energy window which will measure all photons of interest but will discriminate any spurious spikes in the data. The detector used was a scintillation counter.*

The alignment of the instrument was monitored with a strip chart recorder before and after every scan and realignment was necessary after an average of 10 to 12 experimental runs.

Data accumulation. As mentioned in the preceeding section, the data was recorded automatically according to the set of instructions given at the beginning of each run. A sample of such instructions is given in Appendix VIII. It is more accurate for purposes of comparison

* Scintillation detectors are reputed to have long life, less prone to damage, uniform spectral sensitivity and very short dead-times during counting.

between scans to keep the number of counts constant rather than fix the time for which counting is done. An upper limit of 60 seconds per counting event was arbitrarily preset to keep experimental durations within reasonable bounds.

The chlorine in PVC has a much higher mass absorption coefficient (μ/ρ) than the other elements. The values of linear and mass absorption coefficients for both PVC and PCL are shown in Table IV and these values were used to estimate⁹² the optimum thicknesses t_m from the relation

$$t_m = \frac{1}{\mu} \quad (92)$$

The μ values for the blends were estimated using the relation

$$\left(\frac{\mu}{\rho}\right)_{BL} = W_{PCL} \left(\frac{\mu}{\rho}\right)_{PCL} + W_{PVC} \left(\frac{\mu}{\rho}\right)_{PVC} \quad (93)$$

where W represents weight fractions.

On account of the presence of such a highly absorbing element like chlorine, the number of present counts was on an average kept at 5000 at the beginning of a run and gradually lowered as necessary. Compositions richer in PCL not only had less chlorine but had higher crystallinities and counts as high as 10,000 are feasible. The number of counts should be as high as possible when the intensity exhibits a high slope, or where a maximum in intensity occurs. This is roughly estimated by scanning each new composition at larger intervals and small preset counts. 5000 counts would result in a probable error of $< 1\%$.²¹⁶

The final scanning was done at intervals of 1 to 3 minutes (i.e., 0.017 to 0.05 degree) with four counting events at each angular

TABLE IV

Absorption Coefficients of PCL and PVC for Cu K_{α}

Components	PCL	PVC
Chemical Composition	$C_6H_{10}O_2$	C_2H_3Cl
Molecular Weight (Repeat Unit)	114.146	62.496
Density ρ (g.cc ⁻¹ , 25°C)	1.145	1.398
X Mass Absorp. Coeff. μ/ρ (cm ² .g ⁻¹)	6.158	61.986
Linear Absorp. Coeff. μ (cm ⁻¹)	7.05	87.00
Optimum Thickness $t_m = \mu^{-1}$ (cm)	.142	.015

increment. A check on noise in the data is made using program DATA (Appendix VII) and a "coefficient of variation" (COV) of $\leq 3^\circ$ was arbitrarily chosen as acceptable. If a spurious data point was discovered, it was eliminated and estimated by interpolation if the data on either side was sufficiently clean to justify such smoothening. Scans with frequent error were not processed. For each composition at least four to five scans were superimposed to check for reproducibility. This would be the equivalent of 16 to 20 data points per angular increment. Also, the intensity of the incident beam was monitored as frequently as possible with an auxiliary sample of polyethylene and with a calibrated Lupolen sample provided by Professor Kratky.

With the collimation system used, the scans could be started at 8 minutes (.1333 deg., 665 Å) and were stopped after the counting times for 10 consecutive increments in angle showed no further change.

Following each scan with the sample in the scattering position (Fig. 2), another was taken with it in the non-scattering position to estimate the parasitic scattering of the system due to slit-edges, air-scattering, absorption of some of the incident radiation by the sample, etc. The sample is kept just before the first collimator slit for this purpose. However, this subjects the sample to intense radiation from the tube and for PVC rich compositions degradation was evident. The sample was thus kept immediately after the first collimator. The intensity so obtained is subtracted as shown below.

Another parameter needed is the attenuation of scattered intensity due to absorption by the sample. This is done by measuring the intensity of an auxiliary sample at a convenient angle (say 20

corresponding to 150 \AA , i.e., approximately 0.6°) with and without the experimental sample in an absorbing position (e.g., right after the first collimator) and taking the ratio of the two intensities.

The mean of four readings each for 10,000 counts was taken for all measurements for all samples when the absolute intensity and the attenuation factor were measured.

Data processing. This section is concerned with the various corrections employed to SAXS data.

The various terms used henceforth are defined below:

$\tilde{I}_{\text{EXPT}}(m) \equiv$ raw intensity data straight from the machine without any modification whatsoever.

$\tilde{I}_B(m) \equiv$ parasitic scattering due to instrument with no sample in the beam in any position. (This may be measured but is not recommended.)

$\exp(-\mu t) \equiv$ absorption or attenuation factor due to the sample's particular chemical composition and thickness.* This is identical with the factor A_s^{217} where,

$$A_s = \tilde{I}_{A,1} / \tilde{I}_{A,2} \quad (\text{See Appendix IX})$$

$\tilde{I}_{A,1} =$ intensity of auxiliary sample at convenient scattering angle

$\tilde{I}_{A,2} =$ intensity of auxiliary sample at same angle but with the primary beam weakened by the experimental sample in a non-scattering position.

* $\exp(-\mu t)$ can also be computed theoretically but errors in μ and t make the experimental value more reliable.

$\tilde{I}_B(m) \cdot \exp(-\mu t)$ = attenuated background intensity with sample in non-scattering position. This is measured as a composite term rather than multiplying $\tilde{I}_B(m)$ and $\exp(-\mu t)$.

$$\tilde{I}(m) = \tilde{I}_{\text{EXPT}}(m) - \tilde{I}_B(m) \cdot \exp(-\mu t) \quad (94)$$

$\tilde{I}(m)$ thus represents the intensity corrected for instrumental background as modified by the sample's absorption.

If comparison between samples of different compositions or treatments is to be made, the above intensities must be further corrected for absorption due to the volume of the sample. Thus,

$$\tilde{I}(m) = \frac{\tilde{I}_{\text{EXPT}}(m) - \tilde{I}_B(m) \cdot \exp(-\mu t)}{A_B t \exp(-\mu t)} \quad (95)$$

where A_B = area of sample irradiated

t = sample thickness.

Due to the smallness of the angles involved and the narrowness of the range scanned, the absorption factor is angularly independent⁹² as shown in equation (95). It can thus be treated as a constant and introduced at any stage.

The polarization factor commonly written as $P = (1 + \cos^2 2\theta)/2$ reduces to unity for very small values of 2θ , and the multiplicity factor j used in WAXD is also set equal to 1.⁹² The role of the Lorentz factor L is crucial in certain respects and will be discussed shortly.

Intensities in equations (94) or (95) can now be desmeared to give $I(m)$ or processed as is.

The desmearing is done for the simple reason of knowing the undistorted profile so that parameters like the position of maximum intensity and the narrowness or broadness of the profile (FWHM) can be quantitatively measured for meaningful comparisons. The desmeared data, however, must precede the Lorentz correction as the form in which it is used is valid only for ideal pinhole collimation.

The desmearing operation (Appendix II) sharpens the intensity profile and also causes the peak to move to higher angles. The Lorentz correction also apparently sharpens the profile still further and causes the peak to move towards still larger angles. The form of the correction factor is simply θ^{-2} (Appendix I), i.e., the desmeared intensity is to be further multiplied by its reciprocal viz θ^2 . Thus

$$I_{\text{correct}}(m) = I(m) \cdot \theta^2 \quad (96)$$

The form of the Lorentz factor is a somewhat debated topic and not all authors favor its use in their analysis although their numbers are growing. There is no apriori reason to justify its omission.^{92,128}

In fact, it is implicitly used in the analysis of SAXS data as, m^2 , s^2 , etc., for the calculations of the "desmeared invariant" as shown below.

$$Q(m) = \int_0^{\infty} m^2 \cdot I(m) \, dm \quad (97)$$

Crist has discussed this factor in more detail.¹²⁸

The Lorentz corrected data is then interpreted in terms of a suitable model. The Buchanan-Tsvankin¹³³ analysis (Appendix V) needs the

position of maximum intensity and the width at half the maximum intensity (FWHM). If more than one order of reflection is present then the ratio of their angular positions can be checked for a ratio of 2 and interpreted according to the analysis of Crist.^{127,128} Wenig and Kilian¹³⁴ have proposed a theoretical curve fitting model approach which has several parameters. While it is true that a best fit can be obtained with sufficient parameters, it is instructive to do so and compare with the results of other approaches. Some of the data was so processed.

The above approaches are suited for ordered lamellar morphology that exist in crystalline compositions. For amorphous compositions no apriori model can be assumed and it is more instructive to estimate the general parameters.

The scattering power $\langle \eta^2 \rangle$ was estimated for all compositions and so also was the specific surface O/V. The trend in their values is instructive of the changing morphology. Also the absolute value of $\langle \eta^2 \rangle$ can be matched with reasonable models to check for compatibility, partial compatibility or incompatibility. The O/V gives an idea of the fineness of the dispersion. The Porod chord lengths can substantiate this result along with the Debye correlation distance.

The transition zone thickness was estimated by the Stein-Khambatta theory and compared with values using Bonart's method.

Of course the SAXS analysis was continuously compared with trends from other experiments and whenever ambiguities arise, the possibility that fits the trend as seen by a combination of techniques is considered to be the most reliable.

Small-Angle Light Scattering Apparatus

In the case of SALS the photographic technique developed in this laboratory is more convenient to use as compared to the photometric one, on account of its speed and simplicity of operation.

Essentially, the photographic technique as shown in Fig. 12 consists of a laser light source, a polarizer, an analyzer and a camera. The laser provides an intense, coherent and monochromatic source of radiation which, after passing through a polarizer, impinges on the sample. The scattered radiation is then photographed with a high speed Polaroid film such as Type 57 after passing through an analyzer either in the crossed (H_V) or parallel (V_V) position. In most cases exposures as low as 1/100 second suffice. Since the laser beam is very fine (small diameter) one does not need a very large sample area. For the same reason the pattern could be speckled due to insufficient material in the path of the beam and also not be a very good representation of the average morphology. This difficulty can be circumvented by using a beam-splitter and increasing the exposure times proportionately.

The same principle as above is used in the photometric apparatus except that the light source is replaced by a Hg vapor lamp and the camera by a detector which is mounted on a movable arm of the goniometer much like the SAXS apparatus. The incident light is suitably attenuated and monochromatised by a series of optical filters and the detector signal after filtration for noise is averaged by a boxcar integrator before being displayed on an oscilloscope screen. The apparatus is best suited for dynamic light scattering studies and was used in the static

mode for this study. It is suitably described elsewhere²¹⁸ regarding the function of each of its components. The scattering angle θ is changed manually and a resolution up to 0.1° is possible.

Corrections. The various corrections necessary in SALS can be divided into three main types, viz.

- (i) general corrections
- (ii) those due to external disorder
- (iii) those due to internal disorder.

General. These include corrections due to the refractive index of the sample as mentioned before, refraction of the light as it passes through the sample, reflection of light at the various interfaces of differing refractive indices and the internal rescattering of scattered light termed as multiple-scattering.

In order to minimize loss of intensity due to reflection, optical continuity must be maintained as mentioned before for the sample and glass (cover slips) composite. Since the experimental intensity (I_{EXPT}) measured as raw data, contains a background component (I_B) due to the parasitic scattering of the instrumental geometry it must be subtracted. I_B is measured using just the two cover slips with some silicone oil in between, the same way as the sample scattering. The corrected intensity $I_1(\theta, \mu)$ is then given by

$$I_1(\theta, \mu) = I_{\text{EXPT}}(\theta, \mu) - I_B(\theta, \mu) \quad (98)$$

with the assumption that no absorption takes place. It is preferable to have the refractive index of the silicone oil as close to that of the sample as possible.

According to the construction of the dynamic light scattering apparatus, the incident beam is split by a partially silvered mirror for purposes of monitoring it during dynamic experiments. This causes the transmitted light which would otherwise be depolarized to be slightly polarized by a variable factor along the azimuthal direction (μ) and correction for this can be made by multiplying by the depolarization factor (DPF) as tabulated in Table V.²¹⁸ The DPF is independent of θ .

In order to estimate the apparatus constant "k", one has to calibrate the apparatus suitably. This constant k represents a certain proportionality between the physical condition of the apparatus and the data obtained under the same conditions. It thus includes geometry, alignment, the detector response, etc. The determination of "k" needs some known physical standard such as benzene but pure benzene does not scatter as highly as semi-crystalline polymeric films and the dynamic light scattering apparatus is not sensitive enough to detect benzene scattering accurately.

Thus, using benzene, a Brice-Phoenix light scattering apparatus was at first calibrated by Prud'homme²⁰⁹ and, using this calibration, a Ludox solution was calibrated as a secondary standard which, on account of the particular cell geometry, necessitated a tertiary calibration procedure using a PET film whose scattering power at high angles was estimated. Assuming a direct proportionality to its scattering at small angles the constant "k" was estimated. The entire procedure is explained in detail elsewhere.²⁰⁹

For a given sample τ is related to its transmittance T by the following equations, i.e.,

$$\tau = \frac{1}{d} \ln \left[\frac{100}{T} \right] \quad (101)$$

$$T = \left[\frac{I_{\text{SAMPLE}}(\theta = 0^\circ)}{I_{\text{BLANK}}(\theta = 0^\circ)} \right]_{V_v} \times 100 \quad (102)$$

Thus τ and T are inversely related. It is common practice to keep T as high as possible, say 70% or so, but this is not always possible. One of the ways is to make thinner samples but there is a limit to this if the bulk morphology is to be preserved. Samples which transmit less than 20% due to excessive multiple scattering will consequently have a larger error in their results.

An assumption made in the definition of T is that the sample scattering at angles very close to the incident beam is negligible so that $[I_{\text{SAMPLE}}(\theta = 0^\circ)]$ is essentially just the attenuation of the beam due to the physical presence of the sample in its path.

External disorder. Densely packed spherulites cannot be considered as spherical entities as they continue to fill the volume after impingement with other spherulites. Thus they are truncated entities of polygonic shapes. Also due to randomness in the locations of the nuclei, the truncated polygons have a certain size distribution. Lastly, due to their dense packing for reasons analogous to those in SAXS, there is interspherulitic interference. All this leads to non-ideality in scattering and must be corrected for.

The major effect of the size distribution is to wash out the higher order peaks.^{164,165} The interspherulitic interference has been shown to have little effect when the number of spherulites is large¹⁶⁶⁻¹⁷⁰ for H_v . The effect of truncation¹⁷² has been shown to shift θ_{\max} to smaller angles. This is due to the fact that the larger spherulites get weighed more heavily than the smaller ones. Equations (82) and (83) show that $I \sim V^2 \sim (R_s^3)^2 \sim R_s^6$ and so small differences in relative radii are enough to cause a shift in θ_{\max} . Besides truncation contributes excess intensity at small and large angles while suppressing it at intermediate ones. The corrections for truncation are best handled using a so-called "truncation parameter" $\langle \sigma^2 / \bar{a}^2 \rangle$ where, as shown in Fig. 16, a_i is the distance from the center to the truncated boundary and σ is the standard deviation of the average radius of the spherulites defined by \bar{a} . (\bar{a} is the arithmetic mean of all a_i for any truncated spherulite.)

Thus, correcting for truncation involves a shifting of θ_{\max} to higher angles to nullify the weighting of larger spherulites and to then raising the intensity by a constant multiplying factor. It is therefore implied that the two steps can be performed independently. For a randomly nucleated system, $\langle \sigma^2 / \bar{a}^2 \rangle$ was estimated to be 0.132¹⁷⁹ which necessitates multiplying θ_{\max} by 1.3 and the scattered intensities by 1.39¹⁸⁰ according to Fig. 17. Albeit this correction is without much refinement at the present and has a relatively minor effect on the final results. Therefore, the θ_{\max} used to estimate the spherulite radius R_s from equation (84) in principle ought to be corrected as just shown.

Following corrections for truncation, one can then correct for multiple scattering. The multiple scattering factor K is theoretically

estimated by dividing the sample thickness into a series of layers mathematically, the number of which is chosen on grounds of computation times and realistic probabilities. The computed curves of K as a function of rd are shown in Fig. 18 for various combinations of U and μ . Thus the procedure is to choose U in multiples of its maximum, i.e., 4, 8, 12, etc., and multiply the corresponding intensities corrected so far for other factors by the appropriate values of K in order to modify the intensity scan. Since K is a function of θ and μ the corrected intensity scan will change its shape much like when a desmearing operation is done on SAXS data although no analogies are drawn. K is not very sensitive to δ and $\langle \sigma^2/a^2 \rangle$, but nevertheless bears functionality to them.

Internal disorder. In the ideal Stein-Rhodes¹⁵⁹ model, the assumption was made that the optic axis was parallel or perpendicular to the radial direction. van Aartsen's¹⁵⁵ calculations showed that the same equations were valid for the case of the optic axis normal to the radius. There is, however, no reason a priori to believe that there is no fluctuation in its orientation about its most probable direction. The problem was considered preliminarily^{162,173} and later refined by the Stein-Yoon^{174,175} lattice theory in which δ is defined as a disorder parameter, the magnitude of which is a measure of the "wander" in the orientation of the optic axis. One of the assumptions is that the more the "wander" in a preceeding step, the higher the probability of the optic axis returning to its ideal orientation in the next one. It was found that orientational disorder results in excess intensities at both small and large angles and lower values at θ_{\max} .

Thus, the δ parameter also distorts the intensity scan in a certain manner. It is estimated by finding the ratios of $[I_{H_V}(U = 4)/I_{H_V}(U = x)]_{\mu=45^\circ}$ or $[I_{H_V}(\mu = 45^\circ)/I_{H_V}(\mu = x)]_{U=4}$ and then reading off the values from the theoretical plots^{175,180} as a function of x for fixed values of $\langle \sigma^2/a^2 \rangle$. Thus, for a θ scan, one can have ratios between $U = 4$ and $U = 8, 12, 16$, etc., and the mean δ is estimated.

First attempts by Stein and Yoon¹⁷⁴ were made for a two dimensional case in which the spherulites were considered as two dimensional discs divided into concentric rings with subdivision into rectangular cells. This was done in order to keep computation times reasonable. However, more recent calculations on three dimensional disorder have been done¹⁷⁶ and preliminary indications are that for a given value of $I_{H_V}(U = 4.0)/I_{H_V}(U = 15)$, the intensity loss at $I_{H_V}(\text{max.})$ is a little larger than for the corresponding two dimensional case. Results of I_{H_V} will be discussed in the next chapter for both the above cases.

The necessary corrections having been performed, one can now compare experimental and theoretical Rayleigh ratios. This comparison is done for $\theta = \theta_{\text{max}}$, i.e., $U = 4.1$ and $\mu = 45^\circ$. The Rayleigh ratio for three dimensional perfect spherulites in the H_V mode is written as²⁰⁴

$$R_{H_V}(\theta, \mu) = \frac{144\pi^4}{\lambda_o^4} N_s V^2 (\alpha_t - \alpha_r)^2 \left[\cos^2\left(\frac{\theta}{2}\right) \sin\mu \cos\mu \cos\rho {}_2P_2^{\Phi_{H_V}}(U) \right]^2 \quad (103)$$

where λ_o = wavelength of light in vacuum

N_s = number of spherulites per cm^3

V = volume of the spherulite

$$\phi_{H_v}(U) = (4\sin U - U \cos U - 3 \sin^3 U)/U^3 \quad (104)$$

$$\text{and } \cos^2 \rho_2 = \cos^2 \theta / (\cos^2 \theta + \sin^2 \theta \sin^2 \mu)^{1/2} \quad (105)$$

The other terms have been previously defined.

On substituting

$$\begin{aligned} \lambda_o &= 5461 \text{ \AA} \text{ (for the green filtered radiation)} \\ &= 5461 \times 10^{-8} \text{ cm} \end{aligned}$$

$$N_s V = 1.0 \text{ (for volume filling system)}$$

$$\begin{aligned} V &= \frac{4}{3} \pi R_s^3 = 4.19 R_s^3 \text{ (for isolated spherulites)} \\ &\approx 4.91 R_s^3 \text{ (for truncated spherulites)} \end{aligned}$$

$$(\alpha_t - \alpha_r) \approx X_{cr} (\alpha_t - \alpha_r)_{cr} \text{ (per cc.) (as discussed before)} \quad (106)$$

one gets

$$R_{H_v}(\theta, \mu) = 7.8 \times 10^{21} X_{cr}^2 (\alpha_t - \alpha_r)_{cr}^2 \left[\cos^2\left(\frac{\theta}{2}\right) \sin \mu \cos \mu \cos \rho_2 \phi_{H_v}(U) \right]^2 \quad (107)$$

The angular terms are estimated below.

$$\cos^4\left(\frac{\theta}{2}\right) \approx 1.0 \quad \text{for small } \theta$$

$$\cos^2 \mu = \sin^2 \mu \approx 0.5 \quad \text{for } \mu = 45^\circ$$

$$\cos^2 \rho_2 \approx 1.0 \quad \text{for small } \theta$$

$$\text{and } \phi_{H_v}^2(U) \approx 0.0073 \quad \text{for } U = 4.1 \text{ (i.e., } \theta_{\max})$$

Thus, on substituting into equation (107) it further reduces to

$$\begin{aligned} R_{H_V}(\theta_{\max}, 45^\circ) &= 7.8 \times 10^{21} \times 0.0018 [X_{cr}^2 R_S^3 (\alpha_t - \alpha_r)_{cr}^2] \\ &= 1.4 \times 10^{19} [X_{cr}^2 R_S^3 (\alpha_t - \alpha_r)_{cr}^2] \end{aligned} \quad (108)$$

For polyethylene $(\alpha_t - \alpha_r)_{cr} = 0.0029$

For PCL $(\alpha_t - \alpha_r)_{cr} = 0.00522$ (Appendix VI)

$$R_{H_V}(\theta_{\max}, 45^\circ) = 3.56 \times 10^{14} (X_{cr}^2 R_S^3) \quad (109)$$

where R_S is expressed in cm units.

Equation (109) is then divided by F_{dis} which accounts for the effect of the δ parameter. After the average δ has been estimated as explained before, one can use the plot of $[I_{H_V}(\delta = 0)/I_{H_V}(\delta = x)]$ for $U = 4$ and $\mu = 45^\circ$ against δ .^{175,180} Thus

$$R_{H_V}(\theta_{\max}, \mu = 45^\circ) = \frac{356 X_{cr}^2 R_S^3}{F_{dis}} \quad (110)$$

where R_S is expressed in microns. The above Rayleigh ratio is the theoretically calculated one using appropriate system parameters. It is compared with the experimental Rayleigh ratio which is merely the value of R_{H_V} at $U = 4.1$ after the experimental curve has been corrected for multiple scattering. This is the same as multiplying the above curve for $[F_{dis}]^{-1}$ and comparing it with equation (110).

C H A P T E R V

RESULTS AND DISCUSSION

The discussion which follows is based primarily of SAXS and SALS data and evidence from supplementary techniques such as optical microscopy, SEM, WAXD, DSC, etc., is included so as to complement the principal data.

Since the blends exhibited primarily two main kinds of morphologies, viz. semi-crystalline and amorphous, the chapter will be broadly classified into two sections. Crystalline morphologies are explained using the Buchanan-Tsvankin analysis of SAXS and absolute intensities of SALS in terms of Rayleigh Ratios. The amorphous morphologies are discussed in terms of the Debye correlation distance, Porod chord lengths and transition zone thicknesses. The more general parameters such as "scattering power" and "specific surface" are applicable to all morphologies and serve as a connecting thread.

Semi-Crystalline Morphologies

General. A preliminary look at the compositions rich in PCL shows distinct turbidity to the eye and the presence of a spherulitic morphology under the polarizing microscope. The spherulites are truncated resulting in a volume filling superstructure up to 60/40 compositions as shown in Fig. 19. The 50/50 composition shows presence of isolated pockets of non-spherulitic regions in an otherwise partially

truncated system, while PCL shows the most severe case of impingement, so much as to almost obliterate the identity of the individual spherulites. Beyond 50/50 no spherulites were observed nor was any kind of birefringence noted under the microscope. These initial observations suggest that with increase in the PVC content beyond 50%, crystallinity is either very low or almost nonexistent.

The spherulites exhibit the typical "maltese cross" in the direction of the cross polaroids and possess a banded appearance showing concentric rings, with a simultaneous variation in size. The banded appearance is discussed later. When the optical micrographs are compared with photographs of H_v SALS in Fig. 20 and SEM in Fig. 21, one can see a consistent trend in their sizes as plotted in Fig. 22 against the blend composition. The size variation goes through a maximum around the 90/10 composition and then drops off linearly within experimental error ($\pm 2\mu$). While the SEM observations could be the most ambiguous of the four independent techniques used, and for which reason a range has been shown, the observations of the other three techniques are in satisfactory agreement. For reasons explained later, a size estimation for the case of pure PCL is difficult to make by photometric SALS (H_v) but due to its statistical averaging it is the least ambiguous. However, both microscopic and photographic H_v SALS show a definitely smaller superstructure for PCL. A similar trend in spherulite sizes has been reported by Natov and coworkers⁴² from their observations on semi-crystalline blends of polyethylene-adipate and polyvinylacetate. This behavior goes to the heart of some other related observations and is discussed below.

Spherulite size. The formation of a certain size distribution of volume filling spherulites must depend on nucleation density, i.e., densely nucleated systems will breed spherulites closer to each other and under favorable growth conditions they will grow until they run into each other and fill up the whole volume. If the density of nucleation was less, the spherulites would grow outwards again and like before run into each other if they are able to grow large enough giving truncated spherulites of a larger size distribution than before in a volume-filling system. However, their growth is governed by crystallization kinetics which depends on the viscosity of the medium in which crystallization occurs, i.e., the T_g of the system, and undercooling (ΔT), the difference between the temperature of crystallization T_c and the melting point of the crystallites T_m . If the medium is so viscous as to prevent the diffusion of polymeric chains to a crystal-melt growth face, crystallization will be kinetically impeded and if the supercooling (ΔT) is small, the driving force for crystallization is again correspondingly reduced.

A look at Table VI which lists the data of Ong¹⁰ available for certain blend compositions and some more recent observations of Goldfarb and coworkers for pure PCL, shows that even at 45°C, the growth rate (G) of PCL is at least an order of magnitude higher than for the blends. Besides, with the addition of PVC to PCL, a slight but nevertheless real depression in nucleation density (N) is noticed with a simultaneous significant drop in growth rate (G) and an even more dramatic increase in $t_{1/2}$ the half time of crystallization. The latter is a measure of the over all rate of crystallization. A correlation of these data with

TABLE VI

Crystallization Kinetics Data of PCL/PVC Blends

Blend	T _c °C	k	G(μm/min)	N̄(#/cm ³)	t _{1/2} (min)
*PCL	45		2.20		
70/30	30	5.0 x 10 ⁻⁴	7.9 x 10 ⁻¹	0.98 x 10 ⁸	20 (25°C)
65/35	30	2.6 x 10 ⁻⁵	3.25 x 10 ⁻¹	1.66 x 10 ⁸	37 (25°C)
60/40	30	1.2 x 10 ⁻⁶	1.06 x 10 ⁻¹	0.78 x 10 ⁸	58 (25°C)
50/50	30	2.2 x 10 ⁻⁹	1.20 x 10 ⁻²	0.69 x 10 ⁸	595 (25°C)

k = Avrami constant

n = Avrami exponent ≈ 3.00 ± 0.25 (all compositions)

G = spherulite growth rate

N̄ = nucleation density

t_{1/2} = half-time crystallization

*Data of Goldfarb L. et. al., Die Makromol. Chemie 175, 2483 (1974).

the corresponding depression in the melting points (T_m) and increase in the glass transition temperatures (T_g) as shown in Table VII shows that initially for PCL which has a high nucleation density at the isothermal temperature of 30°C studied, and a high rate of growth the spherulites run into each other very rapidly and form a truncated volume filling morphology. With the addition of 10% PVC, the melting point is depressed so the supercooling is lowered while the T_g is raised. Even though the growth rate is impeded, the lower nucleation density permits larger spherulites to grow and since 90% of the material is still PCL by weight, there is enough of it to form a volume filling spherulitic morphology.

It would seem from this train of thought that with a further lowering in N with the addition of more PVC, the spherulite sizes should continue to show an upward trend. However, one needs to consider two related factors, i.e., as ΔT gets lower in magnitude and so does T_m , the requirements for the critical nucleus size (r^*) are altering, i.e., larger r^* are needed to nucleate as $r^* \sim (T_m/\Delta T)$ and the PCL which crystallizes has to be able to diffuse through the initially well mixed system of PCL and PVC, in an increasingly viscous medium. All the PCL than can potentially crystallize is not free to do so in a blended system such as this in which films were cast from dilute solutions under carefully controlled conditions as explained before.

As the T_g of the bulk polymer (blended films) is raised above room temperature, the blends are glassy with their morphologies frozen in. For those like 50/50 and 60/40 where the T_g values are a little above room temperature, a limited amount of crystallization is possible

TABLE VII

Glass Transition Temperatures and Melting Points of Blends

Blend Comp. (PCL/PVC)	Glass Transition Temperature T _g (°C)		Melting Point by DSC T _m (°C)
	Ong ¹⁰	Koleske ⁷	
PCL	-52	-71	63.2
90/10	-44	-63	62.5
75/25	-16	-48	60.2
50/50	9	-20	57.3
PVC	78	--	--

as seen by the low values of G and N not to mention the very dramatic increase in $t_{1/2}$. All this combines to give spherulites of smaller sizes which partially truncate giving non-volume-filling systems. It thus seems that the spherulite sizes must go through a maximum where optimum conditions prevail and this appears to be around the 90/10 composition.

The phenomenon is obviously complex and depends on an interplay of several interdependent parameters but the trend is believed to be real in view of its reproducibility and agreement in the analysis of four independent techniques of measurement.

The Avrami exponent n has a value of 3.00 ± 0.25 independent of composition indicating a heterogeneously nucleated three dimensional spherical growth according to both Ong¹⁰ and Goldfarb and coworkers.

Nevertheless, for spherulitic morphologies that are volume filling, the obvious question is about the location of PVC within the spherulites. The work of Keith and Padden¹⁶ on the crystallization of polyblends indicates that the non-crystallizing component is rejected at the advancing growth front as an impurity whose concentration keeps building in the melt as crystallization proceeds. Simultaneously, the rejected impurity, in this case PVC, due to its inability to diffuse away, gets trapped between the crystalline fibrils and resides there. For volume-filling cases where no matrix exist eventually all of the rejected PVC must therefore be interlamellar by this line of reasoning and ample support exists.

If all the PVC does not exist between the lamellae of the spherulites then some of it must be within the lamellae. This could be either

as trapped isolated pockets of PVC in the lamellae or as PVC co-crystallized with PCL. The latter is a remote possibility and quickly discounted on the basis of WAXD evidence. If co-crystallization did occur then the unit cell dimensions of PCL should change and cause a shift in the "d" spacing. WAXD photographs, as shown in Fig. 23, show no shift in the "d" spacings of PCL thereby suggesting that the lamellae are exclusively PCL.

The assumption all along has been that PVC does not itself undergo any crystallization, i.e., its contribution to crystallinity has been neglected. Commercial PVC such as this was⁷ is known to have crystallinities $<10\%$ ¹¹⁻¹⁵ because it is atactic and this prevents PVC chains from packing together in large enough sequences to form crystallites. It is reasonable to assume that whatever little crystallinity is possible due to isolated areas of small ordered arrays of PVC chains, blending with a foreign molecule like PCL further lowers the already poor crystallinity. Such low values of crystallinity are very difficult to detect as common estimates of even higher values have ~5% experimental errors. Besides a WAXD photograph of PVC used in this work shows a broad diffuse halo and no diffraction rings. Ong's estimates of PVC crystallinity by infra-red spectroscopy and WAXD also indicate about 5% crystallinity. Moreover, no detectable superstructure in PVC is seen either by microscopy or SALS. Hence, for all practical purposes in this work, PVC is considered to be amorphous.

Having established that PVC is interlamellar, it is instructive to know how it is distributed viz, whether it is well mixed with inter-

lamellar PCL or whether it is partially so or completely segregated. SAXS gives insight regarding this particular detail.

Long-period. SAXS curves of PCL as shown in Fig. 24 show the presence of diffraction maxima. This maxima as was discussed before is due to what is commonly called the long-period. The long-period (c) results from the presence of a macro-lattice formed by centers of adjacent lamellae. The value for PCL as shown in Table VIII agrees well with that of Perret and Skoulios. Also, with the inclusion of PVC, the values of the long-period increase as listed in Table VIII and shown in Fig. 30. This implies that with the addition of PVC the lamellae are pushed further apart so as to accomodate more PVC with a subsequently larger amorphous fraction of PCL also. This is in qualitative agreement with the electron microscopy work of Ong.¹⁰

Two values of long period are listed for each composition in order to show the effect of the Lorentz correction on the peak positions. Figs. 25 through 29 show the effect of desmearing and Lorentz correction on the smeared intensity profile. Each curve is then analyzed for its long-period using the peak position and FWHM by the Buchanan-Tsvankin model according to the procedure outlined in Appendix V.

It is also obvious from Figs. 24 through 29 that as one goes from PCL to 50/50 composition, the maxima become broader and more diffused. This makes their location and widths difficult to estimate with enough precision for meaningful analysis. For the 50/50 blend even the Lorentz corrected curve shows poor resolution for which reason no Lorentz corrected data is shown in Table VIII.

TABLE VIII
Long-Period of PCL/PVC Blends

Blend (PCL/PVC)	Desmeared Long Period		Desmeared & Lorentz Corrected Long Period	
	Directly	Tsvankin-Buchanan Model	Directly	Tsvankin-Buchanan Model
	(\AA)	(\AA)	(\AA)	(\AA)
PCL	161 (155*)	168	148	158
90/10	166	187	148	165
80/20	190	220	160	181
70/30	221	265	183	216
60/40	265	300	204	246
50/50	322	345	---	---

*Data of Perret R. and Skoulios A., Die Macromol Chemie,
156, 157 (1972).

While the Lorentz corrected profile is in principle the correct one and adopted for analysis, it is nevertheless instructive to note that the Lorentz factor has little or no effect on the FWHM of the curve although an apparent sharpening of the profile occurs. This is because it affects the lower angle data much more than at higher ones. For the same reason the first order reflection is shifted towards higher angles or lower long periods but hardly any shift is noticed for the second reflection when it is present. A hardly noticeable and ill-defined weak second maximum also becomes more noticeable.

The rationale behind the Tsvankin model is to utilize the width of the single diffraction maximum to obtain more information on the scattering system. Its physical assumptions and the mathematical treatment are debatable. According to Crist and Morosoff¹²⁸ the all important width of the diffraction peak which must be determined solely by disorder of the second kind (para-crystallinity) is shown not to be so for PE and POM.

Table IX shows that the effect of the Lorentz correction is to bring the ratio $(2\theta_2/2\theta_1)$ closer to an integral value of 2 after the desmearing operation. This is in agreement with the observations of Crist and Morosoff¹²⁸ on PE and POM. However, $(2\theta_2/2\theta_1) \rightarrow 2$ as the crystallinity vanishes and according to the Tsvankin model, the opposite behavior is expected as more amorphicity leads to more assymetric lattice statistics. This apparent anomaly could be resolved if one considers amorphicity to be synonymous with more disorder for highly crystalline homopolymers like PE and POM, but not necessarily so for blends. The morphological situation for blends is very often unique and for a system

TABLE IXComparison of $(2\theta_2/2\theta_1)$ ratios for (PCL/PVC) Blends

Blend	$(2\theta_2/2\theta_1)$ Desmeared	$(2\theta_2/2\theta_1)$ Desmeared and Lorentz corrected
PCL	2.73	2.61
90/10	2.59	2.43
80/20	2.50	2.31
70/30	2.36	2.10
60/40	--	2.04

such as PCL/PVC which has been classified as "compatible" in spite of very different crystallization behavior by each component, it is even more so. There is evidence from photometric SALS to suggest that as a consequence of higher PVC concentrations, while the crystallinity drops the SALS maxima are better resolved. Micrographs also show that the spherulites are better defined as one goes from PCL to 60/40 possibly due to slower crystallization kinetics. Photographic SALS in the V_v mode complement the banding of the spherulites observed microscopically. Banding is due to regular in-phase twisting of the lamellae and this is indicative of supermolecular order. Thus in the complex world of blends such an unexpected result can be accommodated. One also needs to point out that the above ideas are rather simplistic and not without limitations.

Crystallinity. Simultaneous to the long periods, one is also able to estimate a one dimensional crystallinity parameter (k) from the Buchanan calibration plots. k represents crystallinity in the direction normal to the alternating crystalline and amorphous layers, and is defined as

$$k = \frac{\text{crystallite size}}{\text{long period}} = \frac{a}{c}$$

k is a linear measure of crystallinity in one dimension. As shown in Fig. 30, k drops appreciably with increasing PVC content as a consequence of the PVC pushing the lamellae further apart. An estimate of k allows one to evaluate an average value for the crystallite size denoted by "a" as shown in Fig. 30. The effect of Lorentz correction on k was <5%.

If one assumes that the sandwich lamellar structures completely fill the volume of the system the above decrease in the value of the linear crystallinity k may be quantitatively related to the corresponding change in the weight fraction crystallinity X_c using equations 111(a) and 111(b) (for deviation of 111(a) see Appendix XII).

$$k = \phi_{\text{PCL}} \phi_c \quad (111(a))$$

$$X_c = \frac{\phi_c \rho_c}{\phi_c \rho_c + (1 - \phi_c) \rho_a} \quad (111(b))$$

where, ϕ_{PCL} = volume fraction PCL in the blend

ϕ_c = volume fraction crystallinity of PCL

k = volume fraction crystallinity of blend

X_c = weight fraction crystallinity of PCL

ρ_c = crystalline density of PCL = 1.178 g.cc^{-1}
(x-ray, ref. 201)

ρ_a = amorphous density of PCL = 1.094 g.cc^{-1}

Thus, estimation of k from Buchanan's analysis allows one to obtain ϕ_c which being a volume fraction crystallinity, must be converted to X_c before SAXS crystallinities can be compared to those from other independent methods such as the density column and heat of fusion. The latter can be computed by assuming additivity of specific volumes. Therefore

$$V_{\text{BL}} = W_{\text{PCL}} V_{\text{PCL}} + W_{\text{PVC}} V_{\text{PVC}} \quad (112)$$

$$V_{\text{PCL}} = X_c V_{\text{PCL}}^c + (1 - X_c) V_{\text{PCL}}^a \quad (113)$$

where V represents specific volume, W represents weight fraction and c and a denote crystalline and amorphous states respectively. The specific volumes are obtained from the reciprocals of the corresponding density values viz.

$$V_{PCL}^c = \rho_c^{-1}$$

$$V_{PCL}^a = \rho_a^{-1}$$

$$V_{PVC} = \rho_{PVC}^{-1} \quad (\rho_{PVC} = 1.398 \text{ g.cc}^{-1})$$

$$V_{BL} = \rho_{BL}^{-1} \quad (\rho_{BL} = \text{experimental})$$

Since the original composition of the blend is known, equation (112) allows one to estimate V_{PCL} which, when substituted in equation (113) gives X_c . A comparison of the weight-fraction crystallinities by the different techniques is shown in Fig. 31.

It is seen that the values of X_c agree very well up to 40% PCL substantiating the treatment of data and its interpretation. With higher amounts of PVC the fraction crystallinity determined by SAXS is higher than that determined by other methods. This discrepancy arises because the SAXS method characterizes the local crystallinity of those regions where the sandwich structures occur while the other methods characterize the average crystallinity of the polymer as a whole. If the sandwich structures prevail throughout the entire volume of the polymer, the two will be identical. However, if the sandwich structures fill only part of the volume of the polymer, the SAXS method will lead to a higher X_c since this feature is not included in the

TABLE X

Comparison of One Dimensional Blend Crystallinities

Comp. PCL/PVC	Blend Crystallinity (Vol.)	
	^k _{Buchanan} Calib. Plots	^k _{Theoretical} Tsvankin Model
PCL	63.0	63.2
90/10	56.0	54.2
80/20	47.5	47.0
70/30	42.4	41.5
60/40	36.0	34.1
50/50	30.0	24.8

Tsvankin model. In fact, the ratio of the correct and overestimated (SAXS) values can be used to estimate the volume fraction of spherulites for treatment of SALS data as will be discussed later.

The two major implications of the above analysis are that (i) the one dimensional crystallinity approximates the three dimensional case satisfactorily and (ii) no significant secondary crystallization of PCL occurs between the lamellae.

Crystallite size. The small positive slope in the value of the crystallite size with composition is an unexpected result. It can be phenomenologically explained on the basis of a depression of T_m (melting point) as shown in Table VII. Sanchez and Eby²¹⁹ have predicted for a copolymer with randomly arranged non-crystalline sequences that the crystallite size must increase with increase in the concentration of the non-crystalline component. Albeit theirs is an inclusion model where the non-crystalline component has a lesser degree of freedom in mobility compared to a blend and the comparison is to a certain extent speculative. Also as mentioned before, the Buchanan-Tsvankin analysis is a model that could be further refined and the increase in crystallite size (~10%) could well be an artifact of the analysis. Nevertheless, the slope is small and within experimental error could be treated as negligible.

An independent way to check the crystallite size would be by the particle size analysis of WAXD profiles using the Scherrer equation

$$L_{hkl} = \frac{K\lambda}{\beta_o \cos\theta} \quad (114)$$

where L_{hkl} is the mean dimension of the crystallites perpendicular to the planes (hkl), β_o is the integral breadth or breadth at half-maximum intensity of the pure reflection profile in radians and K is a constant commonly assigned a value of unity.

The technique, however, is very sensitive to small errors and demanding on equipment and experimental precision. Monochromatization is needed along with good resolution of the profiles in order to analyze their broadening. This necessitates good counting statistics as small errors in the width of profiles make relatively large differences in the final results. Moreover, the technique is fraught with assumptions and separation of broadening effects due to small crystallite size and lattice distortions is not a routine exercise.

The application was attempted inspite of the above difficulties on a GE-XRD5 diffractometer but without success. In the case of PCL which has an orthorhombic unit cell, the (00 ℓ) reflections necessary for the line broadening analysis (to estimate crystallite sizes in the direction of the chain axis) are rather weak and difficult to resolve. This can in principle be indirectly estimated by using the (0k ℓ) and (0k0) reflections but the latter was not resolvable with the available instrumentation. If the (hk0) and (h00) reflections are used, a different aspect of the crystallite dimensions is estimated and this is thought to be the reason for the significant decrease in Ong's¹⁰ values of crystallite sizes with increasing PVC concentration. The least ambiguous method is the Fourier Transform method of Buchanan and Miller²⁰⁰ but such an extensive study was not undertaken.

It must be pointed out that the above analysis was for a transition zone parameter $\epsilon = 0.2$, i.e., 20%. While there is no apriori justification for this value, it is in most cases reasonable. ϵ can be changed but as long as $\epsilon > 0$ it does not affect the calibration curves. Nevertheless, β/α the crystallite size distribution parameter was also chosen to be 0.2 as previous work has justified.¹⁹⁸⁻²⁰⁰ The calibration curves however are sensitive to the choice of β/α and this in turn can be used as a fitting parameter. β/α will depend on the kinetics of crystallization and there is justification that with the blend composition β/α could change.

Asymmetry of distribution function. By the method of Crist¹²⁷ when more than one diffraction maxima exist, one can use the ratio of their angular positions, i.e., $(2\theta)_2/(2\theta)_1$, to estimate the skewness of the crystallite size distribution. According to Crist, positively skewed distributions give a ratio >2.0 . Negatively skewed distributions or symmetric (Gaussian) distributions would give ratios ≤ 2.0 .

Reinhold et al.¹²⁹ have discussed the meaning of positively skewed and negatively skewed distributions more fully. Table IX shows the ratios of $(2\theta)_2/(2\theta)_1$ for the various compositions. This suggests that for PCL rich compositions where crystallization is rapid, the distributions are more positively skewed than for those compositions where the kinetics are lower. This is also consistent with the analysis of 90/10 compositions by the Wenig-Kilian method¹³⁴ which indicates an asymmetry of 0.3 (30%). The technique needs extensive computation time and was not applied for other compositions. It also indicates a transition zone of approximately 12 \AA which, for a crystallite size of approximately

100 Å gives $\epsilon \sim 0.12$. Another parameter obtained is N, the approximate number of lamellae in parallel array on an average and the best fit was obtained for N=6 comparable with polyethylene. N could be used as a measure of the coarseness of the spherulites or openness of the structure and correlated with both the long-period and observations by electron microscopy.

While the positions of the two maxima were compared as done by Crist, it needs to be pointed out that the origin of the second maxima is poorly understood. It could be a true second order of the same morphology that is responsible for the primary maximum but it could in some cases also be due to an altogether different morphological periodicity.¹²⁶ In our case, the fact that the second maxima progressively broadens and washes away ultimately with a corresponding drop in crystallinity makes the former more probable.

SALS. The analysis of SAXS is further complemented by results of SALS as discussed below. Fig. 19 shows banded spherulites by light microscopy, believed to be due to in-phase coordinated twisting of the lamellae such that it is very regular or periodic. Such twisting has also been observed before on other systems¹⁵⁹ and on the same by Ong.¹⁰ Photographic H_v and V_v experiments show intensity arcs at higher angles which are also believed to be due to the same phenomenon.¹⁵⁹ Values of twist periods estimated by microscopy and SAXS show good agreement by both techniques as shown in Fig. 32. The periodicity is proportional to the spherulite's radius. Whether the twisting is real or false is a debated subject and falls outside the scope of this study.

The most interesting SALS information can be had from the Rayleigh ratio calculations as outlined in Table XI. The I_{H_v} vs θ scans along

L

TABLE XI

SALS Rayleigh Ratios of PCL/PVC Blends

Blend Comp. Wt. % PCL	Spherulite Crystallinity	$R_{H_v}(\theta_{\max}, \mu_{45^\circ}) \times 10^{-3}$	
		Experiment	Theory
100	.63	--	--
90	.56	16.07	29.60
80	.48	5.19	8.35
70	.42	2.90	2.87
60	.36	2.24	1.82
50	.29	0.24	0.24

$\mu = 45^\circ$ are shown in Fig. 51 and were used to estimate the Rayleigh ratios.

The Rayleigh ratio as expressed in equation (91) takes into account all the various corrections discussed before, viz. background subtraction due to scattering by a blank specimen, normalization of scattered intensities to the incident intensity, corrections for reflection, refraction and multiple-scattering and also those due to external and internal disorders.

In the expression for Rayleigh ratio as given by equation (108), one needs the term $(\alpha_t - \alpha_r)^2$ which, as shown in Appendix VI, was estimated to be 0.00522. For volume filling systems $N_{SPH} V$ reduces to unity and V was taken as $4/3\pi R^3$, i.e. $4.19 R^3$ because the truncation effect is already corrected for once by both shifting the entire curve to larger angles by a predetermined factor depending on $\langle \sigma^2/a^2 \rangle$ and also raised in intensity by multiplying it by another constant factor again dependent on $\langle \sigma^2/a^2 \rangle$. The truncation parameter was assumed to be 0.132 i.e., for random nucleation as already estimated before¹⁷⁹ and for this value the shift factor for the curve is given as 1.37 while the multiplication factor is given as 1.39.¹⁸⁰ Using $\lambda_0 = 5461 \text{ \AA}$ in the equation for Rayleigh ratio, the expression reduces to

$$R_{H_V}(\theta_{\max}, 45) = \frac{312 R_s^3 X_{CR}^2}{F_{dis}} \quad (115)$$

for a volume-filling system subject to the above assumptions. For a non-volume-filling system $\langle \sigma^2/a^2 \rangle = 0$ and no shift factor nor multiplication of the intensity by a constant factor is necessary. However, under these

conditions, $N_{SPH} V^2$ reduces to $\phi_s \left(\frac{4}{3}\pi R^3\right)$ as shown below, where ϕ_s is the volume fraction spherulites.

$$\begin{aligned}\phi_s &= \text{volume fraction spherulites} \\ &= \text{volume of all spherulites} / \text{total volume of system} \\ &= \left(\frac{\text{volume}}{\text{spherulite}} \times \text{number of spherulites} \right) \times \frac{1}{\text{total volume of system}}\end{aligned}$$

Now,

$$\begin{aligned}X_{CR} &= \text{crystallinity of system (= crystallinity of spherulite only in volume-filling case)} \\ &= \frac{\text{crystalline volume}}{\text{total volume}}\end{aligned}$$

and

$$\begin{aligned}k_{BUCH} &= \text{crystallinity of spherulite} \\ &= \frac{\text{crystalline volume}}{\text{volume of spherulite}} \quad (\text{assuming matrix is completely amorphous})\end{aligned}$$

Thus,

(116)

$$\frac{X_{CR}}{k_{BUCH}} = \frac{\text{volume of spherulites}}{\text{total volume}} = \phi_s$$

$$\text{and } \phi_s = \left(\frac{4}{3}\pi R^3\right) N_{SPH}$$

From this

$$\begin{aligned}N_{SPH} V^2 &= \phi_s \left(\frac{4}{3}\pi R^3\right)^{-1} \left(\frac{4}{3}\pi R^3\right)^2 = \phi_s \left(\frac{4}{3}\pi R^3\right) \\ &= 4.19 \phi_s R^3\end{aligned}$$

Using these values, equation (115) reduces to

$$R_{H_v}(\theta, \mu) = \frac{312 (\phi_s R^3) X_{CR}^2}{F_{dis}} \quad (117)$$

for a non-volume-filling system.

The multiple scattering corrections were done using the plot shown in Fig. 18 as explained before and δ value estimates using the two dimensional theoretical predictions showed a constancy with composition in the range $\delta = 0.2 \pm 0.02$.

The denominator F_{dis} in equation (115) and (117) is estimated from a plot of F_{dis} versus δ and the Rayleigh ratio so estimated agrees well with the maximum value in the corrected experimental curve within a factor of 2.

In view of the approximate nature of some of the assumptions, particularly the truncation correction and the 2-dimensional parameter, such agreement is considered fair although further refinement is certainly necessary. In the semi-crystalline blends, the truncation does vary and ideally $\langle \sigma^2/a^2 \rangle$ must too, which would involve similar modifications of the end result.

The H_v scattering is proportional to $[X_{CR}(\alpha_t - \alpha_r)]^2$ and since $(\alpha_t - \alpha_r)^2$ stays constant the variation of X_{CR}^2 as estimated from independent techniques serves well to compare the two Rayleigh ratios. The sudden drop in the intensity of 50/50 composition is due to the building up of a non-spherulitic matrix and the volume fraction crystallinity of the spherulites (i.e., ϕ_s) was taken as the ratio of the crystallinity by the density method and that estimated by SAXS. This gives a good comparison once again confirming the validity of the approach.

The curves are seen to become broader for the more crystalline compositions due to the severity of the truncations and consequent size distribution in spherulite sizes.

Since the H_v pattern has its lobes at 45° to the direction of the crossed polaroids, the optic axis is either in the 0° or 90° orientation to the radius. Since PCL is very similar to PE in most respects and the optic axis of PE is the chain axis at 90° to the radius, the same can be said of PCL.

No photometric data for pure PCL could be taken due to the tremendous turbidity of the sample due to a highly anisotropic unit cell structure.²⁰¹ This gives rise to a high degree of multiple scattering. The transmittance of a PCL sample < 1 mil thick was barely 5%. Any lower thicknesses would distort the bulk morphology and invalidate comparison with the blends.

Long time crystallization. It was discovered that the 40/60 composition classified all along as amorphous developed a non-volume-filling spherulite structure after more than a year's annealing at ambient temperatures. This can be seen both microscopically where no truncation is evident and also by SALS where the H_v pattern is large and weak and the V_v pattern is elliptical and much stronger. The same phenomenon was observed for 50/50 but less than 6 months after isothermal crystallization at 30°C . This is in agreement with Ong's¹⁰ observations that beyond the 50/50 composition $t_{1/2}$ is very high as shown in Table VI.

Hence this confirms that given enough time, the very slow kinetics of phase separation ultimately allow for it. Results of 50/50 and 40/60 compositions therefore should be strictly speaking examined with care due to the transient nature of their morphologies.

Amorphous Morphologies

The scattered intensities of compositions from 40/60 to PVC are shown in Fig. 33 through 37. The curves show rather broad diffuse maxima which are spread out over a considerable angular range but nevertheless represent some complex discrete scattering phenomena which will be discussed later. In spite of the presence of these maxima, one cannot readily adopt a model to explain their discrete scattering. This is best treated instead in terms of the more general parameters of theories proposed by Debye^{95,96} and Porod^{84,85} for random morphologies.

It was mentioned before that every part of a scattering curve is in some way a manifestation of some particular detail of the system's morphology. According to Kratky,¹⁸⁴ the scattering curves for solutions exhibit Gaussian behavior in the very low angle regions, Debye-scattering in the intermediate region and conform to Porod's law in the tail region as shown in Fig. 38. When the scattered intensities of the amorphous blends are analyzed by the Debye method of plotting $1/\sqrt{I}$ against θ^2 the data is found to conform to linear behavior as predicted by equation (40) in the intermediate angular range as shown in Fig. 39. This permits the estimation of \bar{l}_c the "correlation distance" from the slope and intercept according to equation (42) and the Porod "inhomogeneity lengths" \bar{l}_{PCL} and \bar{l}_{PVC} from equations (45) and (46). Fig. 40 shows the trend in the values of the above three parameters as the blend composition varies.

It is interesting to note that as the system becomes richer in PCL, the inhomogeneity lengths of both components approach each other

in magnitude and will ultimately become indistinguishable as to which is the matrix and which is the dispersed phase. At this stage the system must be on the verge of phase inversion and varying the composition any further in the direction of more PCL should lead to it. This is precisely what is observed microscopically and by SALS. The 50/50 composition is semi-crystalline (non-volume-filling) and the phase inversion allowed the PCL to undergo some crystallization as volume fraction wise PCL was now the dominant component.

It is also important to note that the value of $\bar{\ell}_{\text{PCL}}$ for 10/90 composition is of the order of magnitude of 30 to 35 Å which is about the size of an isolated PCL molecule implying by this analysis that it is molecularly dispersed at that concentration. If then the PCL domains increase with composition, the logical question is why does this isolated mass of PCL not crystallize? For crystallization to take place one must have nucleation such that conditions are favorable for stable nuclei to be formed before any crystalline growth can occur. Stable nuclei must have dimensions larger than the critical nucleus size given by r^* .

r^* is proportional to T_m the crystalline melting point and varies inversely as ΔT the supercooling. For the amorphous compositions, the melting point of PCL is not only depressed enough to prevent crystallization but the temperature of crystallization T_c (30°C) is below the glass transition of the blend as shown in Table VII. The very fact that only one T_g is observed implies that either the domains of PCL if at all they exist, are very small or that the PCL is so well mixed with PVC that at 30°C it cannot free itself by diffusion so as to form a nucleus

> r^* and thus crystallize. If so then is there any significance to the Porod chord lengths for PCL, viz. are the values of $\bar{\lambda}_{\text{PCL}}$ real? The reasons shown below help explain their significance.

To begin with, in application of both the Debye and Porod theories the implicit assumption is that there are two phases which are homogeneous in their densities and that they are separated by sharp boundaries. Leaving the latter condition aside for the time being, the definition of homogeneous phases could include two possibilities, viz. 1) that both PCL and PVC are completely segregated into pure components, and 2) that there are domains which are not chemically pure but physically homogeneous. In other words, one can conceive of a situation that has a dispersed phase rich in one component and a matrix which is rich in the other, and both are homogeneous within themselves. Such a situation however implies good mixing within the domains and it follows that if indeed mixed domains occur then sharp boundaries are less favorable and that the transition zone from the domains to the matrix must be rather diffuse. It also follows that one ought to observe two glass transitions each for the domain and the matrix. For two T_g 's to be detected the phases must be large enough to be detected by whatever method the T_g is measured. However, the data of Koleske⁷ and that of Ong¹⁰ do not seem to indicate such an occurrence. This is not unreasonable if the phase dimensions are small enough and a measure of their fineness of dispersion can be had from their specific surface values (O/V) as listed in Table XII.

Another important point is that even the pure PVC gives a Debye correlation distance value of approximately 22 Å, due to its excess

TABLE XII

Specific Surface of Amorphous Blends

Blend (PCL/PVC)	Specific Surface O/V (\AA^{-1})	k_2 (Porod's Slope)
10/90	8.58×10^{-3}	.138
20/80	11.47×10^{-3}	.186
30/70	12.86×10^{-3}	.206
40/60	14.64×10^{-3}	.242

scattering. This implies some heterogeneity in PVC as a pure amorphous polymer should not scatter if its electron density is truly homogeneous. In fact, the PVC in this work not only gives excess scattering but also exhibits a barely perceptible maximum in the raw experimental data. This gradually becomes more noticeable after the various corrections are performed. The origin of this maximum is not well understood and discussed later.

In order to eliminate the scattering contribution of PVC from that of the blend one can apply the following relation.

$$(I_{BL})_c = I_{BL} - I_{PVC} \cdot W_{PVC} \quad (118)$$

where I_{BL} is the intensity which includes the contribution of PVC, I_{PVC} is that due to PVC and W_{PVC} is the weight fraction of PVC depending on the blend's composition. When the corrected intensity $(I_{BL})_c$ was re-plotted as $1/\sqrt{(I_{BL})_c}$ against θ^2 as shown in Fig. 41, all the compositions showed zero intercepts giving infinite values of $\bar{\ell}_c$ since

$$\bar{\ell}_c = \frac{\lambda}{2\pi\sqrt{\frac{\text{slope}}{\text{intercept}}}}$$

This result does not make sense and the reason responsible for this is thought to be the continuously changing scattering behavior of PVC with the blend composition. In other words, the contribution of PVC cannot be subtracted simply by applying equation (118) but is more complex.

Thus, the simple minded analysis of Debye and Porod is not applicable from a point of view of absolute significance towards the study of complex morphologies such as above, but nevertheless very helpful in

following a trend. The Debye-Porod approach is sound in principle but the system deviates from ideality enough to make absolute relevance to their parameters doubtful.

It must be mentioned at this point that the scattering due to the amorphous compositions has so far been given the single-particle treatment when discussed in terms of the Debye-Porod parameters. The single-particle scattering theories were originally derived for isotropic (spherically symmetric) scattering particles for which a "Lorentz correction" is not required. In view of this, the desmeared intensities were used to process the data for the Debye-Bueche correlation distance and Porod chord length as shown in Figures 39 through 42.

From a discussion of Figure 41, it is apparent that the complexities of the amorphous morphologies will need more than one kind of analysis for their meaningful characterization. A second approach is to consider the scattering maxima observable in each composition and to treat these discrete effects as originating from some kind of statistical periodicity in their morphology.

Discrete-effects. The presence of discrete scattering effects for all amorphous compositions inclusive of PVC is an unexpected result at first glance, but literature contains several indirect references to the fact that PVC has a tendency to agglomerate and form clusters of various dimensions.²²⁰⁻²²⁵ Before proceeding to any discussion of these maxima, it should be pointed out that the data represents the average values of several scans which were all reproducible. An error analysis of the original data always showed a coefficient of variation <5%. This is a reasonable figure especially in view of the fact that the PVC rich

blends on account of their high absorption coefficients are not so transparent to x-rays resulting in very low intensities. Due to the heterogeneities the blends richer in PCL scatter more than the others in the low angle region but in the tail region the scattered intensities are low enough for all compositions and high counting times were necessary for appropriate resolution from background scattering.

Since the maxima are diffuse and broad, the desmearing operation will further introduce a magnification of the original experimental error and such an error analysis was done as shown in Fig. 42. A synthetic curve with a monotonic decrease in intensity was desmeared in order to compare for the magnification in error. It is seen that the "discrete" effect continues to persist and is thus accepted as real and not due to any experimental artifacts such as long time variations in instrumental stability.

In a dense system such clustering would give rise to a quasi-periodicity in the electron density of the material and when combined with the inter-particle interference effects inherent in dense systems,⁸³⁻⁸⁵ the presence of maxima which are relatively broad and diffuse, is not totally unreasonable even in the absence of crystallinity. According to Guinier⁸³ and Porod⁸⁵ such maxima in non-crystalline systems are phenomenologically predicted but the application of Bragg's law and discussion in terms of "d" spacings is strongly discouraged. Nevertheless, without attaching any absolute significance to these numbers, it is possible to compare values of "d" spacings on a relative scale in order to get an order of magnitude approximation and to follow a trend with composition.

Values of the "d" spacing which, if loosely defined, represent some sort of an average periodicity in the electron density are listed in Table XIII after desmearing, both with and without the Lorentz corrections.

The application of the Lorentz correction factor and the subsequent Bragg treatment is not unreasonable if the aim is to estimate a trend on a relative scale. Moreover, as will be shown later, the rather large transition zone values and inconsistent volume fractions by the Stein-Khambatta treatment combined with the inter and intra particle interference effects due to denseness, justify the above analysis for diffuse-scattering.

This shows an increase in the "d" spacing occurs with the addition of PCL to PVC, i.e., whatever the scattering entities are, their centers are getting further apart much like the separation of lamellae by excess PVC. An exactly similar trend was observed in plasticized PVC by Geil and Gezovich²²⁰⁻²²⁵ but without any maxima for pure PVC. In view of very small differences in densities between clusters and their surroundings, PVC scattering is difficult to detect and also quite sensitive to the sample's history. Nevertheless by EM, Geil's^{220, 225} conclusion is that the fundamental building blocks of PVC morphology are particles of $\sim 100 \text{ \AA}$ size which cluster to give larger aggregates in the micron range and these are detected more easily by EM. These EM particles are more visible after annealing. Thus from Geil's work it can be concluded that the PVC clusters of 100 \AA size are increasingly separated by the addition of low molecular weight plasticizers and is in good agreement with the present data both qualitatively and quanti-

TABLE XIII

Relative Trend in Periodicity of
Scattering Entities for Amorphous

Blend	Before Lorentz Corrections (Å)	After Lorentz Corrections (Å)
40/60	143	102
30/70	123	95
20/80	113	91
10/90	110	84
PVC	104	80

tatively. More recent support to this comes from the work of Neilson and Jabarin²²⁴ who, while not observing any maxima in the SAXS of PVC, conclude from a Guinier plot analysis that a particle diameter of 120 Å for PVC is not unreasonable. Considering the fact that EM is difficult to quantize statistically and that the "radius of gyration" method is strictly applicable only to very dilute systems at very small angles, the agreement about the approximate dimensions of PVC is considered to be fair.

There is evidence to believe¹¹⁻¹⁵ that the small but finite crystallinity of PVC is due to favorable chain alignment located throughout the morphology such that the small crystallites so formed act as stable crosslinks that hold the gel particles together and that due to the high melting point of these crystallites their total elimination is not achieved without risk of degradation in the absence of thermal stabilizers. For our PVC that was neither stabilized nor stirred at high temperatures these gel particles are believed to have persisted.

In fact, recent work by Collins²²⁶ indicates that in the absence of heating PVC solutions at elevated temperatures for extended periods of time, the resulting morphologies show 100 Å particles that persist from the virgin polymer, due to incomplete dissolution. Hence, the occurrence of a SAXS maximum is not unreasonable.

Statton⁸² has proposed that the presence of microvoids is sometimes responsible for spurious discrete effects. If microvoids are indeed responsible for the above maxima, then the scattering power of the system must greatly exceed that in the absence of voids due to the large electron density difference between polymer and voids according to

equation (29). This was not found to be the case as shown in Table XIV. In fact, as the PCL concentration increases, so does the mixing as the 50/50 composition is reached. This shows a reverse trend than if voids did occur. Another way to check this possibility is to swell the polymer with a suitable solvent. The filling of voids by solvent should lower the scattering power due to a lowering of the electron density difference.

The simplest case is to imagine spherical PVC domains densely packed and interconnected with transition zones over which a continuous density difference, although small, exists. One can then try to compare the scattering power of such a model to that obtained experimentally. The next case would be to check if the model is consistent with the scattering power of blends, i.e., does the PCL merely separate the PVC clusters or does it enter the clusters, or is it well mixed in the transition zone between clusters, etc.?

Table XIV lists the various models tried for pure PVC.

Adopting the gelation model, one can then follow the trend with the blends by assuming that the gel particles are separated by an average distance such that for pure PVC $a = 2R$ where R is the radius of the gel particles. As PCL is added a increases to a^* but R remains the same as in Fig. 43. Thus, $a^{*3} = a^3 / \phi_{\text{PVC}}$ and taking $a \approx 80 \text{ \AA}$ as seen after Lorentz correction, the corresponding a^* values agree very well with the SAXS periodicity as shown in Table XV.

Further insight into the morphology is gained by the transition zone analysis, in the next section.

TABLE XIV

Comparison of Various Models for PVC

$$\langle \eta^2 \rangle_{\text{Expt}} = 0.403 \times 10^{-3} \text{ (mole elec/cc)}^2$$

Model	Type	$\langle \eta^2 \rangle$ model	Result	Remarks
1	Void Model (Statton)	0.403×10^{-3}	$<0.1\%$ voids	Most polymers can have 1 part in 1000
2	Density depletion in amorphous phase due to formation of crystallites ($<10\%$ crystallinity) (proposed for alloys by Guinier)	0.403×10^{-3}	$\rho_a = 1.46 \text{ g. cc}^{-1}$ $\rho_a = 1.32 \text{ g. cc}^{-1}$ for $X_{\text{CR}} \approx 9\%$	ρ_{AM} is quite low but possible
3	Gelation Model maximum packing of spherical gel particles giving $\phi_{\text{gel}} = 0.74$	0.403×10^{-3}	$\rho_{\text{gel}} = 1.435$ $\rho_{\text{matrix}} = 1.350$	Most probably (only $\pm 3\%$ fluctuation in ρ from ρ_{AV} of 1.39)

TABLE XV

Comparison of Lorentz Corrected Periodicities
with those of the Gel model for
Amorphous Compositions

$$a^* = 80 / (3 \sqrt{\phi_{\text{PVC}}})$$

Blend	a^* (Å)	Lorentz corrected values (Å)
40/60	98	102
30/70	92	95
20/80	87	91
10/90	83	84

Transition zone. The two models used for the above analysis are the Stein-Khambatta model and the Bonart model. For each of the compositions, the $\langle \eta^2 \rangle_{\text{EXPT}}$ value was matched to the $\langle \eta^2 \rangle_{\text{TH}}$ to estimate the volume fraction of the transition zone by the Stein-Khambatta model using the relation

$$\langle \eta^2 \rangle = [\phi_1 \phi_2 - \frac{\phi_3}{6}] (\rho_1 - \rho_2)^2 \quad (119)$$

and the results are tabulated in Table XVI.

While finite positive values are obtained for ϕ_3 , the values are very high and suggest a high proportion of the morphology to be as a diffuse transition zone which implies very good compatibility. This is consistent with the single glass transitions observed. However, the ϕ_3 values are inconsistent with those of ϕ_1' and ϕ_2' according to

$$\phi_1' = \phi_1 - \phi_3/2 \quad (120)$$

$$\phi_2' = \phi_2 - \phi_3/2 \quad (121)$$

This is due to the dense nature of the system where a high degree of overlapping of the zones occurs and leads to their overestimation.

The Bonart method is somewhat more useful in this respect and values of B are tabulated in Table XVII from Fig. 44 through 47.

These results show that the zone thickness increases with the addition of PCL implying better compatibility as 50/50 composition is approached. Also the fraction of diffuse boundaries shows a corresponding trend in the same direction.

TABLE XVI

Volume Fraction of Transition Zone by the Stein-Khambatta Model

Blend	$\langle \eta^2 \rangle_{\text{EXPT}} = \langle \eta^2 \rangle_{\text{TH}}$ (mole elec/cc) ²	ϕ_3
10/90	.554 x 10 ⁻³	.39
20/80	.975 x 10 ⁻³	.65
30/70	1.278 x 10 ⁻³	.82
40/60	1.35 x 10 ⁻³	.90

TABLE XVII

Transition Zone Thickness by Bonart's Method
for Amorphous Compositions

Blend	$B(\text{\AA})$	Fraction of diffuse zones
10/90	28 ± 3	0.78
20/80	33 ± 3	0.83
30/70	32 ± 2	0.85
40/60	36 ± 2	0.90

If this behavior is true then by the Debye-Beuche method, one ought to get a straight line when plotting $K_4 \langle \eta^2 \rangle$ against ϕ_{PCL} and Fig. 48 shows that this is indeed so. The slope of Fig. 48 indicates a fractional thickness of about 25 to 27% which would in turn indicate that for domains of the order of 100 \AA the thickness should be of the order of 25 \AA . This agrees very well with values of Helfand and Tagami^{143,144} and Meier^{145,194} who predict thicknesses of the order of 15 \AA to 20 \AA for incompatible systems and higher values for compatible ones like PCL/PVC.

The specific surface (O/V) ratios and values of k_2 (Porod's slope) are listed in Table XII. They also show a trend towards increased compatibility as 50/50 compositions are approached. O/V is a measure of the improved surface contact between the components. k_2 is a measure of the amount of segmental mixing that contributes to background scattering at higher angles. Thus, with more PCL, the mixing seems to improve and mixed phases should be favored.

This is further explained in the next section.

Scattering power. A much more powerful tool on account of its unambiguous nature is the "scattering power" of the system denoted by $\langle \eta^2 \rangle$ in Fig. 49. It is a measure of the total heterogeneity of the system and should pass through a maximum at $\phi_{\text{PCL}} = \phi_{\text{PVC}} = 0.5$ for a two phase model according to equation (29). If the abscissa in Fig. 49 were in volume fractions, this is seen to be the case. However, according to equation (29), a two phase model with homogeneous phases should give zero values of $\langle \eta^2 \rangle$ for $\phi_{\text{PCL}} = 0$ and $\phi_{\text{PVC}} = 0$. When $\phi_{\text{PCL}} =$

0, we have only PVC and a finite value of $\langle \eta^2 \rangle$ is a clear indication of its heterogeneity which may be related to the gel structure already discussed. $\phi_{\text{PCL}} = 0$ is for the PCL composition and a finite value in this case is obviously due to its semi-crystalline nature.

One also notices that the plot is not symmetric about the maximum. This could be due to the deviation of the morphologies of the various compositions from the one idealized in equation (29) (where the phases are often considered synonymous with the components) to one which may have mixed phases or three different phases or the presence of diffuse transition zones. The various possibilities are explored below.

These experimental values of $\langle \eta^2 \rangle_{\text{EXPT}}$ may be compared with theoretically calculated values of $\langle \eta^2 \rangle_{\text{Theor.}}$ based upon various assumed models to gain insight into the distribution of phases. A case in point is the amorphous blend containing $W_{\text{PVC}} = 0.70$ or $\phi_{\text{PVC}} = 0.65$ for which the experimental $\langle \eta^2 \rangle = 1.28 \times 10^{-3}$ (moles electrons/cm³)² as shown in Table XVIII. A calculation of $\langle \eta^2 \rangle$ based upon Equation (29) where the two phases are the two components, gives a value of 3.18×10^{-3} which is too high. This rules out this model since, if anything, the experimental value is too high as a consequence of structure within the phases. A possibility is to utilize Equation (62) or Equation (119) which gives a lower $\langle \eta^2 \rangle$. However, to account for the experimental value, it is necessary to assume that if two phases are coexistent, they cannot be pure components. We may assume a phase A which is PVC rich and phase B which is PCL rich. If ϕ_A and ϕ_B are the volume fractions of the two phases (where $\phi_A + \phi_B = 1$) and, for example ϕ_{PCL}^A and ϕ_{PVC}^A are the volume

TABLE XVIII

Comparison of Various Models for 30/70 (PCL/PVC)

$$\langle \eta^2 \rangle_{\text{Expt.}} = 1.28 \times 10^{-3} \text{ (mole elec./cc)}^2$$

Model	Domain/Matrix	Domain/Tr. Zone/Matrix	Domain/Matrix
Phases	PCL/PVC	PCL/Mixed/PVC (Stein-Khambatta)	Mixed/Mixed
Tr. Zone	Sharp	Diffuse	Sharp
Expression	$\phi_1 \phi_2 (\rho_1 - \rho_2)^2$	$(\phi_1 \phi_2 - \phi_3 / 6) (\rho_1 - \rho_2)^2$	$\phi_1 \phi_2 (\rho_1 - \rho_2)^2$
$\langle \eta^2 \rangle$ model	3.18×10^{-3}	1.28×10^{-3}	1.28×10^{-3}
Remarks	$\phi_{\text{PCL}} = 0.354$	$\phi_3 = 0.82$	multiple possibilities. limiting vol. fr.
	$\phi_{\text{PVC}} = 0.646$	Not consistent with ϕ_1' and ϕ_2'	upper(PCL)0.200 0.937
	overestimates		lower(PCL)0.037 0.641

fractions of the two components in Phase A (where ϕ_{PVC}^A and $\phi_{PCL}^A = 1$) it must then follow that

$$\phi_{PVC} = \phi_A \phi_{PVC}^A + \phi_B \phi_{PVC}^B \quad (122)$$

and

$$\phi_{PCL} = \phi_A \phi_{PCL}^A + \phi_B \phi_{PCL}^B \quad (123)$$

Then

$$\langle \eta^2 \rangle = \phi_A \phi_B (\rho_A - \rho_B)^2 \quad (124)$$

where, assuming additivity

$$\rho_A = \phi_{PCL}^A \rho_{PCL} + \phi_{PVC}^A \rho_{PVC} \quad (125)$$

and

$$\rho_B = \phi_{PCL}^B \rho_{PCL} + \phi_{PVC}^B \rho_{PVC} \quad (126)$$

where ρ_A and ρ_B are the electron densities of phases A and B and ρ_{PCL} and ρ_{PVC} are the electron densities of the homopolymers. The task is to find values of ϕ_A , ϕ_{PCL}^A and ϕ_{PCL}^B consistent with the known ϕ_{PVC} so as to give a $\langle \eta^2 \rangle$ in Equation (124) which fits the experimental value.

There is not a unique solution to this problem but rather a range of concentrations which will satisfy this condition ranging from a lower limit of $\phi_{PCL}^A = 0.037$ and $\phi_{PCL}^B = 0.641$ up to $\phi_{PCL}^A = 0.200$ and $\phi_{PCL}^B = 0.937$.

The most likely situation is that there may be two mixed phases with a transition zone between them. However, this model involves more parameters than can be experimentally characterized.

The situation is more complex in a concentration range where the PCL is partly crystalline. A typical case is that of $W_{\text{PVC}} = 0.10$ for which the experimental $\langle \eta^2 \rangle$ is 0.77×10^{-3} (moles electrons/cc)² as shown in Table XIX. One model is that possessing two phases, a crystalline PCL phase and a homogeneous amorphous phase consisting of a solution of the amorphous PCL with the PVC. This model leads to a too low value of $\langle \eta^2 \rangle$ of 0.21×10^{-3} . The amorphous phase is evidently not homogeneous. Thus, the system must be described as a three phase one. If the phase boundaries are sharp, a generalization of equation (29) gives

$$\langle \eta^2 \rangle_{\text{av}} = \phi_1 \phi_2 (\rho_1 - \rho_2)^2 + \phi_1 \phi_3 (\rho_1 - \rho_3)^2 + \phi_2 \phi_3 (\rho_2 - \rho_3)^2 \quad (127)$$

One possibility is that the PVC and PCL are completely incompatible in the amorphous phase. This leads to a value of $\langle \eta^2 \rangle$ of 1.02×10^{-3} which gives a disagreement of ~20% between experiment and theory not uncommon in estimations of $\langle \eta^2 \rangle$. The disagreement for PCL is even higher, viz. ~30%. However, one needs to point out two aspects to qualify the above statements further. Firstly, if the incompatibility in the amorphous phase between PVC and PCL is indeed real then it must be so at a level which does not affect the glass transition behavior in order to be consistent with the work of Koleske,⁷ Ong¹⁰ and Bares.⁷³ This clearly points out the ambiguity in the very definition of "compatibility". Secondly, as shown in Fig. 50, a plot of the Porod slope k_2 versus composition shows a sudden upturn between 90/10 and PCL.

According to Luzatti and coworkers¹⁸⁹ the Porod slope (k_2) is a collective measure of all kinds of deviations from the ideal two phase

TABLE XIX

Comparison of Various Models for 90/10 (PCL/PVC)

$$\langle \eta^2 \rangle_{\text{Expt.}} = 0.77 \times 10^{-3} \text{ (mole elec./cc)}^2$$

Model	Cryst/AM	Cryst/AM/AM	Cryst/AM/AM
Phases	PCL/Mixed	PCL/PCL/PVC	PCL/Mixed/Mixed
Expression	$\phi_1 \phi_2 (\rho_1 - \rho_2)^2$	$\phi_1 \phi_2 (\rho_1 - \rho_2)^2 + \phi_2 \phi_3 (\rho_2 - \rho_3)^2 + \phi_3 \phi_1 (\rho_3 - \rho_2)^2$	
$\langle \eta^2 \rangle$ Model	0.21×10^{-3}	1.02×10^{-3}	0.77×10^{-3}
Remarks	underestimates	overestimates but probable	multiple possibilities for amorphous phase limiting volume fr.
			AM(1) AM(2)
			upper(PCL) .997 .332
			lower(PCL) .933 .062

model. These deviations could be inhomogeneity due to impurities, crystalline imperfections, nonuniformity of the amorphous phase, frozen in strains, etc. All these could cause excessive scattering in the tail of the profile and must be corrected for. In the case of PCL we have also seen the inability to characterize it very well microscopically. All this could be due to very high rates of crystallization which may be the reason for the rather disconcerting disagreement between its theoretical and experimental values of $\langle \eta^2 \rangle$. Therefore, one should not necessarily consider such a high discrepancy as characteristic of all the other compositions and consider the option of mixed amorphous phases for the crystalline compositions also as shown in Table XIX. The conclusions, as with the purely amorphous polymer, is that the amorphous phase involves a partially compatible mixture of at least two components, each of which consists of a mixture of the two components. The distribution of components cannot be uniquely determined on the basis of a comparison of experimental and theoretical values of $\langle \eta^2 \rangle$ but the range of compositions may be established.

It is evident from the conclusion from these comparisons of $\langle \eta^2 \rangle_{av}$ that the amorphous phases do not consist of pure components. Hence, the assumptions inherent in the resolution of ℓ_c into $\bar{\ell}_{PVC}$ and $\bar{\ell}_{PCL}$ are not valid. The best that can be done is to resolve ℓ_c into $\bar{\ell}_A$ and $\bar{\ell}_B$. However, this requires a knowledge of ϕ_A and ϕ_B which cannot be uniquely obtained from the invariant analysis. The same limitation is inherent in our treatment of the transition zone thickness.

C H A P T E R VI

SUMMARY AND CONCLUSIONS

The main theme of this work was to study the morphology of polymer blends using SAXS and SALS as the principal independent techniques and to correlate information between them as well as with other independent methods such as WAXD, SEM, DSC, optical microscopy and density measurements. The system chosen for the study was a blend of PCL and PVC across the entire compositional range, the same having been previously classified as "compatible" by the independent works of Koleske and Lundberg,⁷ and later by Price and Ong.¹⁰

Insofar as the observance of a single glass transition was reported by both the above groups, the system is undoubtedly compatible and exceptionally so in view of the fact that some of the compositions are crystalline whereas crystallinity inherently implies phase separation. A single T_g , however, is necessary but not a sufficient condition for compatibility, since systems that respond as compatible by the criteria of one technique are not necessarily so by another.³⁵

The estimation of "scattering power" using absolute intensities for SAXS indicate that neither complete segregation of phases (i.e., incompatibility) nor complete mixing at the segmental level (i.e., compatibility) occurs for any of the compositions across the entire range from PCL to PVC. The most favored possibility is that for mixed phases that coexist with diffuse transition zones in the amorphous state. Thus

the measurement of scattering power becomes a very powerful independent way of studying the state of mixing in a blended system.

SAXS analysis also shows that there can be several possibilities for such mixing to occur viz., the composition and sizes of the domains could cover a large spectrum. Since mixed domains are favored, the existence of diffuse transition zones established from SAXS analysis in this work, becomes an even more acceptable reality. One can thus conceive of a morphology in which the electron density varies gradually from PCL rich areas to those rich in PVC and smear out any phase separation in the ideal sense. The observation of single glass transition temperatures is consistent with such a morphological model of limited compatibility, if the domains are sufficiently small.

✓ It is important to realize that for the analysis of small-angle x-ray data one needs other independent information in order to make the choice of any particular model as realistic as possible. This was done by analyzing the system by other supplementary techniques as mentioned before and also by using the results of others on the same system. Nevertheless, a convenient model is very often a compromise between "idealism" and "realism". The more realistic a model, the more complex it is likely to be and in order to make its application feasible one sacrifices some of its rigor to assumptions that can strictly be justified only for an ideal state of affairs. Thus, when data are analyzed by any particular model, the analysis will be dependent on the model's sophistication. With this in mind, more importance should be given to the relative trend in the analysis as the composition is varied rather than attach absolute significance to numerical values. Simply stated,

any change in model details will cause a corresponding change in numerical values but the trend should be preserved.

For the semi-crystalline compositions, the Tsvankin model, as modified by Buchanan, was applied. It is not completely rigorous and apriori assumption of certain parameters is necessary for its application. Nevertheless, it incorporates the main features of a semi-crystalline lamellar kind of morphology as evidenced by other independent techniques. In other words, it provides a good compromise and case of operation once the calibration curves have been evaluated. It is sophisticated enough to be sensitive to changing morphological details as the blend composition is varied. The increase in long period and one dimensional crystallinity are consistent with theoretical calculations. Refinement of the model should improve its utility. For example, for low values of crystallinities, such as the 60/40 and 50/50 compositions due to the rather poorly defined maxima which makes the evaluation of their position and breadth of reflections less precise, the analysis will contain a larger experimental error with consequent ambiguity in interpretation. However, under favorable circumstances when more than one order of reflection is present and the maxima are more well defined, this model can be used in conjunction with the analysis of Crist. This and the curve fitting method of Wenig and Kilian, along with independently obtained values of weight crystallinities, etc., give consistent and encouraging results.

For the analysis of amorphous morphologies, the models of Debye and Porod are much too ideal and better suited to incompatible systems where domains of pure phases separated by sharp boundaries, contribute

a higher electron density difference by not smearing it out over the morphology. The one dimensional Stein-Khambatta model is sound in principle and only assumes non-overlapping transition zones. In a densely packed system such as blends in the solid state with the domains within high proximity of each other and perhaps even interpenetrating each other, one can readily see that the transition zones associated with these domains can overlap. In fact, the application of the Stein-Khambatta model by virtue of its above assumption points out an important truth in our system viz., that for high enough concentrations of PCL, the system is densely packed and this aspect is in some measure responsible for the discrete but broad maxima seen in the amorphous compositions. Dense packing causes interparticle interference effects which can give rise to discrete scattering. This is thus consistent with other morphological evidence. Hence the failure of the Stein-Khambatta model in its inability to estimate correct values of ϕ_3 (internally consistent) for this particular system, is however beneficial in describing a related and important detail.

The fact that these maxima by a rough approximation of Bragg's equation, agree in trend and magnitude both with an analogous system studied by Geil²²⁰ and for a model of densely packed spherical gel particles for PVC whose centers get further apart as the PCL gets between them seems to ratify the model. Gel formation due to incomplete dissolution of PVC in the absence of any heating is thought to be cause for the anomalous scattering observed.

Bonart^{141,142} provides an elegant and very realistic approach towards analyzing systems with domains of mixed compositions having

diffuse as well as sharp boundaries. The analysis, however, needs rather precise data as the evaluation of transition zone thickness and percent diffuse boundaries is sensitive to small errors. It was mentioned that, due to the high mass absorption coefficient of PVC, a certain amount of precision had to be sacrificed, especially for data accumulated in the tail region of the curve. This is precisely the range of applicability of Bonart's analysis as it is in principle a more sophisticated version of Porod's law which was formulated for ideal systems. Hence, the values of Bonart's parameters, though once again useful to follow a trend, must be accepted with some reservations. However, in spite of this, the values of transition zone thicknesses are consistent with the theoretical predictions formulated for incompatible systems as found. A more rigorous application of Bonart's ideas is needed for a complete analysis which was not possible to accomplish in this thesis.

Coming to the application of SALS, agreement between the experimental and theoretical Rayleigh ratios within a factor of two is very encouraging, especially in view of the fact that previous efforts to correlate them in these laboratories had resulted in much wider disagreements. The fair agreement can be considered as a justification for the various correction procedures adopted, but it must simultaneously be pointed out that in view of the non-rigorous nature of some correction procedures as already discussed before, and also due to certain apriori assumptions during their application, the possibility of compensating errors cannot be ruled out. Nevertheless, the assumption of random

nucleation, the estimation of ϕ_s from X_{CR} and k_{BUCH} and the use of 2-dimensional disorder theory do not seem to cause any significant discrepancy.

While much remains to be done for a more thorough understanding of the morphology of blends, particularly those which exhibit partial to good compatibility, the application of SAXS and SALS in this study have served to prove them as indispensable tools of characterization. Not only have they proved their worth as independent techniques in providing information complimentary to each other and consistent with other techniques, but in so doing made it possible to compliment and extend previous research efforts on the same system.

C H A P T E R VII

SUGGESTIONS FOR FURTHER RESEARCH

The suggestions that follow are to a certain extent paradoxial because on the one hand, extension of work on the same system is advocated in order to complete the story on its morphology and on the other, the need to choose a simpler system for reasons of more precise interpretation of data is also emphasized. The former could be a major undertaking but so could the latter in view of the fact that much is already known about the PCL/PVC system.

Extension of work on PCL/PVC system:

1. It was mentioned that the raw experimental data was processed through a series of corrections before any analysis was undertaken. No mention was made of the background correction due to all other aspects of the morphology, except heterogeneity due to the mixing of two components and this needs to be done by subtracting out the amorphous scattering contributions of both PCL and PVC. Thus, ideally speaking

$$(I_{BL})_{CORRECT} = (I_{BL}) - (I_{PCL} \cdot W_{PCL} + I_{PVC} \cdot W_{PVC})$$

where I_{PCL} = scattering due to pure amorphous PCL

I_{PVC} = scattering due to pure amorphous PVC

W_i = weight fraction of component i for a given blend composition

I_{BL} = scattering due to blend as measured

I_{PCL} can be obtained by melting PCL and I_{PVC} can be obtained by casting PVC from a solution that was heated sufficiently long to dissolve PVC completely before casting. PVC cannot be melted at a high enough temperature unless it is thermally stabilized.

2. More intermediate compositions need to be studied for the following reasons.
 - (i) Between PCL and 90/10, an obvious change in both SAXS scattering and spherulite size takes place.
 - (ii) Between 60/40 and 40/60, the crystallinity drops very fast and the morphology transforms from truncated spherulites to amorphous via an intermediate non-volume-filling case. Thus, a few more compositions in this range should show the trend with better precision.
3. The very elegant method of Bonart should be carried to completion with the estimation of the damping factor and the corrected invariant as he advocates.
4. The semi-crystalline compositions should also be studied in the melt by SALS so as to study the effect of only the heterogeneities due to the two components in the absence of any crystallinity.
5. The three-dimensional disorder parameter calculations of Yoon and Chu must be applied and compared with the two-dimensional case.
6. The blends should be stretched and tested for affine deformation with respect to the various morphological details, using the photographic SALS technique.

7. A more rigorous calculation of the dynamic SALS apparatus is necessary in order to have better confidence in comparing Rayleigh ratios.
8. Even the amorphous blends should be studied by SALS so as to check for any macro-heterogeneity using the correlation function approach of Debye.
9. The blends should be also studied by the Kratky camera to extend this study to lower angles. It is not expected to yield any new information for the semi-crystalline morphologies but the same cannot be said apriori of the amorphous compositions.
10. The V_v theory of Yoon must also be applied to complement the photographic work done in this thesis, especially for compositions where the system is just beginning to become non-volume-filling. From values of the polarizability of the extra-spherulitic medium one could gain valuable information about the state of mixing and check the partial-mixing conclusions of this work for amorphous phases.
11. The Tsvankin-Buchanan approach should be more thoroughly checked with other kinds of model calculations. It would perhaps be very useful to obtain Vonk's computer program about his correlation function method and try it out. This is a much less ambiguous approach and should be quite expeditious on the new Cyber computer at the University of Massachusetts.
12. Both the Weighting Function Program and the Desmearing Program should be converted for use on the Cyber computer.

13. Some more SEM work would be helpful, especially using the EDAX for non-volume-filling compositions.

Choosing an alternate system:

1. Since PCL/PVC is a rather compatible system, the evaluation of certain parameters is blurred as they are not morphologically well defined in the system, e.g., the thickness of the transition zone. A system known to be incompatible by other techniques and one which yet has a sufficient electron density difference should be adopted for testing some of the theoretical aspects before being applied to compatible systems.
2. Even if homogeneous PVC samples can be made, the high absorption coefficient due to the Cl atoms cuts down the already low intensity due to collimation. One way around it could be to run PVC rich samples using the much longer slits of the Kratky camera in order to get a higher precision in measurement.
3. The PMMA/PVF₂ and PEMA/PVF₂ systems are very analogous to PCL/PVC in that the PVF₂ crystallizes and the acrylates do not. The electron density difference is very favorable and the absorption coefficient is low. Besides the acrylates are not known to form gels unlike PVC. These systems are industrially very important and should be looked into.

APPENDIX I

LORENTZ FACTOR

In conventional wide-angle x-ray diffraction work, the Lorentz correction is routinely done in combination with the polarization correction and standard texts on WAXD have the composite Lorentz-Polarization factor listed in tables. In SAXS work, the polarization correction $\frac{(1 + \cos^2 2\theta)}{2}$ reduces to unity because of the small angles involved ($\cos^2 2\theta \approx 1$ for $2\theta \leq 2^\circ$) but the Lorentz correction has not been always applied in the correction of experimental data. There are some instances of its inclusion in SAXS analysis¹⁻⁷ and no apriori justification for its omission exists. There is reason to believe that this is due to two main reasons, viz.

- (i) If model calculations are not performed, but only general parameters such as $\langle \eta^2 \rangle$ and (O/V) are derived, then the correction need not be done as it is implicitly included⁸ in the theoretical formulations as shown by Guinier⁹ and Porod,¹⁰ i.e.,

$$Q = \int_0^\infty m^2 \cdot I(m) \, dm$$

contains m^2 as the Lorentz factor as is shown above and similarly for (O/V) .

- (ii) Its precise formulation is debated and many workers have preferred to avoid including any ambiguity that may result from its application.

In the analysis of discrete maxima, however, the position of the ones that are at the smallest angles are affected most by this correction. The peak position shifts to smaller long periods after the correction and the shift is proportional to the smallness of the angles and the breadth of the reflection. Thus, if reliable conclusions are to be drawn, this correction ought to be included after the desmearing operation, as its formalism makes no provision for inclusion of the profile distortion due to a slit geometry.

The Lorentz factor is a geometrical or trigonometrical factor which influences the intensity of the scattered beam. It is in reality a combination of three factors¹¹

$$\begin{aligned}\text{Lorentz factor} &= \left(\frac{1}{\sin 2\theta}\right)(\cos \theta)\left(\frac{1}{\sin 2\theta}\right) \\ &= \frac{1}{4\sin^2 \theta \cos \theta}\end{aligned}$$

For small 2θ , i.e., small θ , $\sin \theta \approx \theta$ and $\cos \theta \approx 1$ giving

$$\text{Lorentz factor} = \frac{1}{\theta^2}$$

(the constant 4 may be dropped).

Crist⁶ has given a much more rigorous derivation which leads to the same result and so have Hosemann and Bagchi¹² using the paracrystalline model approach.

Thus, the experimental intensities must be multiplied by θ^2 after the desmearing has been performed if slit collimation is used, i.e.,

$$\tilde{I}(2\theta)_{\text{OBS}} \rightarrow I(2\theta)_{\text{OBS}}$$

$$I(2\theta) = I(2\theta)_{\text{OBS}} \cdot \theta^2$$

For lattices in which the lateral dimensions are much larger than the identity period, the above formalism is rigorously correct.

References

1. Burmester, A. F., Ph.D. Thesis, Case Western Reserve University, (1970).
2. Vonk, C. G., and Kortleve, G., Kolloid Z. Z. Polym., 220, 19 (1967).
3. Fischer, E. W., Goddard, H. and Schmidt, G. F., Makromol. Chem., 118, 144 (1968).
4. Fulcher, K. U., Brown, D. S., and Wetton, R. E., J. Polym. Sci., C38, 315 (1972).
5. Brämer, R., and Kilian, H., Paper presented at IUPAC Symposium on Macromolecules, Helsinki, III-6, (1972).
6. Crist, B., and Morosoff, N., J. Polym. Sci., 11, 1023 (1973).
7. Wenig, W., Ph.D. Thesis, University of Ulm, W. Germany (1974).
8. Alexander, L. E., X-Ray Diffraction Methods in Polymer Science, Wiley-Interscience, New York, 1969, Ch. 5.
9. Guinier, A., and Fournet, G., Small-Angle Scattering of X-Rays, Wiley, New York, 1955, Ch. 2.
10. Porod, G., Kolloid -Z., 124, 83 (1951).

References (cont.)

11. Cullity, B. D., Elements of X-Ray Diffraction, Addison Wesley, 1967, Ch. 4.
12. Hosemann, R. and Bagchi, S. N., Direct Analysis of Diffraction by Matter, North Holland, Amsterdam, 1962, Ch. 12.

APPENDIX II

DESMEARING TECHNIQUES AND COMPUTER PROGRAM

As was mentioned already, in order to optimize the scattered intensity, a point-like primary beam often used for photographic SAXS is replaced by a line shaped beam instead. This affects the distribution of scattered intensities due to reasons explained before, and results in a distortion of the true profile. The true profile, however, can be recovered from the experimental one by a "desmearing operation" and several methods have been proposed.¹

From a mathematical point of view, the problem can be formulated as a deconvolution² which suggests the applicability of Fourier Transform methods. Mathematical treatments were proposed by Kranjc³ and Ruland.⁴ The methods are laborious involving a series of complex operations and Kratky, Porod and Skala⁵ have raised strong doubts about the possibilities of routinely applying them. Lake⁶ has proposed an iterative method whereby successive approximations of the true curve are "smeared" by inversion of the desmearing equation and the results then compared with the observed data. Dijkstra, Kortleve and Vonk⁷ on the other hand, approximate the observed scattering curve by an orthogonal (Fourier) series which is then easily differentiated. Schmidt and Hight⁸ outlined a fairly simple approach of avoiding the differentiation of the experimental curve by the method of integrating by parts. Among the more recent methods proposed is that of Strobl.⁹

A slit has finite dimensions in both height and breadth. When their ratio is very high, the slits are essentially infinitely long, e.g., the slits of a Kratky camera where the ratio is approximately 5000 (5 cm. long and 10 μ wide). For such a case, the experimental intensity $\tilde{I}(S)$ is related to the undistorted one by the Guinier-Fournet¹⁰ equation

$$\tilde{I}(S) = \int_0^{\infty} W(\phi) I \sqrt{(S^2 + \phi^2)} d\phi$$

where $W(\phi)$ is a weighing function, the form of which depends on the collimation geometry.¹ For infinitely long and narrow slits $W(\phi) = 1$ and the above equation can be appropriately solved.

The slits used in this work had a length to width ratio of approximately 100, i.e., they are of finite length relative to their breadth. For such systems $W(\phi)$ can often be approximated by a Gaussian function according to Kratky, Porod and Kahovec,¹¹ as

$$W(\phi) = \frac{2p}{\sqrt{\pi}} \exp(-p^2 \phi^2)$$

and

$$I(S) = - \frac{\exp(p^2 S^2)}{p \sqrt{\pi}} \int_0^{\infty} \frac{N'[S^2+t^2]^{1/2} dt}{(S^2+t^2)^{1/2}}$$

in which

$$N(S) = \tilde{I}(S) \exp(-p^2 S^2)$$

defines the intensity function of which N' is the first derivative.

The technique of calculating $I(S)$ from experimentally measured intensities $\tilde{I}(S)$ by a numerical method developed by Schmidt¹² is given below as PROGRAM SAXSC and the estimation of $W(\phi)$ is done by the method of Hendricks and Schmidt¹³ using PROGRAM WEIGHT. Both programs are for the CDC-3600 computer.*

References

1. Alexander, L. E., X-Ray Diffraction Methods in Polymer Science, Wiley-Interscience, New York, 1969.
2. Hosemann, R., Ergebn, Exakt. Naturw., 24, 142 (1951).
3. Kranjc, K., Acta Cryst., 7, 709 (1954).
4. Ruland, W., Acta Cryst., 17, 138 (1964).
5. Kratky, O., Porod, G., Skala, Z., Acta Phys., Austriaca, 13, 76 (1960).
6. Lake, J. A., Acta Cryst., 23, 191 (1967).
7. Dijkstra, A., Kortleve, G. and Vonk, G., Kolloid-Z. U.Z. Polymer, 210, 121 (1966).
8. Schmidt, P. W. and Hight, R. Jr., Acta Cryst., 13, 480 (1960).
9. Strobl, G., Acta Cryst., A26, 367 (1970).

*Ideally speaking, the desmearing operation should also include distortions due to the slit-width, but as a general rule for studies below 1000 Å in the angular range, this can be neglected as it was in this work.

References (cont.)

10. Guinier, and Fournet, Small Angle X-Ray Scattering, New York, Wiley (1955).
11. Kratky, O., Porod, G. and Kahovec, L., Z. Elektr. Chem., 55, 53 (1951).
12. Schmidt, P. W., Acta Cryst., 19, 938 (1965).
13. Hendricks and Schmidt, P., Acta Phys. Austriaca, 26, 97 (1967).

5.5A

01/31/73

PROGRAM MAIN

C		10
C		20
C		30
C	PROGRAM WEIGHT	40
C		50
C	R.W. HENDRICKS, AUTHOR	60
C		70
C	SEE ORNL-TM-1950	80
C	REVISION 2	90
C		100
C	SEPTEMBER 1, 1971	110
C		120
C		130
	DIMENSION BCD(4)	
	DIMENSION AANS(202), AMOMNT(202), APLTZ(5000), FHX(1001), FWZ(1001),	140
	IG(P), F(8), SD(8), SIMPY(1001), SIMPZ(1001), TD(8), UDIF(202), UA(96),	141
	2UAA(256), UB(96), UBB(256), UFE(6), UIF(16), UIO(16), UL(202), ULL(2),	142
	3UGO(6), USTORE(202), UUL(2), UVAL(202), WCE(1), WCE(8), WCO(8), WM(1),	143
	4WLU(202), WWU(202), WWUP(202), XANS(202), XAU(202), XBU(202), XIE(16),	144
	5XINT(1001), XIO(16), XMAXD(1), XMIND(1), XRAY(1001), XVAL(50), XWX(50),	145
	6XXF(6), YXD(6), ZANS(202), ZAU(202), ZBU(202), ZIE(4), ZINT(1001),	146
	7ZIO(4), ZJE(4), ZJO(4), ZVAL(50), ZWZ(50)	147
	INTEGER TITLE(80)	
	DATA (BCD=8HW W (U) ,6HW L (U) ,8H EFFECTI,8HVE)	
	DATA (BLANK=8H)	
	DATA (BLNK=609)	
5	FIRSTM=0.	200
	SECONDM=BLANK	210
	THIRDM=BLANK	220
	FRSTM=BLANK	230
	SCNDMM=BLANK	240
	THRDMM=BLANK	250
	IUAAA=0	260
	CALL TIMER(0)	270
	DO 10 I=1,80	280
10	TITLE(I)=BLNK	290
	READ(5,8000)TITLE	
	IF (EOF,5)600,11	
11	CONTINUE	
8000	FORMAT(80A1)	310
	READ(5,8005) M,N,NU,KK,JJ,IOUT,IFZ,IEX,NUMZ,NUMX,KOUT,IPLOT,ILNGTH	320
8005	FORMAT(13I5)	330
	ITWONU=10*(NU-1)	340
	TWONU=ITWONU	350
	ITONU=ITWONU+1	360
	DO 15 K=1,8	370
	SD(K)=BLANK	380
	TD(K)=BLANK	390
	H(K)=BLANK	400
	G(K)=BLANK	410
15	CONTINUE	420
	M2=2+K	430
	N2=2+N	440
	READ(5,8010)EL,ELO,WCE(1)	450
	WCO(1)=-WCE(1)	460

5,5A

01/31/73

```

8010 FORMAT(3F10.4)
      READ(5,8015)(SD(I),I=1,M2)
      READ(5,8015)(H(I),I=1,M2)
      READ(5,8015)(TD(J),J=1,N2)
      READ(5,8015)(G(J),J=1,N2)
8015 FORMAT(8F10.3)
C
C... TEST M AND N
C
      IF(M,LE,4) GO TO 20
      WRITE(6,8020)
8020 FORMAT(1H1,20X,'TOO MANY EDGES BETWEEN FOCAL SPOT AND SAMPLE'//)
      M=4
      M2=8
20   IF(N,LE,4) GO TO 25
      WRITE(6,8025)
8025 FORMAT(1H1,20X,'TOO MANY EDGES BETWEEN SAMPLE AND DETECTOR'//)
      N=4
      N2=8
C
C... SET UP FWZ ARRAY
C
25   IF(IFZ)30,60,30
30   READ(5,8030)(ZVAL(I),ZWZ(I),I=1,NUMZ)
8030 FORMAT(8F10.3)
      ZINCR=(ZVAL(NUMZ)-ZVAL(1))/TRONU
      SIMPZ(1)=ZVAL(1)
      DO 35 LA=2,ITONU
35   SIMPZ(LA)=SIMPZ(LA-1)+ZINCR
      DO 55 LA=1,ITONU
      DO 45 LO=1,NUMZ
      IF(SIMPZ(LA)-ZVAL(LO))50,40,45
40   FWZ(LA)=ZWZ(LO)
      GO TO 55
45   CONTINUE
50   FAX(LA)=YLAG(SIMPZ(LA),ZVAL,ZWZ,0,IFZ,NUMZ,IEC)
55   CONTINUE
      CALL SIMP(SIMPZ,FWZ,ZINT,ITONU)
C
C.... SET UP EWX ARRAY
C
60   IF(IEY)65,95,65
65   READ(5,8030)(XVAL(I),XWX(I),I=1,NUMX)
      XINCR=(XVAL(NUMX)-XVAL(1))/TRONU
      SIMPX(1)=XVAL(1)
      DO 70 LB=2,ITONU
70   SIMPX(LB)=SIMPX(LB-1)+XINCR
      DO 90 LB=1,ITONU
      DO 80 LP=1,NUMX
      IF(SIMPX(LB)-XVAL(LP))85,75,80
75   EXX(LB)=XWX(LP)
      GO TO 90
80   CONTINUE
85   FAX(LB)=YLAG(SIMPX(LB),XVAL,XWX,0,IEY,NUMX,IEC)
90   CONTINUE
C...

```


5.5A

01/31/73

```

C... LOOP ONE
C...
95  IFLAG=0
    DO 100 I=1,M
      NDX=2*I
      MDX=NDX-1
C
C... CHECK TO SEE THAT THE SD ARRAY CONTAINS PAIRS OF EDGES EQUIDISTANT
C... FROM THE SAMPLE PLANE TO THE I-TH EDGE, I=1,2,...,2*M
C
    IF(SD(MDX).EQ.SD(MDX-1))GO TO 100
    IFLAG=1
    WRITE(6,8035)
8035 FORMAT(1H1,3X,8HSD ARRAY///)
    WRITE(6,8040)MDX,SD(MDX),MDX,SD(MDX)
8040 FORMAT(1H ,3HSD(,13,34)= ,F10.5,10H*****ERROR/
13HSD(,13,34)= ,F10.5,10H*****ERROR)
100  CONTINUE
C
C... END LOOP ONE
C
C
C... START LOOP TWO
C
    DO 105 I=1,N
      NDX=2*I
      MDX=NDX-1
C
C... CHECK TO SEE THAT THE TD ARRAY CONTAINS PAIRS OF EDGES EQUIDISTANT
C... THE SAMPLE PLANE TO THE J-TH EDGE, J=1,2,...,2*N
C
    IF(TD(MDX).EQ.TD(MDX))GO TO 105
    IFLAG=1
    WRITE(6,8045)
8045 FORMAT(1H1,3X,8HTD ARRAY///)
    WRITE(6,8050)MDX,TD(MDX),MDX,TD(MDX)
8050 FORMAT(1H ,3HTD(,13,34)= ,F10.5,10H*****ERROR/1H ,
13HTD(,13,34)= ,F10.5,10H*****ERROR)
105  CONTINUE
C
C... END LOOP TWO
C
C... WERE ERRORS DISCOVERED IN THE SD AND/OR TD ARRAYS
C... IF YES, PROCESS THE NEXT CASE
    IF(IFLAG.EQ.1) GO TO 5
C
C... CALCULATE ALLOWABLE RANGE OF X VALUES
C
    JO=0
    DO 115 L=1,N
      LEVN=2*L
      LODD=LEVN-1
      DO 110 J=1,N
        IF(J.GE.L) GO TO 115
        JO=JO+1
        JEVN=2*J

```

5.5A

01/31/73

```

JODD=JEVN-1
WCO(JO)=-(G(LEVN)*(EL-TD(JODD))+G(JODD)*(EL-TD(LEVN)))/
1 (TD(LEVN)-TD(JODD))
110 WCE(JO)=(G(LDDO)*(EL-TD(JEVN))+G(JEVN)*(EL-TD(LDDO)))/
1 (TD(LDDO)-TD(JEVN))
115 CONTINUE
CALL SUBMAX(WCO,WCO,XMIN,JO,0)
CALL SUBMIN(WCE,WCE,XMAX,JO,0)
WM(1)=XMIN
WC(1)=XMAX
C
C... CALCULATE U(I,IPRIME) AND U(I,J)
C
NUM1=0
DO 120 I=1,M
DO 120 IP=1,M
IF(I.LE.IP) GO TO 120
NUM1=NUM1+1
LIE=2+I
LIO=LIE-1
LPE=2+IP
LPO=LPE-1
UEF(NUM1)= WM(1)/EL-((EL+SD(LPO))*H(LIE)+(EL+SD(LIE))*H(LPO))/
1 (EL*(SD(LIE)-SD(LPO)))
JOD(NUM1)= WC(1)/EL+((EL+SD(LPE))*H(LIO)+(EL+SD(LIO))*H(LPE))/
1 (EL*(SD(LIO)-SD(LPE)))
120 CONTINUE
NUMA=0
DO 125 I=1,M
DO 125 J=1,N
NUMA=NUMA+1
IEVN=2+I
IDD=IEVN-1
JEVN=2+J
JODD=JEVN-1
C1=SD(IDD)*(EL-TD(JEVN))
C2=SD(JEVN)*(EL-TD(JODD))
UIE(NUMA)= WC(1)*(SD(IDD)+TD(JEVN))/C1 + H(IDD)/SD(IDD) +
1 (EL+SD(IDD))*G(JEVN)/C1
125 UIE(NUMA)= WM(1)*(SD(JEVN)+TD(JODD))/C2 - H(JEVN)/SD(JEVN) -
1 (EL+SD(JEVN))*G(JODD)/C2
C
C... CALCULATE U(I,IPRIME,K,J) AND U(I,J,K,L)
C
NUM1JK=0
DO 135 I=1,M
IEVN=2+I
IDD=IEVN-1
DO 135 IP=1,M
IF(I.LE.IP) GO TO 135
IPEVN=2+IP
IPODD=IPEVN-1
CA=-(H(IEVN)*(EL+SD(IPODD))+H(IPODD)*(EL+SD(IEVN)))/
1 (SD(IEVN)-SD(IPODD))
CB=(H(IDD)*(EL+SD(IPEVN))+H(IPEVN)*(EL+SD(IDD)))/
1 (SD(IDD)-SD(IPEVN))

```

5.5A

01/31/73

```

DO 130 K=1,M
KEVN=2*K
KODD=KEVN-1
DO 130 J=1,N
JEVN=2*J
JODD=JEVN-1
NUMIJK=NUMIJK+1
CAA=-(H(KODD)*(EL-TD(JEVN))+G(JEVN)*(EL+SD(KODD)))
CBB=-(H(KEVN)*(EL-TD(JODD))+G(JODD)*(EL+SD(KEVN)))
C1=SD(KODD)+TD(JEVN)
C2=1./(TD(JEVN)*(EL+SD(KODD)))
C3=SD(KEVN)+TD(JODD)
C4=1./(TD(JODD)*(EL+SD(KEVN)))
UA(NUMIJK)=C1+C2*CA+C3+CAA
UB(NUMIJK)=C3+C4*CB+C4+CBB
130 CONTINUE
135 CONTINUE
NUMJKL=0
DO 155 I=1,M
IEVN=2*I
IODD=IEVN-1
DO 155 J=1,N
JEVN=2*J
JODD=JEVN-1
CA=-(H(IEVN)*(EL-TD(JODD))+G(JODD)*(EL+SD(IEVN)))
CB=-(H(IODD)*(EL-TD(JEVN))+G(JEVN)*(EL+SD(IODD)))
C1=SD(IEVN)+TD(JODD)
C2=SD(IODD)+TD(JEVN)
DO 155 K=1,M
KEVN=2*K
KODD=KEVN-1
DO 155 L=1,N
LEVN=2*L
LODD=LEVN-1
NUMJKL=NUMJKL+1
C3=SD(KODD)+TD(LEVN)
C4=SD(KEVN)+TD(LODD)
AIJKLA=SD(IEVN)*(EL-TD(JODD))*C3-SD(KODD)*(EL-TD(LEVN))*C1
IF(AIJKLA.LE.0.) GO TO 140
CAA=-(H(KODD)*(EL-TD(LEVN))+G(LEVN)*(EL+SD(KODD)))
UAA(NUMJKL)=(C3*CA+C1*CAA)/AIJKLA
GO TO 145
140 UAA(NUMJKL)=-999.
145 AIJKLB=SD(IODD)*(EL-TD(JEVN))*C4-SD(KEVN)*(EL-TD(LODD))*C2
IF(AIJKLB.LE.0.) GO TO 150
CBB=-(H(KEVN)*(EL-TD(LODD))+G(LODD)*(EL+SD(KEVN)))
UBB(NUMJKL)=(C4*CB+C2*CBB)/AIJKLB
GO TO 155
150 UBB(NUMJKL)=999.
155 CONTINUE
C
C... WRITE OUT INTERMEDIATE COMPUTATIONS
C
IF(KOUT.EQ.0) GO TO 160
WRITE(6,0055)
0055 FORMAT(1H1,20X,INTERMEDIATE COMPUTATIONS*//17X,NOTE THAT THESE D

```

5,5A

01/31/73

```

DATA ARE PRINTED*/21X,*PRIOR TO U-AXIS INVERSION*//)
WRITE(6,8050) NUMI
8060 FORMAT(1H0,20X,*UEE*,10X,*NUMI = *,15//)
WRITE(6,8065)(UEE(I),I=1,NUMI)
8065 FORMAT(2E14.6)
WRITE(6,8070) NUMA
8070 FORMAT(1H0,20X,*UIE*,10X,*NUMA = *,15//)
WRITE(6,8065)(UIE(I),I=1,NUMA)
WRITE(6,8075) NUMIJK
8075 FORMAT(1H0,20X,*UA*,10X,*NUMIJK = *,15//)
WRITE(6,8065)(UA(I),I=1,NUMIJK)
WRITE(6,8080) NUMJKL
8080 FORMAT(1H0,20X,*UAA*,10X,*NUMJKL = *,15//)
WRITE(6,8065)(UAA(I),I=1,NUMJKL)
WRITE(6,8085)
8085 FORMAT(1H0,20X,*UOO*/)
WRITE(6,8065)(UOO(I),I=1,NUMI)
WRITE(6,8090)
8090 FORMAT(1H0,20X,*UIO*/)
WRITE(6,8065)(UIO(I),I=1,NUMA)
WRITE(6,8095)
8095 FORMAT(1H0,20X,*UB*/)
WRITE(6,8065)(UB(I),I=1,NUMIJK)
WRITE(6,8100)
8100 FORMAT(1H0,20X,*UBB*/)
WRITE(6,8065)(UBB(I),I=1,NUMJKL)
C
C... CALCULATE UAAA AND UBBB
C
160 CALL SUBMAX(UA,UAA,ULL(1),NUMIJK,NUMJKL)
CALL SUBMIN(UB,UBB,UUL(1),NUMIJK,NUMJKL)
CALL SUBMAX(UIE,UEE,ULL(2),NUMA,NUMI)
CALL SUBMIN(UIO,UOO,UUL(2),NUMA,NUMI)
CALL SUBMAX(ULL,UA,UAAA,2,0)
CALL SUBMIN(UUL,UB,UBBB,2,0)
IF(UAAA.LT.UBBB) GO TO 165
IUAAA=1
GO TO 350
165 UINC=(UBBB-UAAA)/FLOAT(NU-1)
C
C.... START U LOOP
C
C2=EL+ELO
DO 330 L=1,NU
UVAL(L)=UAAA+FLOAT(L-1)*UINC
C
C... CALCULATE x(I,IPRIME)
C
I00=0
DO 170 I=1,M
DO 170 IP=1,M
IF(I.LE,IP) GO TO 170
I00=I00+1
LIE=2*I
LIO=LIE-1
LPE=2*IP

```


3.5A

01/31/73

```

LPO=LPE-1
XXO(100)=(EL*(SD(L10)-SD(LPE))*UVAL(L)+(EL+SD(LPE))*H(L10)
1      *(EL+SD(L10))*H(LPE))/(SD(L10)-SD(LPE))
XXE(100)=(EL*(SD(L1E)-SD(LPO))*UVAL(L)+(EL+SD(LPO))*H(L1E)
1      *(EL+SD(L1E))*H(LPO))/(SD(L1E)-SD(LPO))
170 CONTINUE
C
C... CALCULATE X(I,J)
C
IO=0
DO 175 I=1,M
DO 175 J=1,N
IO=IO+1
IXE=2*I
IXO=IXE-1
JXE=2*J
JXO=JXE-1
XIE(10)=(EL-TD(JXO))*SD(IXE)+UVAL(L)+H(IXE)*(EL-TD(JXO))+G(JXO)*
1(EL+SD(IXE))/(SD(IXE)+TD(JXO))
175 XIO(10)=(EL-TD(JXE))*SD(IXO)+UVAL(L)+H(IXO)*(EL-TD(JXE))-G(JXE)*
1(EL+SD(IXO))/(SD(IXO)+TD(JXE))
C
C... CALCULATE XB(U) AND XA(U)
C
CALL SUBMIN(XIE,XXE,XMIN,10,100)
CALL SUBMAX(XIO,XXO,XMAX,10,100)
XMIND(1)=XMIN
XMAXD(1)=XMAX
CALL SUBMAX(XMAXD,WM,XAU1,1,1)
CALL SUBMIN(XMIND,WC,XBU1,1,1)
XBU(L)=XBU1
XAU(L)=XAU1
XINC=(XBU(L)-XAU(L))/FLOAT(MU-1)
C
C..... START X LOOP
C
DO 270 MM=1,MU
XRAY(MM)=XAU(L)+FLOAT(MM-1)*XINC
IE=0
C1=EL*UVAL(L)-XRAY(MM)
C
C... CALCULATE Z(I)
C
DO 180 I=1,M
IE=IE+1
IEVN=2*I
IODD=IEVN-1
ZIC(IE)=(EL0-SD(IODD))*C1+C2*H(IODD)/(EL+SD(IODD))
180 ZIE(IE)=(EL0-SD(IEVN))*C1-C2*H(IEVN)/(EL+SD(IEVN))
C
C... CALCULATE Z(J)
C
JE=0
C1=EL0*UVAL(L)
DO 185 J=1,N
JE=JE+1

```

5,5A

01/31/73

```

      JEVN=2*J
      JODD=JEVN-1
      ZJO(JE)=C1-((ELD+TD(JODD))*XRAY(MH)-C2*G(JODD))/(EL-TD(JODD))
185  ZJE(JE)=C1-((ELD+TD(JEVN))*XRAY(MH)+C2*G(JEVN))/(EL-TD(JEVN))
C
CALCULATE ZB(X,U) AND ZA(X,U)
C
      CALL SUBMIN(ZIO,ZJO,ZBOI,IE,JE)
      CALL SUBMAX(ZIE,ZJE,ZAOI,IE,JE)
      ZBO(MH)=ZBOI
      ZAO(MH)=ZAOI
C
C.....DO Z INTEGRATION
C
      IF(IFZ) 190,265,190
190  IF(ZAU(MH).GE.SIMPZ(1).AND.
1  ZAU(MH).LE.SIMPZ(1TONU)) GO TO 195
      WRITE(6,8105)
8105 FORMAT(1H0,20X,*ZAU OUT OF RANGE OF ZVAL INPUT*/
1  20X,*TERMINATE PROCESSING*//)
      GO TO 5
195  IF(ZRU(MH).GE.SIMPZ(1).AND.
1  ZRU(MH).LE.SIMPZ(1TONU)) GO TO 200
      WRITE(6,8110)
8110 FORMAT(1H0,20X,*ZRU OUT OF RANGE OF ZVAL INPUT*/
1  20X,*TERMINATE PROCESSING*//)
      GO TO 5
200  AREAB=0.
      AREAT=0.
      IF(ZAU(MH)-SIMPZ(1))205,205,210
205  IF(ZRU(MH)-SIMPZ(1TONU))230,260,260
210  DO 220 INTB=2,1TONU
      IF(ZAU(MH)-SIMPZ(INTB))215,225,220
215  FWZINB=FWZ(INTB-1)+(ZAU(MH)-SIMPZ(INTB-1))*(FWZ(INTB)+FWZ(INTB-1))
1/ZINCR
      AREAB=0.5*(SIMPZ(INTB)-ZAU(MH))*(FWZ(INTB)+FWZINB)
      GO TO 225
220  CONTINUE
225  IINTB=INTB
      GO TO 235
230  IINTB=1
235  DO 245 INTT=IINTB,1TONU
      IF(ZBU(MH)-SIMPZ(INTT))240,250,245
240  FWZINT=FWZ(INTT-1)+(ZBU(MH)-SIMPZ(INTT-1))*(FWZ(INTT)+FWZ(INTT-1))
1/ZINCR
      AREAT=0.5*(ZBU(MH)-SIMPZ(INTT-1))*(FWZ(INTT-1)+FWZINT)
      GO TO 255
245  CONTINUE
250  AREAT=ZINT(INTT)-ZINT(INTT-1)
255  ZANS(MH)=ZINT(INTT-1)-ZINT(INTB)+AREAB+AREAT
      GO TO 270
260  ZANS(MH)=ZINT(1TONU)
      GO TO 270
265  ZANS(MH)=ZBU(MH)-ZAU(MH)
270  CONTINUE
C

```

5.5A

01/31/73

```

C.....END X LOOP
C
C.....DO X INTEGRATION
C
      IF(IFX)275,305,275
275 DO 300 MM=1,NU
      IF(XRAY(MM) .GE. SIMPX(1) .AND.
1 XRAY(MM) .LE. SIMPX(ITONU)) GO TO 280
      WRITE(6,6115)
8115 FORMAT(1H0,20X,'XRAY OUT OF RANGE OF XVAL INPUT*//
1 20X,'TERMINATE PROCESSING*//)
      GO TO 5
280 IF(XRAY(MM)-SIMPX(1))285,290,290
285 XINT(MM)=0.
      GO TO 300
290 IF(XRAY(MM)-SIMPX(ITONU))295,295,285
295 XINT(MM)=ZANS(MM)*YLAG(XRAY(MM),SIMPX,EWX,0,2,ITONU,IEC)
300 CONTINUE
      GO TO 315
305 DO 310 I=1,NU
310 XINT(I)=ZANS(I)
C
C....WRITE INTERMEDIATE COMPUTATIONS
C
315 IF(KOUT)320,325,320
320 WRITE(6,6120)UVAL(L),XAU(L),XBU(L),(ZAU(ML),ZBU(ML),ZANS(ML),XINT(
1ML),ML=1,NU)
8120 FORMAT(1H1,3H1U=,F9.5,5X,4HXAU=,E14,6,5X,4HXBU=,E14,6,3X,2(3HZAU,
111X,3HZBU,11X,4HZANS,10X,4HXINT,10X)/(1X,8E14,6))
C
C.... CALCULATE UNNORMALIZED WW(U)
C
325 CALL SIMP(XRAY,XINT,XANS,NU)
      WWUP(L)=XANS(NU)*EL*ELO/(EL+ELO)
C
330 CONTINUE
C
C.....END U LOOP
C
C.... CALCULATE AW (NORMALIZATION FACTOR)
C
      CALL SIMP(UVAL,WWUP,AANS,NU)
      IF(AANS(NU) .NE. 0.) GO TO 335
      WRITE(6,6125)
8125 FORMAT(1H0,20X,'AANS(NU) = 0.*//)
      GO TO 5
C
C....CALCULATE NORMALIZED WW(U) AND CONVERT TO MILLIRADIANS
C
335 AW=AANS(NU)
      DO 340 L=1,NU
      WWU(L)=WWUP(L)*0.001/AW
      IF(WWU(L) .LT. 0.) WWU(L)=0.
      UVAL(L)=1000.*UVAL(L)
340 CONTINUE

```

5,5A

01/31/73

```

C
C... INVERT U-AXIS
C
      JM=NU/2
      TEMP=-1000.*U888
      U888=-1000.*UAAA
      UAAA=TEMP
      DO 345 L=1,JM
      IU=NU-L+1
      TEMP1=-UVAL(L)
      UVAL(L)=-UVAL(IU)
      UVAL(IU)=TEMP1
      TEMP2=WMU(L)
      WMU(L)=WMU(IU)
      WMU(IU)=TEMP2
345   IF(MOD(NU,2).NE.0) UVAL(JM+1)=-UVAL(JM+1)
C
C... START PRINT-OUT
C
350   WRITE(6,8130)
8130  FORMAT(1H1,20X,*,INPUT DATA*//)
      IF(ILNGTH.EQ.0) GO TO 355
      WRITE(6,8135)
8135  FORMAT(1H0,8X,*,THIS IS A LENGTH WEIGHTING FUNCTION*//)
      GO TO 360
355   WRITE(6,8140)
8140  FORMAT(1H0,8X,*,THIS IS A WIDTH WEIGHTING FUNCTION*//)
360   WRITE(6,8145)M,N,NU,KK,JJ,IFZ,NUMZ,ICX,NUMX,ELO,EL,WCE(1),WM,WC
8145  FORMAT(1H0,5X,*,THERE ARE*,I2,*, PAIRS OF EDGES BETWEEN THE FOCAL SP
101  AND THE SAMPLE*/
2     8X,*,THERE ARE*,I2,*, PAIRS OF EDGES BETWEEN THE SAMPLE A
3ND THE DETECTOR*/
4     6X,I3,*, DATA POINTS WILL BE COMPUTED*/
5     6X,*,COMPUTE THE*,I2,*, MOMENT ABOUT THE ORIGIN*/
6     6X,*,COMPUTE THE*,I2,*, MOMENT ABOUT THE MEAN*/
7     6X,*,INTERPOLATION IN THE F(Z) ARRAY WILL BE BY A*,I2,*,
8POINT LAGRANGIAN*/
9     6X,*,THESE ARE*,I2,*, POINTS IN THE E(Z) ARRAY*/
9     6X,*,INTERPOLATION IN THE E(X) ARRAY WILL BE BY A*,I2,*,
9POINT LAGRANGIAN*/
9     6X,*,THESE ARE*,I2,*, POINTS IN THE E(X) ARRAY*/
9     6X,*,THE FOCAL SPOT TO SAMPLE DISTANCE IS*,F6,1,*, MM*/
9     6X,*,THE SAMPLE TO DETECTOR DISTANCE IS*,F6,1,*, MM*/
9     6X,*,THE RECEIVING SLIT WIDTH IS 2X*,F6,3,*, MM*/
9     6X,*,THE LOWER LIMIT OF X VALUES IS*,F6,3,*, MM*/
9     6X,*,THE UPPER LIMIT OF X VALUES IS*,F6,3,*, MM*//)
      WRITE(6,8150)
8150  FORMAT(1H0,2X,12H SUBSCRIPT I,10X,12H SUBSCRIPT J)
      WRITE(6,8155)(SD(I),TD(I),I=1,8),(H(I),G(I),I=1,8)
8155  FORMAT(1H0,
2(5HD(1)=,F7,3,11X)/2(6H D(2)=,F7,3,10X)/2(6H D(3)=
1,F7,3,10X)/2(6H D(4)=,F7,3,10X)/2(6H D(5)=,F7,3,10X)/2(6H D(6)=,F
27,3,10X)/2(6H D(7)=,F7,3,10X)/2(6H D(8)=,F7,3,10X)/2(6H H(1)=,F7,3
3,10X)/2(6H H(2)=,F7,3,10X)/2(6H H(3)=,F7,3,10X)/2(6H H(4)=,F7,3,10
4X)/2(6H H(5)=,F7,3,10X)/2(6H H(6)=,F7,3,10X)/2(6H H(7)=,F7,3,10X)/
52(6H H(8)=,F7,3,10X))
      IF(ICX)365,370,365

```


5.5A

01/31/73

```

365 CALL WOUT1(NUMX,XVAL,XX) 5040
370 IF(IF2)375,380,375 5050
375 CALL WOUT2(NUMZ,ZVAL,ZHZ) 5060
380 WRITE(6,8150) TITLE 5070
8160 FORMAT(1H1,20X,80A1,///) 5080
      IF(1UAAA.EQ.0) GO TO 385 5090
      WRITE(6,8155) 5100
8165 FORMAT(1H1,20X,*UAAA GREATER THAN UBRB*) 5110
      GO TO 5 5120
385 WRITE(6,8170) 5130
8170 FORMAT(1H ,10X,*WEIGHTING FUNCTION BEFORE SHIFT ABOUT FIRST MOMENT 5140
      1*///) 5141
      WRITE(6,8200) 5150
      NNU=NU/2 5160
      DO 8201 I=1,NNU
      J=I+NNU
      WRITE(6,8205)UVAL(I),WNU(I),UVAL(J),WNU(J)
8201 CONTINUE
      IF(MOD(NNU,2))390,395,390 5180
390 WRITE(6,8175) UVAL(NNU),WNU(NNU) 5190
8175 FORMAT(1P ,52X,F11.6,E13.5) 5200
395 WRITE(6,8180) AW 5210
8180 FORMAT(1P,24HNORMALIZATION FACTOR AW=,E13.5///) 5220
C 5230
C... CALCULATE MOMENTS ABOUT THE ORIGIN 5240
C 5250
      IF(KK) 430,430,400 5260
400 DO 425 MAP=1,KK 5270
      DO 405 LAP=1,NU 5280
405 USTORE(LAP)=(UVAL(LAP)+*MAP)*WNU(LAP) 5290
      CALL SIMP(UVAL,USTORE,AMOMNT,NU) 5300
      IF(MAP-2) 410,415,420 5310
410 FIRSTH=AMOMNT(NU) 5320
      GO TO 425 5330
415 SECONDH=AMOMNT(NU) 5340
      GO TO 425 5350
420 THIRDDH=AMOMNT(NU) 5360
425 CONTINUE 5370
C 5380
C... CALCULATE MOMENTS ABOUT THE MEAN 5390
C 5400
430 IF(JJ) 465,465,435 5410
435 DO 460 MAP=1,JJ 5420
      DO 440 LAP=1,NU 5430
440 UDIF(LAP)=((UVAL(LAP)-FIRSTH)+*MAP)*WNU(LAP) 5440
      CALL SIMP(UVAL,UDIF,AMOMNT,NU) 5450
      IF(MAP-2) 445,450,455 5460
445 FRSTHH=AMOMNT(NU) 5470
      GO TO 460 5480
450 SCNDHH=AMOMNT(NU) 5490
      GO TO 460 5500
455 THRDHH=AMOMNT(NU) 5510
460 CONTINUE 5520
465 DO 470 I=1,NU 5530
470 UVAL(I)=UVAL(I)-FIRSTH 5540
      IF(IOUT) 475,430,475 5550

```

5,5A

01/31/73

```

475 WRITE(7,8185) NU, AW
8185 FORMAT(15,E20.8)
WRITE(7,8190) (UVAL(I),WWU(I),I=1,NU)
8190 FORMAT(2E20.8,40X)
480 IF(KK,20,0) GO TO 495
WRITE(6,8150) TITLE
WRITE(6,8195)
8195 FORMAT(1H,10X,WEIGHTING FUNCTION AFTER SHIFT ABOUT FIRST MOMENT
1.////)
WRITE(6,8200)
8200 FORMAT(1H0,4X,2H U,7X,6H WW(U),37X,2H U,7X,6H WW(U)///)
DO 8202 I=1,NU
J=I+NU
WRITE(6,8205)UVAL(I),WWU(I),UVAL(J),WWU(J)
8202 CONTINUE
8205 FORMAT(1H,F11.6,E13.5,28X,F11.6,E13.5)
IF(MOD(U,2))485,490,485
485 WRITE(6,8175) UVAL(NU),WWU(NU)
490 WRITE(6,8190) AW
495 IF(ILNGTH,NE,0) GO TO 520
IF(KK) 500,590,500
500 WRITE(6,8210)FIRSTM,SECONDM,THIRDM
8210 FORMAT(1H0,40HMENTS OF THE FUNCTION ABOUT THE ORIGIN///1X,5H1ST
1E15.5,10X,5H2ND =,E15.5,10X,5H3RD =,E15.5)
DO 505 I=1,NU
II=NU+1-I
IF(WWU(II),NE,0) GO TO 510
505 CONTINUE
510 RESOLV=1.5417/(UVAL(II)+0.001)
WRITE(6,8215) RESOLV, UVAL(II)
8215 FORMAT(1H0,THEORETICAL LIMIT OF RESOLUTION =,F10.1,*, ANG.*/
1
OR = *,F10.2,*, MR.*///)
IF(JJ) 515,590,515
515 WRITE(6,8220)FIRSTM,SECONDM,THIRDM
8220 FORMAT(1H0,36HMENTS OF THE FUNCTION ABOUT THE MEAN///1X,5H1ST =,
1E15.5,10X,5H2ND =,E15.5,10X,5H3RD =,E15.5)
GO TO 590
C
C... COMPUTE EFFECTIVE SLIT-LENGTH WEIGHTING FUNCTION
C
520 IF(ILNGTH,NE,1) GO TO 590
IF(-UAAA,GT,U333) GO TO 525
DELU=U333/LOAT(NU-1)
GO TO 530
525 DELU=-UAAA/LOAT(NU-1)
530 DO 555 L=1,NU
UL(L)=LOAT(L-1)*DELU
IF(UL(L),GT,U333) GO TO 535
TEMP1=YL4G(UL(L),UVAL,WWU,0.3,NU,IEC)
GO TO 540
535 TEMP1=0.
540 IF(-UL(L),LT,UAAA) GO TO 545
TEMP2=YL4G(-UL(L),UVAL,WWU,0.3,NU,IEC)
GO TO 550
545 TEMP2=0.
550 WLU(L)=(TEMP1+TEMP2)/2.

```

5.5A

01/31/73

```

-----
IF(WLU(L) .LT. 0.) WLU(L)=0.
555 CONTINUE
IF(IOUT) 560,565,560
560 WRITE(7,8195) NU,AW
WRITE(7,8196)(UL(I),WLU(I),I=1,NU)
565 WRITE(6,8225)
8225 FORMAT(1H1,20X,'EFFECTIVE SLIT-LENGTH WEIGHTING FUNCTION*//')
WRITE(6,8200)
DO 8203 I=1,NUU
J=I+NUU
WRITE(6,8205)UL(I),WLU(I),UL(J),WLU(J)
8203 CONTINUE
IF(MOD(NU,2)) 570,575,570
570 WRITE(6,8175)UL(NU),WLU(NU)
575 C1=WLU(1)+0.99
DO 580 L=1,NU
II=L
IF(WLU(L) .LT. C1) GO TO 585
580 CONTINUE
585 WRITE(6,8230) UL(II)
8230 FORMAT(1H0,'THEORETICAL LIMIT OF RESOLUTION*//
1 * IN THE INFINITE BEAM APPROX = *,F6.2,* MR*//')
590 CALL TIMER(1)
IF(IPLT .EQ. 0) GO TO 5
IF(IPLT .LT. 0) GO TO 595
CALL PLOTS(APLTZ,5000)
IPLT=-IPLT
595 CALL LINE(-NU,1,0VAL,1,.07,WLU)
CALL SYMBOL(1.0,10.6,0.14,TITLE(1),0.0,80)
CALL SYMBOL(5.0,0.1,0.14,16HU (MILLIRADIANS),0.0,16)
N=1
IF(ILNGTH .NE. 0) N=2
CALL SYMBOL(0.0,4.0,0.14,BCD(N),90.0,8)
CALL PLOT7525(13.0,0.0,0,-3)
IF(ILNGTH .NE. 1) GO TO 5
CALL LINE(-NU,1,UL,1,.07,WLU)
CALL SYMBOL(1.0,10.6,0.14,TITLE(1),0.0,80)
CALL SYMBOL(5.0,0.1,0.14,16HU (MILLIRADIANS),0.0,16)
CALL SYMBOL(0.0,4.0,0.14,BCD(2),90.0,24)
CALL PLOT7525(13.0,0.0,0,-3)
GO TO 5
600 STOP
END

```


5.5A

12/19/74

PROGRAM SAXSC

SLIT-LENGTH-COLLIMATION-CORRECTION-FOR-GAUSSIAN-WEIGHTING-FUNCTION
(REVISED MARCH, 1969)

THIS PROGRAM SAXSC IS USED FOR CORRECTING SMALL ANGLE X-RAY SCATTERING INTENSITY FROM A FINITE SLIT SYSTEM WITH A GAUSSIAN WEIGHTING FUNCTION. THE USER IS REFERRED TO (P.W. SCHMIDT, ACTA CRYSTA. 19, 938 (1969)) FOR THE PROCEDURE AND INPUT DATA ARE EXPLAINED AS FOLLOWS. THE ANGULAR INCREMENT IS A MILLIRADIANS. THE INTENSITY VALUES $F(I)$ ARE GIVEN FOR SCATTERING ANGLES FROM A THROUGH $A+IMAX$, (THE FORTRAN SYMBOL $*$ WILL BE USED TO DENOTE MULTIPLICATION, ZEROES ARE USED FOR $F(I)$ FOR INTENSITIES AT WHICH EXPERIMENTAL DATA ARE NOT AVAILABLE.) FIVE INTENSITY VALUES ARE PUT ON EACH CARD IN (5E11.4) FORMAT. THE PROGRAM CALCULATES CORRECTED INTENSITIES FROM $J0+A$ MILLIRADIANS THROUGH $N1+A$ MILLIRADIANS WITH AN ANGULAR INCREMENT $N2+A$ MILLIRADIANS. CORRECTED INTENSITIES ARE COMPUTED NEXT FROM $(N1+N4)+A$ MILLIRADIANS THROUGH $N3+A$ MILLIRADIANS WITH AN INCREMENT $N4+A$, AND THEN FROM $(N3+N6)+A$ MILLIRADIANS THROUGH $N5+A$ MILLIRADIANS WITH AN INCREMENT $N6+A$, PROVIDED $N5$ DOES NOT EXCEED $IMAX$, CORRECTED INTENSITIES ARE NOT CALCULATED FOR ANGLES EXCEEDING $IMAX+A$ MILLIRADIANS, REGARDLESS OF THE VALUES OF THE NUMBERS ON CARD 3 BELOW. (THIS $IMAX$ VALUE IS THE VALUE FOR THE CURVE BEING CORRECTED.)

IN THE USE OF THIS PROGRAM, THE CARDS ARE ARRANGED AS FOLLOWS:

CARD 1. A

CARD 2. $J0$ AND $IMAX$, (THE VALUE OF $J0$ ON THIS CARD MUST EQUAL THE SMALLEST $J0$ VALUE USED WITH ANY OF THE SCATTERING CURVES BEING CORRECTED; THE $IMAX$ VALUE ON THIS CARD MUST EQUAL THE LARGEST $IMAX$ VALUE USED FOR ANY OF THE CURVES BEING CORRECTED.)

CARD 3. $N1, N2, N3, N4, N5, N6$

CARD 4. $J0$ AND $IMAX$ FOR THE FIRST CURVE

CARD 5. THE FIRST CARD OF THE SET OF CARDS WITH THE INTENSITIES $F(I)$

THE OTHER CARDS FOR THIS CURVE THEN FOLLOW. FOR EXAMPLE, IF THERE ARE 60 $F(I)$ IN THE FIRST CURVE, $IMAX = 80$, AND THERE 16 CARDS IN THE SET, FOR EACH SUCCEEDING CURVE, THE SET OF $F(I)$ CARDS IS PRECEDED BY A CARD GIVING $J0$ AND $IMAX$ FOR THIS CURVE.

AFTER THE LAST CURVE HAS BEEN CORRECTED, THE COMPUTER GIVES A STATEMENT INDICATING THAT THE END OF THE DATA HAS BEEN REACHED.

USUALLY IT IS MOST CONVENIENT TO HAVE THE VALUES OF $N3$ AND $N5$ BE AT LEAST AS LARGE AS $N1$ AND $N3$, RESPECTIVELY, WITH $N2$ AND $N4$ BEING NO LESS THAN $N4$ AND $N6$, RESPECTIVELY. HOWEVER, THESE CONDITIONS ARE NOT NECESSARY. FOR EXAMPLE: IF CORRECTED VALUES ARE DESIRED ONLY FOR A SINGLE ANGULAR INCREMENT, THE APPROPRIATE VALUES OF $N1$ AND $N2$ CAN BE CHOSEN, AND $N3, N4, N5$, AND $N6$ CAN ALL BE SET EQUAL TO ZERO, OR THESE POSITIONS CAN BE LEFT BLANK ON CARD 3.

THE LARGEST VALUES ALLOWED FOR THE NUMBERS ON CARDS 2, 3, AND 4 ARE DETERMINED BY THE DIMENSION STATEMENT AT THE BEGINNING OF THE PROGRAM. (THIS STATEMENT CAN BE CHANGED WHEN NECESSARY.) NO $IMAX$ VALUE ON CARDS 2 OR 4 CAN EXCEED 400, AND NO INPUT CURVES CAN HAVE MORE THAN 400 DATA POINTS, ACCORDING TO THE DIMENSION STATEMENT USED IN THIS PROGRAM. WITH THE NUMBER 50 USED IN THE SECOND SUBSCRIPT OF $T(1, J0)$ IN THE DIMENSION STATEMENT, CORRECTED INTENSITIES CAN BE CALCULATED AT UP TO 50 ANGLES. THE ANGLES AT WHICH CORRECTED DATA ARE OBTAINED ARE SPECIFIED BY THE NUMBERS ON CARDS 2, 3, AND 4.

THE WIDTH OF THE GAUSSIAN WEIGHTING FUNCTION IS DETERMINED BY THE

5,5A

12/19/74

C CONSTANT SL DEFINED EARLY IN THE PROGRAM, FOR A BEEMAN-TYPE FOUR-SLIT
 C COLLIMATION SYSTEM WITH 50 CM. BETWEEN SUCCESSIVE SLITS AND WITH THE X-
 C RAY BEAM UNIFORMLY ILLUMINATING THE ENTIRE LENGTH OF THE ENTRANCE SLIT, SL
 C IS EQUAL TO THE SLIT LENGTH IN CENTIMETERS. THE CONSTANT SL MUST BE SPEC-
 C IFIED FOR EACH SLIT SETTING FOR WHICH CORRECTIONS ARE CALCULATED.
 C IN OUR CASES, THE WIDTH OF THE GAUSSIAN WEIGHTING FUNCTION IS
 C THEORETICALLY CALCULATED BY THE METHOD REPORTED BY R.W. HENDRICKS AND P.W.
 C SCHMIDT (1966). WE HAVE A SEPARATED PROGRAM CALLED WEIGHT FOR THIS
 C CALCULATION.
 C THE CONSTANTS L0, L1, AND L2 IN THE INPUT AND OUTPUT STATEMENTS MUST
 C BE DEFINED AT THE BEGINNING OF THE PROGRAM,
 C IN STEP 103. ALOG IS A NATURAL LOGARITHM. THIS NOTATION MAY HAVE TO
 C BE CHANGED FOR SOME COMPUTERS.
 C ***2 BANKS ARE REQUIRED FOR UNASS SYSTEM***

C
 C COMPUTATION OF LEAST SQUARES FIT TO
 C DIMENSION T(220,100), F(200)
 C DOUBLE PRECISION SL, PDELH, SCPI, A, SJ1(220), SJ2(220),
 C 1 SJ3(220), B, C, D, F, DD, EE, F, UIJ, V32IJ, V33IJ,
 C 2 T31IJ, DEL51, DEL52, DEL53, DEL42, VV
 C L0=60
 C L1=61
 C L2=62
 C PDELH = 0.0096600
 C SCPI = 1.77245385100
 C 1 FORMAT(F6,4)
 C 2 FORMAT(2I4)
 C 3 FORMAT(6I4)
 C 4 FORMAT(1H1,4X,10HANGLE(RAD),9X,10HANGLE(DEG),8X,14HCORRECTED INT.,
 C 19X,14HMEASURED INT.,7X,9HTHEFA SC.,7X,10HDEBYF INT.,7X,
 C 17HLORENTZ,7)
 C 5 FORMAT(5H11,4)
 C 6 FORMAT(1X,F12,6,8X,F12,6,4X,E20,8,2X,E18,6,6X,F13,4,4X,E14,4,4X,
 C 1F12,4,4)
 C 7 FORMAT(5X,F10,6,E15,6,5X,F10,6,2F15,6)
 C READ (L0,1) A
 C READ (L0,2) J0, IMAX
 C READ (L0,3) N1, N2, N3, N4, N5, N6
 C N = N1
 C NN = N2
 C J00 = J0
 C JJ = 0
 C 100 DO 105 J = J0, N, NN
 C IM = IMAX - J + 12
 C JJ = JJ + 1
 C DO 102 I = 6, 10
 C SJ1(I) = 0.0
 C SJ2(I) = 0.0
 C 102 SJ3(I) = 0.0
 C R = J
 C IM1 = IM + 1
 C DO 104 I = 11, IM1
 C C = 1 - 10
 C D = C * C - 2 * D * C * R
 C F = (C - 1 * D0) * (C - 1 * D0) + 2 * D0 * D * (C - 1 * D0)
 C DD = DSQRT(D)

FTN5,5A

12/19/74

```

      EF= DSORT(E)
103- SJ1(I)=PLOG((C+P+DD)/((C+P-1DD+FEA)
      SJ2(I)=(C+R-0.5DD)*SJ1(I)-DD+EF
104- SJ3(I)= 0.5DD*((C+B)**2-1DD/3DD+n.5DD*P**2)*SJ1(I)
      1 -0.75DD*(C+B)*DD+(0.75DD*(C+P)+0.25DD)*EE
      H=-A*-PDELH
      DO 105 I = 10, 1M
      C=-1-12
      U1J=DEXP(-(H*H)*(C+C+2DD*B+C))/(H*SOP1)
      V321J=SJ2(I-1DD)-2DD*SJ2(I-2DD)+SJ2(I-3DD)
      V331J=SJ3(I)-3DD*SJ3(I-1DD)+3DD*SJ3(I-2DD)-SJ3(I-3DD)
      T311J=U1J*(SJ1(I-1DD)-SJ1(I-2DD)+V321J+V331J)
      DEL51= SJ1(I+1DD)-5DD*SJ1(I)+1DD*SJ1(I-1DD)-1DD*SJ1(I-2DD)+5DD*
1- SJ1(I-3DD)-SJ1(I-4DD)
      DEL52 = SJ2(I+1DD)-5DD*SJ2(I)+1DD*SJ2(I-1DD)-1DD*SJ2(I-2DD)
1- +5DD*SJ2(I-3DD)-SJ2(I-4DD)
      DEL53=SJ3(I+1)-5DD*SJ3(I)+1DD*SJ3(I-1)-1DD*SJ3(I-2)
1- +5DD*SJ3(I-3)-SJ3(I-4)
      DEL42=SJ2(I)-4DD*SJ2(I-1)+6DD*SJ2(I-2)-4DD*SJ2(I-3)+SJ2(I-4)
      VV=-2DD*DEL51+DEL52+9DD*DEL42+2DD*DEL53
105 T(I,JJ) = T311J + (5.*U1J*VV)/126.
      IF (N=N3) 110,-111,-111
110 N = N3
      NN=N4
      JO = N1 + N4
      JO1=JJ-1
      GO TO 100
111 IF (N=N5) 112,-200,-200
112 N = N5
      NN=N6
      JO = N3 + N6
      JO2=JJ-1
      GO TO 100
C SLIT LENGTH CORRECTION
200 READ (L0,2) JO, IMAx
      WRITE (L1,4)
      READ (L0,5) (F(I), I = 1, IMAx)
      IF (JO=N1) 201, 204, 204
201 NN = N2
      JJ = (JO - JO0)/N2
      IF (N1 = IMAx) 202, 203, 203
202 N = N1
      GO TO 220
203 N = IMAx
      GO TO 220
204 IF (JO = N3) 205, 208, 208
205 NN = N4
      JJ = JO1 + (JO - N1)/N4
      IF (N3 = IMAx) 206, 207, 207
206 N = N3
      GO TO 220
207 N = IMAx
      GO TO 220
208 NN = N6
      JJ = JO2 + (JO - N3)/N6
      IF (N5 = IMAx) 209, 210, 210

```

FTN5,5A

12/19/74

```

      EE= DSQRT(E)
103 SJ1(I)=DLOG((C+B+D)/((C+B+D)+FE))
      SJ2(I)=(C+H-0.5D)*SJ1(I)-DE+EE
104 SJ3(I)= 0.5D*((C+B)**2-1D)/3D+0.5D*(B**2)*SJ1(I)
      1 -0.75D*(C+B)*D+(0.75D*(C+B)+0.25D)*EE
      H = A - PDELH
      DO 105 I = 10, 1H
      C = I - 12
      U1J=DEXP(-(H*H)*(C+C+2D*B+C))/(H*SOP1)
      V321J=SJ2(I-1D)-2D*SJ2(I-2D)+SJ2(I-3D)
      V331J=SJ3(I)-3D*SJ3(I-1D)+3D*SJ3(I-2D)-SJ3(I-3D)
      T311J=U1J*(SJ1(I-1D)-SJ1(I-2D)+V321J+V331J)
      DEL51= SJ1(I+1D)-5D*SJ1(I)+1D*SJ1(I-1D)-10D*SJ1(I-2D)+5D*
1 -SJ1(I-3D)-6J1(I-4D)
      DEL52 = SJ2(I+1D)= 5D*SJ2(I)+10D*SJ2(I-1D)-10D*SJ2(I-2D)
1 -+ 5D*SJ2(I-3D)-SJ2(I-4D)
      DEL53=SJ3(I+1)-5D*SJ3(I)+10D*SJ3(I-1)-10D*SJ3(I-2)
1 -+ 5D*SJ3(I-3)-SJ3(I-4)
      DEL42=SJ2(I)-4D*SJ2(I-1)+6D*SJ2(I-2)-4D*SJ2(I-3)+SJ2(I-4)
      VV=-2D*DEL51+DEL52+9D*DEL42+7D*DEL53
105 T(I,JJ) = T311J + (5.*U1J*VV)/126,
      IF (N - N3)-110,-111,-111
110 N = N3
      NN = N4
      J0 = N1 + N4
      J01 = JJ - 1
      GO TO 190
111 IF (N - N5)-112,-200,-200
112 N = N5
      NN = N6
      J0 = N3 + N6
      J02 = JJ - 1
      GO TO 190
C. SLIT LENGTH CORRECTION
200 READ (L0,2) J0, IMAx
      WRITE (L1,4)
      READ (L0,5) (F(I), I = 1, IMAx)
      IF (J0 - N1) 201, 204, 204
201 NN = N2
      JJ = (J0 - J00)/N2
      IF (N1 - IMAx) 202, 203, 203
202 N = N1
      GO TO 220
203 N = IMAx
      GO TO 220
204 IF (J0 - N3) 205, 208, 208
205 NN = N4
      JJ = J01 + (J0 - N1)/N4
      IF (N3 - IMAx) 206, 207, 207
206 N = N3
      GO TO 220
207 N = IMAx
      GO TO 220
208 NN = N6
      JJ = J02 + (J0 - N3)/N6
      IF (N5 - IMAx) 209, 210, 210

```

FTN5,5A

12/19/74

```

209 N = N5
   GO TO 220
210 N = IMAX
220 DO 230 J = J0, N, NN
   IMAX1 = IMAX + 12 = J
   JJ = JJ + 1
   SUM = 0.0
   DO 225 I = 10, IMAX1
   K = J + I - 12
225 SUM = SUM + F(K) * T(I, JJ)
   X = J
   X = .001 * A * X
   Y = X * 57.29578
   THETA = X / 2.
   THETASQ = THETA ** 2
   ACF = 2205.
   SUM = SUM * ACF
   ALORENTZ = THETASQ * SUM
   DERYF = 1. / (SQRT(SUM))
230 WRITE (L1, 6) X, Y, SUM, F(J), THETASQ, DERYF, ALORENTZ
   IF (N = IMAX) 251, 200, 200
251 IF (N = N3) 252, 261, 261
252 J0 = N1 + N4
   GO TO 205
261 IF (N = N5) 262, 200, 200
262 J0 = N3 + N6
   GO TO 208
END

```


APPENDIX III

EXPRESSION FOR SCATTERING POWER $\langle \eta^2 \rangle$ 1. Ideal 2-Phase Model

Phases homogeneous in their electron densities (ρ_i).

Phase boundary is sharp.

$$\begin{aligned} \eta &= \text{fluctuation in local electron density } (\rho_i) \text{ from average } (\bar{\rho}) \quad (1) \\ &= (\rho_i - \bar{\rho}) \end{aligned}$$

$$\bar{\rho} = \phi_1 \rho_1 + \phi_2 \rho_2 \quad (2)$$

ϕ_i = volume fraction of phase i.

$$\eta^2 = (\rho_i - \bar{\rho})^2 \quad (3)$$

$$\langle \eta^2 \rangle = \sum_i \phi_i (\rho_i - \bar{\rho})^2 \quad (4)$$

$$= \phi_1 (\rho_1 - \bar{\rho})^2 + \phi_2 (\rho_2 - \bar{\rho})^2$$

$$= \phi_1 (\rho_1 - \phi_1 \rho_1 - \phi_2 \rho_2)^2 + \phi_2 (\rho_2 - \phi_1 \rho_1 - \phi_2 \rho_2)^2$$

$$= \phi_1 [\rho_1 (1 - \phi_1) - \phi_2 \rho_2]^2 + \phi_2 [\rho_2 (1 - \phi_2) - \phi_1 \rho_1]^2$$

$$= \phi_1 [\rho_1 \phi_2 - \phi_2 \rho_2]^2 + \phi_2 [\phi_2 \rho_2 - \phi_1 \rho_1]^2$$

$$\begin{aligned}
&= \phi_1 \phi_2 [\rho_1 - \rho_2]^2 + \phi_2 \phi_2 [\rho_1 - \rho_2]^2 \\
&= \phi_1 \phi_2 [\rho_1 - \rho_2]^2
\end{aligned}
\tag{5}$$

2. 2-Phase Model with Diffuse Boundary

Electron density varies continuously across boundary

Assumptions: Both phases are homogeneous

Density gradient is linear

Density profile is trapezoidal

No overlap of transition zones (dilute dispersion
of domains in an otherwise dense system)

ϕ_1 = volume fraction of component 1 (starting composition)

ϕ_1' = volume fraction of phase 1 (homogeneous portion)

ϕ_3 = volume fraction of boundary layer

ϵ = thickness of transition zone

$$\phi_1' = \phi_1 - \phi_3/2 \text{ (linear gradient assumption)} \tag{6}$$

$$\text{Similarly } \phi_2' = \phi_2 - \phi_3/2 \tag{7}$$

$\rho_3(x)$ = density variation in transition zone in direction x

$$= \rho_1 + (\rho_2 - \rho_1)(x/\epsilon) \quad (8)$$

$$\begin{aligned} \langle \eta^2 \rangle &= \sum_i \phi_i (\rho_i - \bar{\rho})^2 \\ &= \phi_1' (\rho_1 - \bar{\rho})^2 + \phi_2' (\rho_2 - \bar{\rho})^2 = \phi_3 [\rho_3(x) - \bar{\rho}]^2 \end{aligned} \quad (9)$$

Using equation (8)

$$\begin{aligned} (\rho_3(x) - \bar{\rho}) &= \rho_1 + (\rho_2 - \rho_1)\left(\frac{x}{\epsilon}\right) - \phi_1 \rho_1 - \phi_2 \rho_2 \\ &= (\rho_2 - \rho_1)(x/\epsilon - \phi_2) \end{aligned} \quad (10)$$

$$\overline{(\rho_3(x) - \bar{\rho})^2} = (\rho_2 - \rho_1)^2 \frac{1}{\epsilon} \int_0^\epsilon \left(\frac{x}{\epsilon} - \phi_2\right)^2 dx \quad (11)$$

$$= (\rho_2 - \rho_1)^2 \frac{1}{\epsilon} \int_0^\epsilon \left(\frac{x^2}{\epsilon^2} + \phi_2^2 - \frac{2x\phi_2}{\epsilon}\right) dx$$

$$= \frac{(\rho_2 - \rho_1)^2}{\epsilon} \left[\frac{x^3}{3\epsilon^2} + \phi_2^2 x - \frac{2x^2\phi_2}{2\epsilon} \right]_0^\epsilon$$

$$= \frac{(\rho_2 - \rho_1)^2}{\epsilon} \left[\frac{1}{3} + \phi_2^2 - \phi_2 \right] \epsilon$$

$$= (\rho_2 - \rho_1)^2 \left[\frac{1}{3} - \phi_1 \phi_2 \right] \quad (12)$$

Substituting (12) into (9) gives

$$\langle \eta^2 \rangle = \phi_1' (\rho_1 - \bar{\rho})^2 + \phi_2' (\rho_2 - \bar{\rho})^2 + \phi_3 (\rho_2 - \rho_1)^2 \left(\frac{1}{3} - \phi_1 \phi_2 \right) \quad (13)$$

$$= (\rho_2 - \rho_1)^2 [\phi_1' \phi_2^2 + \phi_2' \phi_1^2] + \phi_3 (\rho_2 - \rho_1)^2 \left(\frac{1}{3} - \phi_1 \phi_2 \right)$$

$$= (\rho_2 - \rho_1)^2 \left[\left(\phi_1 - \frac{\phi_3}{2} \right) \phi_2^2 + \left(\phi_2 - \frac{\phi_3}{2} \right) \phi_1^2 + \phi_3 \left(\frac{1}{3} - \phi_1 \phi_2 \right) \right]$$

$$= (\rho_2 - \rho_1)^2 \left[\phi_1 \phi_2 - \frac{\phi_3}{6} \right] \quad (14)$$

APPENDIX IV

BONART'S ANALYSIS

The analysis of Bonart is based on the idea that for the estimation of "specific surface" values for phase separated systems, the values of k_1 as obtained from a simple application of the Porod-Luzzati plot does not suffice.

In the Porod-Luzzati plot the assumption is made that the phase boundary is sharp but that the phases are not very homogeneous and result in excess scattering at higher values of m . This is estimated as the constant k_2 by plotting $m^3 \cdot \tilde{I}(m)$ vs. m^3 and then subtracting the slope to give corrected values of intensity as $(\tilde{I}(m) - k_2)$. The intercept of the same plot is k_1 and appears in the "specific surface" (O/V) relationship as

$$\frac{O}{V} = \frac{8\pi}{\lambda a} \phi_1 \phi_2 \frac{k_1}{Q} \quad (1)$$

Underestimation of k_1 leads to low values of O/V and Bonart's method essentially helps to get more realistic values instead.

According to Bonart, a transition zone of finite thickness will also contribute to the total intensity but in a rather complicated manner. In a system with diffuse boundaries therefore, on applying the Porod-Luzzati plot, one is not estimating the constant k_1 but rather a combined parameter $D^2(m)k_1$ where $D^2(m)$ is a damping factor

and is not a constant unlike k_1 . For the very simplest case $D^2(m)$ can be considered to be a simple Gaussian function with $D^2(0) = 1$. However, this is not so for real systems in which both the sharp and diffuse boundaries can coexist. The sharp boundaries as before contribute a constant excess intensity which is not known unless their volume fraction D_∞^2 is known. The diffuse boundary contribution is lumped together as $(1 - D_\infty^2) G^2(m)$ where $G^2(m)$ is a Gaussian function given by

$$G^2(m) = \exp(-2\pi B^2 m^2 / \lambda^2 a^2) \quad (2)$$

and B is the thickness of the transition zone.

Thus, for the case of both kinds of boundaries occurring simultaneously in the same system, the more refined damping factor is written as

$$D^2(m) = D_\infty^2 + (1 - D_\infty^2) G^2(m) \quad (3)$$

$$D_\infty^2 = k_\infty / k_1 \text{ (as defined by Bonart)} \quad (4)$$

This says that the Porod-Luzzati intercept k_1 is indirectly obtainable from their plot and is equal to an intercept k_∞ divided by a constant D_∞^2 . Thus, if k_∞ and D_∞^2 can somehow be estimated, then that value of k_1 should be used in equation (1) for estimating (O/V) .

This is done as follows:

$$\text{Porod's law} \quad \tilde{I}(m) \xrightarrow{m \rightarrow \infty} \frac{k_1}{3m} \quad (5)$$

Porod-Luzzati combination $\tilde{I}(m) \xrightarrow{m \rightarrow \infty} \frac{k_1}{3} + k_2$

Porod-Luzzati-Bonart combination $\tilde{I}(m) \xrightarrow{m \rightarrow \infty} \frac{D^2(m)k_1}{3} + k_2$

$$\tilde{I}(m) \xrightarrow{m \rightarrow \infty} \frac{k_\infty + (k_1 - k_\infty) G^2(m)}{3} + k_2$$

(It is seen that in the absence of diffuse boundaries $G^2(m) = 0$ and $D_\infty^2 = 1$. Thus, the Porod-Luzzati formalism is reobtained.)

Thus

$$[\tilde{I}(m) - k_2]m^3 - k_\infty = (k_1 - k_\infty) G^2(m) \quad (8)$$

$$= (k_1 - k_\infty) \exp(-2\pi B^2 m^2 / \lambda^2 a^2) \quad (9)$$

$$\ln\{[\tilde{I}(m) - k_2]m^3 - k_\infty\} = \ln(k_1 - k_\infty) - \left(\frac{2\pi B^2}{\lambda^2 a^2}\right) m^2 \quad (10)$$

which shows that a plot of the left side of equation (10) against m^2 should give a straight line of negative slope $(2\pi B^2 / \lambda^2 a^2)$ and intercept of $(k_1 - k_\infty)$.

From the slope one can estimate the transition zone thickness and from the intercept one can calculate D_∞^2 the relative volume fraction of sharp boundaries by combining $(k_1 - k_\infty)$ with the regular intercept k_∞ of the Porod-Luzzati plot. This further leads to $G^2(m)$ which gives a more accurate value for the corrected invariant \tilde{Q}_B defined as

$$\tilde{Q}_B = \int_0^{\infty} m \cdot \left[\frac{\tilde{I}(m) - k_2}{D^2(m)} \right] dm \quad (11)$$

All this then leads to a realistic O/V estimation which can be more conveniently compared with the corresponding values of an ideal system which Bonart refers to as a "comparison system".

References

1. Bonart, R. and Müller, E. H., J. Macromol. Sci. - Phys., B10 (1), 177 (1974).
2. Ibid, B10 (2), 345 (1974).

APPENDIX V

PROCEDURE FOR USING CALIBRATION CURVES
OF MODIFIED BUCHANAN METHOD

1. Experimental Peak Position (d)
2. Experimental Full Width (of peak) at Half Max Intensity* (q)
3. $(p) = dq$
4. Read off k , X_m , p as functions of (p) from Calibration Plots (Fig. 11)

$$(p) = p/X_m \quad p = cq \quad X_m = c/d$$
5. Long Period (c) $c = X_m d \text{ (\AA)}$
6. Crystallite Size (a) $a = kc \text{ (\AA)}$
7. Inter-Lamellar Region (l) $l = c-a \text{ (\AA)}$
8. Crystallinity (k) $k = \frac{a}{l+a} = \frac{a}{a+l} = \frac{a}{c}$
One dimensional

*Commonly referred to as FWHM.

APPENDIX VI

BOND POLARIZABILITIES AND $(\alpha_t - \alpha_r)_{cr}$ PCL Unit Cell Dimensions (\AA)

<u>a</u>	<u>b</u>	<u>c</u>	
7.496	4.974	17.297	Bittiger et al. ²⁰¹
7.470	4.980	17.050	Chatani et al. ²⁰²

ϕ = angle between chain backbone plane and b axis

= 41° [Bunn²⁰³ for PE]

= 55° [Zuganmeier as quoted by Bittiger et al.²⁰¹]

= 40° [Chatani et al.²⁰² for PCL]

All bond angles and ϕ are from Chatani et al.²⁰²

Number of Segments per unit volume (N_s):

$$N_s = \frac{\text{Density of crystalline phase}}{\text{Molecular weight/repeat unit}} \times \text{Avogadro's Number}$$

$$= \frac{1.178}{114.146} \times 6.02 \times 10^{23} = 6.20 \times 10^{21} \text{ (segments/cc)}$$

Polarizabilities

$$P_j = \sum_i \rho_i = \sum_i [(b_\ell - b_T)_i \cos^2 \theta_i + (b_T)_i] \quad (87)$$

on substituting the appropriate values of the bond polarizabilities from Bunn and Daubeny²⁰³ and the bond angles from Chatani et al.²⁰² one gets:

$$P_a = 109.68 \times 10^{-25}$$

$$P_b = 109.68 \times 10^{-25}$$

$$P_c = 126.64 \times 10^{-25}$$

substituting these values into equation (89)

$$(\alpha_t - \alpha_r)_{cr} = N_s \left(\frac{P_a + P_c}{2} - P_b \right)$$

one gets for PCL

$$(\alpha_t - \alpha_r)_{cr} = .00522$$

APPENDIX VII

COMPUTER PROGRAM FOR SMALL-ANGLE X-RAY CORRECTIONS

LIST DATA

```

10 PROGRAM DATA
11*ERROR ANALYSIS OF RAW DATA FOR QUICK CHECK ON NOISE
12*CONTENT AND ANY NEEDED EDITING.
13*CALCULATES CPS, STD. DEV., ERROR LIMITS AND COEFF. OF VAR.
20 DIMENSION M(10),N(10),K(10),B(10),X(10),C(10),D(10),DATA(50)
30 INPUT, COMP,A1,A2,A3,J2,J3,JMAX
35 J1=1
40 PRINT 45
45 FORMAT (///,20X,*STATISTICAL CHECK OF RAW DATA*/)
50 PRINT 55,COMP
55 FORMAT (21X,*ELEMEN COMPOSITION = *F6.2,/)
60 PRINT 65,A1,J1,J2,A2,J2+1,J3,A3,J3+1,JMAX
65 FORMAT (5X,*PRESET COUNT = *,F5.,3X,*J = *,I3,3X,*TO J = *
66C,I3,/,18X,*= *,F5.,5X,*= *,I3,10X,*= *,I3,/,18X,*= *,F5.,
67C5X,*= *,I3,10X,*= *,I3,/)
70 PRINT 75
75 FORMAT (5X,*ANGLE*,8X,*CPS*,8X,*STANDARD*,8X,*LIMITS*,8X,
76C*COEFFICIENT*)
78 PRINT 80
80 FORMAT (3X,*DEG.*,2X,*MIN.*,15X,*DEVIATION*,7X,*OF ERROR*,
81C6X,*OF VARIATION*/,*=====
32C=====*/)
90 COUNT=A1
95 DO 320 J=J1,J2
100 READ 110,(M(I),N(I),I=1,5)
110 FORMAT (1X,10(I4,2X))
120 DO 160 I=2,5
130 K(I)=60*M(I)+N(I)
140 B(I)=K(I)
150 X(I)=COUNT/B(I)
160 CONTINUE
170 Y=(X(2)+X(3)+X(4)+X(5))/4.
180 DO 210 I=2,5
190 C(I)=ABS(X(I)-Y)
200 D(I)=C(I)**2
210 CONTINUE
220 E=(D(2)+D(3)+D(4)+D(5))/3.
230 F=SQRT(E)
240 G=.6745*F
250 G=ABS((C(2)+C(3)+C(4)+C(5))/4.)
260 F=SQRT(4./3.)*G
270 R=2.55*F
280 S=(F/Y)*100.
300 PRINT 310,M(1),N(1),Y,F,R,S
310 FORMAT (1X,2(I4,2X),F10.4,F12.4,2F16.4/)
320 CONTINUE
330 IF (J2.EQ.JMAX)430,340
340 IF(J1.EQ.1) 350,390
350 J1=J2+1
360 J2=J3
370 COUNT=A2
380 GO TO 95
390 J1=J3+1
400 J2=JMAX
410 COUNT=A3
420 GO TO 95
430 STOP
440 END
450 ENDPROG

```

APPENDIX VIII

PRELIMINARY

Using the PDP-8 Data Gathering Interface
with the Low Scattering Angle Diffractometer

I. Assumptions

1. It is assumed that the user is familiar with the PDP-8 and the Small Computer Handbook (DEC). (In particular, Chapter 2, pages 2-1 through 2-8 on the Console and 2-11 through 2-19 on loading a program. The diagram on page 2-19 is particularly useful to a beginning operator.)

2. The user should also be familiar with the operation of the Low Angle Scattering Diffractometer and the DAC model 200.

II. Starting Procedures

1. Turn on the X-Ray apparatus as usual.

2. Place the PDP-8 Run/Halt switch (Note: Console switches will appear underlined.) in the Halt position (Down) and turn on the PDP-8 using the key. This should turn on the DAC, Teletype and Interface. (The Interface has a separate power switch on its left-hand side and a small pilot light; this light should be ON.)

3. Check the operation of the DAC by pressing in sequence its stop, reset, start switches when it is in the test mode. (i.e.,

Preset time off, Preset count in, Test in, Preset count of 100.)

The DAC should count up to 100 and stop.

4. The Data Gathering Program should be in the machine. If it is not, load it in using the Binary Loader (See Page 2-19 of the DEC handbook for instructions).

5. Place 1200_8 in the Switch Register (see Appendix I) and press the Load Ads Switch. Raise the Run/Halt switch, press Clear and then Continue. The Program is now running.

6. Follow the directions as typed on the teletype, the operating dialogue is described in the next section.

III. Operating Dialogue - Teletype Printout in CAPITALS, operator responses in lower case.

1. ENTER RUN IDENTIFICATION

type a name for this run (Maximum of 30 Alpha-Numeric Chars).

2. ENTER STARTING ANGLE, DEG

type starting angle, between plus and minus 20 deg.

3. ENTER NUMBER OF SEGMENTS

type the number of segments for this run (Maximum 8).

4. ENTER STEP SIZE, MIN

type the step size for this segment (Maximum 60 min).

5. ENTER STOPING ANGLE, DEG

type the stoping angle for this segment.

Note: The sequence 4,5 will be repeated as many times as there are segments in this run.

6. ENTER NUMBER OF READINGS

type the number of readings to be made on the DAC (min 1, max 4).

7. ENTER DAC PRESET COUNT

type 6 numbers - the preset count on the DAC.

8. ENTER MAX TIME FOR STEP, MIN

type the maximum time for a reading of the DAC (max 60 min).

9. SET ARM TO STARTING ANGLE

SET CLUTCH TO SLOW SPEED

SET MOTOR TO FORWARD DIRECTION

HIT CONTINUE WHEN READY

perform the tasks requested, when finished hit the continue key on the console

10. SET MOTOR TO FORWARD DIRECTION

TURN ON TAPE PUNCH

HIT CONTINUE WHEN READY

perform the tasks requested, if a tape copy of the run is wanted for later processing turn the punch on otherwise it may be left off. Hit the continue key.

This ends the operating dialogue, the run is now in progress.

IV. The Run

At the end of the operating dialogue, the PDP-8 will punch leader tape and then the following data (as well as printing it):

Run Identification

Starting Angle

Number of segments

Step size, stopping angle

for each segment

• • •

Number of readings

DAC Preset count

Max time for step

This data will be followed by additional leader tape.

The run data printed (and punched) will consist of

Angle (deg), Angle (min), Time (min), Time (sec), ...

repeated for multiple readings.

V. End of Run

At the end of the run the PDP-8 will punch trailer tape and then ring the teletype bell until any key on the keyboard is struck.

After a key has been struct it will type:

TURN OFF TAPE PUNCH

END OF RUN

A new run may be started by pressing the continue key on the console.

VI. Abnormal Run

If at any time during a run either during the beginning dialogue or in the process of taking readings you would like to STOP and RESTART, simply depress the RUN/HALT switch. To restart, follow these directions from section II-5. If you do not want to restart, turn off the equipment using the on-off key on the console.

Octal Numbers and the Switch Register

The PDP-8 uses the binary number system, which deals with only 0's and 1's. To simplify writing a binary number down the Octal number system (base 8) is used, since one octal digit specifies three binary numbers this saves a lot of space. The conversion between Octal and Binary is as follows:

<u>Octal</u>	<u>Binary</u>
0	000
1	001
2	010
3	011
4	100
5	101
6	110
7	111

When entering a number into the switch register a 1 means the switch is up, a 0 means the switch is down. For example, the number 1200_8 (the 8 means octal) is 001 010 000 000 binary which becomes dn,dn,up,dn,up, dn,dn,dn...in terms of switch positions.

APPENDIX IX

The method of estimating absolute intensities and other related parameters has been included in this Appendix as received from Professor Kratky without any modification.

The pages were originally numbered 1 to 9 and have been renumbered as part of this thesis.

KRATKY X-RAY SMALL ANGLE SYSTEM

Application of the Lupolen platelet designated with 17/4 as a calibration sample for the determination of the absolute scattered intensity and of the primary energy in the case of slit-collimation

The figures refer to the $\text{CuK}\alpha$ -fraction of the scattering resp. the primary energy. Therefore one has to:

- a) work with reflected radiation, that is fully monochromatically, or
- b) use the filter difference method, or
- c) use a proportional counter in connection with a suitably adjusted impulse height discriminator and an additional nickel foil 0,01 mm thick. Omission of the nickel foil may cause an error of several percents, since it is practically not possible, to remove the β -line by means of the impulse height discriminator.

The indices used in the following mean:

C ... calibration sample

S ... scattering sample (= sample to be investigated)

A ... auxiliary sample

In particular the notations mean:

P_S ... energy per 1 cm length of the primary beam after weakening by the scattering sample

P_C ... energy per 1 cm length of the primary beam after weakening by the calibration sample.

We assume, that the scattered intensity is determined by impulse counting. Further we assume a primary beam of line shaped cross section. This brings about a collimation effect ("Längsver-schmierung"). We designate all figures effected by this collimation

effect with a tilde, as example: \tilde{I} . Figures obtained after the collimation error has been eliminated, do no more contain the tilde¹⁾.

For all measurements, the same primary beam (unchanged adjustment of the collimation system and the X-ray unit) and the same counting tube slit must be used.

The determination of the absolute intensity is done as follows.

1) a = distance centre of sample-registering plane, has to be measured in cm,

2) provision must be made that the length of the homogeneous part of the primary beam in the registering plane is between $0.1a$ and $0.25a$ and the length of the counting tube slit is $\leq 0.05a$.

3) The calibration sample is adjusted. Then, with the same slit conditions as will be used by the measurement proper, the scattering of the CuK_α -line is measured for a scattering angle $= 35.3' = 0.0103$ radians, corresponding to a Bragg's value of 150 \AA . The measured number of impulses/min shall be denoted with:

$$(\tilde{\text{imp/min}})_{C, 150 \text{ \AA}}$$

4) The factor of attenuation A_S of the scattering sample (= sample to be investigated) is determined for the CuK_α -line. This is done best by inserting any other, well scattering sample (auxiliary sample) into the camera in the normal way, and measuring its scattering at any angle. It shall be:

$$\tilde{I}_{A,1}$$

1) Here we want to refer to a summarizing treatment discussing all questions pertinent to the collimation effect: O.Kratky, G.Porod and Z.Skala, Acta Physica Austriaca 13, 76 (1960).

Now the primary beam is weakened by the scattering sample. To this end, the latter is inserted into the path of the radiation at a place, where it cannot contribute to the scattering. Again the scattering of the auxiliary sample is measured, it shall be:

$$\tilde{I}_{A,2}$$

The quotient $\tilde{I}_{A,2}/\tilde{I}_{A,1}$ represents the desired factor of attenuation A_S of the scattering sample. If very high accuracy is not required, the factor of attenuation A_S can eventually be calculated from the chemical composition and the thickness of the scattering sample. The factor of attenuation of the used sample container (capillary, cuvette) must, however, then be taken into account too.

5) For all mass determinations by means of the absolute intensity²⁾ the quotient of both the scattered intensity at zero angle $I_{S,0}$ and the primary energy weakened by the scattering sample P_S is required. For the determination of the first figure, we must measure the number of impulses $(\tilde{\text{imp/min}})_S$ of the scattering sample in dependence of the scattering angle. Following known methods¹⁾, this curve is made free from the collimation effect of the primary beam length, with normalization to the energy of a primary beam of point shaped cross section, which contains the energy of an 1 cm long piece of the actual primary beam. We designate the obtained figures with $(\text{imp/min})_S$. This curve is extrapolated to zero scattering angle: $(\text{imp/min})_{S,0}$. Then, if the individual calibration sample is used, we obtain:

2) For a summarizing paper on the use of the absolute intensity see: O.Kratky, Z.analyt.Chem. 201, 161 (1964). Sufficiently extensive informations are also found in: O.Kratky, Progress in Biophysics 13, 105 (1963).

$$\frac{I_{S,0}}{P_S} = 0,0146 \frac{(\text{imp/min})_{S,0}}{(\widetilde{\text{imp/min}})_{C,150\text{\AA}} \cdot a \cdot A_S} \quad (1)$$

6) For the determination of the average square fluctuation of the electron density there is required the quotient:

$$\frac{\int_0^\infty \widetilde{I}.m.dm}{P_S} \quad \text{whereby } 2\theta \approx \frac{m}{a} \quad (2\theta = \text{scattering angle})$$

In this case, the scattering curve $(\widetilde{\text{imp/min}})_S$ can be used without elimination of the collimation effect. There holds:

$$\frac{\int_0^\infty \widetilde{I}.m.dm}{P_S} = 0,0146 \frac{\int_0^\infty (\widetilde{\text{imp/min}})_S \cdot m dm}{(\widetilde{\text{imp/min}})_{C,150\text{\AA}} \cdot a \cdot A_S} \quad (2)$$

7) If the primary energy P_S per 1 cm length of the primary beam, measured in the registering plane and weakened by the scattering sample under investigation is required, we may make use of the relation valid for the application of the individual Lupolen calibration sample 17/4.

$$P_S = 68,7 \frac{(\widetilde{\text{imp/min}})_{C,150\text{\AA}}}{F} \cdot a \cdot A_S \quad (3)$$

Here F means the counting tube slit area (in cm^2).

Short explanation

The individual Lupolen calibration sample 17/4, for use with a line shaped primary beam (length between 0.1a and 0.25a), at an angle corresponding to a Bragg's value of 150 Å, has a scattering intensity, determined by means of the rotator method³⁾ and recalculated to a counting tube slit area of 1 cm^2 :

3) O.Kratky and H.Wawra, Mh.Chem. 94, 981 (1963)

$$\tilde{I}_{C,150\text{\AA}} = \frac{(\tilde{\text{imp/min}})_{C,150\text{\AA}}}{F} = 0,0389 \frac{P_C}{a} \quad (4)$$

Here P_C denotes the energy of the primary beam per 1 cm length, measured in the registering plane, after weakening by the calibration sample. For the evaluation of the measurement at the scattering sample under investigation, however, the energy per 1 cm length of the primary beam after weakening by the scattering sample is required. If A_C means the factor of attenuation of the individual calibration sample 17/4 (the figure is $A_C = 0,374$), A_S that of the scattering sample, then, as can easily be shown, there holds:

$$P_S = P_C \frac{A_S}{A_C} \quad (5)$$

Combining of (4) and (5) yields:

$$\begin{aligned} P_S \cdot F &= 25,7 (\tilde{\text{imp/min}})_{C,150\text{\AA}} \cdot a \cdot \frac{A_S}{A_C} = \\ &= \frac{25,7}{0,374} (\tilde{\text{imp/min}})_{C,150\text{\AA}} \cdot a \cdot A_S \end{aligned}$$

But this is the relation (1) given above.

As a rule, however, the area of the counting tube slit F need not be determined, as all calculations by means of the absolute intensity²⁾ require the quotient $\frac{I_{S,0}}{P_S}$ or $\frac{\int_0^\infty \tilde{I} \cdot m \cdot dm}{P_S}$. Therefore, instead of the \tilde{I} -resp. I -values we may as well use the values multiplied with F , namely the $(\tilde{\text{imp/min}})_S$ -values respectively the figures obtained therefrom by elimination of the collimation error. At the same time, instead of P_S , the figure $P_S \cdot F$, as given by equation (3), must be inserted. In this way we obtain:

$$\frac{I_{S,O}}{P_S} = \frac{I_{S,O \cdot F}}{P_{S \cdot F}} = \frac{1}{68,7} \cdot \frac{(\text{imp/min})_{S,O}}{(\widetilde{\text{imp/min}})_{C,150\text{\AA} \cdot a.A_S}} =$$

$$= 0,0146 \frac{(\text{imp/min})_{S,O}}{(\widetilde{\text{imp/min}})_{C,150\text{\AA} \cdot a.A_S}} \quad (1)$$

and

$$\frac{\int_0^\infty \widetilde{I} \cdot \text{mdm}}{F \int_0^\infty \widetilde{I} \cdot \text{mdm}} = \frac{1}{68,7} \cdot \frac{\int_0^\infty (\widetilde{\text{imp/min}})_{S \cdot \text{mdm}}}{(\widetilde{\text{imp/min}})_{C,150\text{\AA} \cdot a.A_S}} =$$

$$= 0,0146 \frac{\int_0^\infty (\widetilde{\text{imp/min}})_{S \cdot \text{mdm}}}{(\widetilde{\text{imp/min}})_{C,150\text{\AA} \cdot a.A_S}} \quad (2)$$

The calibration sample has been calibrated at a temperature of 21°C ⁺⁾ . It is recommended to carry out the measurements of the scattered intensity with Lupolen in this temperature range too, since significantly higher or lower temperatures will cause a change in the scattering intensity of the Lupolen.

⁺⁾ The calibration was carried out by I. Pilz, Institut für Physikalische Chemie, Universität Graz, using the procedure described in the following papers:

O.Kratky, I.Pilz and P.J.Schmitz; J.Colloid Interface Science 21, 24 (1966)

I.Pilz and O.Kratky, *ibid.* 24, 211 (1967)

I.Pilz, *ibid.* 30, 140 (1969)

Influence of temperature on the scattered intensity of
Lupolen calibration samples.

We calibrate all samples at a temperature of 21°C . If the Lupolen is used at this temperature for the determination of absolute intensity, then the measured scattering intensity can be inserted immediately into the above relations.

If Lupolen is used at another temperature then for high demands on accuracy a correction must be applied. Within the range of 4° to 30°C this is done as follows: the scattering intensity measured at a temperature ϑ and at 150\AA ($= 0,01025$ radians) shall be $\vartheta I_{150\text{\AA}}$. For the value for 21°C to be inserted into the above relation,

$$^{21^{\circ}}I_{150\text{\AA}}$$

we then have:

$$^{21^{\circ}}I_{150\text{\AA}} = \vartheta I_{150\text{\AA}} / (1 + 0,0077 \Delta\vartheta)$$

here $\Delta\vartheta$ means the positive or negative deviation of the temperature used from the calibration temperature of 21°C .

The analogous linear relations for several other scattering angles are:

$$300\text{\AA} \text{ (} = 0,00513 \text{ radians)} \quad ^{21^{\circ}}I_{300\text{\AA}} = \vartheta I_{300\text{\AA}} / (1 + 0,0088 \Delta\vartheta)$$

$$110\text{\AA} \text{ (} = 0,014 \text{ radians)} \quad ^{21^{\circ}}I_{110\text{\AA}} = \vartheta I_{110\text{\AA}} / (1 + 0,0044 \Delta\vartheta)$$

$$55\text{\AA} \text{ (} = 0,028 \text{ radians)} \quad ^{21^{\circ}}I_{55\text{\AA}} \approx \vartheta I_{55\text{\AA}}$$

It may again be remarked explicitly, that these relations hold only in the temperature range between 4° and 30°C .

Besides it may be mentioned, that a Lupolen platelet, which has been heated to 40° or 50°C and cooled again, can be used for standard measurements only after a few hours, since

only after this time the intensity value characteristic for the low temperature will be restored. If a Lupolen platelet has been heated above 55°C , irreversible intensity variations may occur. That means the platelet requires a new calibration.

Instructions for the treatment of the calibration sample

The calibrated Lupolen platelets can as a rule be used for calibration measurements for several years, when the treatment is appropriate, without any alteration in the scattering intensity. A full guarantee that no change of any sort will take place in the course of years can however not be given, since the qualities of the Lupolen material vary somewhat. For very exact measurements it is thus desirable to have the calibration sample checked by means of a recalibration after a year or two. The recalibration of the returned platelet will be carried out free of charge.

Guiding principles for the treatment of the sample:

1. The sample should be stored at room temperature and should only be used for calibration measurements within a temperature range of 0° to 36°C . If the temperature of a Lupolen platelet is varied within this range, the intensity value characteristic for the temperature used (see p. 7) will appear immediately. If the platelet is heated over 55°C irreversible changes in the scattering intensity must be expected.

2. The sample should if possible be stored in a dark place and not exposed to the rays of the sun for weeks on end.

3. In order to obtain a year-long stability of the scattering intensity the sample should not be exposed unnecessarily to x-rays for hours or days on end. For measurements lasting a long time (e.g. the checking of the constancy of an x-ray generator) that uncalibrated Lupolen platelet is to use which has been delivered already with the Kratky camera by Anton Paar. The individually calibrated sample bears the Nr. ^{17/4}..... . The uncalibrated constancy platelet carries the letter "C".

APPENDIX X

SALS REFERENCE INTENSITY

In order to obtain absolute values for the photometric light scattering intensities, one needs to normalize all the scans to a known reference intensity which represents the incident intensity of the appartus for which the apparatus constant was estimated.

A value of 3300 was obtained for the reference intensity by monitoring the transmitted intensity with the detector photomultiplier at $\theta = 0^\circ$ in the V_v mode with all the filters in the incident beam.

A more complete explanation of the entire procedure has been given by Prud'homme²⁰⁹ but it needs to be said that for the present work all the conditions such as instrumental electronics, filters, collimation geometry, etc. were identical to those used by Prud'homme for estimating the above value. Should any of these conditions be altered, the value of $k = 3300$ will change correspondingly.

APPENDIX XI

COMPUTER PROGRAM FOR SMALL-ANGLE LIGHT-SCATTERING CORRECTIONS

LIST RAJ

```

10 PROGRAM RAJ
20* XN = REFRACTIVE INDEX OF SAMPLE
21* DPF=DPF1*DPF2=DEPOLARIZATION RATIO
22* TRANS = TRANSMITTANCE (%)
23* THICK = SAMPLE THICKNESS IN (MILS)
24* XK = APPARATUS CONSTANT (CM**2)
25* RINC = RADIUS OF INCIDENT BEAM (CM)
26* TETA = ANGLE THETA (IN AIR)
27* PMU = ANGLE MU (AZIMUTHAL)
23* READING = READING OF THE RECORDER (THIS IS TRUE READING
29* MINUS BLANK READING, GIVEN FOR STANDARD IO)
30* CN = REFRACTION CORRECTION
32* REFL = REFLECTION CORRECTION
33* TETAS = ANGLE THETA(IN SAMPLE)
34* ANGR = ANGLE IN (RADIAN)S)
35* RAY = RAYLEIGH RATIO
36* RADII = RADIUS OF SPHERULITE
37*FACTOR=MULTIPLICATION FACTOR FOR TRUNCATION
90 INPUT,C,S
92 PI =3.1415927
100 IF(C.EQ.1.) 101,107
101 PRINT 102
102 FORMAT (//////,25X,*THIS IS A THETA SCAN */,24X,*-----
103C-----*)
104 GO TO 111
107 PRINT 108
108 FORMAT (//////,21X,*THIS IS AN AZIMUTHAL SCAN */,20X,*---
109C-----*)
110 GO TO 113
111 PMU=45.
112 DPF2=1.
113 PRINT 114,S
114 FORMAT(//////,*SAMPLE = *F6.2)
116 PRINT 117
117 FORMAT (/,*DATE = *///)
118 READ,XN,TRANS,THICK,XK,RINC,RADII,VVI,DPF1,FACTOR
119 A=(THICK/1000.)*2.54
120 TD=LOG(100./TRANS)
125 VOL=A*(RINC**2)*PI
130 PRINT 135,XN,TRANS,THICK,XK,RINC,RADII
135 FORMAT(5X,*REFRACTIVE INDEX = *,F7.3,/,5X,
136C*TRANSMITTANCE (%) = *,F7.3,/,5X,*SAMPLE
137C*THICKNESS (MILS) = *,F7.3,/,5X,*APPARATUS CONST
138CANT (SQ.CM.) = *,F9.5,/,5X,*INCIDENT BEAM RADIUS
139C (CM) = *,F7.3,/,5X,*RADIUS OF SPHERULITE (MICR
140CONS) = *,F7.3//)
145 PRINT 146,TD,VOL
146 FORMAT (5X,*TURBIDITY = *,F5.3,/,5X,*VOL. IRRAD.
147C (CC) = *,F7.5,////)
148 PRINT 149
149 FORMAT (3X,*THETA*,5X,*THETA*,7X,*MU*,7X,*READING*,3X,

```

```

150C*RAYLEIGH*,5X,*RED. ANGLE*/
151 PRINT 152
152 FORMAT (3X,*(AIR)*,3X,*(SAMPLE)*,3X,*(AZINUTH)*,3X,*(INSTR)*,
153C4X,*(RATIO)*,3X,*(U)*,/)
155 READ,TETA,READING
165 IF (TETA.EQ.0.) GO TO 390
170 TETAR=TETA*PI/180.
175 SINTET=SINF(TETAR)
180 COSTET=COSF(TETAR)
190 TETASR=ASINF(TETAR/XN)
195 COSTES=COSF(TETASR)
200 TETAS=TETASR*180./PI
205 CN=XN*XN*(SQRTF(1.-(SINTET/XN)**2.)/COSTET)
215 RA=((XN-1.)/(XN+1.))**2.
220 ANGR=ASINF(SINTET/XN)
225 ANGA=TETAR-ANGR
230 ANGB=TETAR+ANGR
235 TANA=TANF(ANGA)
240 TANB=TANF(ANGB)
245 SINA=SINF(ANGA)
250 SINB=SINF(ANGB)
254 XPMU=PMU*PI/180.
255 FC=(SINF(XPMU))**2
260 RC=(FC*(SINA/SINB)**2.)+((1.-FC)*(TANA/TANB)**2.)
265 REFLEC=0.96/((1.-RA)*(1.-RC))
270 U=4.*PI*RADI I*XN*SINF(TETASR/2.)/.5461
275 Z=READING*(3300./VVI)*DPF1*DPF2
285 RAY=KK*CN*(REFLEC/VOL)*Z*FACTOR
295 PRINT 296,TETA,TETAS,PMU,READING,RAY,U
296 FORMAT (F3.3,F10.3,F10.1,F12.1,F12.3,F13.3)
300 GO TO 155
390 END
400 ENDPROG
410 1.563,88.0,0.800,0.00106,0.45,4.60,15250.,1.034,1.00

```


APPENDIX XII

THEORETICAL CRYSTALLINITY (k_{TH}) USING TSVANKIN PARAMETERS
 AS A FUNCTION OF ϕ_c AND BLEND COMPOSITION

$$k_{TH} = \frac{\text{Crystallite Size}}{\text{Long Period}}$$

$$= \frac{a}{a + 1}$$

$$= \frac{K \phi_{PCL} \phi_c}{K \phi_{PCL} \phi_c + K[\phi_{PCL} (1 - \phi_c) + (1 - \phi_{PCL})]}$$

$$k_{TH} = \phi_{PCL} \phi_c$$

K = constant of proportionality

ϕ_{PCL} = volume fraction PCL (composition)

ϕ_c = crystallinity of PCL (volume fraction)

BIBLIOGRAPHY

1. Rosen, S. L., Polymer Eng. Sci., 7, 115 (1967).
2. Feldman, D. and Rusu, M., Europ. Polym. J., 6, 627 (1970).
3. Tobolsky, A. V., Properties and Structures of Polymers, Rheinhold, New York, 1962.
4. Flory, P. J., Principles in Polymer Chemistry, Cornell University Press, Ithaca and London, 1969, p. 555.
5. Tager, A. A., Polymer Sci. USSR, 14, 12, 3129 (1974); Vysokomol Soyed., A14, 12, 2690 (1972).
6. Slonimskii, G. L., J. Polym. Sci., Prague Symp., 30, 625 (1958).
7. Koleske, J. V., and Lundberg, R. D., J. Polym. Sci., A2, 7, 795 (1969).
8. Brode, G. L. and Koleske, J. V., J. Macromol. Sci. (Chem), A6(6), 1109 (1972).
9. Union Carbide Corporation, New Product Information, Bulletin F-42501, Chemicals and Plastics, New York.
10. Ong, C. J., Ph.D. Thesis, University of Massachusetts (1973).
11. Lebedev, V. P., Okladnov, N. A., Minsker, K. S., and Shtarkman, B. P., Polymer Sci. USSR, 7, 724 (1965).
12. McKinney, P. V. and Foltz, C. R., J. Appl. Polym. Sci., 11, 1189 (1967).
13. Juijn, J. A., Gisolf, J. H. and deJong, W. A., Kolloid -Z and Z. Polym., 235, 75 (1969).

14. Ibid, 251, 456 (1973).
15. Koleske, J. V. and Wartman, L. H., in Poly(vinyl chloride), Gordon and Breach Sci. Pub., 1969, p. 33-36.
16. Keith, H. D. and Padden, Jr., J. Appl. Phys., 35, 4, 1270 (1964).
17. Ibid, 35, 4, 1286 (1964).
18. Ibid, 34, 8, 2409 (1963).
19. Stein, R. S., Structure and Properties of Polymer Films, Eds. R. W. Lenz and R. S. Stein, Plenum Publishing Corp., 197, p. 1.
20. Pazonyi, T. and Dimitrov, M., Rubber Chem. Technol., 40, 1119 (1967).
21. Brodsky, P. H., Ph.D. Thesis, Cornell University, Ithaca, NY, 1969.
22. Ichihara, S., Komatsu, A. and Hata, T., Polymer J., 2, 5, 640 (1971).
23. Schneier, B., J. Appl. Polym. Sci., 17, 3175 (1973).
24. Bank, M., Leffingwell, J. and Thies, C., Macromol., 4, 1, 43 (1970).
25. MacKnight, W. J., Stoelting, J. and Karasz, F. E., Advances in Chemistry Series, ACS, Vol. 99, 29 (1971).
26. Noland, J. S., Hsu, N. N. C., Saxon, R. and Schmitt, J. M., *ibid.*, pp. 15.
27. Starita, J. M., Trans. Soc. Rheology, 16, 2, 339 (1972).
28. Hickman, J. J and Ikeda, R. M., J. Polym. Sci., Phys. Ed., 11, 1713 (1973).
29. Paul, D. R. and Altamirano, J. O., Am. Chem. Soc., Polymer Preprints, 15, 1, 409 (1974).

30. Karasz, F. E., MacKnight, W. J., and Tkacik, J. J., Polymer Preprints, 15, 1, 415 (1974).
31. Buchdahl, R. and Nielsen, L. E., J. Appl. Phys., 21, 482 (1950).
32. Nielsen, L. E., J. Am. Chem. Soc., 75, 1435 (1953).
33. Buchdahl, R. and Nielsen, L. E., J. Polym. Sci., 15, 1 (1955).
34. Takayanagi, M., Memoirs Faculty of Eng., Kyushu Univ., 23, 1 (1963).
35. Stoelting, J., Karasz, F. E. and MacKnight, W. J., Polym. Eng. and Sci., 10, 3, 133 (1970).
36. Hammer, C. F., 4, 1, 69 (1971).
37. Merz, E. H. et. al., J. Polym. Sci., 22, 325 (1956).
38. Minoura, Y. et. al., J. Appl. Polym. Sci., 9, 1299 (1965).
39. Hughes, L. T. and Britt, G. E., J. Appl. Polym. Sci., 5, 15, 337 (1961).
40. Paxton, T. R., J. Appl. Polym. Sci., 7, 1499 (1963).
41. Fujino, K. et al., J. Appl. Polym. Sci., 8, 2147 (1964).
42. Natov, M. et. al, J. Polym. Sci., C, 16, 4197 (1968).
43. Feldman, D. and Rusu, M., Europ. Polym. J., 7, 215 (1971).
44. Prest, W. M. and Porter, R. S., J. Polym. Sci., A2, 10, 1639 (1972).
45. Harget, P. J., Norelco Reporter, 18, 25 (1971).
46. Dorby, A. and Boyer-Kawenoki, F., J. Polym. Sci., 2, 90 (1947).
47. Scott, R. L., J. Chem. Phys., 17, 279 (1949).
48. Tompa, H., Trans. Faraday Soc., 45, 1142 (1949).
49. Flory, P. J., J. Chem. Phys., 9, 660 (1941).
50. Flory, P. J., J. Chem. Phys., 10, 51 (1942).

51. Huggins, M. L., J. Chem. Phys., 9, 440 (1941).
52. Huggins, M. L., Ann. N. Y. Acad. Sci., 43, 1 (1942).
53. Krause, S., J. Macromol. Sci., C, 7 (2), 251 (1972).
54. Tompa, H., Polymer Solutions, Butterworths, London, 1956.
55. Hildebrand, J. H. and Scott, R. L., The Solubility of Nonelectrolytes, 3rd Ed., Reinhold, New York, 1950; Dover Publications, New York, 1964.
56. Hildebrand, J. H. and Scott, R. L., Regular Solutions, Prentice-Hall, Englewood Cliffs, New Jersey, 1962.
57. Small, P. A., J. Appl. Chem., 3, 71 (1953).
58. Hoy, K. L., J. Paint Technol., 42, 76 (1970).
59. Bohn, L., Kolloid Z. Z. Polym., 213, 55 (1966); Rubber Chem. Technol., 41, 495 (1968).
60. Gee, G., Quarterly Rev. Chem. Soc., 1, 265 (1947).
61. Gee, G., Trans. Inst. Rubber Inc., 18, 266 (1943); Trans. Faraday Soc., 38, 418 (1942).
62. Kern, R. J. and Slocumbe, R. J., J. Polym. Sci., 15, 183 (1955).
63. Kern, R. J., J. Polym. Sci., 21, 19 (1956).
64. Kern, R. J., J. Polym. Sci., 33, 524 (1958).
65. Briston, G. M., J. Appl. Polym. Sci., 11, 4, 120 (1959).
66. Boyer, R. F., J. Appl. Phys., 20, 540 (1949).
67. Perry, E. J., J. Appl. Polym. Sci., 8, 2605 (1964).
68. Hughes, L. J. and Brown, G. L., Ibid, 5, 580 (1961).
69. Eastmond, G. C. and Smith, E. G., Polymer 14, 509 (1973).
70. Kato, K., Polym. Eng. Sci., 7, 38 (1967).
71. Fox, T. G., Am. Phys. Soc., Bulletin, 2, 123 (1956).

72. Gordon, M. and Taylor, J. S., J. Appl. Chem., 2, 493 (1952).
73. Bares, J., Am. Phys. Soc., Bulletin, Phila., 19, 285 (1974).
74. Breuers, W., Hild W. and Wolff, H., Plaste Kautschuk, 1, 170 (1954).
75. Wolff, H., *ibid*, 4, 244 (1957).
76. Jenckel, E. and Herwig, H. U., Kolloid Z., 148, 57 (1956).
77. Booth, C. and Pickles, C. J., J. Polym. Sci., 11, 595 (1973).
78. Yu, A. J., Advances in Chemistry Series, ACS, Vol. 99, 1970, p. 2.
79. Krishnamurti, P., Indian J. Phys., 5, 473 (1930); Mark, H., Physik und Chemi der Cellulose, p. 139, Springer, Berlin, 1932; Hendricks, S. B., Z. Krist., Mineral. Petrog., A 83, 503 (1932); Warren, B. E., J. Chem. Phys., 2, 551 (1934); Phys. Rev., 49, 885 (1936).
80. Guinier, A., Theses Series A. NR. 1854, Univ. Paris, 1939; Compt. Rend., 204, 1115 (1937); Ann. Physik, 12, 161 (1939).
81. Kratky, O., Naturwissenschaften, 26, 29 (1938); 30, 542 (1942).
82. Statton, W. O., Small-Angle X-Ray Studies of Polymers, in Newer Methods of Polymer Characterization, B. Ke. (Ed.), Interscience, New York, 1964.
83. Guinier, A. and Fournet, G., Small-Angle Scattering of X-Rays, Wiley, New York, 1955.
84. Porod, G., Kolloid - Z., 124, 83 (1951).
85. Porod, G., Kolloid-Z., 125, 51 (1952).
86. Kratky, O., Z. Elektrochem., 58, 49 (1954); *ibid.*, 62, 66 (1958); Kolloid - Z., 144, 110 (1955); J. Polymer Sci., 16, 164 (1955).
87. Beeman, W. W., Kaesberg, P., Anderegg, J. W. and Webb, M. B., "Size of Particles and Lattice Defects" in S. Flugge, Ed., Encyclopedia of Physics. Vol. 32, Springer Verlag, Berlin, pp. 321-442.

88. Kratky, O., *Naturwiss.* 42, 237 (1955); *Angew. Chem.* 72, 467 (1960); *Progress in Biophysics*, 13, 105 (1963).
89. Porod, G., *Fortschr. Hochpolym. Forschg.*, 2, 363 (1961).
90. Hosemann, R. and Bagchi, S. N., *Direct Analysis of Diffraction by Matter*, Interscience, New York (1962).
91. Brumberger, M. (Ed.), *Small Angle X-Ray Scattering*, Gordon and Breach, New York, 1967, Parts I, II and III.
92. Alexander, L. E., *X-Ray Diffraction Methods in Polymer Science*, Wiley-Interscience, New York, 1969, Chapter 5.
93. Ref. 76, p. 48-52.
94. Luzzati, V., *Acta. Cryst.*, 13, 939 (1960).
95. Debye, P. and Bueche, A. M., *J. Appl. Phys.*, 20, 518 (1949).
96. Debye, P., Anderson H. and Brumberger, J., *ibid.*, 28, 679 (1957).
97. Kratky, O., Sekora, A., Treer, R., *Z. Elektrochem.*, 48, 587 (1942); Kratky, O., *Kolloidchem. Taschenbuch*, p. 132. Akad. Verl. Ges. Leipzig, 1943; Remarks to a lecture by R. Hosemann, *Z. Elektrochem.*, 46, 535 (1940).
98. Kratky, O. and Porod, G., *J. Colloid Sci.*, 4, 35 (1949).
99. Bear, Bouldan and Salo, J. *Amer. Leather Chemists Assoc.*, 46, 107 (1951).
100. Hashimoto, T., Nagatoshi, K., Todo, A., Hasegawa, H. and Kawai, H., *Macromolecules*, 7, 3, 364 (1974).
101. Statton, W. O., *J. Polym. Sci.*, 28, 423 (1958).
102. Mandelkern, L., Worthington, C. R. and Posner, A. S., *Science*, 127, 1052 (1958).
103. Sella, C., *Compt. Rend.*, 248, 1819 (1959).

104. Zernicke, F. and Prins, J. A., Z. Physik, 41, 184 (1927).
105. Kratky, O., Z. Physik., 34, 482 (1933); Monatsh, Chem., 76, 311 (1947).
106. Hermans, J. J., Rec. Trav. Chem., 63, 211 (1944).
107. Hosemann, R., Acta. Cryst., 4, 520 (1951).
108. Porod, G., Acta Phys. Austriaca, 3, 66 (1949).
109. Hess, K. and Kiessig H., Z. Physik, Chem. (Leipzig), 193, 196 (1944).
110. Belbeoch, B. and Guinier, A., Makromol. Chem., 31, 1 (1959).
111. Zahn, H. and Kohler, K., Kolloid - Z., 118, 115 (1950); Zahn, H. and Winter, U., Kolloid - Z., 128, 142 (1952).
112. Statton, W. O. and Godard, G. M., J. Appl. Phys., 28, 1111 (1957).
113. Statton, W. O., J. Polym. Sci., 41, 143 (1959).
114. Till, P. H., J. Polym. Sci., 24, 301 (1957).
115. Keller, A., Phil. Mag., 2, 1171 (1957).
116. Fischer, E. W., Z. Naturforsch, 12a, 753 (1957).
117. Keller, A. and O'Connor A., Disc. Faraday Soc. No. 25, 114 (1958).
118. Geil, P. H., Polymer Single Crystals, Interscience, New York 1963.
119. Andrews, E. H., J. Polym. Sci., B3, 353 (1965).
120. Geil, P. H., J. Polym. Sci., C13, 149 (1966).
121. Blais, J. J. B. P. and St. John Manley, J. Macromol. Sci. - Phys., B1(3), 525 (1967).
122. Vonk, C. G. and Kortleve, G., Kolloid - Z. U. Z. Polymere, 220 19 (1967).
123. Ibid, 225, 124 (1968).
124. Kavesh, S. and Schultz, J. M., J. Polym. Sci., A-2, 8, 243 (1970).

125. Ibid, A-2, 9, 85 (1971).
126. Burmester, A. F., Ph.D. Thesis, Case Western Reserve University, 1970.
127. Crist, B., J. Polym. Sci. - Phys., 11, 635 (1973).
128. Crist, B. and Morosoff, N., *ibid*, 11, 1023 (1973).
129. Reinhold, C., Fisher, E. W. and Peterlin, A., J. Appl. Phys., 35, 71 (1964).
130. Blundell, D. J., Acta Cryst., A26, 472 (1970).
131. Tsvankin D. Ya., Polymer Sci. USSR, 6, 2304, 2310 (1964).
132. Tsvankin D. Ya., Zubov, U. A. and Kitaigordskii, J. Polym. Sci., C16, 4081 (1968).
133. Buchanan, D. R., J. Polym. Sci., A-2, 9, 645 (1971).
134. Wenig, W., Ph.D. Thesis, Universitat Ulm, West Germany (1974).
135. Ruland, W., J. Appl. Cryst., 4, 70 (1971).
136. Strobl, G. R., *ibid*, 6, 365 (1973).
137. Blundell, D. J., Acta Cryst, A26, 476 (1970).
138. Strobl, G. R. and Muller, N., J. Polym. Sci., 11, 1219 (1973).
139. Vonk, C. G., J. Appl. Cryst., 6, 2, 81 (1973).
140. Stein, R. S. and Khambatta, F., To be published.
141. Bonart, R. and Müller, E. H., J. Macromol. Sci. - Phys., B10 (1), 177 (1974).
142. Bonart, R. and Müller, E. H. *ibid.*; B10 (2), 345 (1974).
143. Helfand, E. and Tagami, Y., J. Polym. Sci., B9, 741 (1971); J. Chem. Phys., 56, 3592 (1971); J. Chem. Phys., 57, 1812 (1972).
144. Helfand, E., Recent Advances in Polymer Blends, Grafts, and Blocks, L. Sperling (Ed.), ACS Chicago Symposium, August, 1973.

145. Meier, D. J., Am. Chem. Soc., Polymer Preprints, 15, 1, 171 (1974).
146. Stein, R. S., in Proceedings of the Interdisciplinary Conference on Electromagnetic Scattering, Ed. By M. Kerker, Pergamon Press, New York, 1963, pp. 439-458.
147. Stein, R. S., Erhardt, P., Clough, S and van Aartsen, J. J. in Electromagnetic Scattering, Ed. by R. L. Rowell, R. L. and Stein, R., S., Gordon and Breach, New York, 1967, pp. 339-410.
148. Stein, R. S. and Rhodes, M. B., ASTM Special Tech. Pub. No. 348 (Symposium on Resiongraphic Methods), 59 (1963).
149. Clough, S., Rhodes, M. B. and Stein, R. S., J. Polym. Sci., C18, 1 (1967).
150. Stein, R. S., In Newer Methods of Polymer Characterization, B. Ke (Ed.), Interscience, New York , 1964.
151. Peterlin, A., Die Makromol. Chemie, 87, 152 (1965).
152. Goldstein, H. and Michalik, P. R., J. Appl. Phys., 26, 1450 (1955).
153. Stein, R. S. and Wilson, P. R., *ibid*, 33, 1914 (1962).
154. Stein, R. S., Erhardt, P., et. al., *ibid*, 37, 3980 (1966).
155. van Aartsen, J. J., J. Colloid Interface Sci., 39, 583 (1972).
156. Stein R. S. and Hotta, T., J. Appl. Phys., 35, 2237 (1964).
157. Stein, R. S., Erhardt, P., van Aartsen, J. J. and Clough, S., in Small Angle Scattering from Fibrous and Partially Ordered Systems, J. Polym. Sci., C13, 1 (1966).
158. Stein, R. S. and Hashimoto, T., J. Polym. Sci., A2, 8, 1503 (1970).
159. Stein, R. S. and Rhodes, M. B., J. Appl. Phys., 31, 1873 (1960).

160. Stein, R. S. and Rhodes, M. B., *ibid*, 39, 4903 (1966).
161. Samuels, R. J., *J. Polym. Sci.*, A2, 9, 2165 (1971).
162. Stein, R. S. and Chu, W., *J. Polym. Sci.*, A2, 8, 1137 (1970).
163. Samuels, R. J., *Ref. 149*, p. 37.
164. Stein, R. S., Rhodes, M. B. et. al., *Pure and Appl. Chem.*, 4, 219 (1962).
165. Motegi, M., Oda, T., Moritani, M. and Kawai, H., *Polym. J.*, 1, 209 (1970).
166. Stein, R. S. and Picot, C., *J. Polym. Sci.*, A2, 8, 1955 (1970).
167. Picot, C., Stein, R. S. et. al., *Macromolecules*, 4, 467 (1971).
168. Prud'homme, R. E. and Stein, R. S., *J. Polym. Sci., Phys. Ed.*, 11, 1357 (1973).
169. Picot, C., Stein, R. S. et. al., *J. Polym. Sci.*, A2, 8, 2115 (1970).
170. Stein, R. S. and Picot, C., *J. Polym. Sci.*, A2, 8, 2127 (1970).
171. Tatematsu, S., et. al., *Polymer J.*, 3, 488 (1972).
172. Prud'homme, R. E. and Stein, R. S., *J. Poly. Sci., Phys. Ed.*, 11, 1683 (1973).
173. Stein, R. S. and Hashimoto, T., *J. Polym. Sci.*, A2, 9, 1747 (1971).
174. Prud'homme, R. E., Yoon, D. and Stein, R. S., *J. Polym. Sci.*, (1971).
175. Yoon, D. A., *Ph.D. Thesis, University of Massachusetts* (1973).
176. Yoon, D. A., *Private Communication*.
177. Stein, R. S. and Keane, J. J., *J. Polym. Sci.*, 17, 21 (1958).
178. Prud'homme, R. E., Bourland, L., Natarajan, R. T. and Stein, R. S., *J. Polym. Sci., Phys. Ed.*, 12, 1955 (1974).

179. Misra, A., Prud'homme, R. E. and Stein, R. S., J. Polym. Sci., A2, 12, 1235 (1974).
180. Natarajan, R. T., Yoon, D., Prud'homme, R. E. and Stein, R. S., in preparation.
181. Ref.85, p. 283.
182. Kratky, O. and Miholic, G., J. Polym. Sci., Part C, 2, 449 (1963).
183. Ref. 85, p. 74.
184. Kratky, O., Pure and Applied Chemistry, 12, 483 (1966).
185. Stern, F., Trans. Faraday Soc., 51, 430 (1955).
186. Kahovek, L., Porod, G. and Ruck, H., Kolloid - Z., 133, 16 (1953).
187. Ref. 76, p. 15.
188. Yuen, H. K. and Kinsinger, J. B., Macromolecules, 7, 329 (1974).
189. Luzzati, V., Witz, J. and Nicolaieff, A., J. Molec. Biol., 3, 367 (1961).
190. Wendorff, J. H. and Fischer, E. W., Kolloid - Z. U.Z. Polym., 251, 876 (1973).
191. Hosemann, R., Polymer, 3, 349 (1962).
192. Shen, M. and Kaelble, D. H., J. Poly. Sci., B, 8, 149 (1970).
193. Peterlin, A., 46th National Colloid Symposium, University of Massachusetts, Amherst, Massachusetts, 1972.
194. Meier, D. J., Private Communication.
195. Perret, Von R. and Ruland, W., Kolloid - Z. U. Z. Polym., 247, 835 (1971).
196. Kim, H., Macromol., 5, 5, 594 (1972).
197. Roe, R. J. and Gieniewski, C., Macromol., 6, 2, 212 (1973).

198. J. H., Buchanan, D. R. and Bowles, B. B., J. Appl. Polym. Sci., 12, 2067 (1968).
199. Buchanan, D. R., McCullough, R. L. and Miller, R. L., Acta. Cryst. 20, 922 (1966).
200. Buchanan, D. R. and Miller, R. L., J. Poly. Sci., B, 5, 771 (1967).
201. Bittiger, M., Marchessault, R. H. and Niegisch, W. D., Acta. Cryst., B26, 12, 1923 (1970).
202. Chatani, Y., et. al., Polymer Journal, 1, 5, 555 (1970).
203. Bunn, C. W. and Daubeny, P. R. De., Trans. Far. Soc., 50, 1173 (1954).
204. Denbigh, K. G., Trans. Far. Soc., 36, 936 (1940).
205. Kiessig, H., Kolloid-Z., 152, 62 (1957).
206. Ref. 92, p. 103.
207. Kratky, O., in "Kratky x-ray small angle camera" Anton Paar K. G., A-8054 Graz, Austria.
208. Instruction Manual 2202, Rigaku-Denki, Ch. IV.
209. Prud'homme, R. E., Ph.D. Thesis, University of Massachusetts, Amherst, Massachusetts, 1973.
210. Schmidt, P. W., Acta. Cryst. 19, 938 (1965).
211. Hendricks, R. W., and Schmidt, P. W., Acta Phys. Austriaca, 26, 97, (1967).
212. Buchanan, M. G. and Hendricks, R. W., Program Weight: A Fortran IV Program for Evaluation of Weighting Functions Used in Small-Angle X-Ray Scattering, ORNL-TM-1950 (1967).

213. Parrish, W. and Kohler, T. R., Rev. Sci. Instr., 27, 10, 795 (1956).
214. Parrish, W., Philips Tech. Rev., 17, 7-8, 206 (1956).
215. Dowling, P. H., et. al., ibid, 18, 9, 262 (1957).
216. Cullity, B. D., Elements of X-Ray Diffraction, Addison-Wesley Publ. Co., Inc. (1967), p. 204.
217. Kratky, O., Pilz I. and Schmitz, P. J., J. Colloid Interface Sci., 21, 24 (1966).
218. Hashimoto, T., Ph.D. Thesis, University of Massachusetts (1971).
219. Sanchez, I. C. and Eby, R. K. Journal of Research of the National Bureau of Standards - A. Physics and Chemistry, 77A, No. 3, May-June (1973).
220. Gezovich, D. M. and Geil, P. H., Intern. J. Polymeric Mater., 1, 3 (1971).
221. Tsou, P. K. C. and Geil, P. H., ibid, 1, 223 (1972).
222. Berens, A. R. and Folt, V. L., Trans. Soc. Rheology, 11, 1, 95 (1967).
223. Abdel-Alim, A. H. and Hamielec, A. E., J. Appl. Poly. Sci., 17, 3033 (1973).
224. Neilson, F. G. and Jabarin, S. A., J. Appl. Phys., 46, 3, 1175 (1975).
225. Singleton, C., Isner, J., Gezovich, D. M., Tsou, P. K. C., Geil, P. H. and Collins, E. A., Dept. of Macromol. Sci., Case Western Reserve Univ., Tech. Rep. 261 (1973).
226. Daniels, C. A. and Collins, E. A., J. Macromol. Sci. - Phys., B10(2), 287 (1974).

LIST OF FIGURES

- Fig. 1 a)* Hess-Kessig model showing distance between crystallites.
 b)† Statton-Geil STRING-BUNDLE model.
- Fig. 2 Scattering geometry showing 2θ the scattering angle.
- Fig. 3 Two phase random morphology showing the respective chord lengths through each phase.
- Fig. 4 Typical form of the Debye-Bueche correlation function $\gamma(r)$.
- Fig. 5 Electron density profile within a non-crystalline material of random morphology.
- Fig. 6** Paracrystallinity model of Hosemann.
- Fig. 7 Bonart's model showing the successive simplification in the electron density-profiles of the original domain morphology. (i) diffuse (ii) intermediate (iii) sharp.
- Fig. 8 Stein-Khambatta model showing isolated homogeneous domains separated by diffuse transition zones in a homogeneous matrix.
- Fig. 9 Electron density profile of the Stein-Khambatta model showing phase boundary of thickness ϵ .
- Fig. 10 Tsvankin model showing the parallel stacking of crystalline lamellae and amorphous layers and their trapezoidal electron density profile.
- Fig. 11 Buchanan calibration curves for the Tsvankin model for $\epsilon = 0.2$ and (a) $\beta/\alpha = 0.1$ (b) $\beta/\alpha = 0.2$ and (c) $\beta/\alpha = 0.3$.

* By permission of IPC Science and Technology Press Ltd.: Polymer Vol. 3. Fig. 35(a) pp. 379 (1962).

† By permission of John Wiley & Sons, Inc.: Fig. VI-26, pp. 272, Newer Methods of Polymer Characterization, Ed. Bacon Ke, Inter. Sc. 1964.

** By permission of IPC Science and Technology Press Ltd.: Polymer Vol. 3, Fig. 46, pp. 387 (1962).

- Fig. 12 Small-angle light-scattering geometry for photographic studies.
- Fig. 13 Flow chart for automatic step-scanning operation of small-angle x-ray goniometer.
- Fig. 14 Slit-collimation system for small-angle x-ray goniometer.
- Fig. 15 Profile of the incident x-ray beam.
- Fig. 16 A truncated spherulite showing the distance from its center to truncated side.
- Fig. 17 Truncation correction factor F_{TRUNC} versus the truncation parameter $\langle \sigma^2 / \bar{a}^2 \rangle$.
- Fig. 18 Multiple scattering correction factor K versus Td (product of turbidity T and thickness d).
- Fig. 19 Optical micrographs of different blend compositions.
- Fig. 20 a) H_V (SALS) and b) V_V (SALS) both with same sample to film distance and exposure times showing typical patterns. c) V_V (SALS) with different exposures and sample to film distance showing equatorial scattering arcs due to periodic twisting of lamellae.
- Fig. 21 Scanning electron micrographs of crystalline blend compositions showing spherulitic superstructure.
- Fig. 22 Spherulite size versus blend composition.
- Fig. 23 Wide-angle X-ray diffraction photographs showing constancy of 'd' spacing.
- Fig. 24 The variation in relative SAXS intensity with 2θ for PCL.
- Fig. 25 The variation in relative SAXS intensity with 2θ for 90/10.
- Fig. 26 The variation in relative SAXS intensity with 2θ for 80/20.
- Fig. 27 The variation in relative SAXS intensity with 2θ for 70/30.
- Fig. 28 The variation in relative SAXS intensity with 2θ for 60/40.
- Fig. 29 The variation in relative SAXS intensity with 2θ for 50/50.
- Fig. 30 The variation of the long period c, the crystal thickness a, and the linear crystallinity k as a function of the weight fraction of PVC in the blend.

- Fig. 31 The variation of the degree of crystallinity of PCL in PCL-PVC blends with volume fraction PCL as determined from density, DSC and SAXS.
- Fig. 32 The variation of periodicity of helicoidal crystal orientation within spherulites of blends as a function of weight fraction of PVC.
- Fig. 33 The variation in relative SAXS intensity with 2θ for 40/60.
- Fig. 34 The variation in relative SAXS intensity with 2θ for 30/70.
- Fig. 35 The variation in relative SAXS intensity with 2θ for 20/80.
- Fig. 36 The variation in relative SAXS intensity with 2θ for 10/90.
- Fig. 37 The variation in relative SAXS intensity with 2θ for PVC.
- Fig. 38 SAXS curve showing the Guinier, Debye and Porod kind of scattering regions as a function of scattering angle 2θ .
- Fig. 39 Debye-Bueche plots of 30/70, 20/80 and 10/90 compositions showing linearity in the intermediate Debye region.
- Fig. 40 The variation of the Debye correlation distance $\bar{\ell}_c$ and the Porod "inhomogeneity lengths" $\bar{\ell}_{PCL}$ and $\bar{\ell}_{PVC}$ with composition for the amorphous blends.
- Fig. 41 A corrected Debye-Bueche plot of the variation of $(I_{BL})^{-1/2}$ with θ^2 for the amorphous blends.
- Fig. 42 Typical plots of corrected desmeared SAXS intensity with 2θ for 30/70 and 20/80 compositions showing error bars.
- Fig. 43 A proposed gel model for PVC showing the distance between the center of gel particles increasing with the addition of PCL.
- Fig. 44 Transition zone plots by the Bonart method for 40/60.
- Fig. 45 Transition zone plots by the Bonart method for 30/70.
- Fig. 46 Transition zone plots by the Bonart method for 20/80.
- Fig. 47 Transition zone plots by the Bonart method for 10/90.
- Fig. 48 A plot of $K_4 \langle \eta^2 \rangle / \phi_{PCL}$ against ϕ_{PCL} for the amorphous blends.
- Fig. 49 Variation of $\langle \eta^2 \rangle$ with weight fraction PVC in the blends.
- Fig. 50 Variation of Porod slope k_2 with composition.

Fig. 51 A comparison of the variation of the corrected experimental values of $R(\theta, 45^\circ)$ as a function of reduced scattering angle for various compositions.

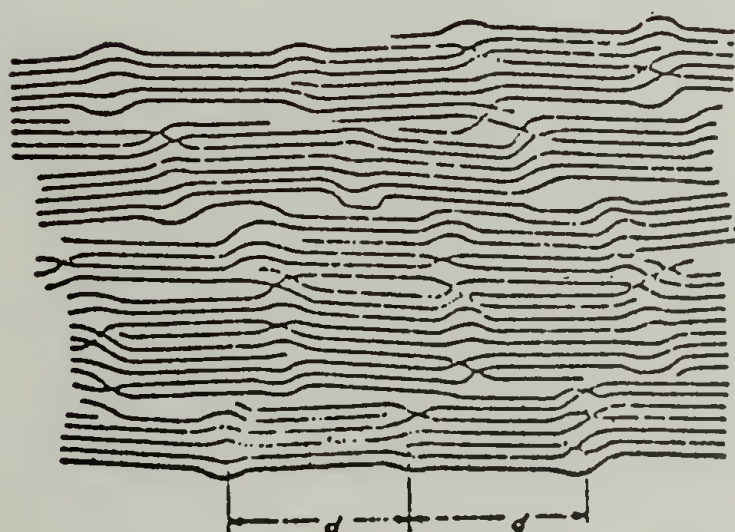


Fig. 1

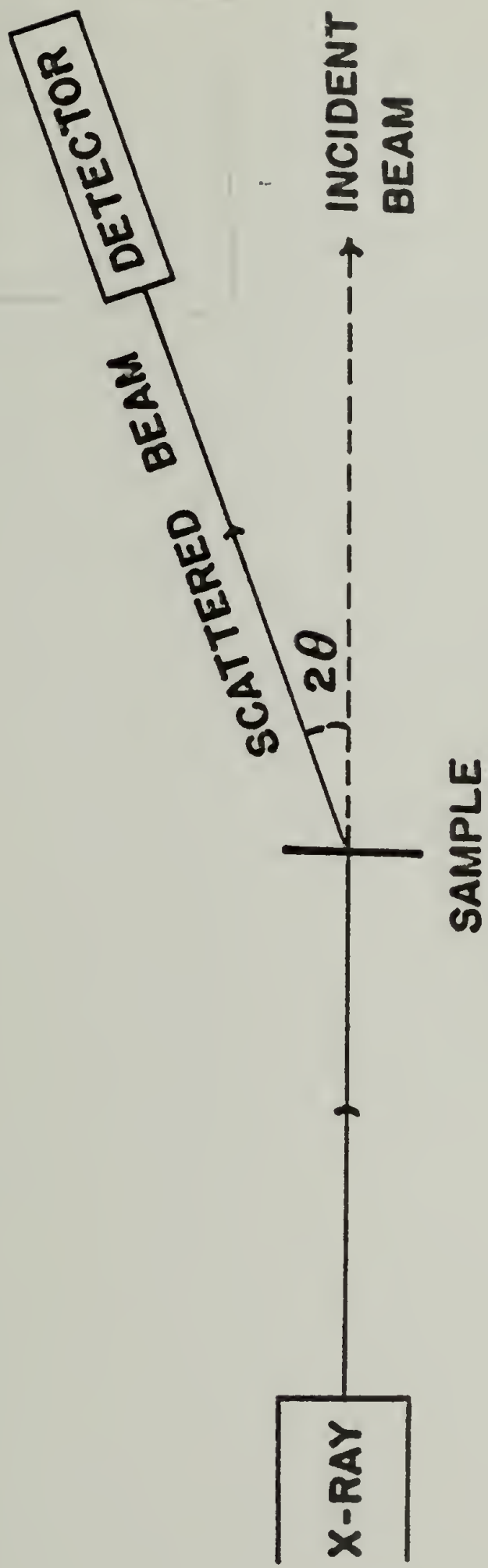


Fig. 2

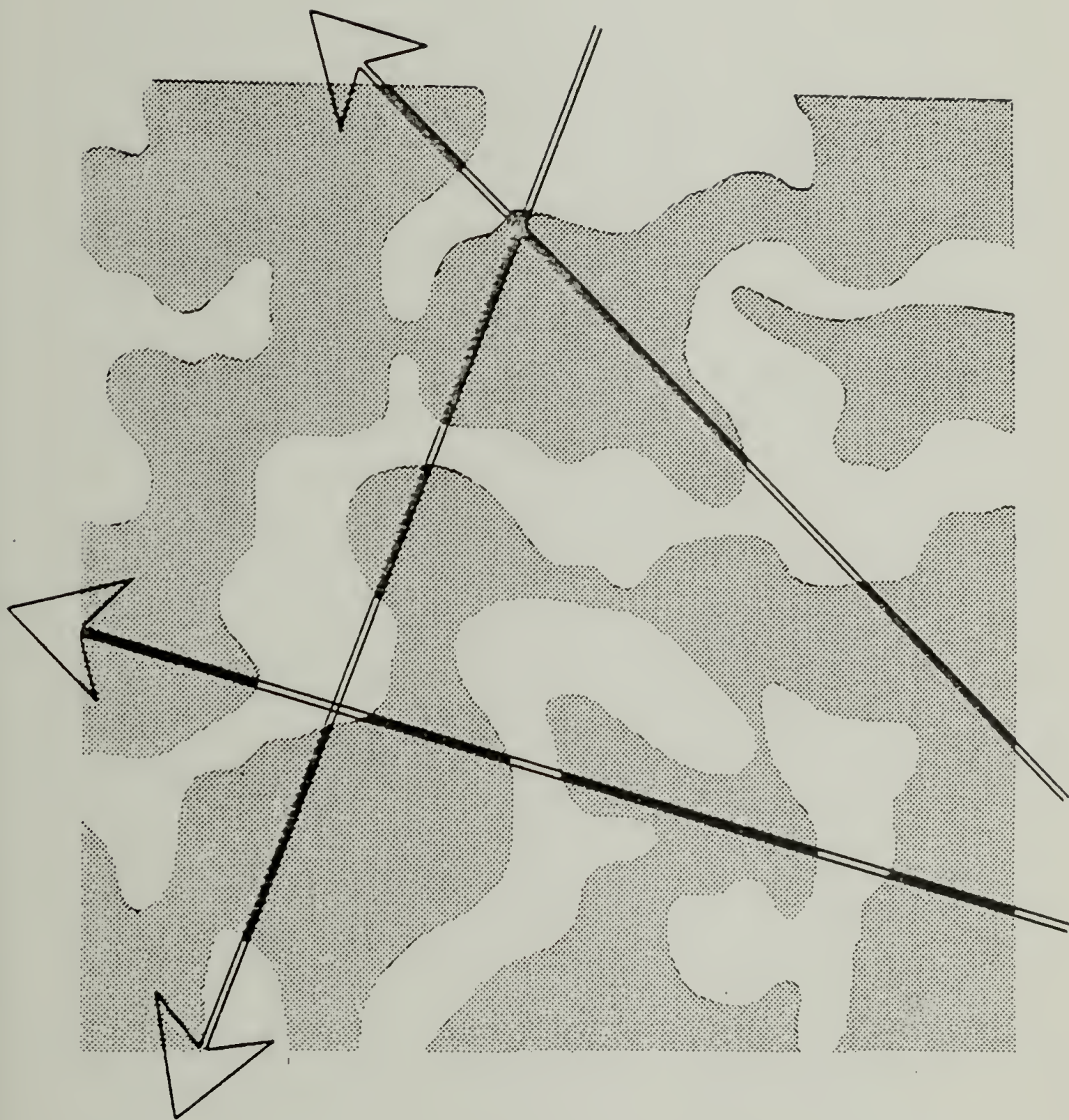


FIG. 3

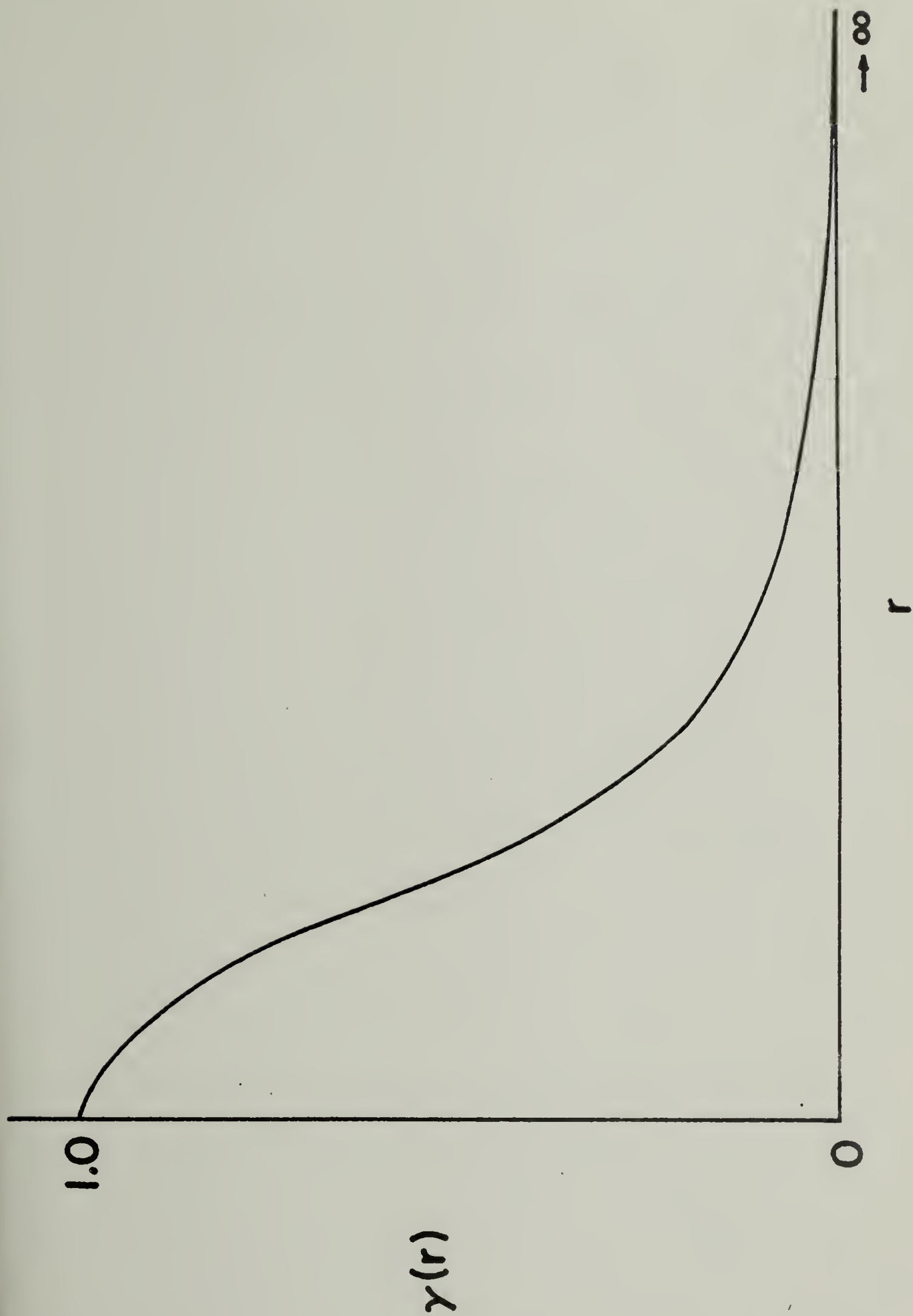


Fig. 4

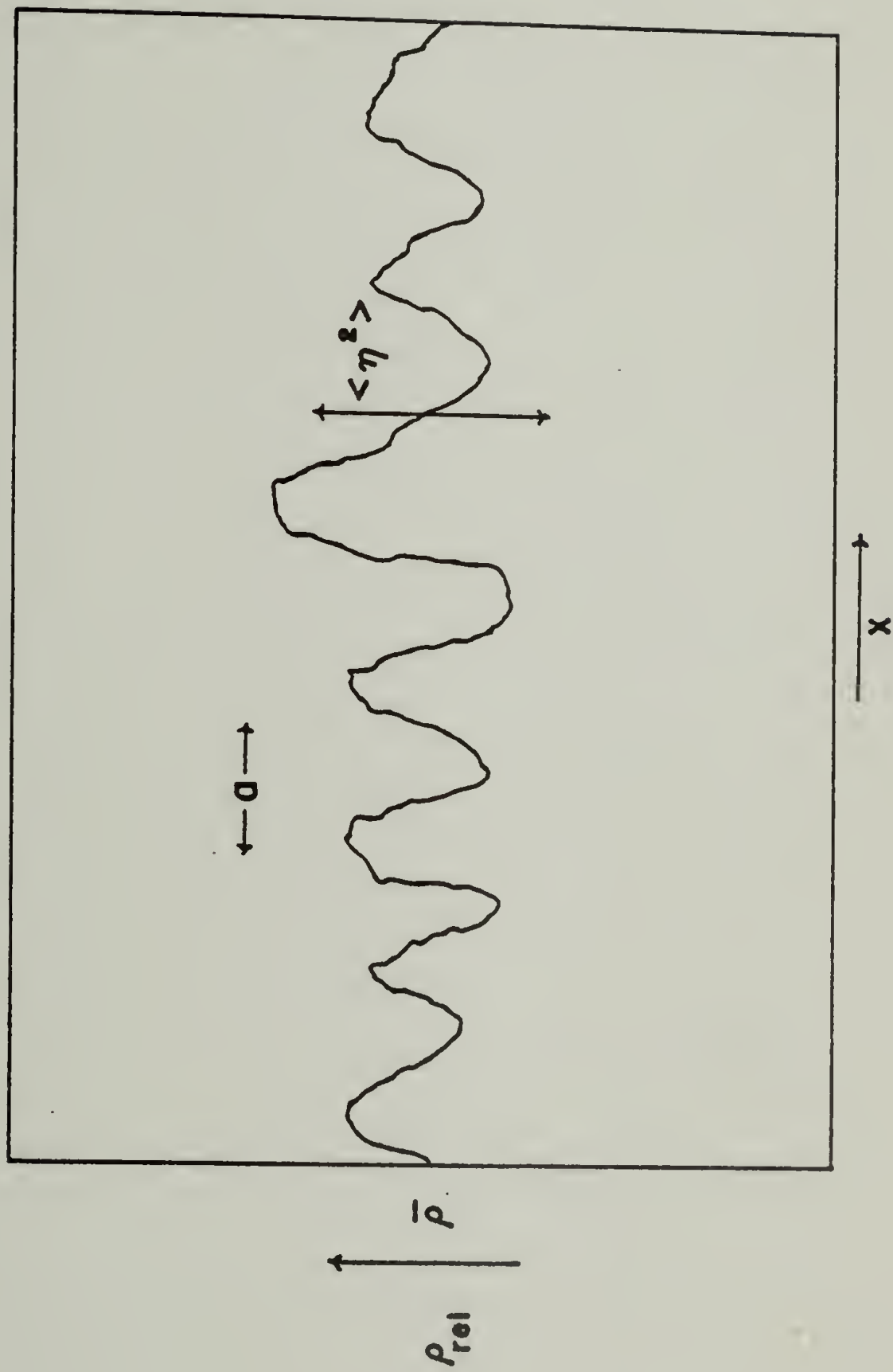


Fig. 5

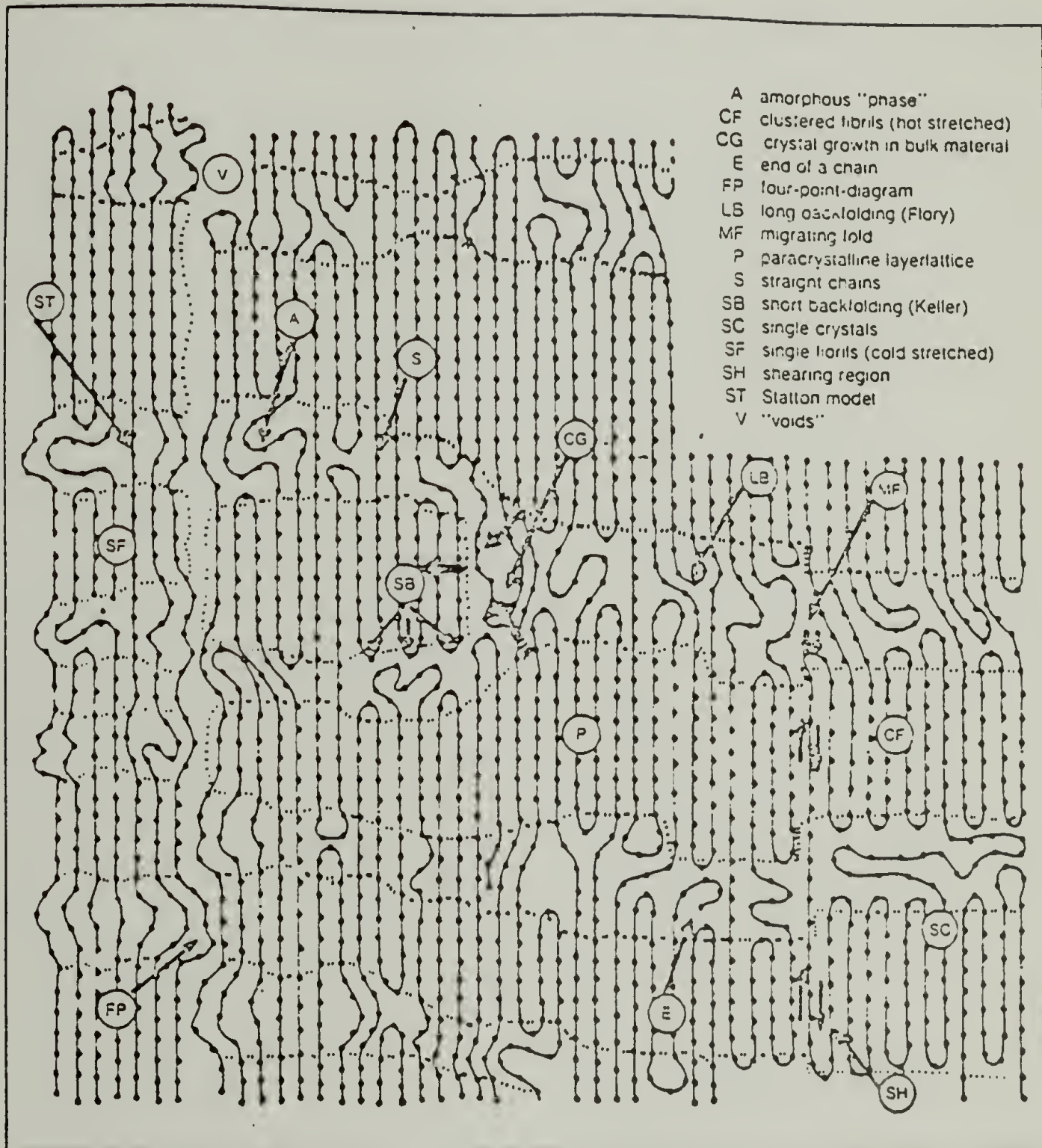


Fig. 6

BONART'S ANALYSIS

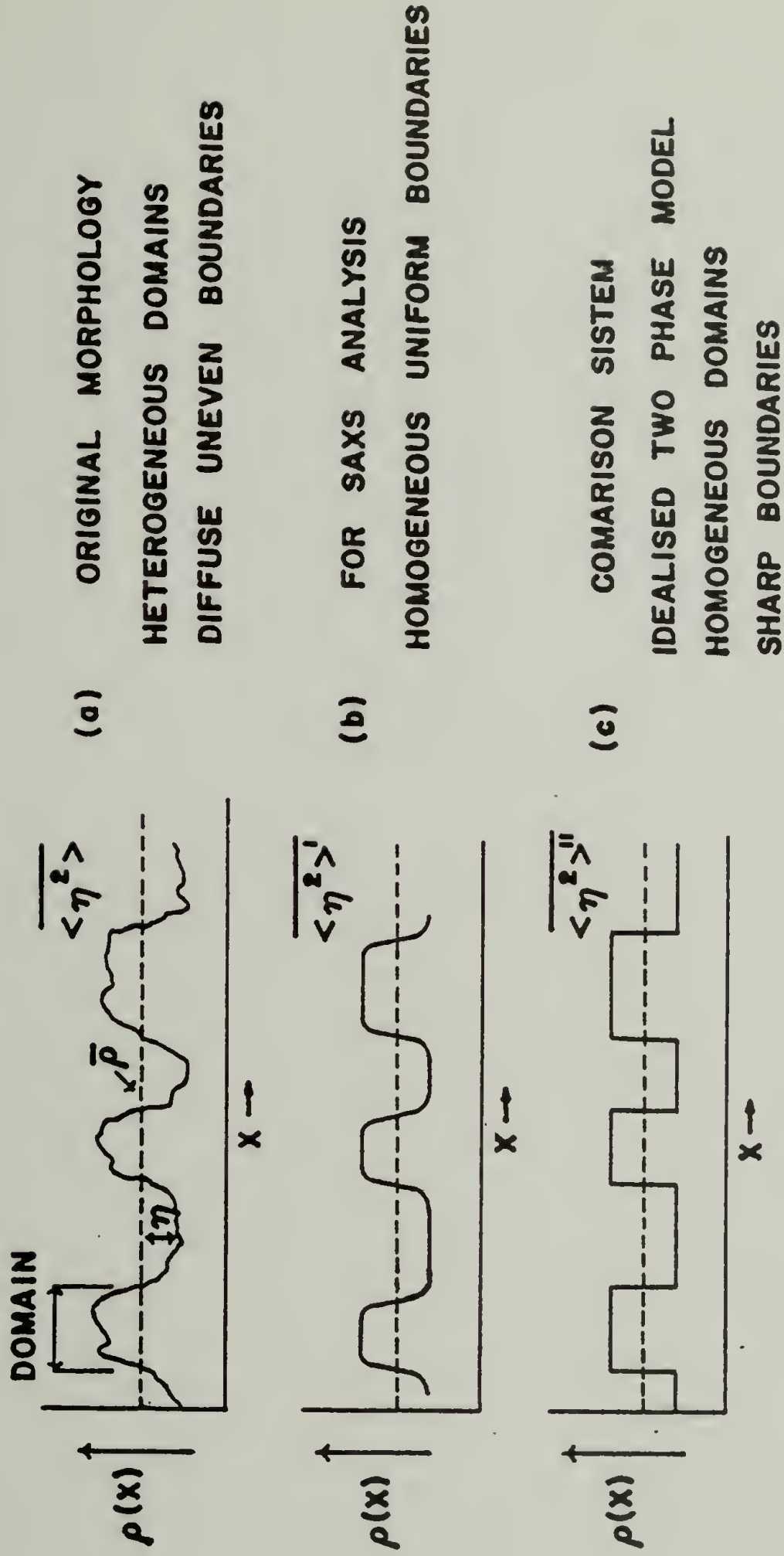


Fig. 7

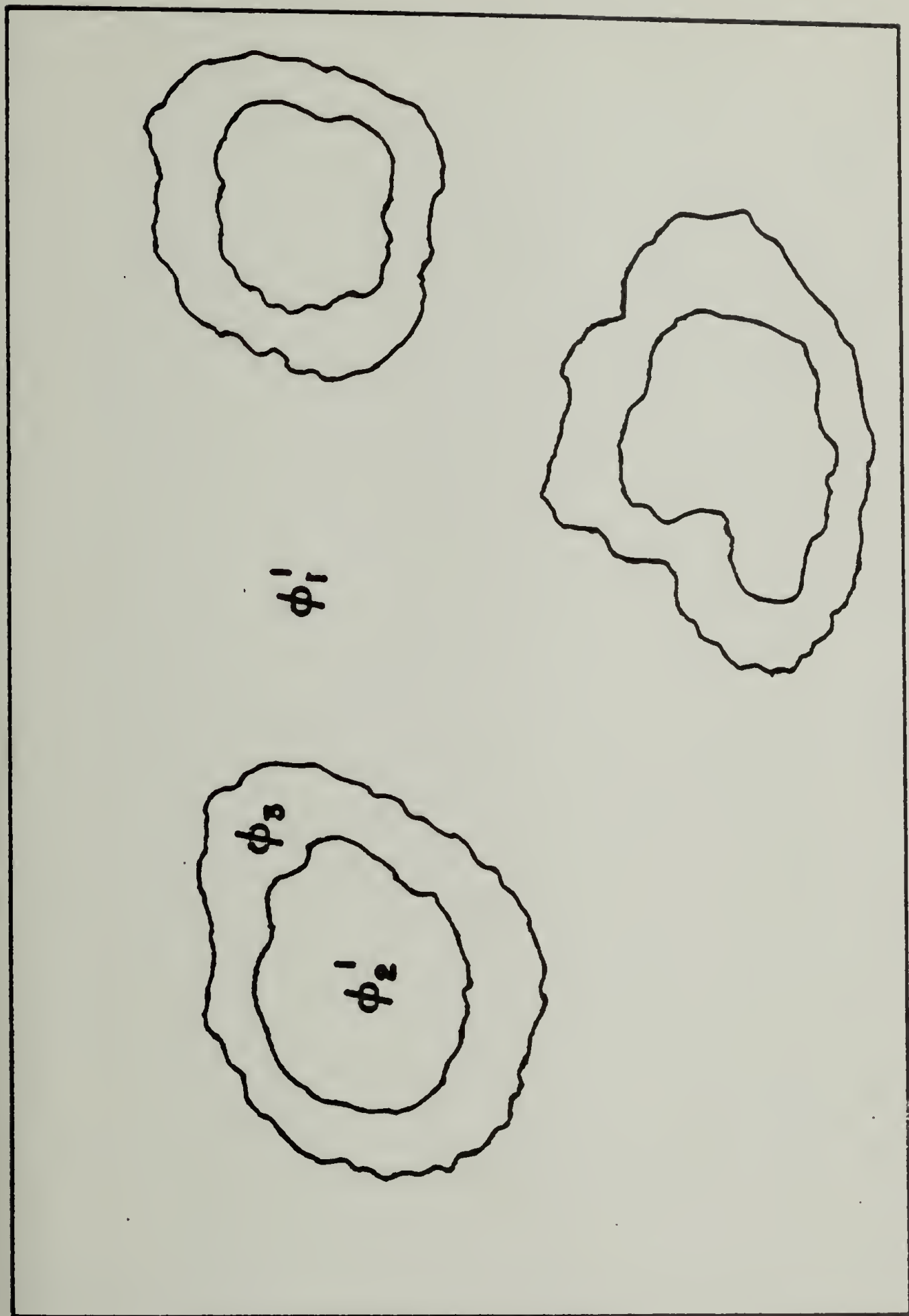


Fig. 8

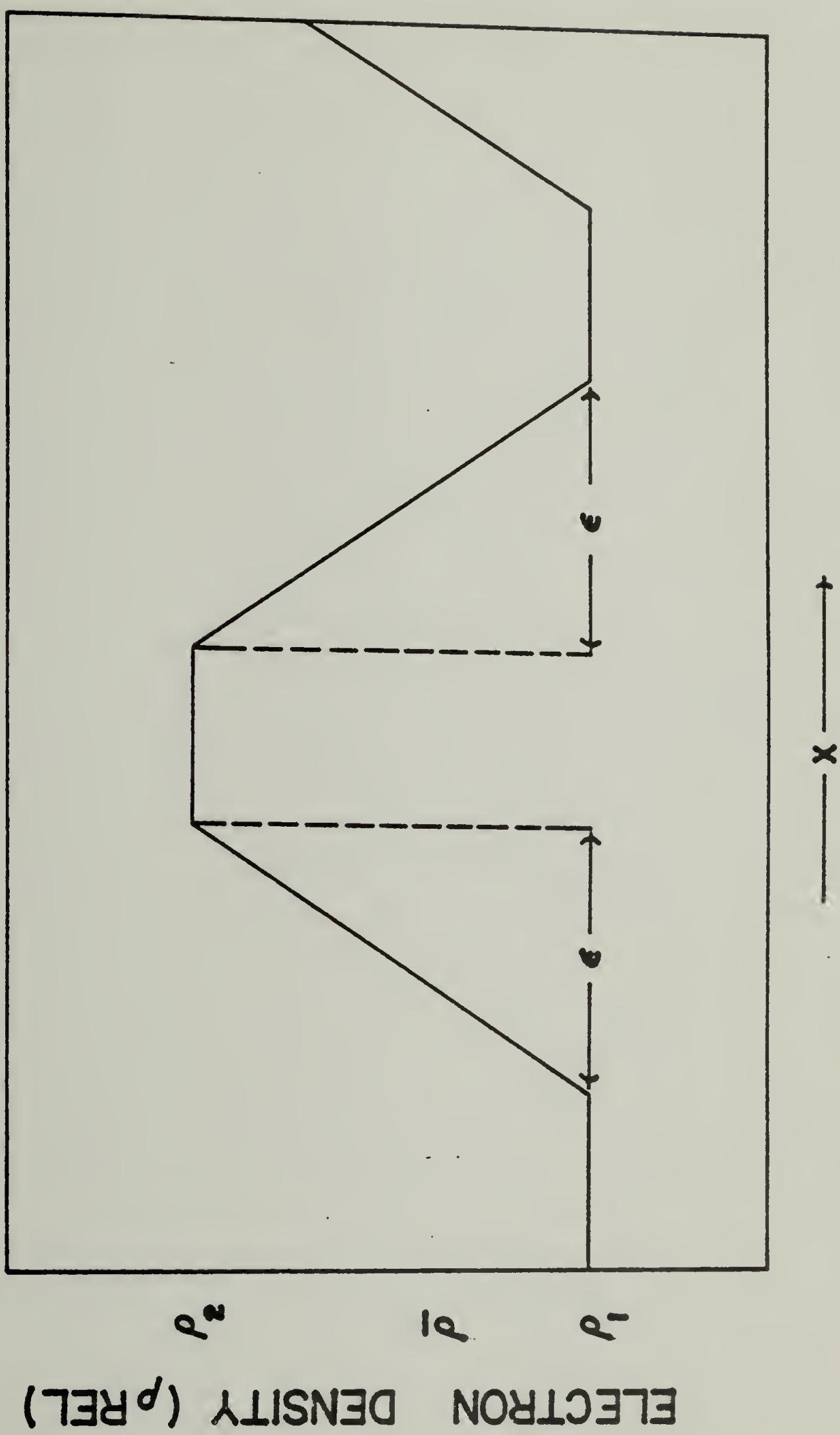
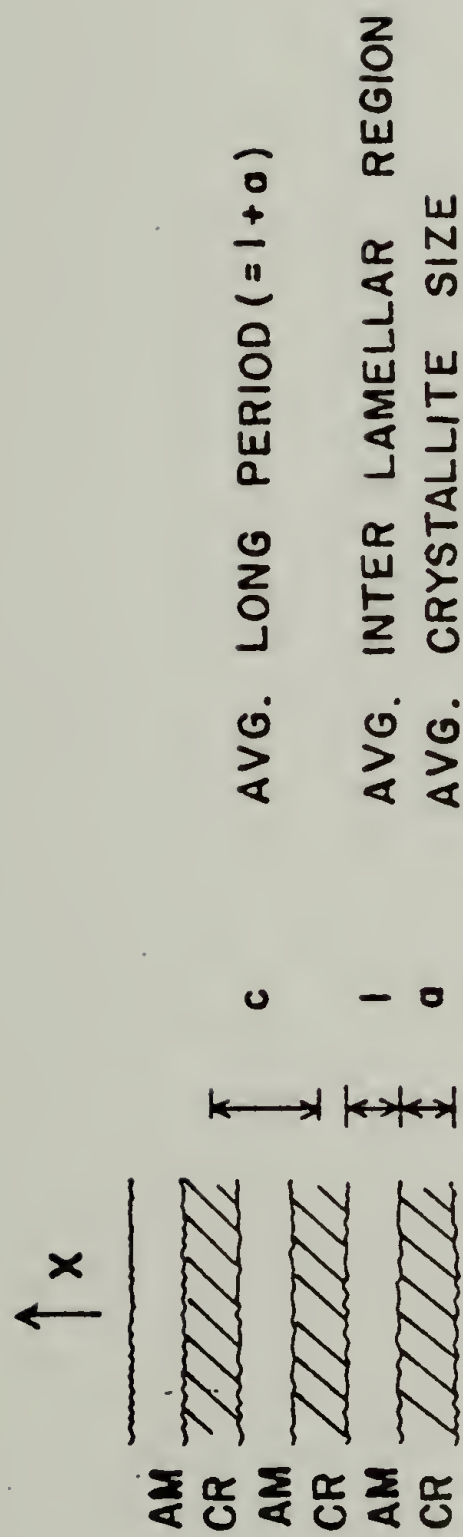


Fig. 9



RELATIVE ELECTRON DENSITY ρ_z WITHIN A CRYSTAL OF LENGTH x

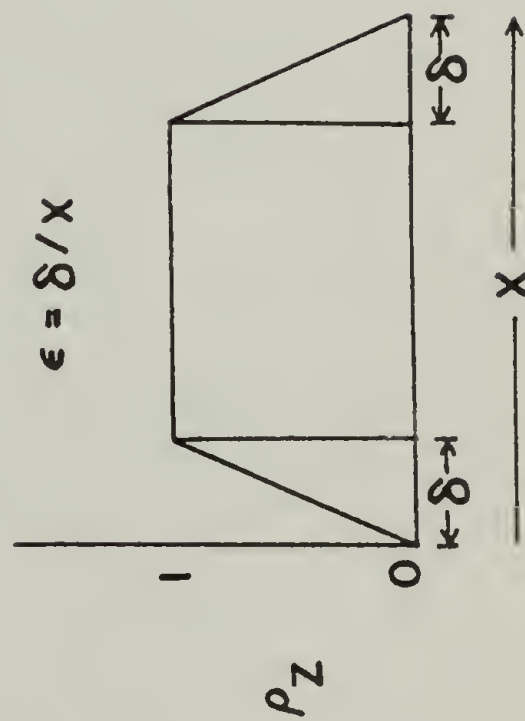


FIG. 10

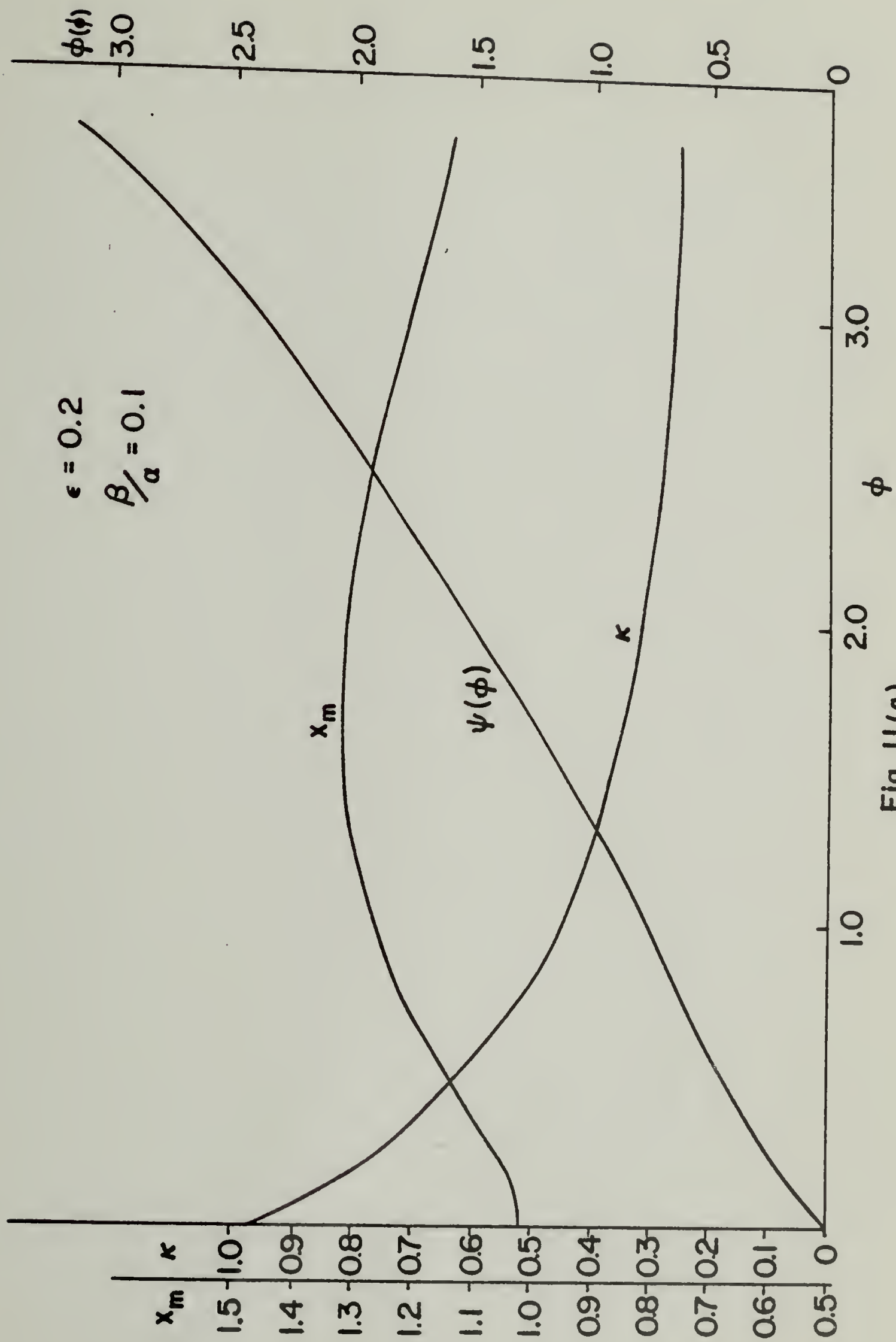


Fig. 11(a)

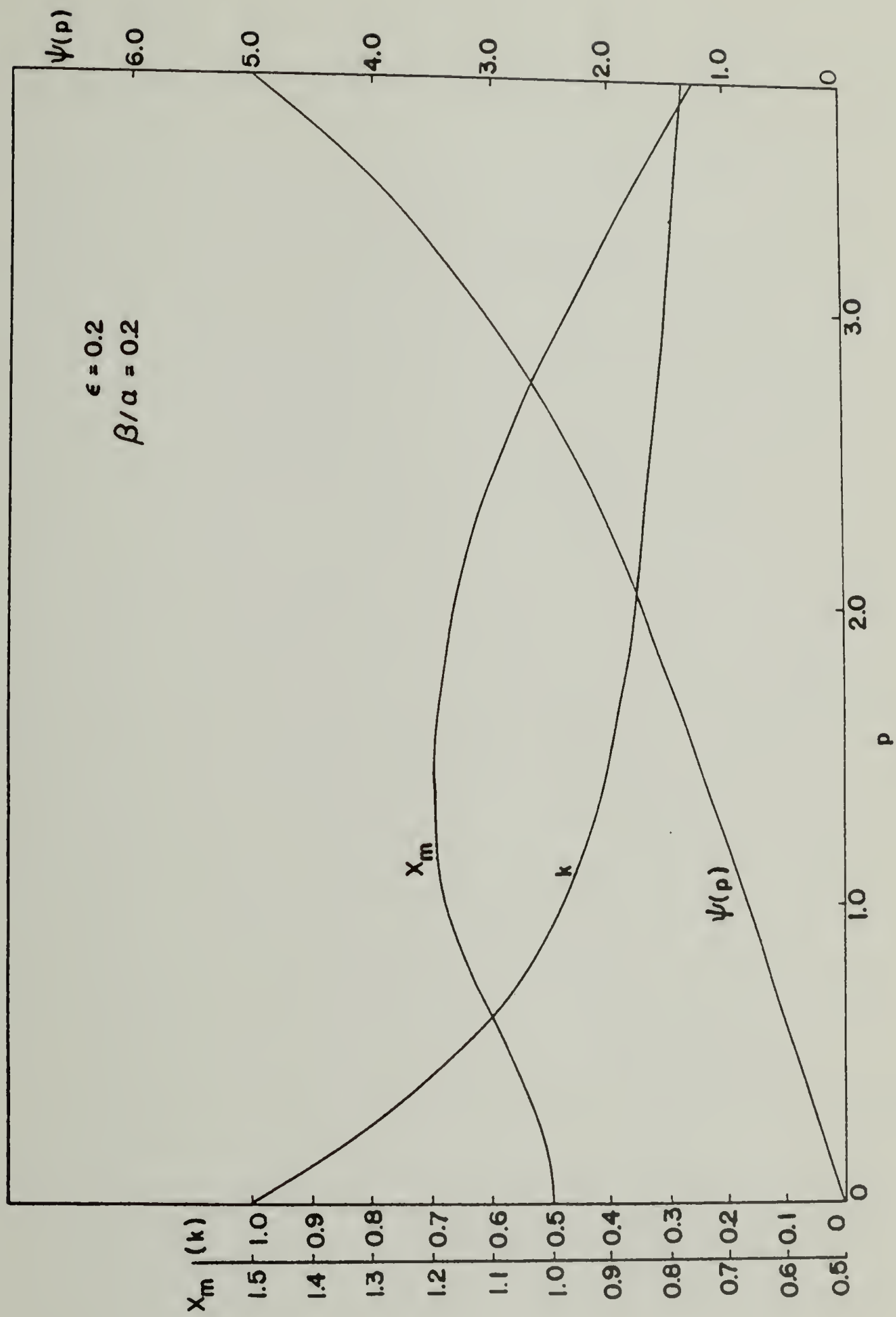


Fig. 11(b)

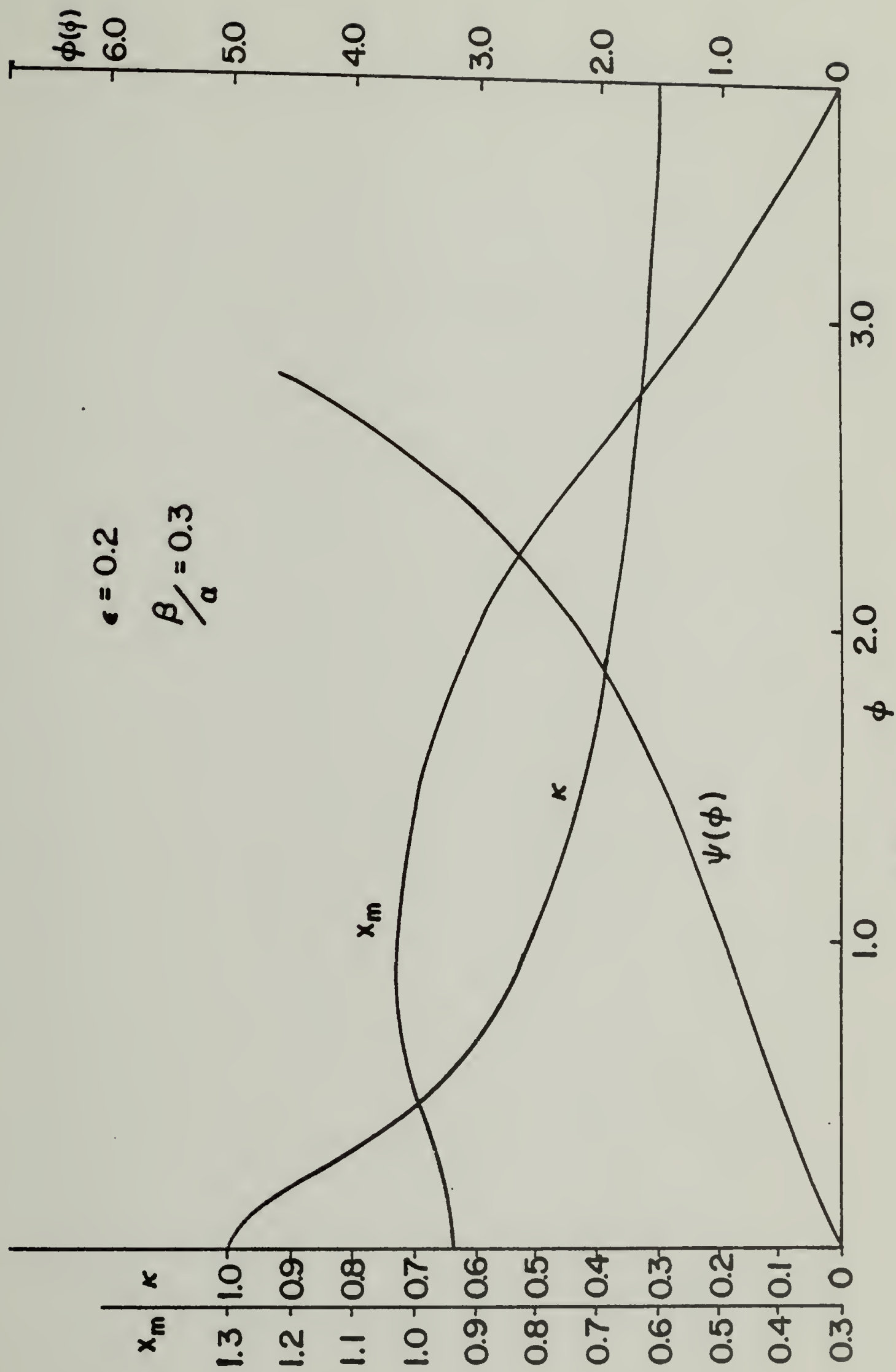


Fig. 11(c)

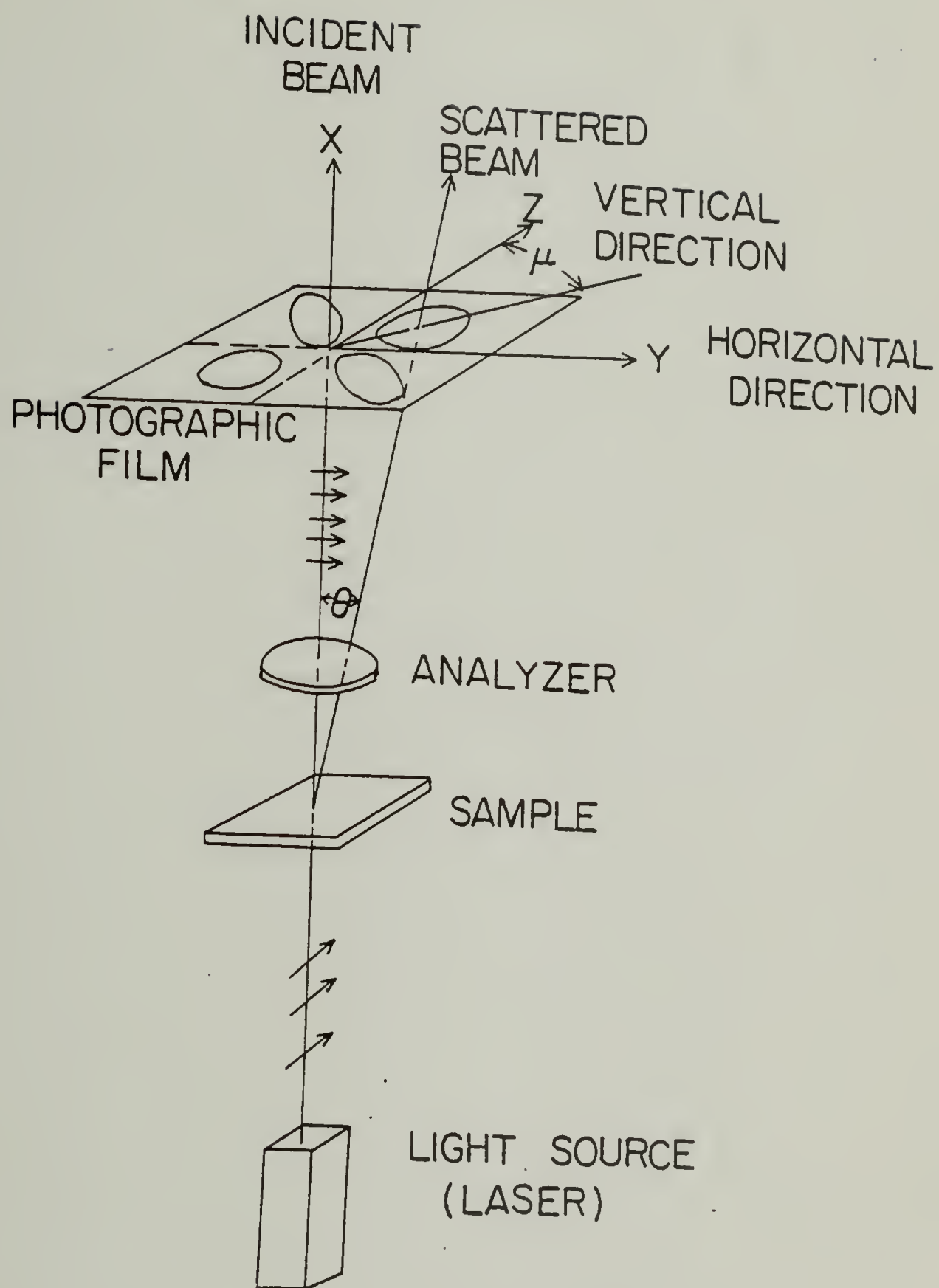


FIG. 12

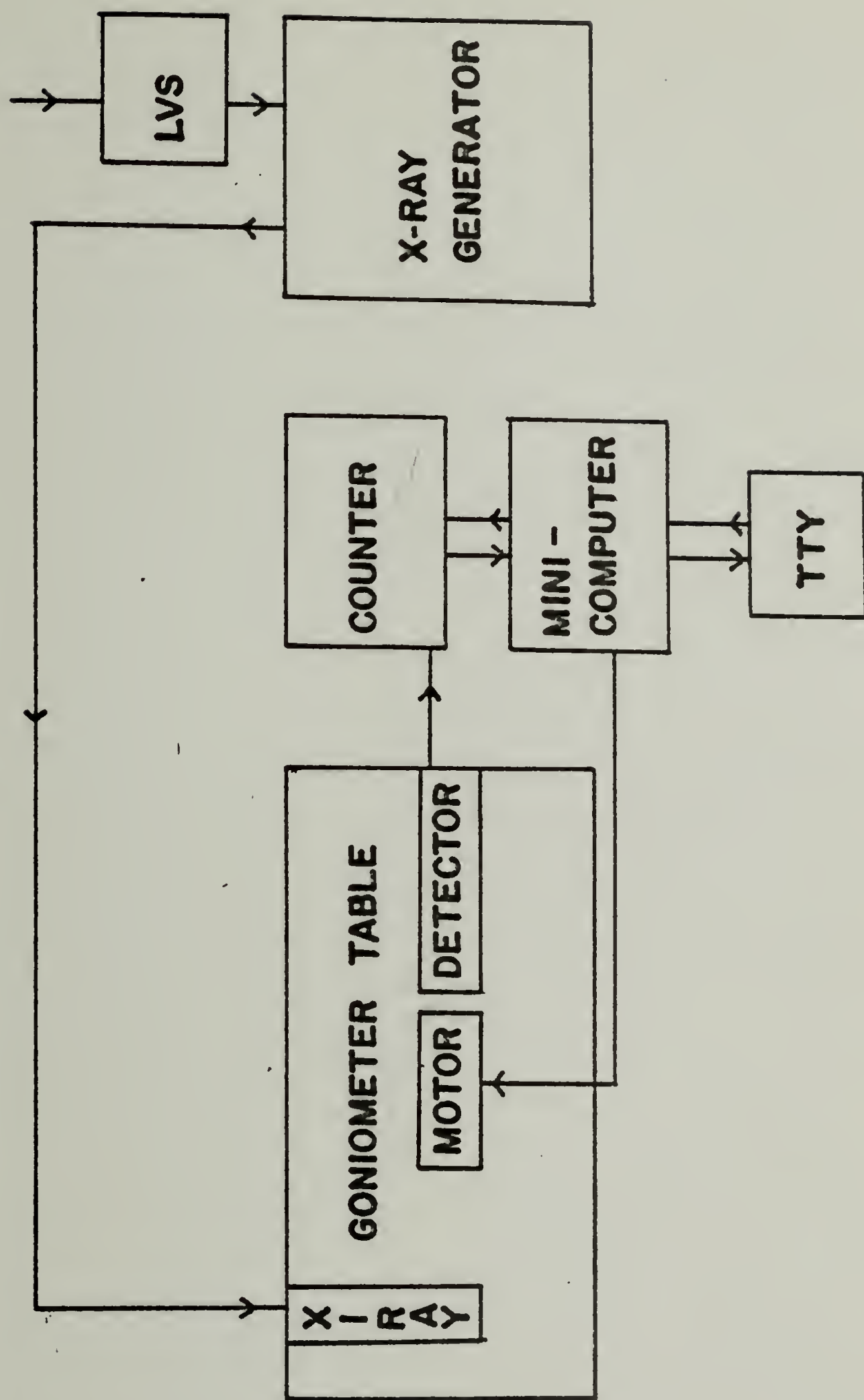


Fig. 13

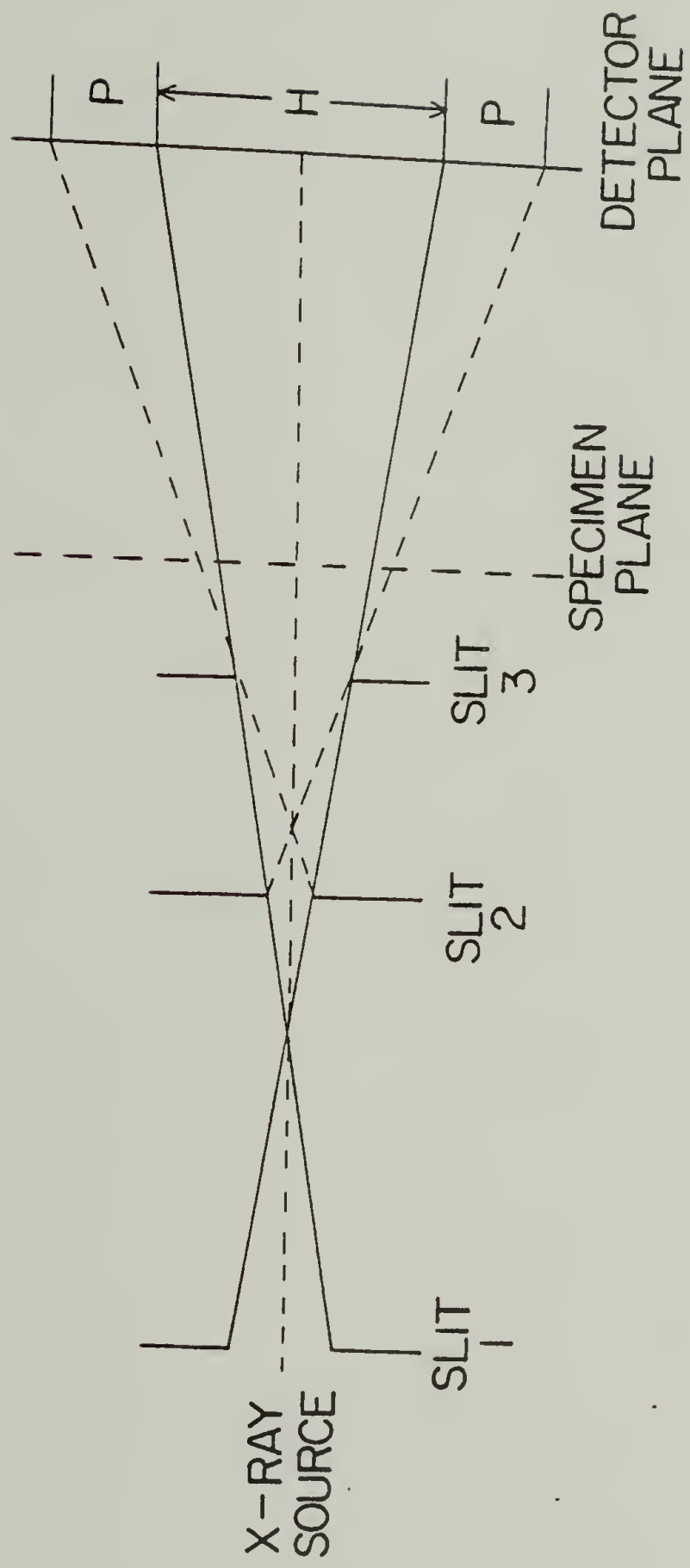


FIG. 14

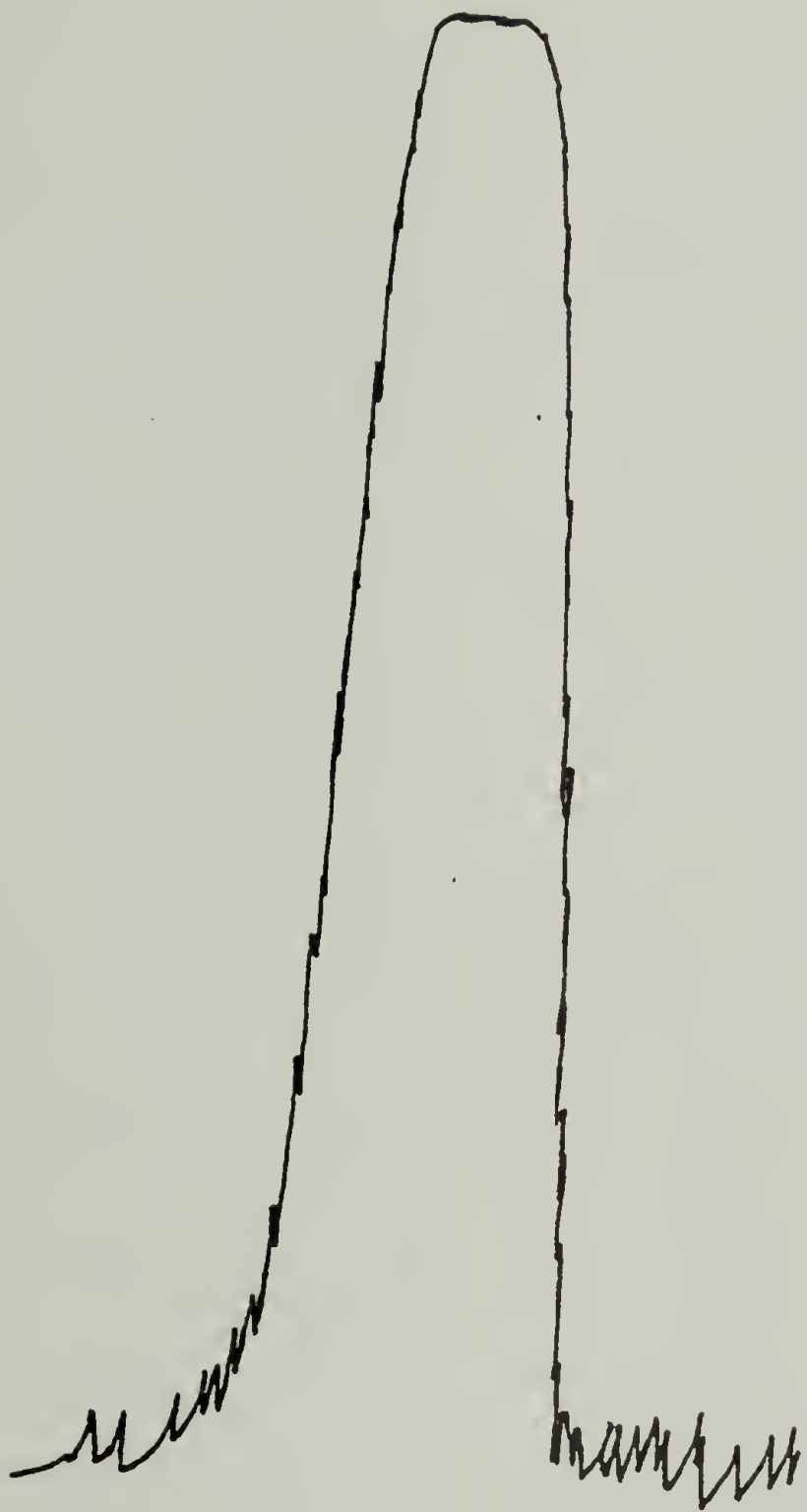


Fig. 15

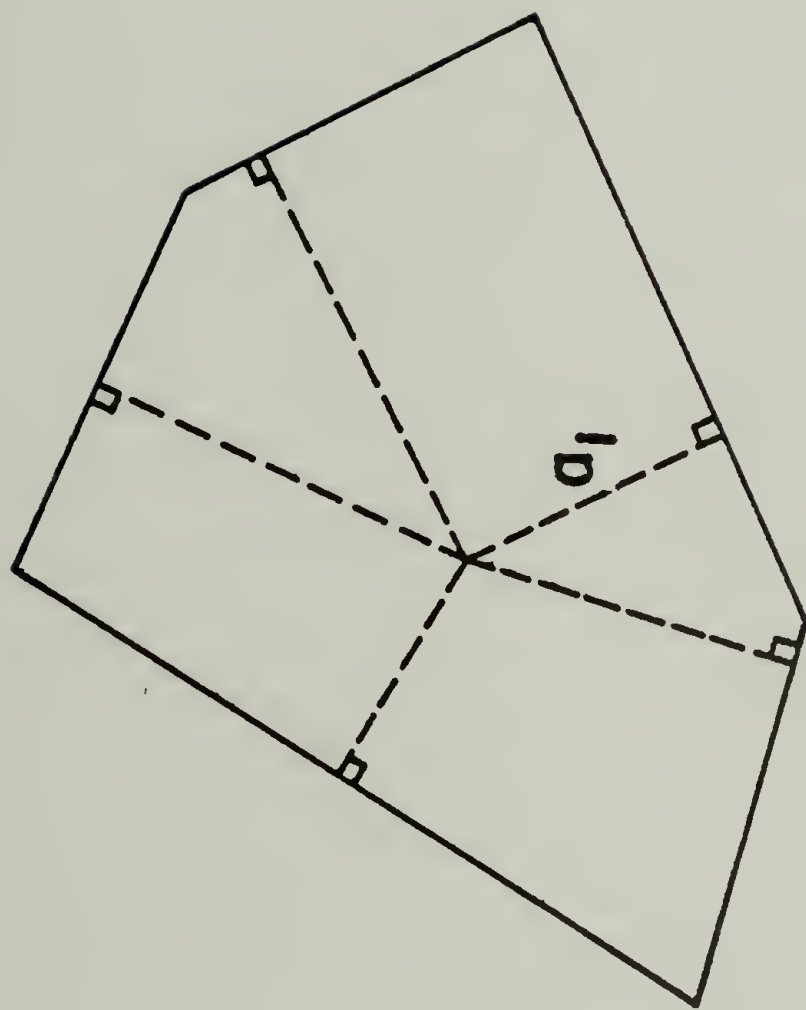


Fig. 16

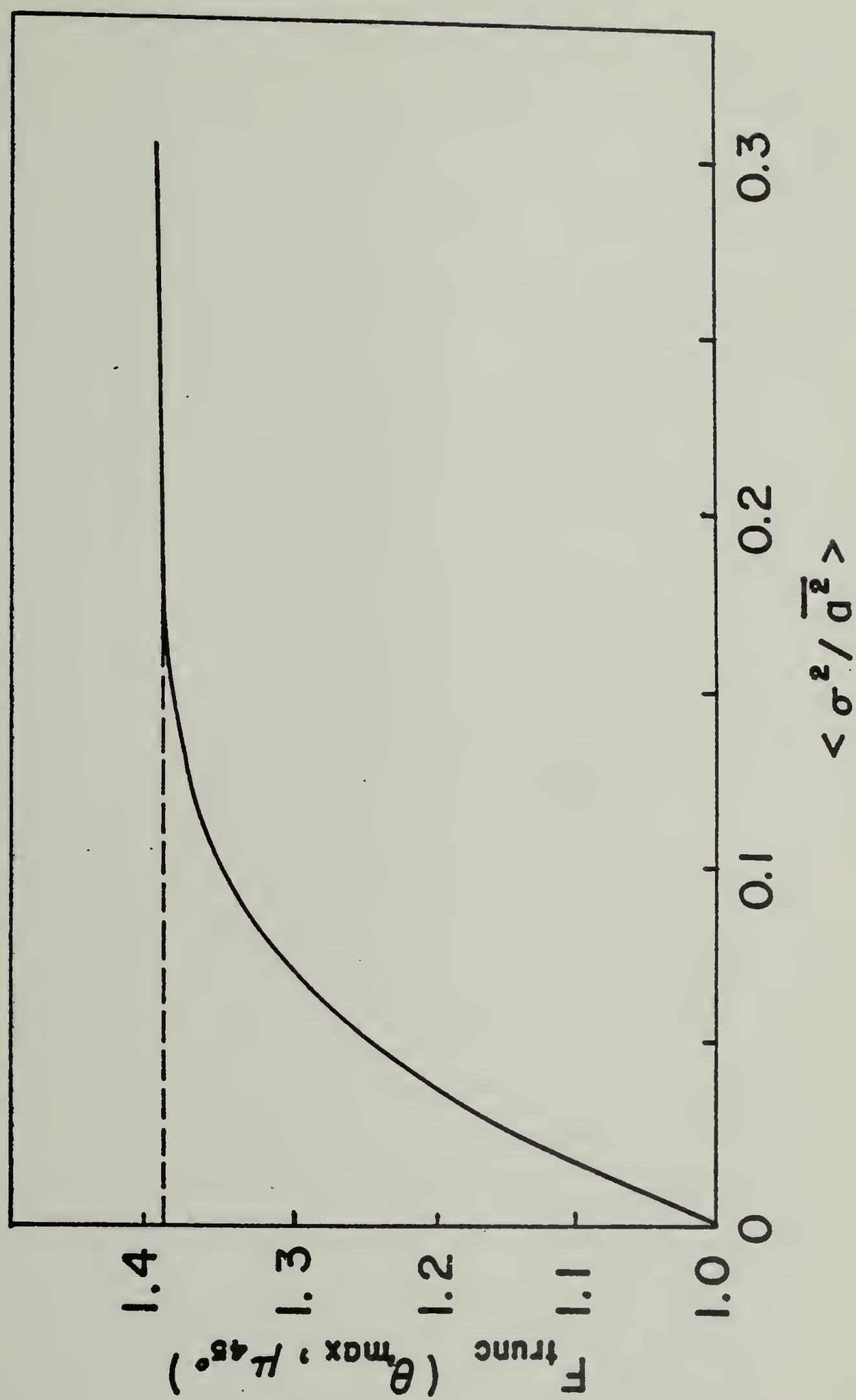


Fig. 17

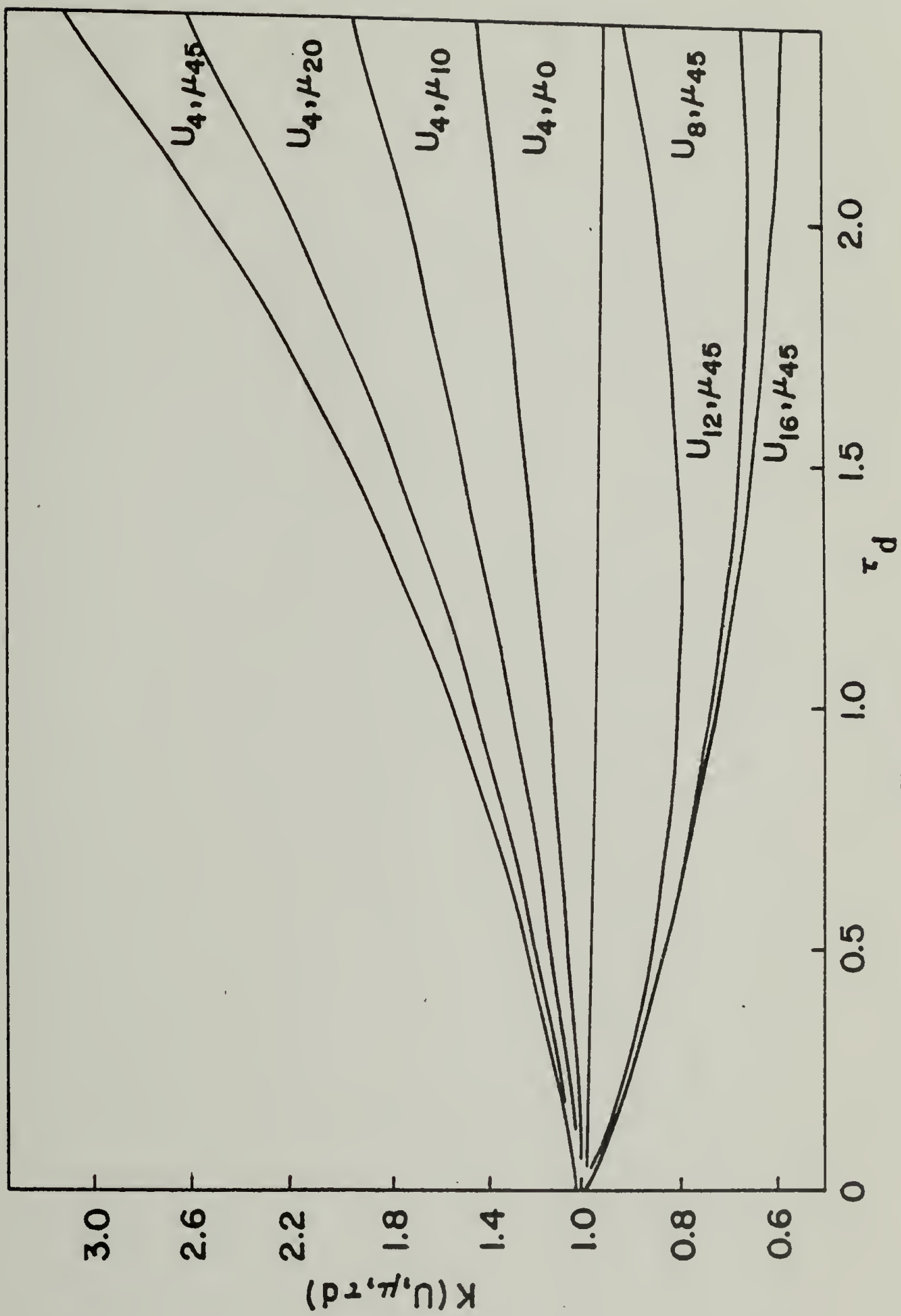
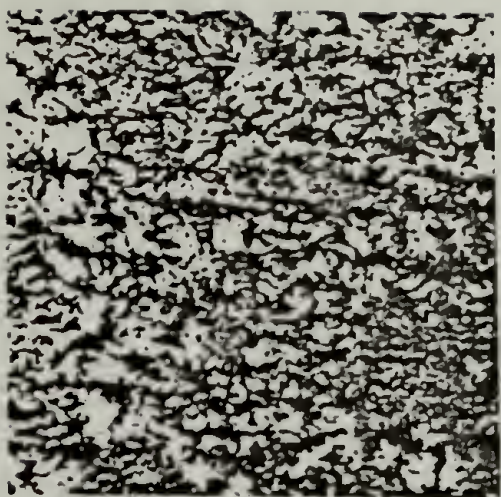
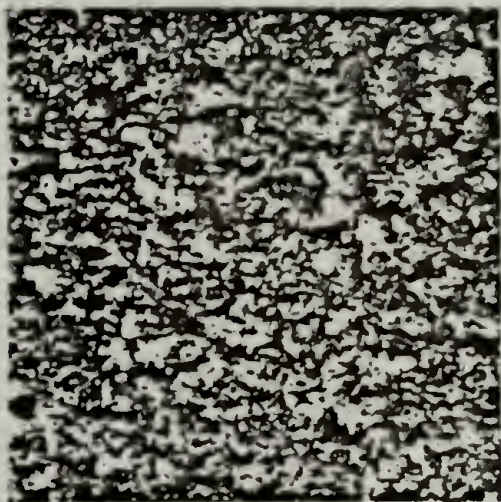


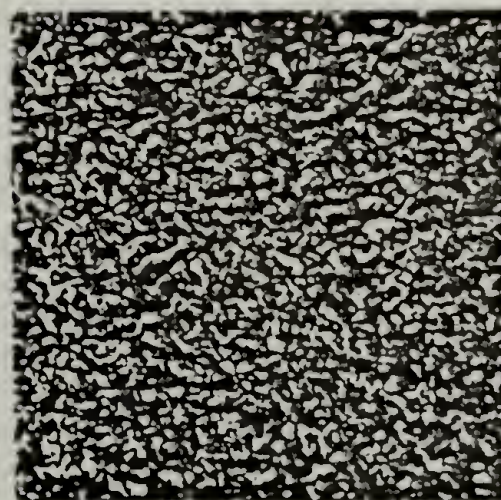
Fig. 18



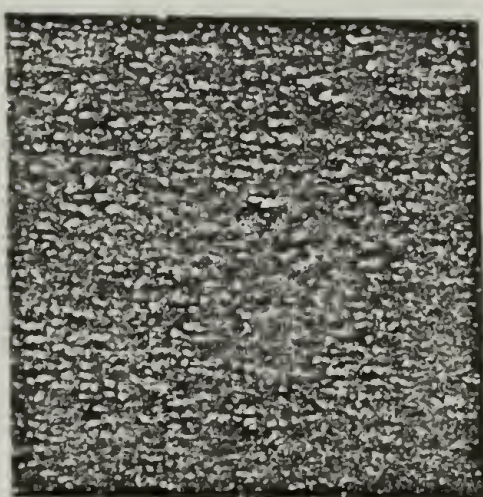
PCL



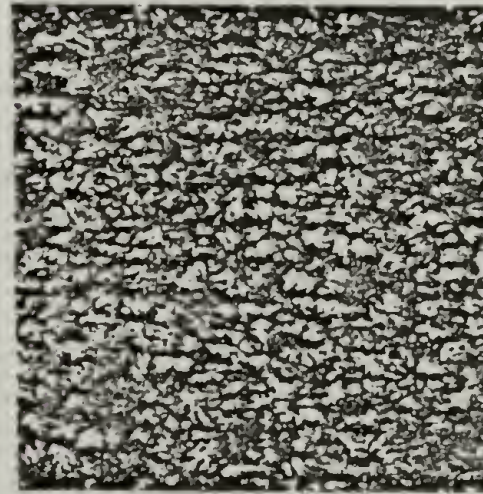
90/10



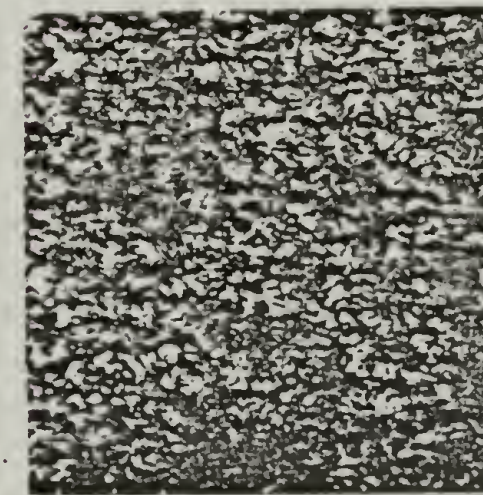
80/20



50/50



60/40



70/30

50 μ

FIG. 19

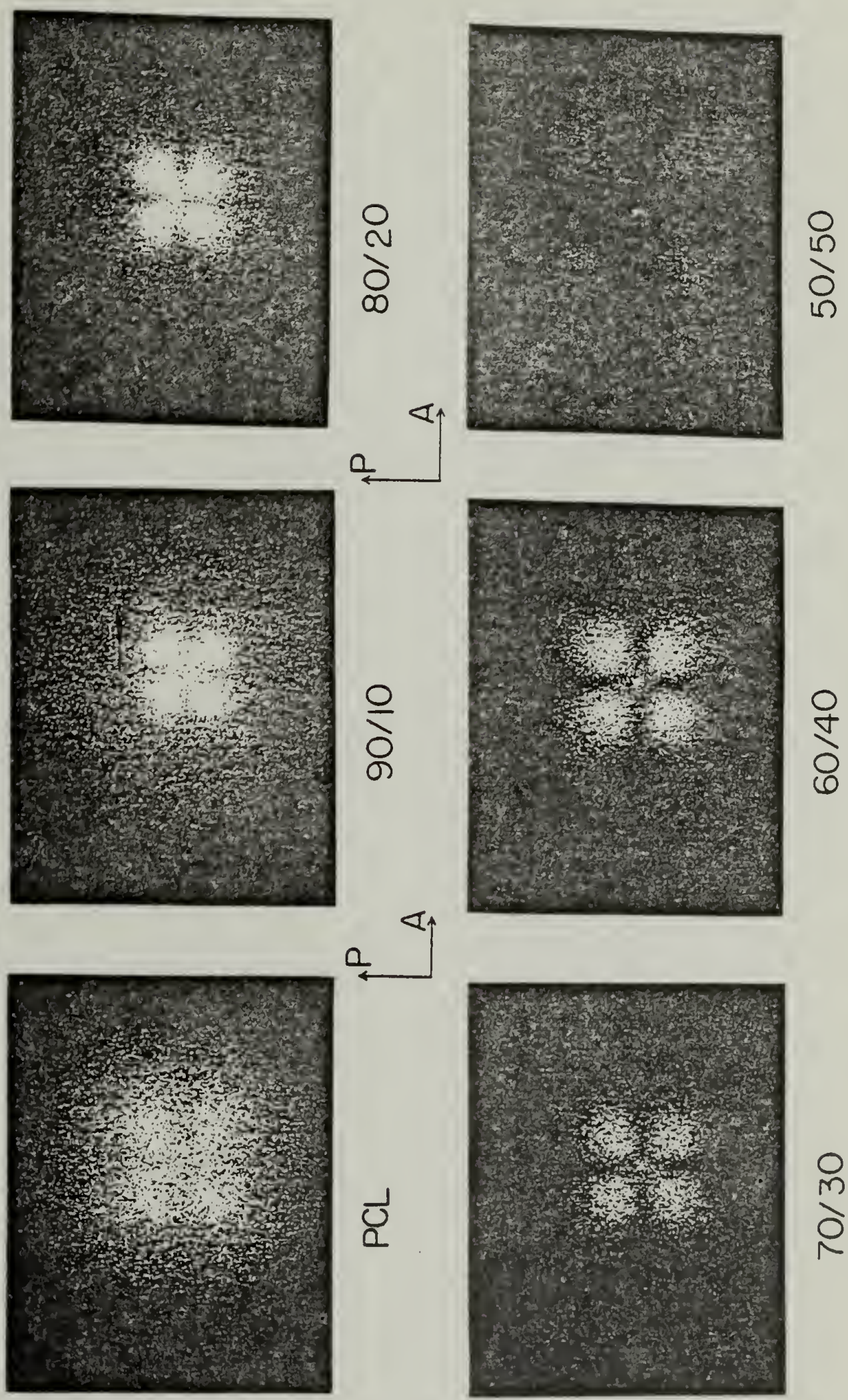
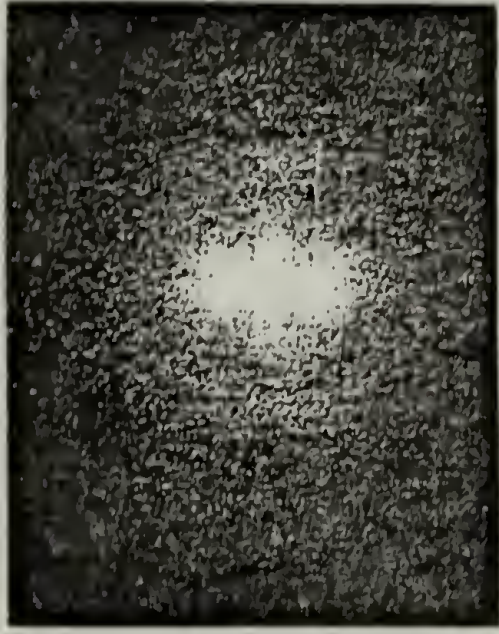


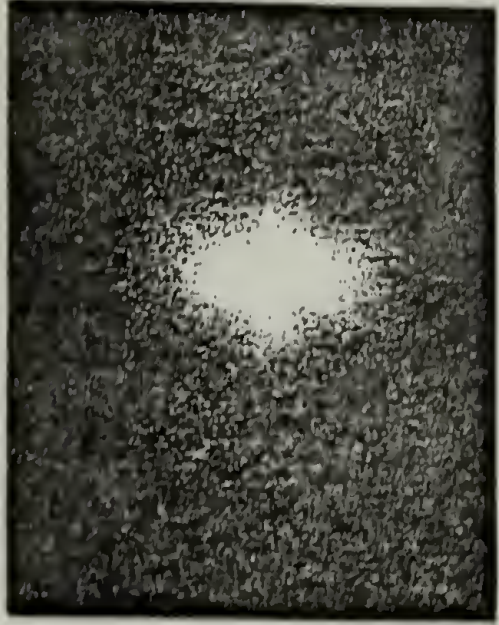
FIG. 20(a)



PCL



90/10

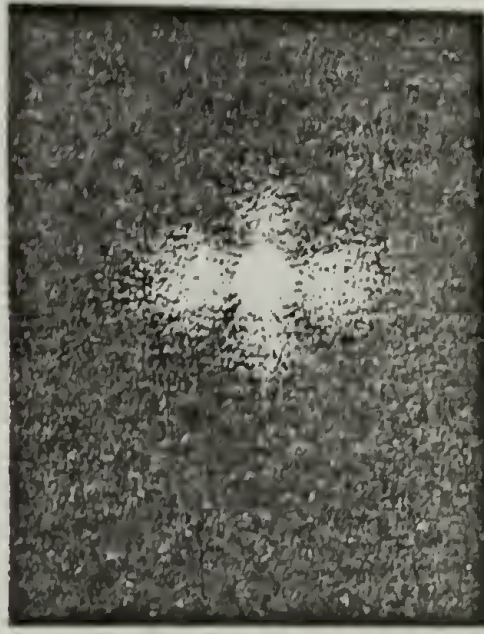


80/20

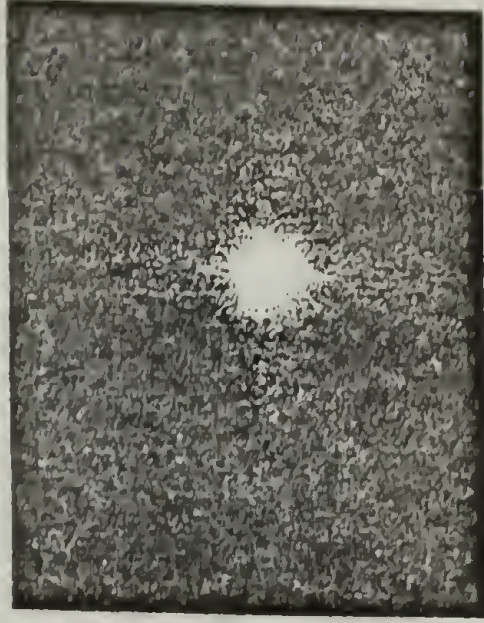
↑
|P,A



70/30

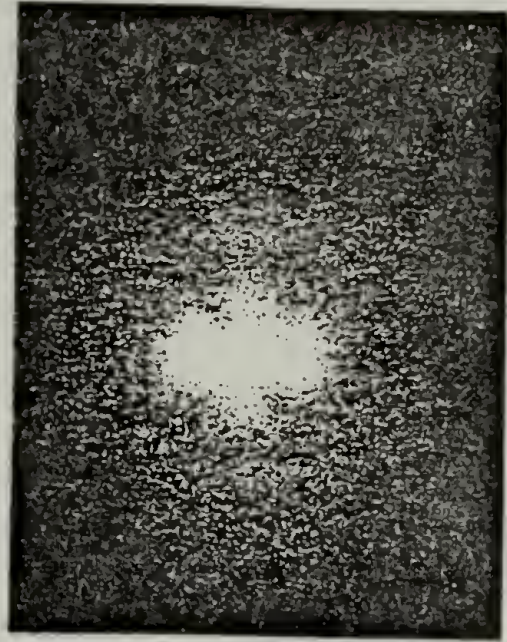


60/40

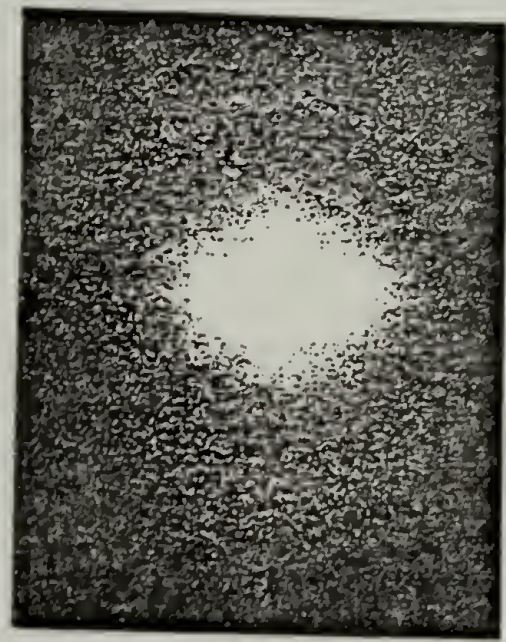


50/50

FIG. 20(b)

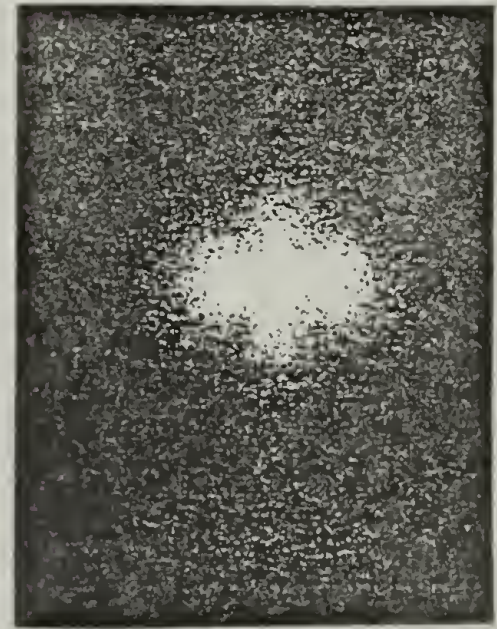


90/10
(1/200, 28CM)

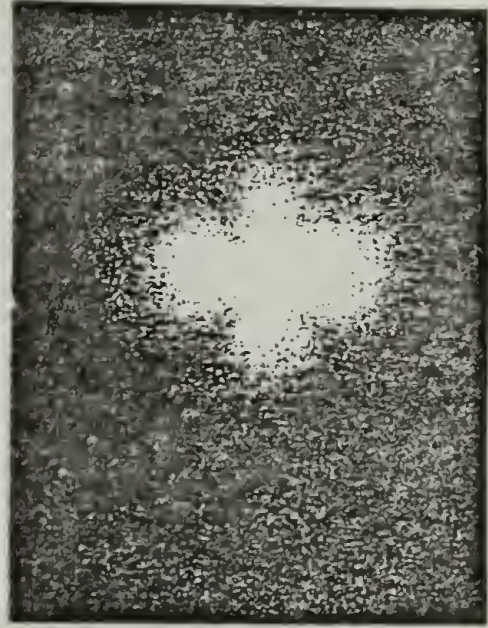


80/20
(1/100, 28CM)

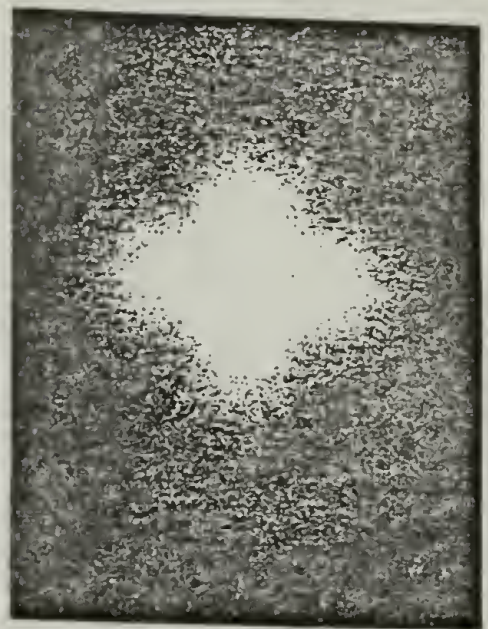
P, A



70/30
(1/100, 28CM)

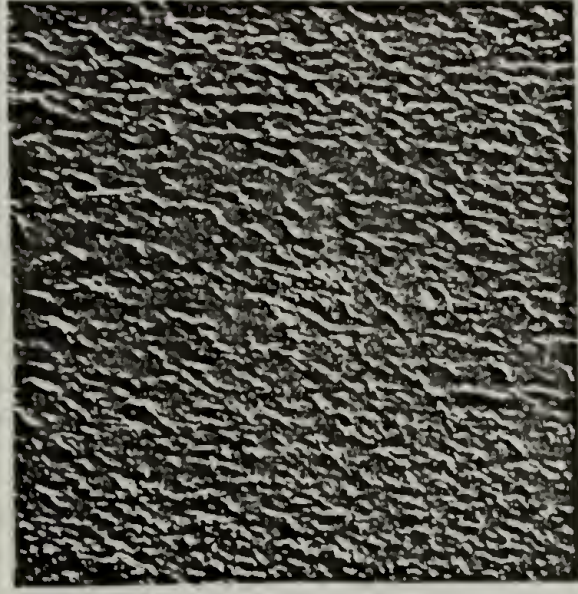


60/40
(1/50, 28CM)



50/50
(1/25, 18CM)

FIG. 20(c)



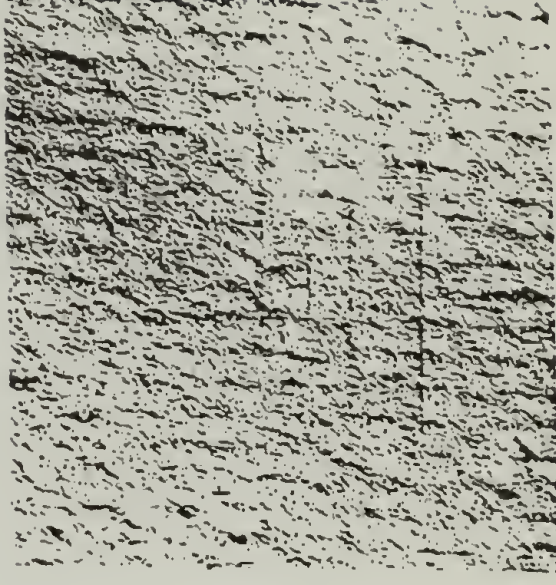
PCL



90/10



80/20



70/30

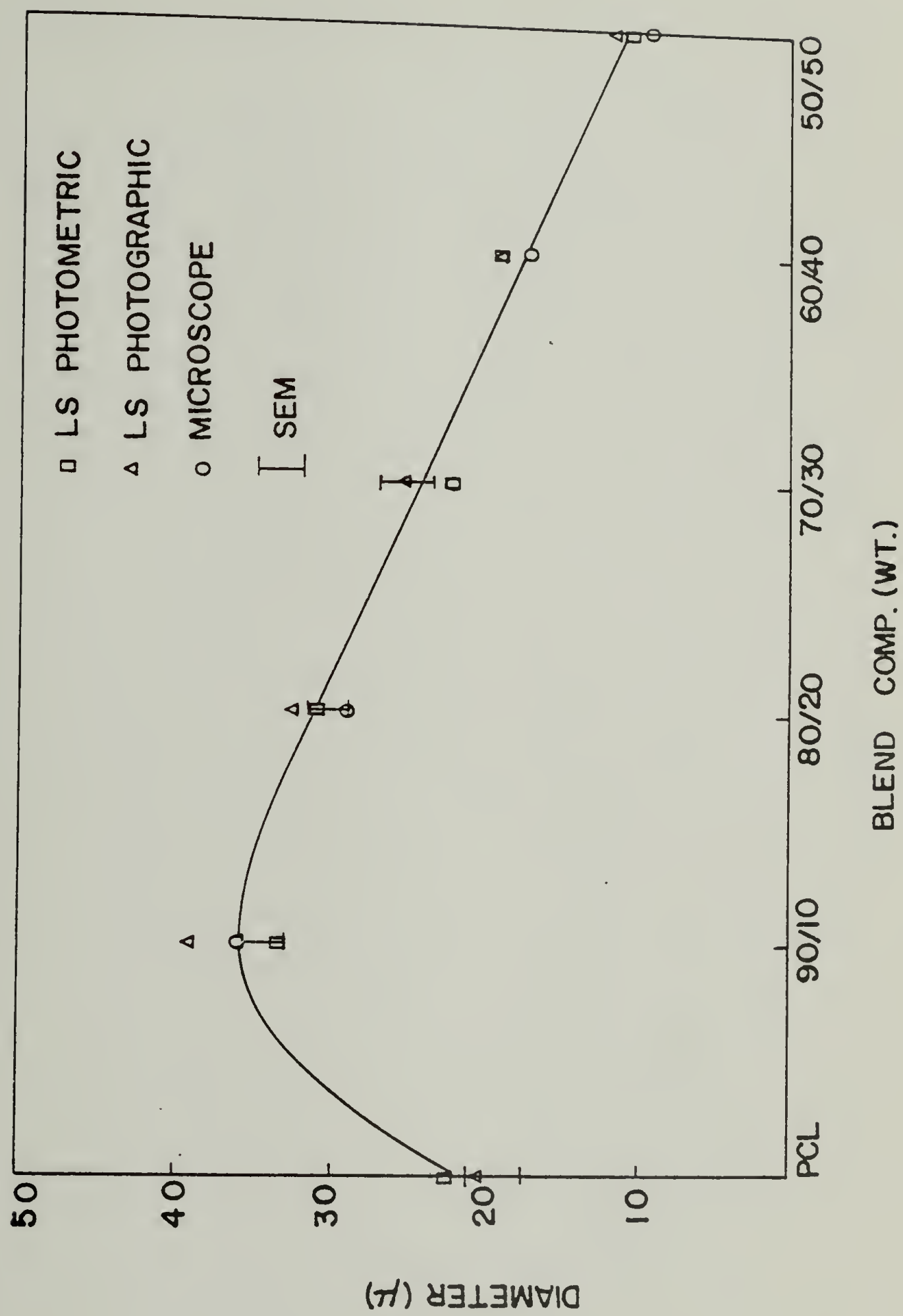
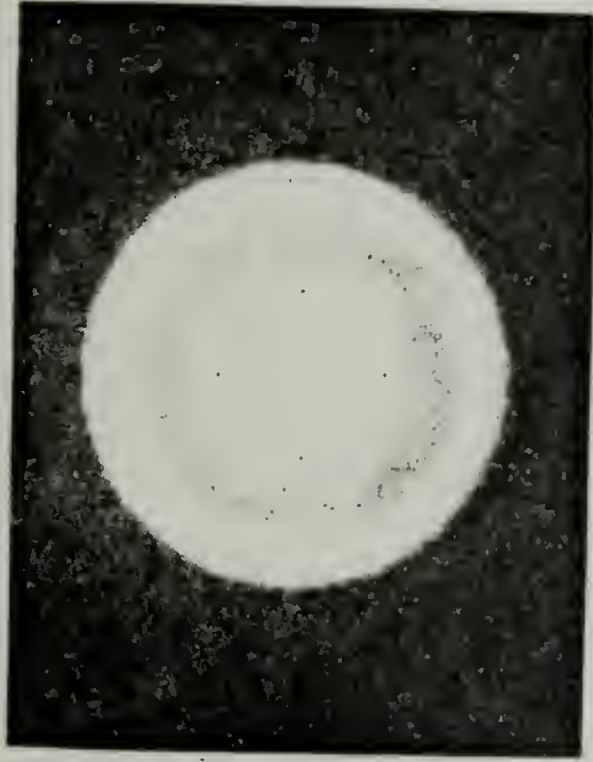


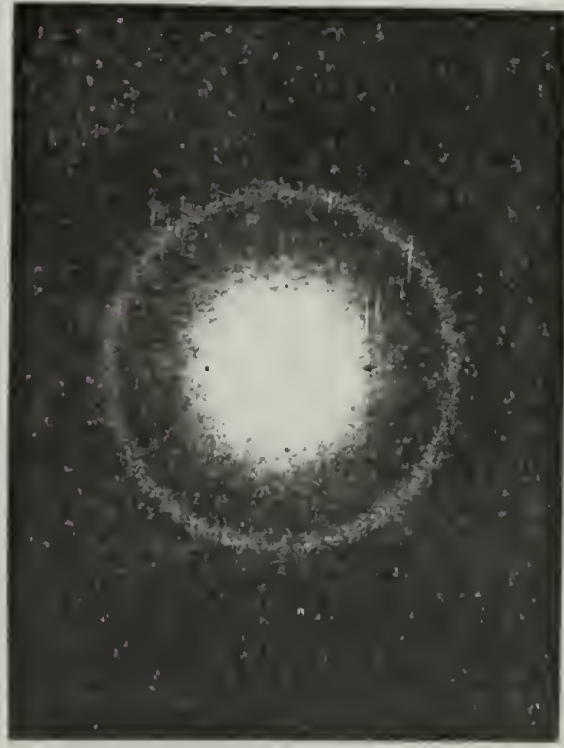
FIG. 22



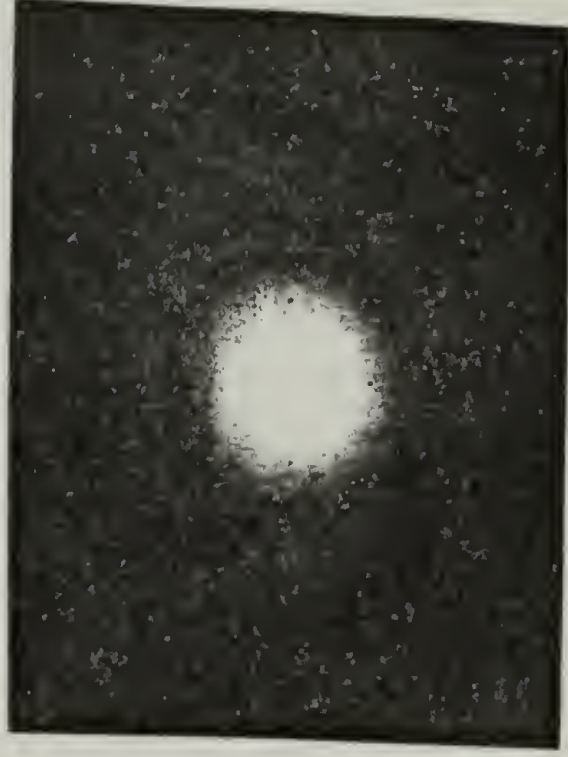
PCL



90/10



70/30



50/50

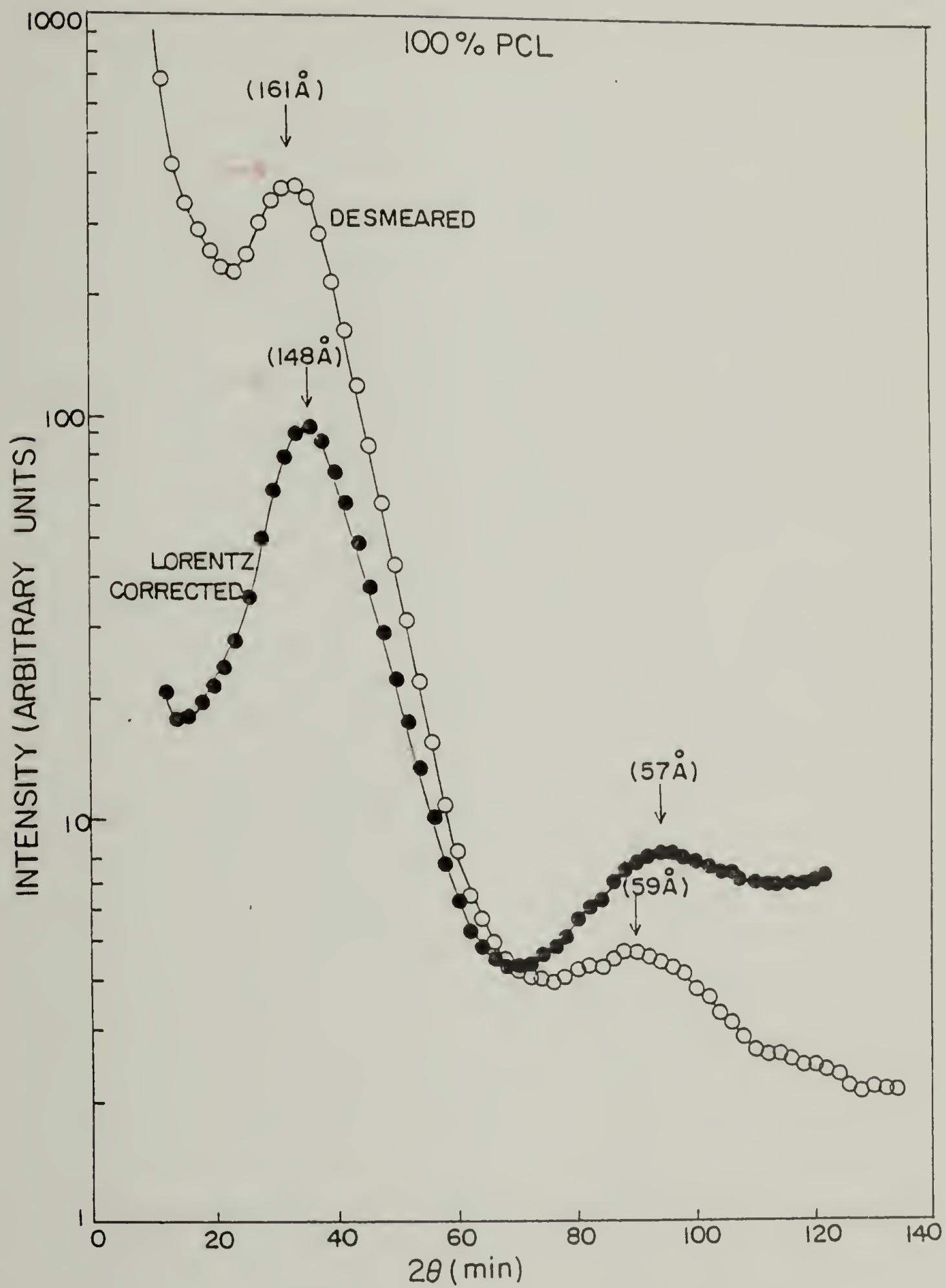


FIG. 24

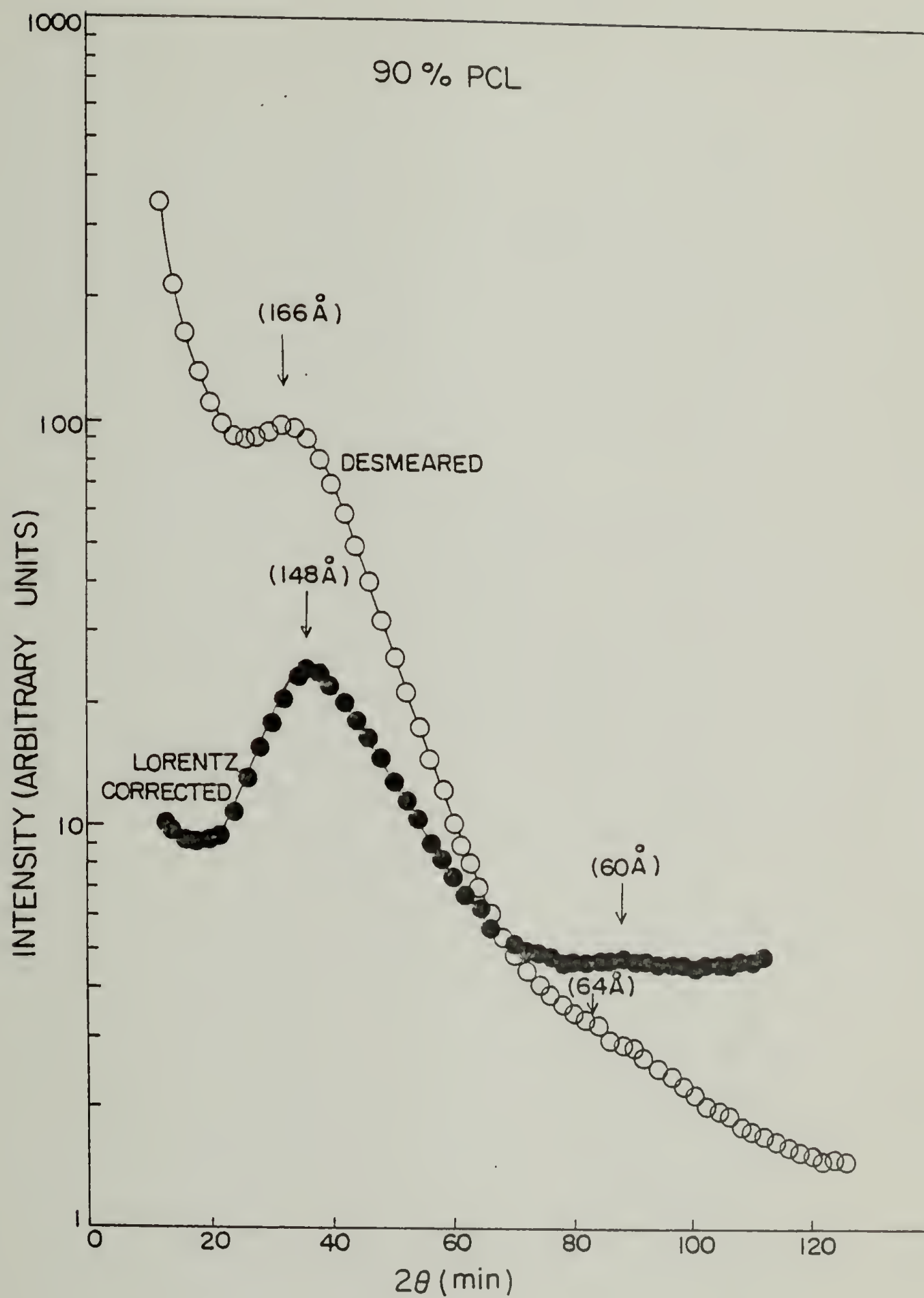
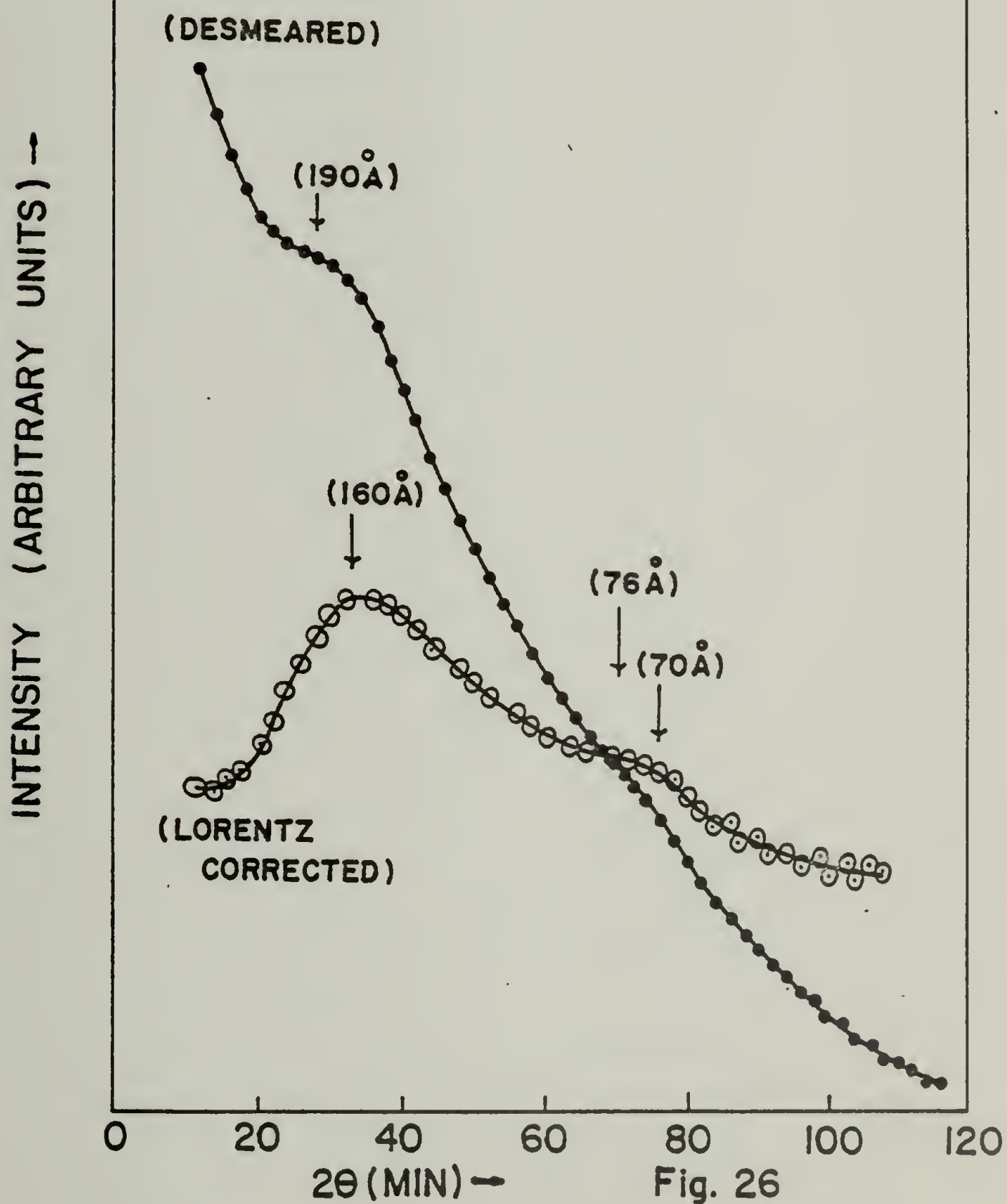
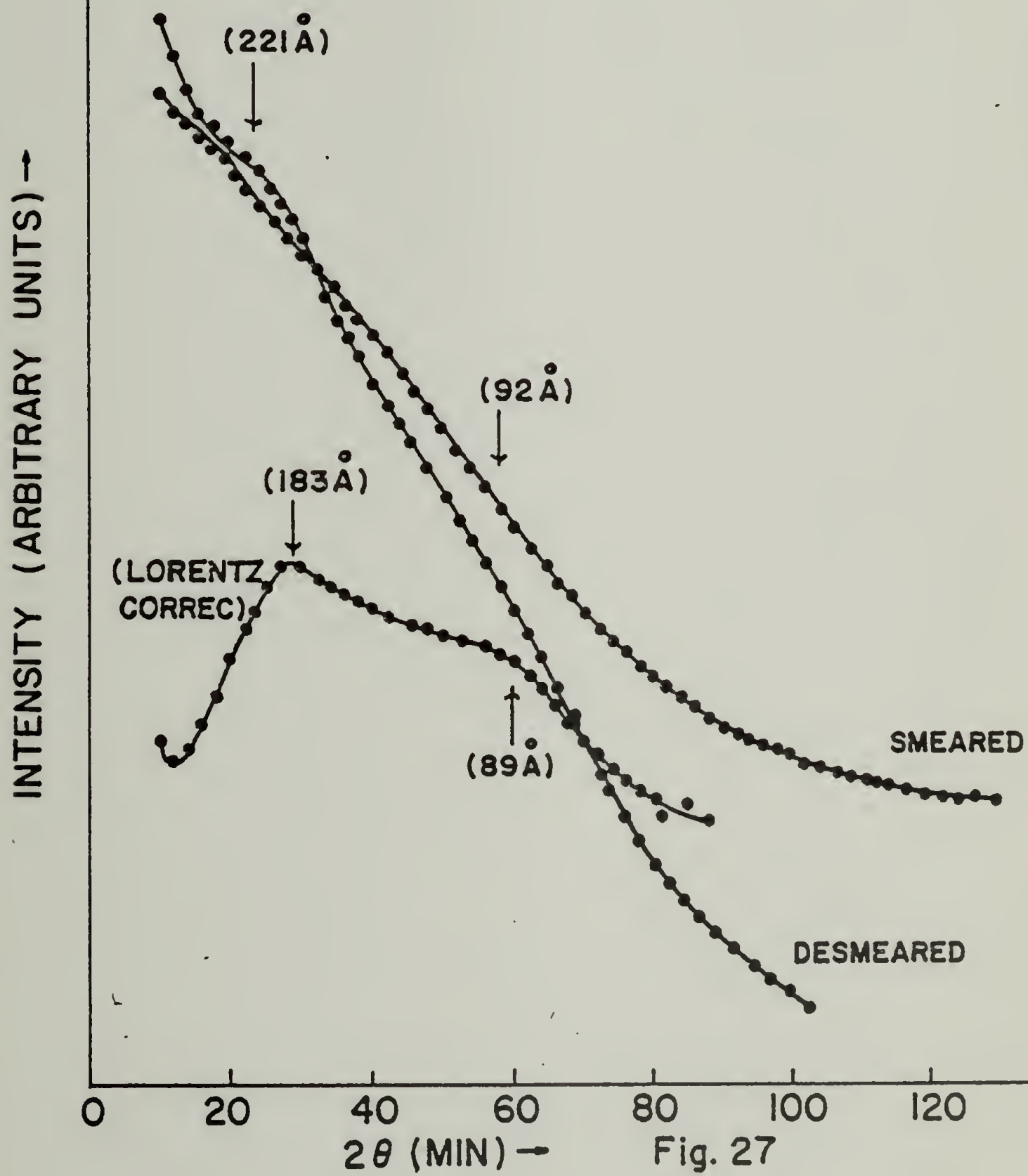


FIG. 25

SAXS OF 80/20 (PCL/PVC)



SAXS OF 70/30 (PCL/PVC)



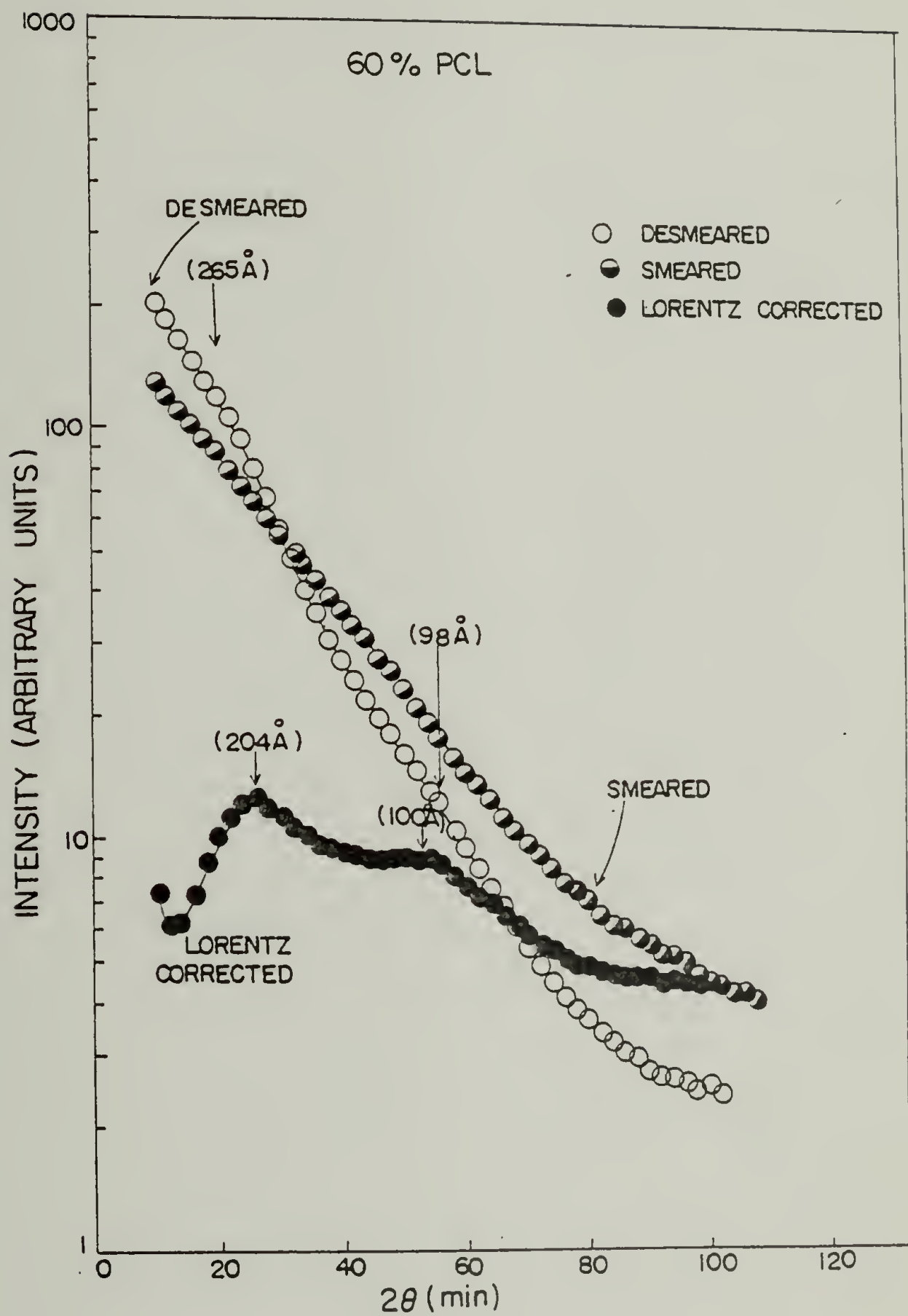
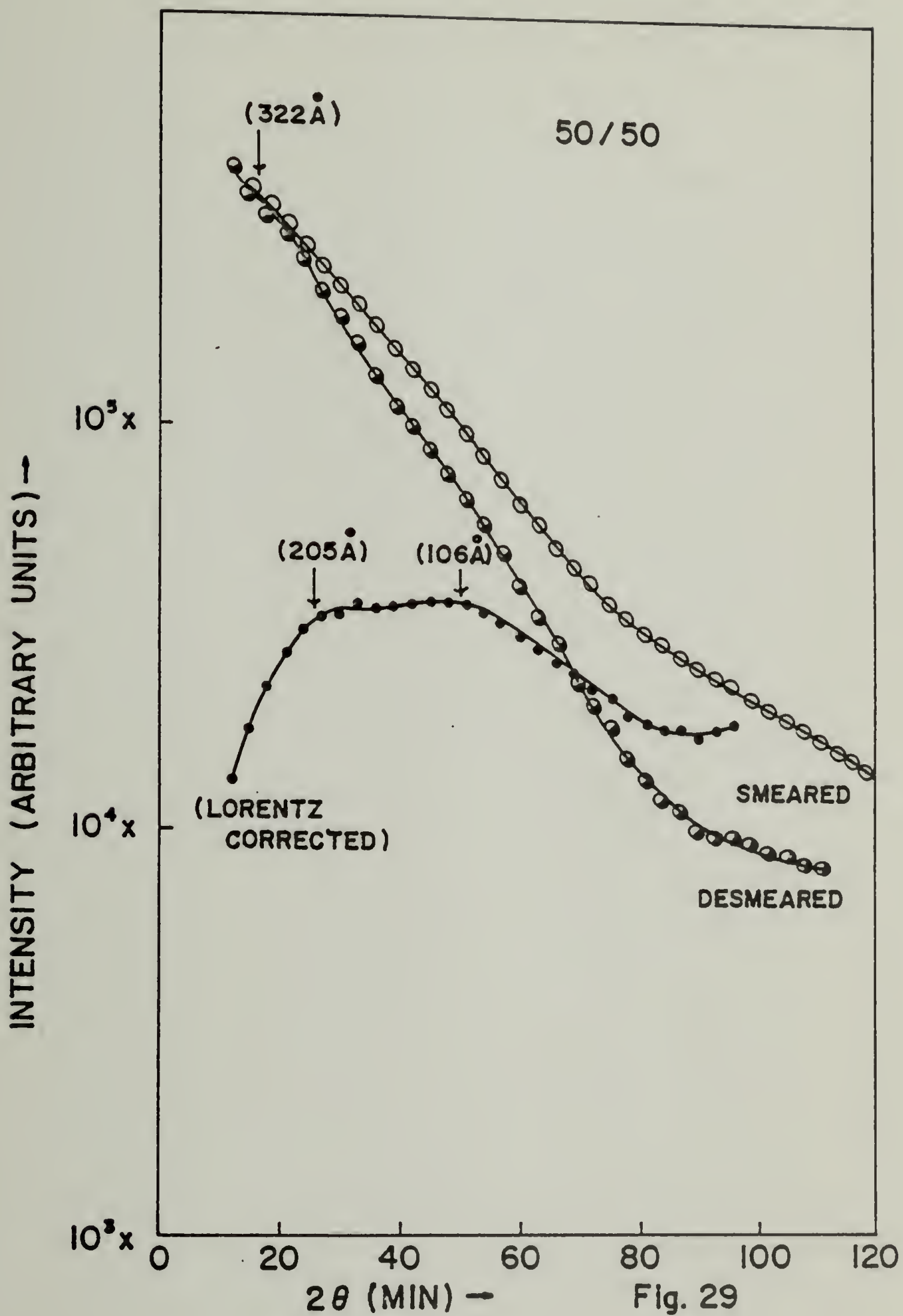


FIG. 28



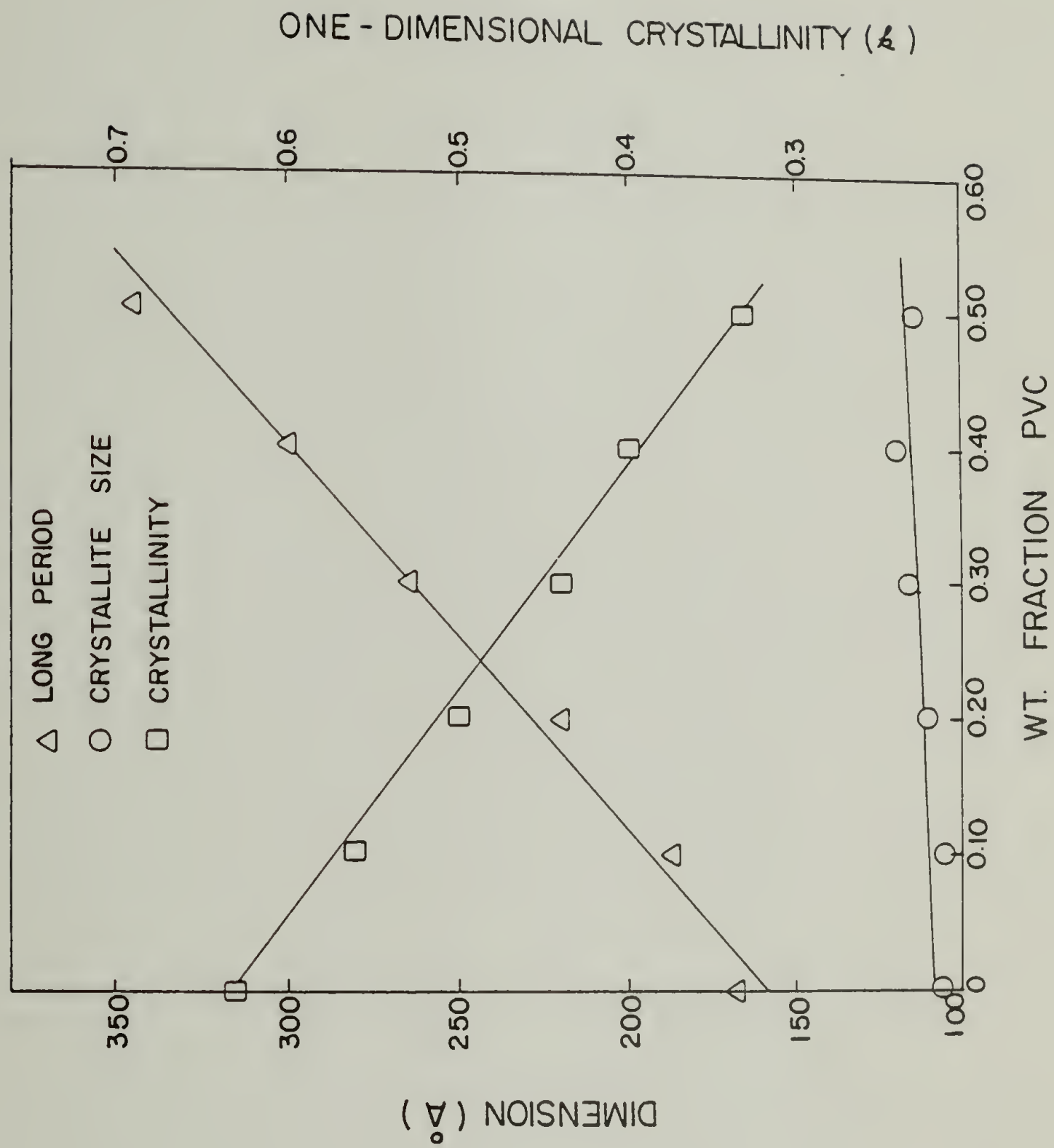


FIG. 30

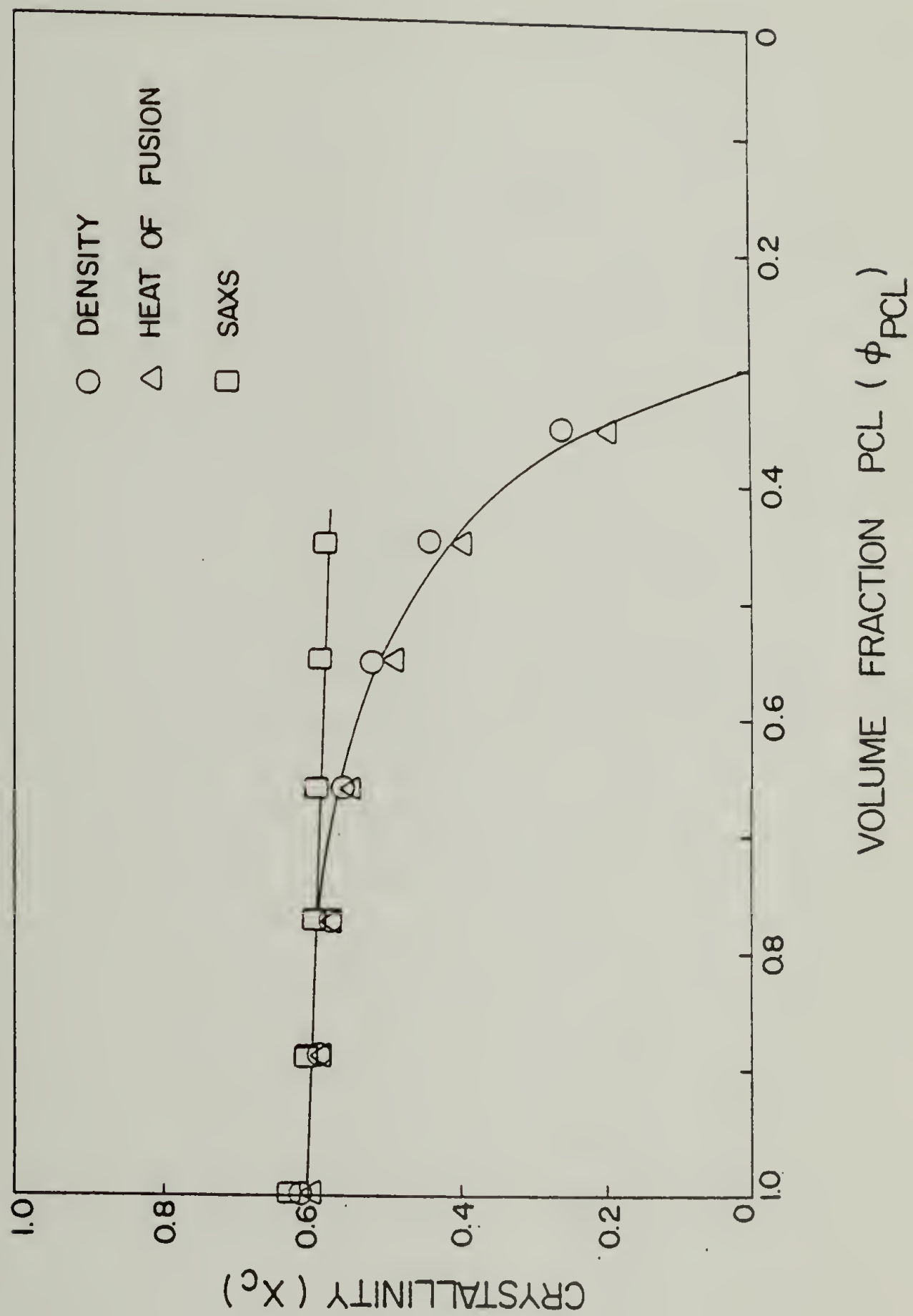


FIG. 31

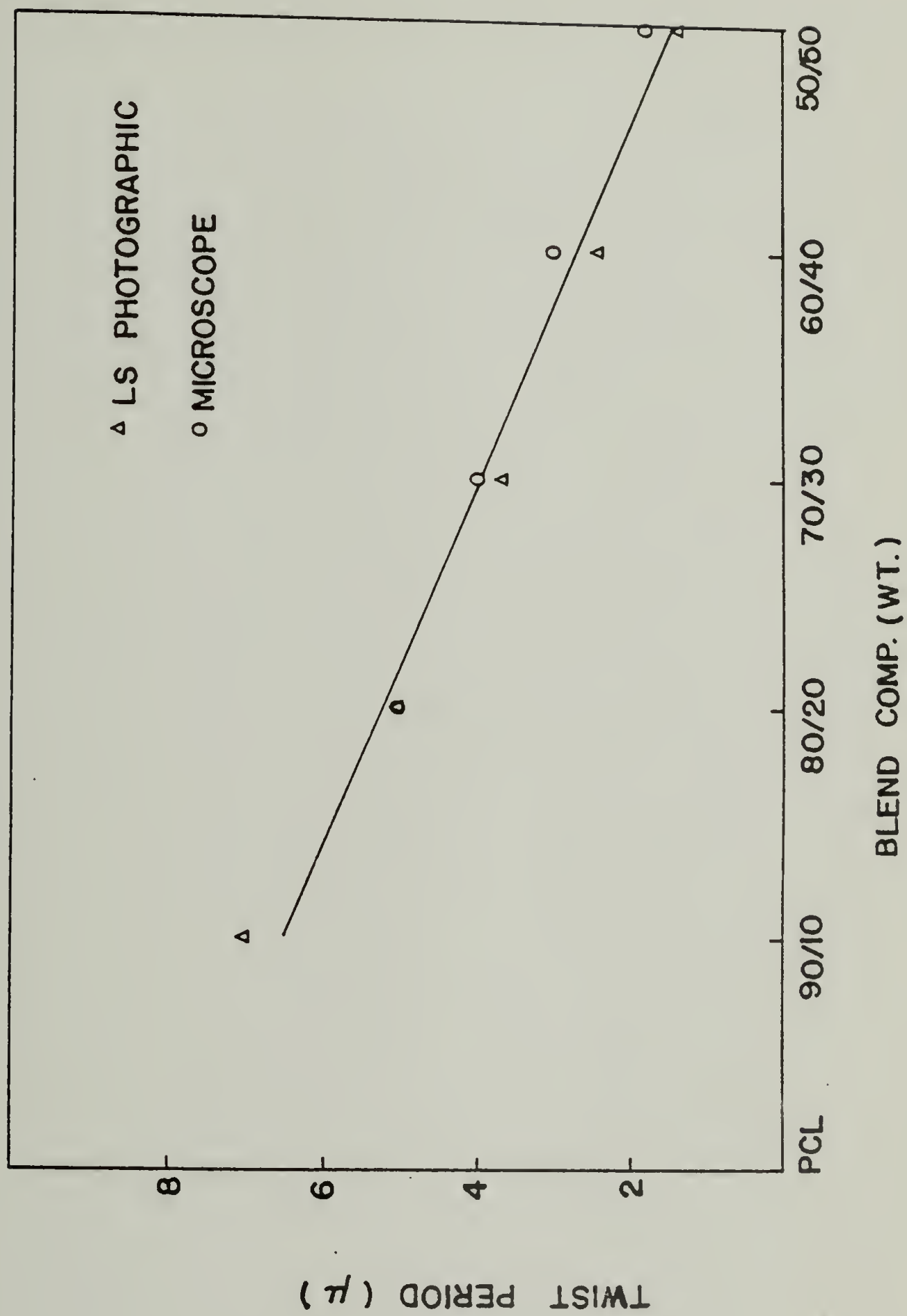


FIG. 32

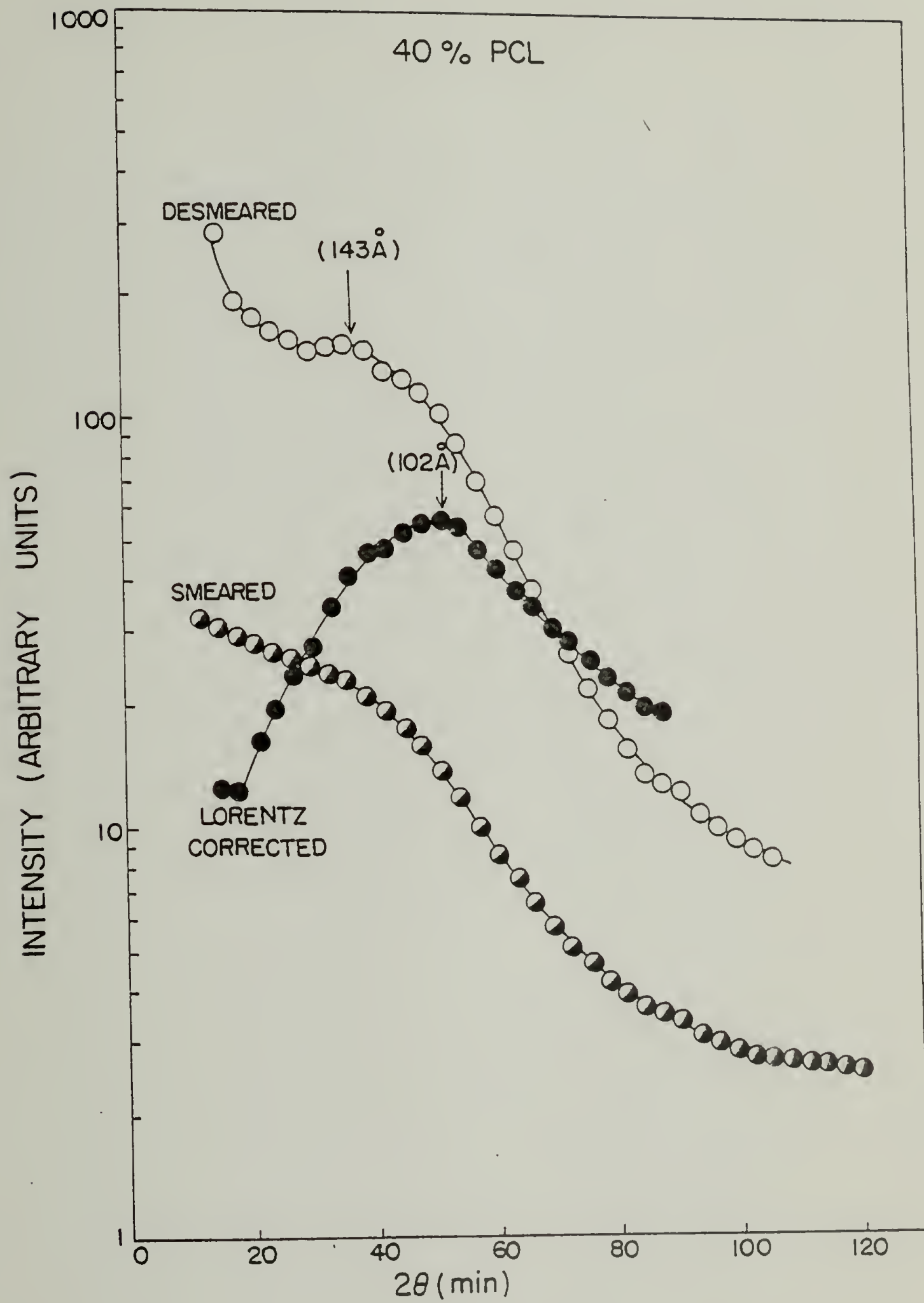


FIG. 33

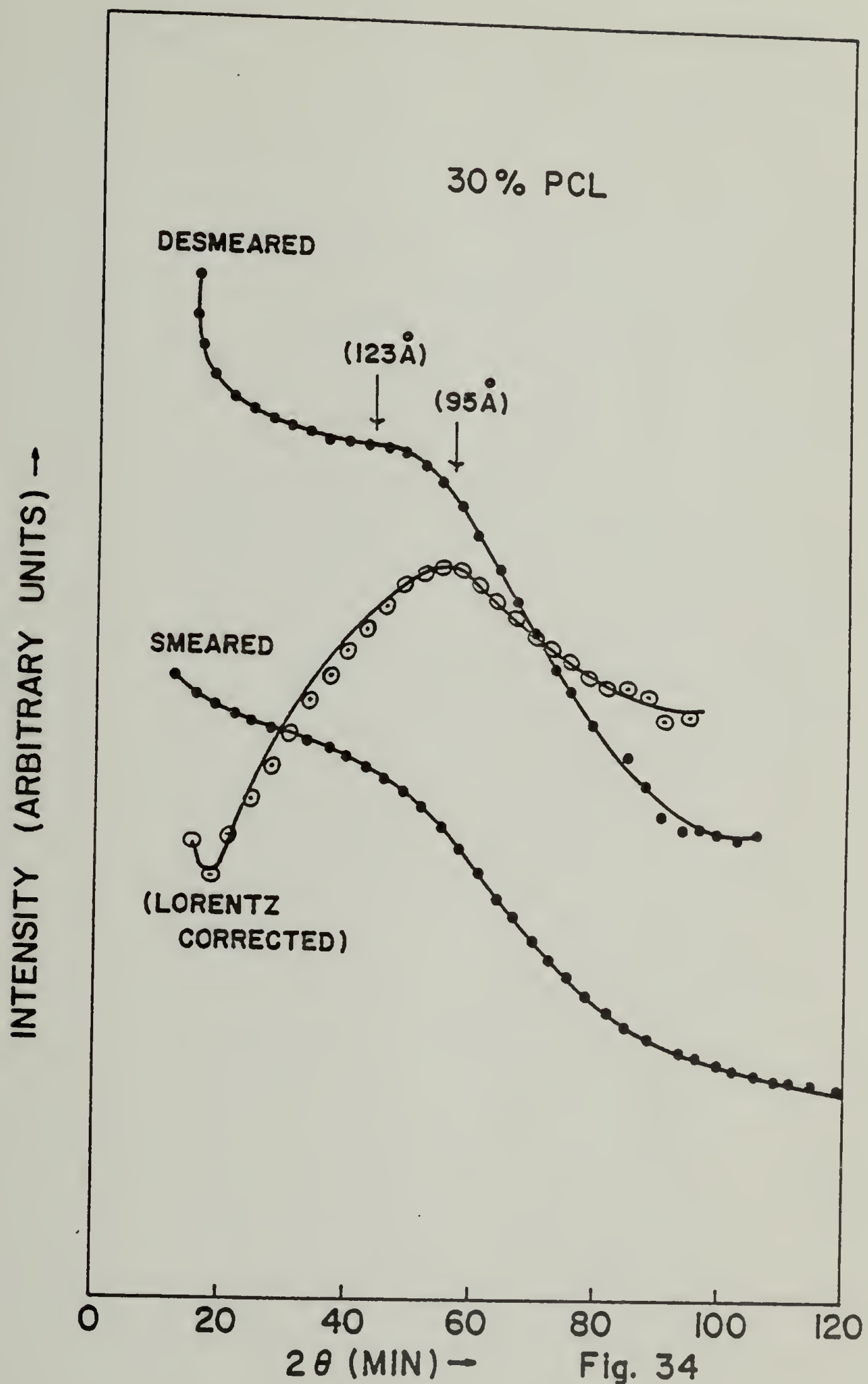


Fig. 34

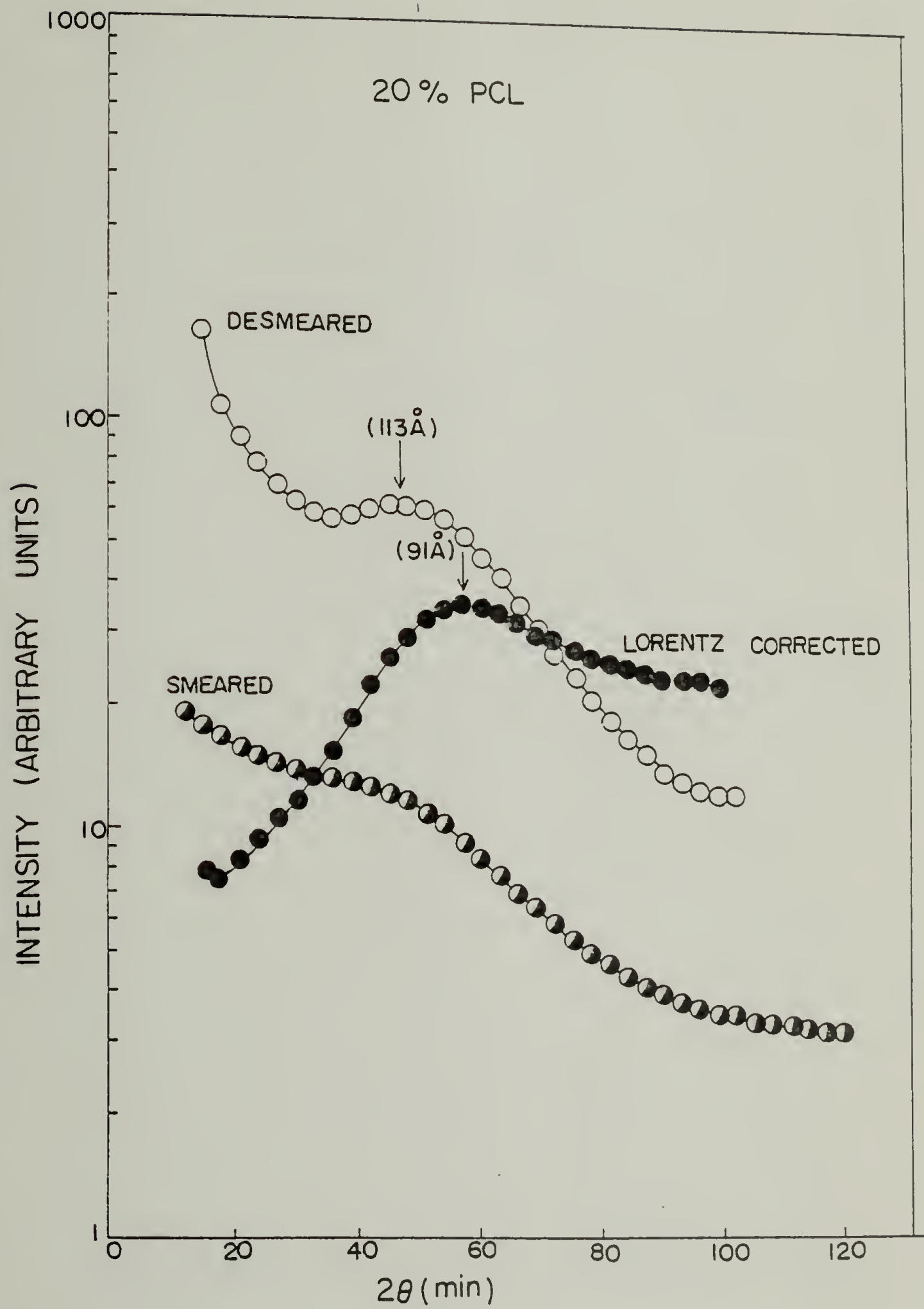


FIG. 35

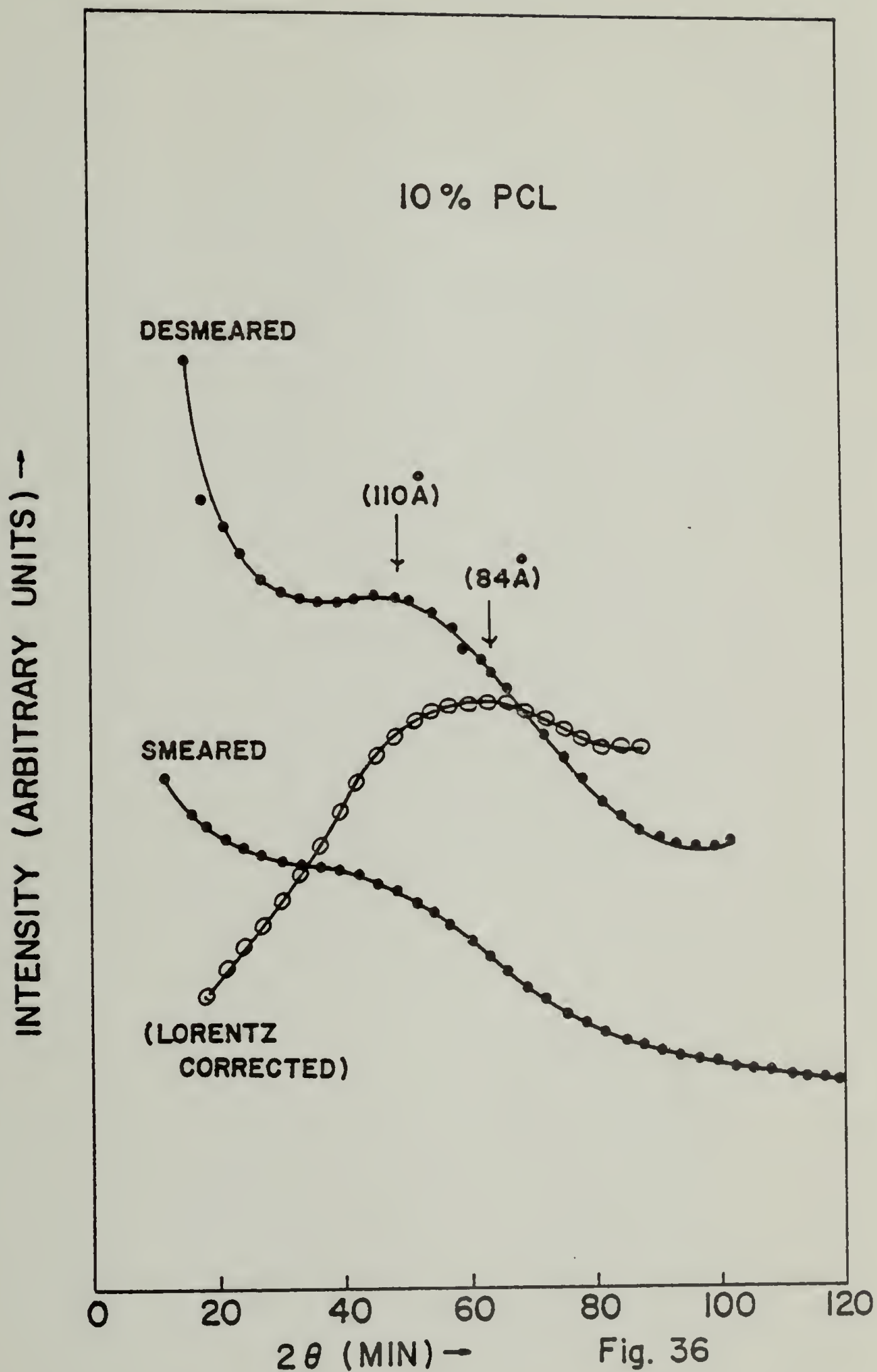
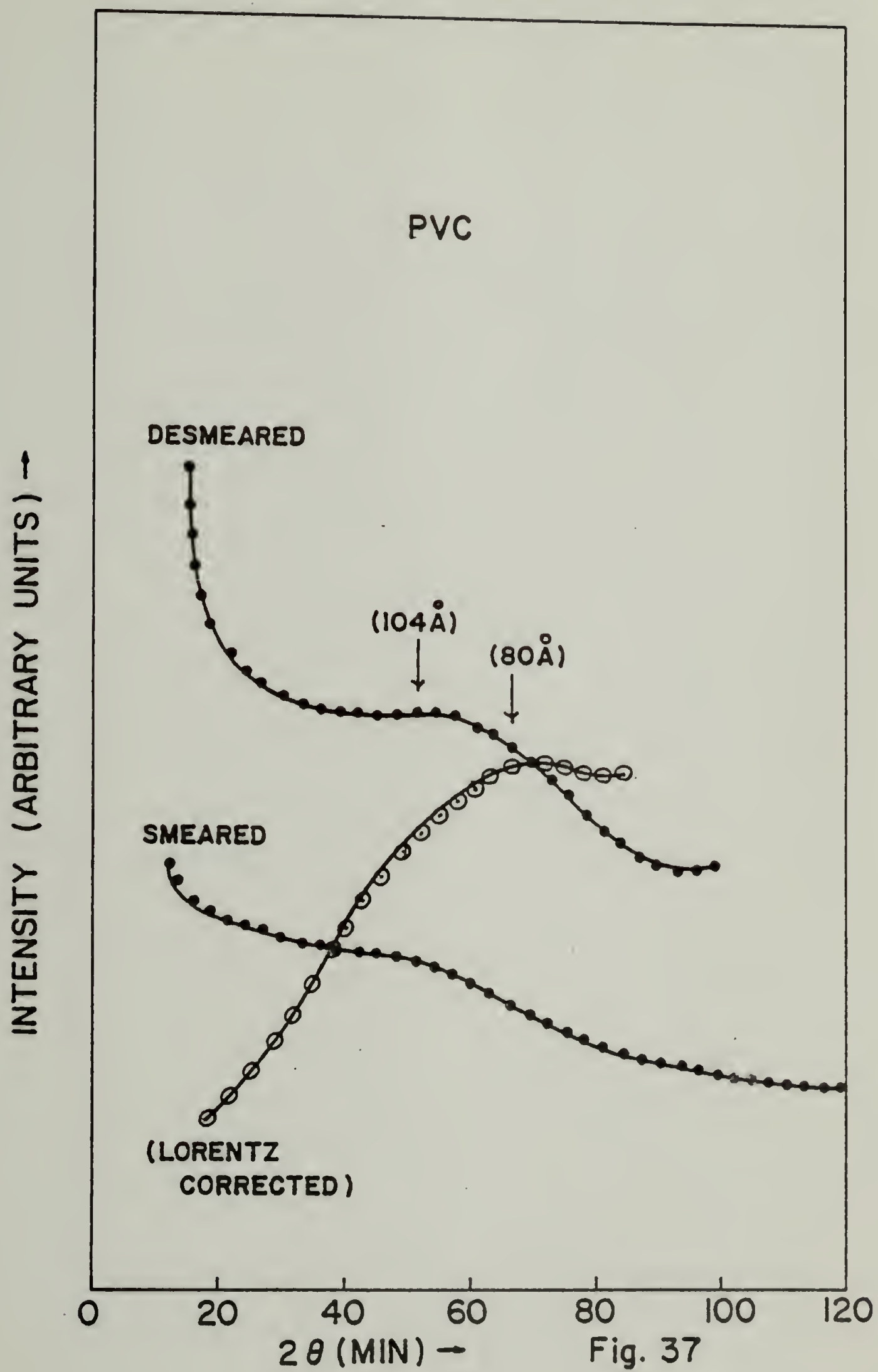


Fig. 36



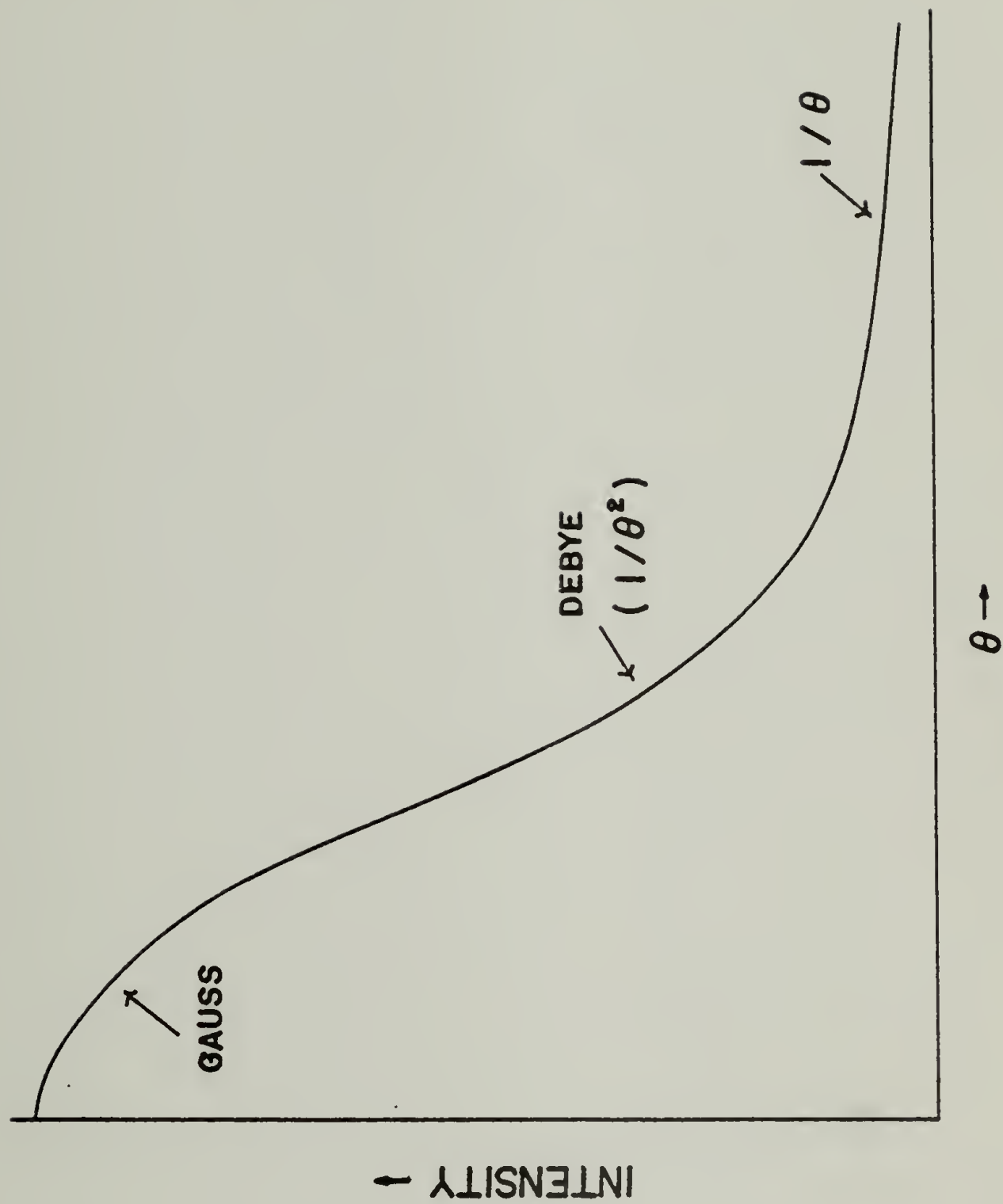


Fig. 38

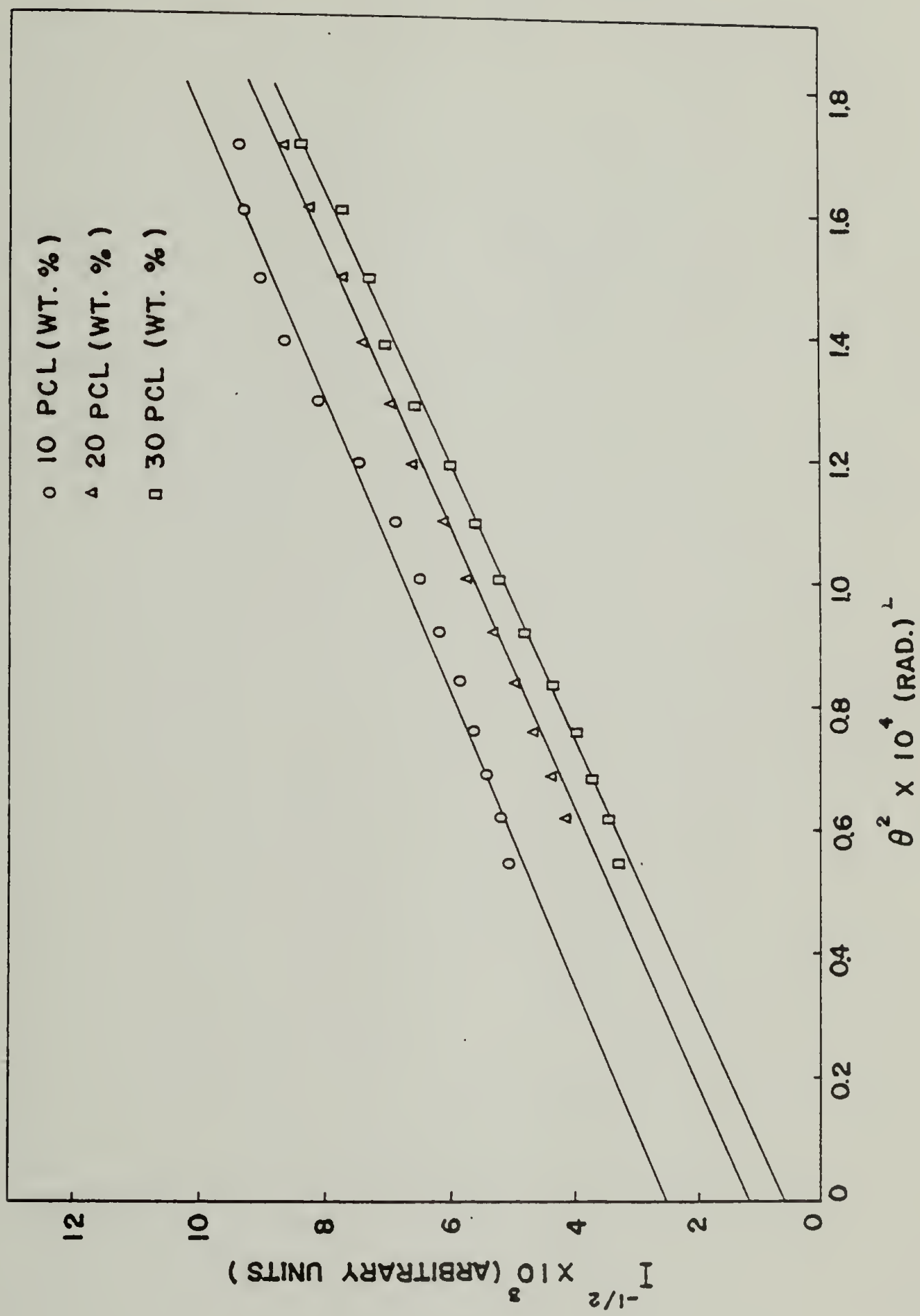


FIG. 39

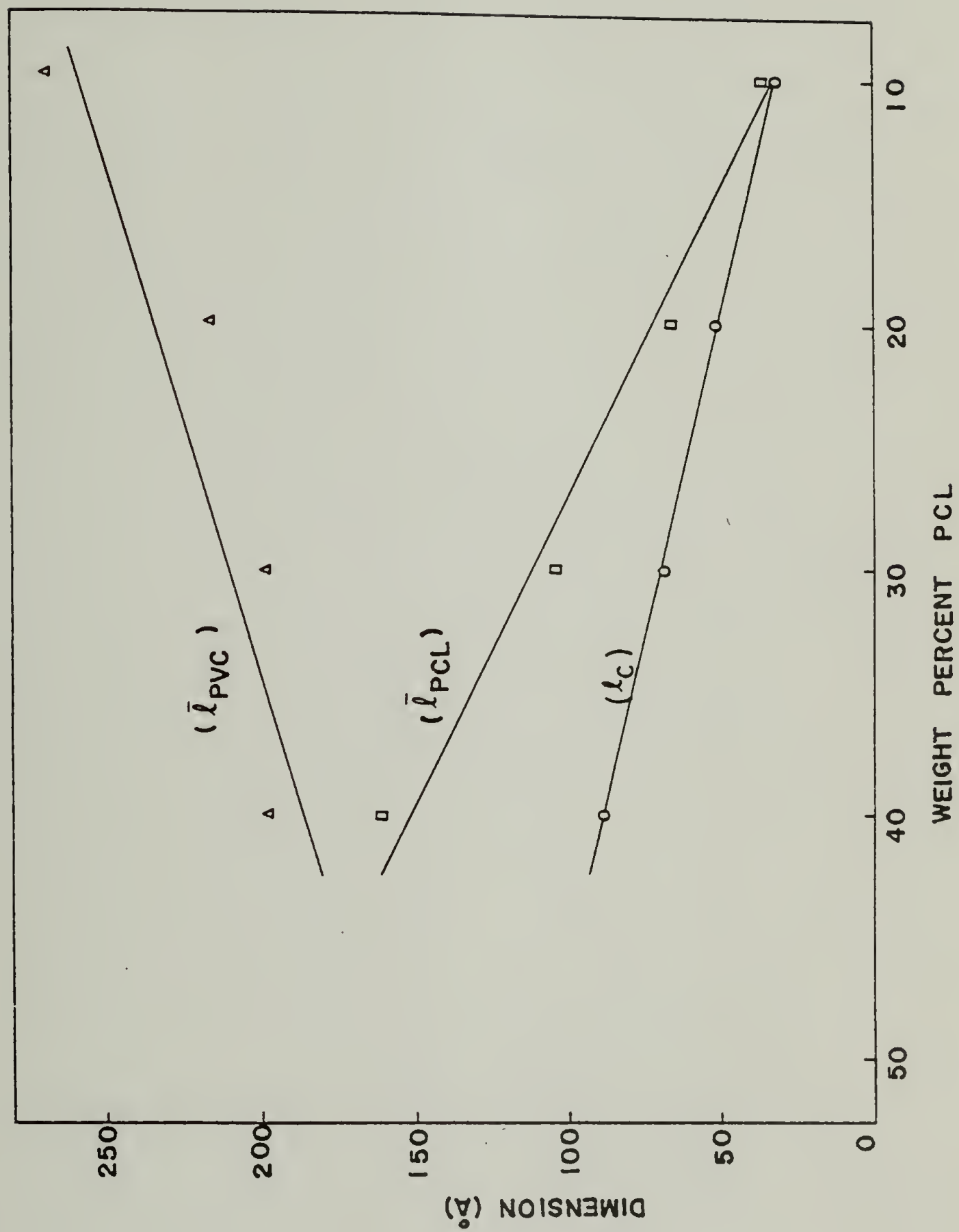


FIG. 40

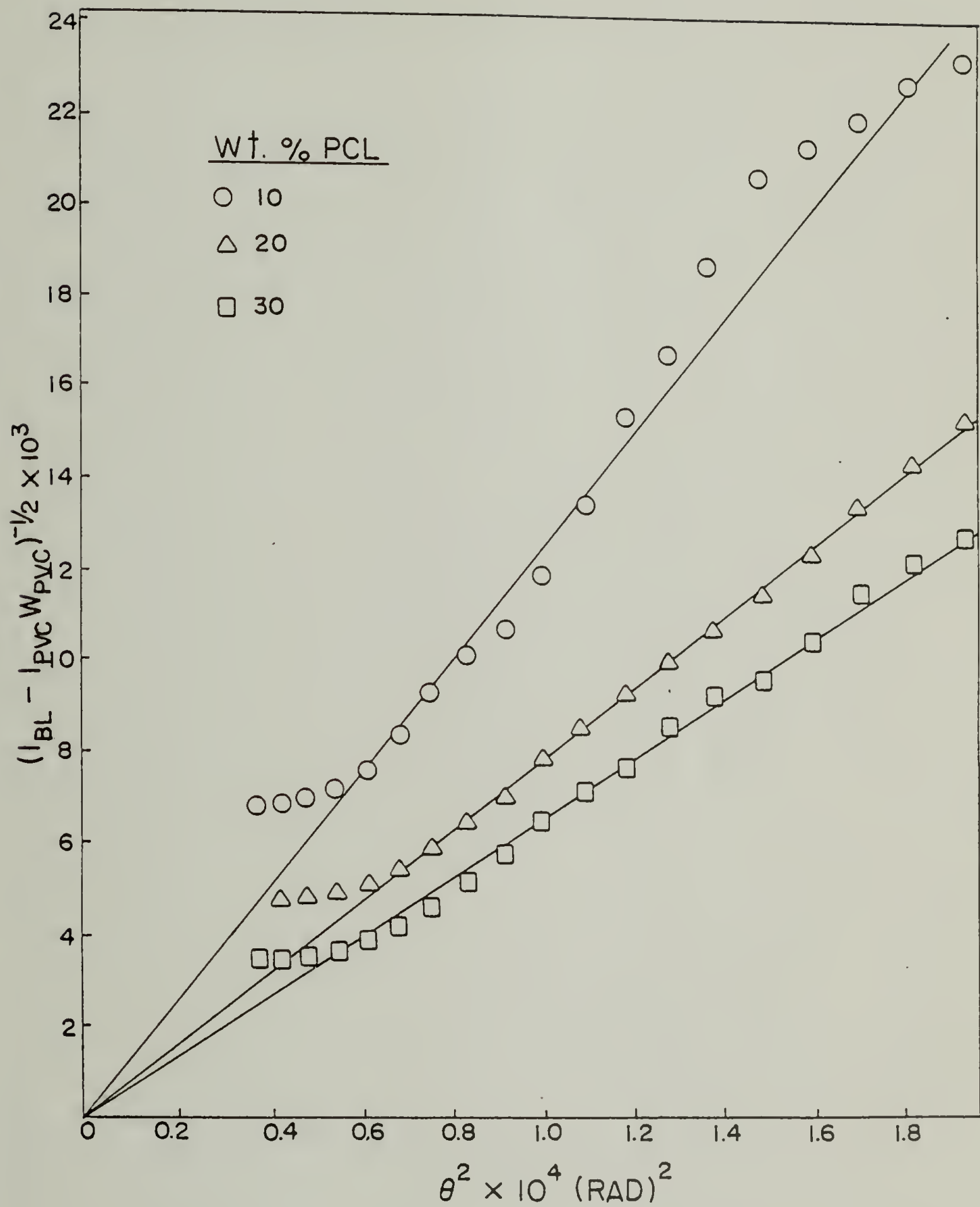


FIG. 41

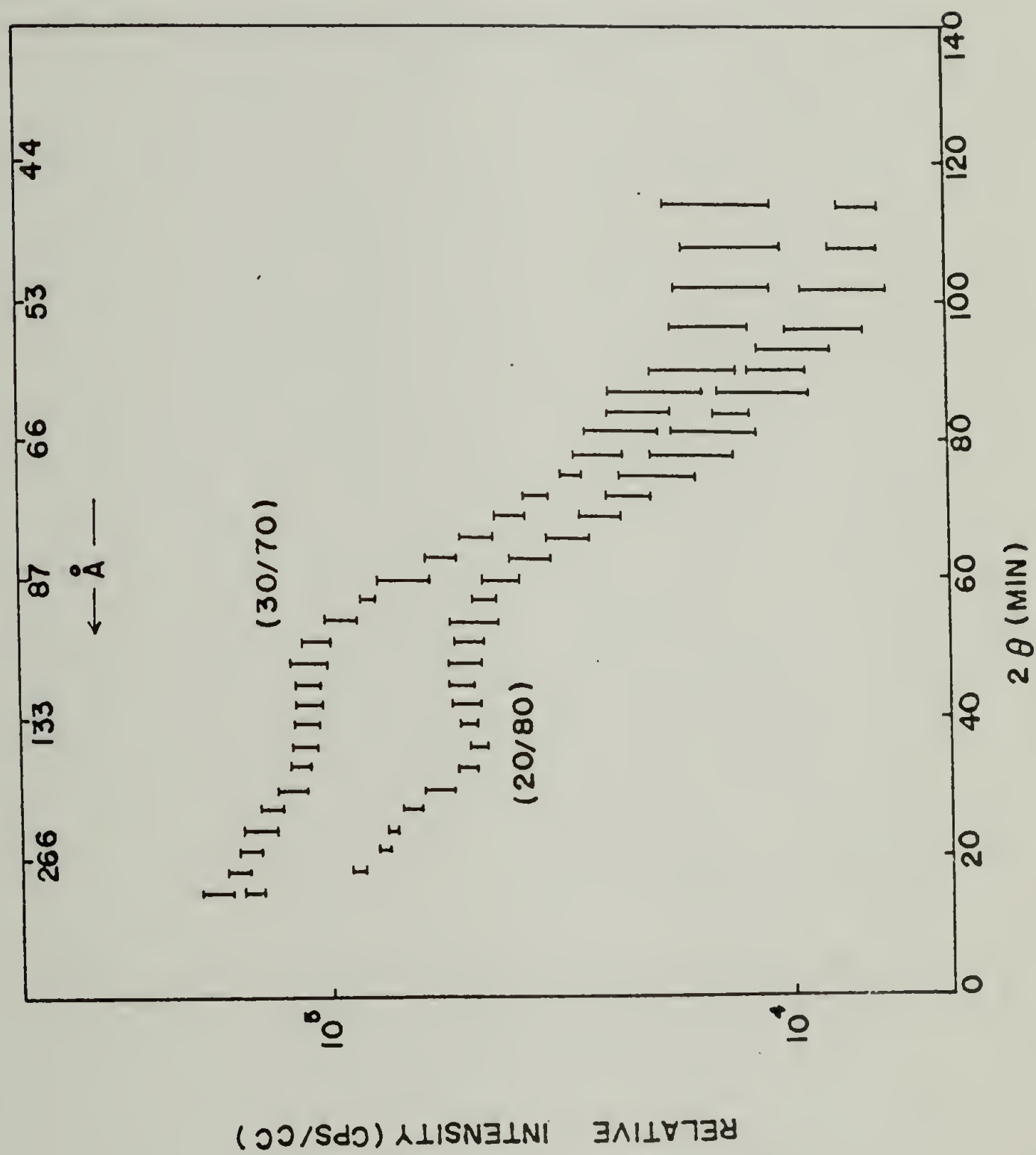
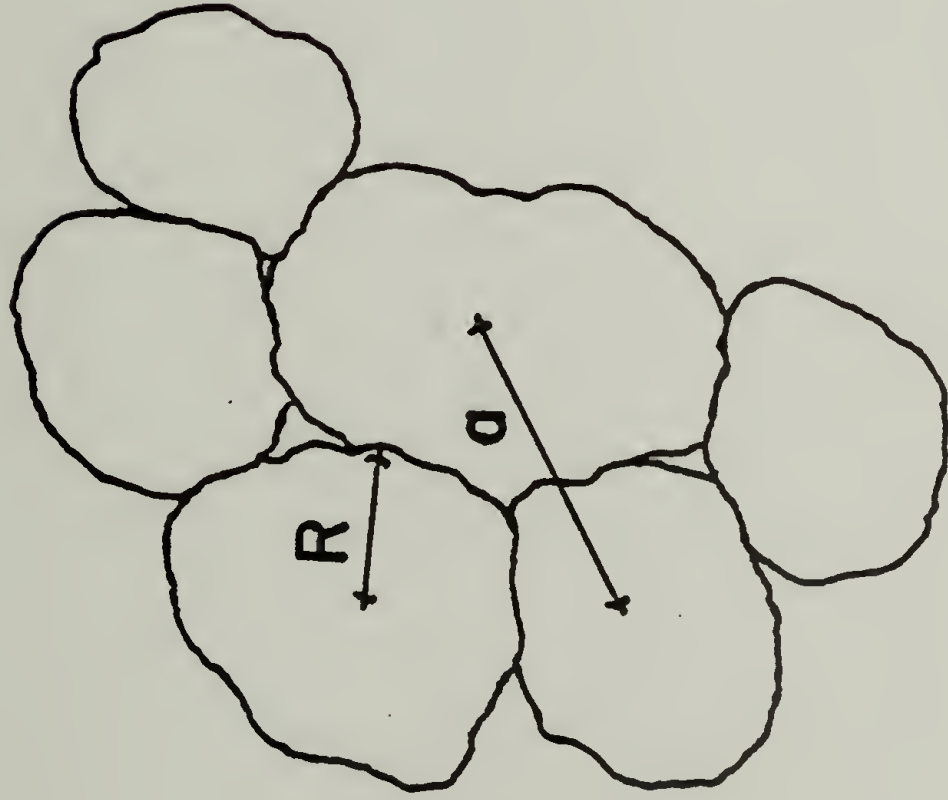
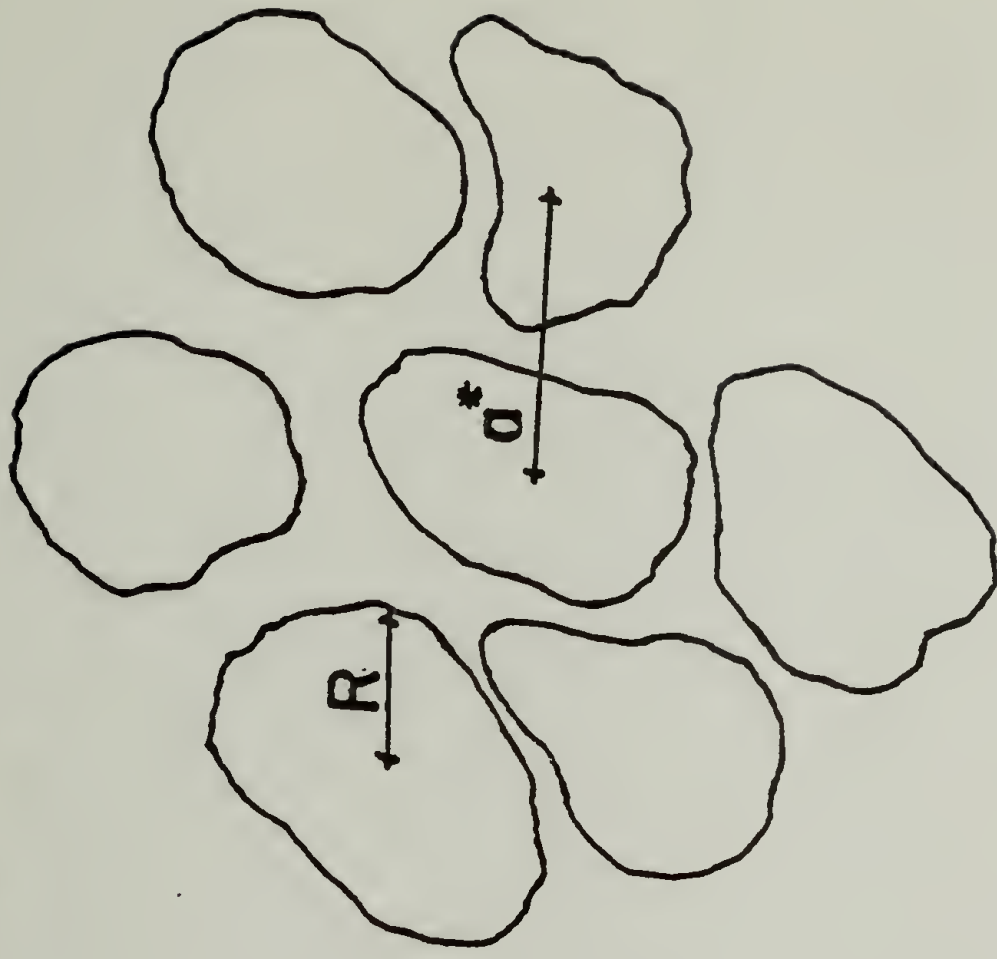


FIG. 42

PVC GEL MODEL



(PVC)



(PVC + PCL)

Fig. 43

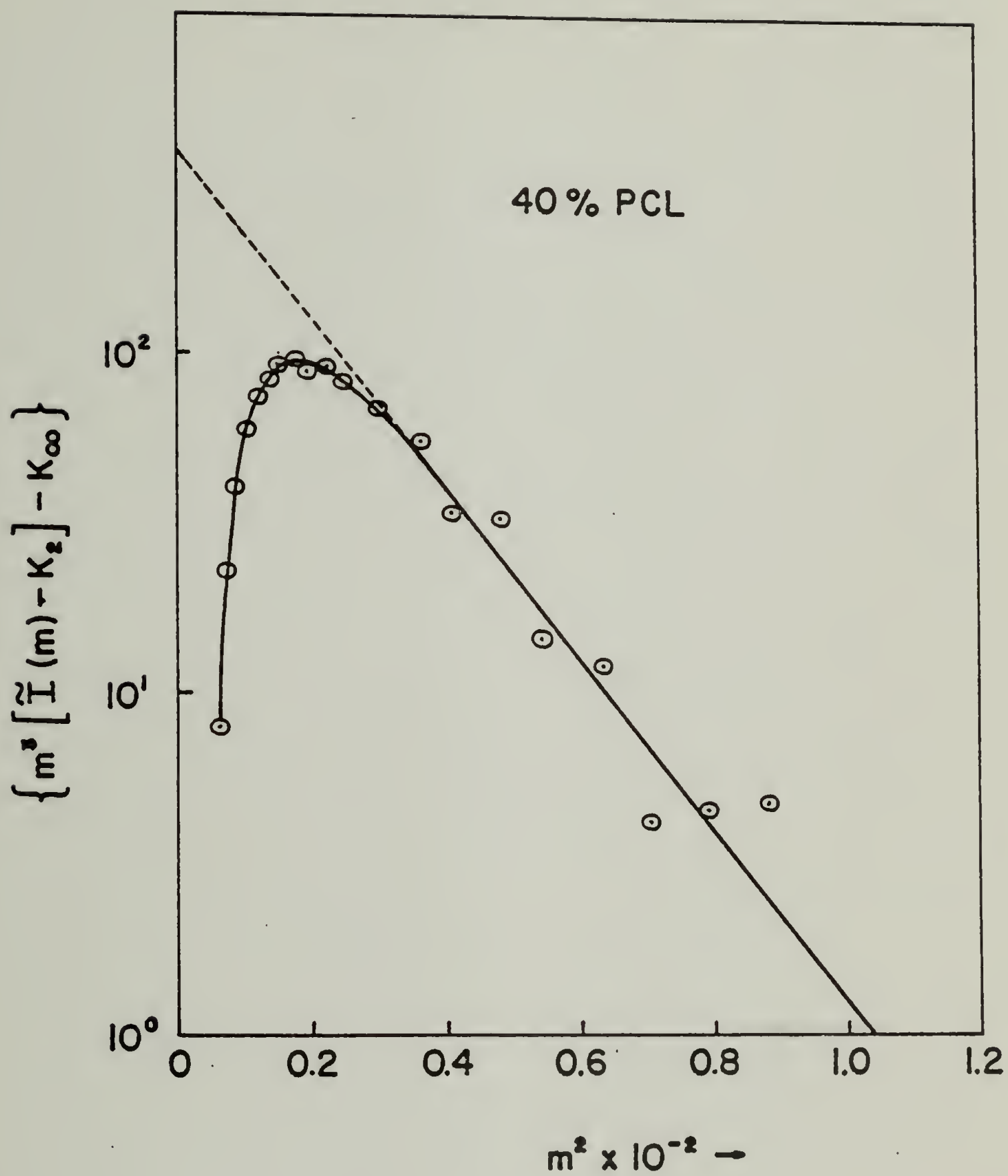


Fig. 44

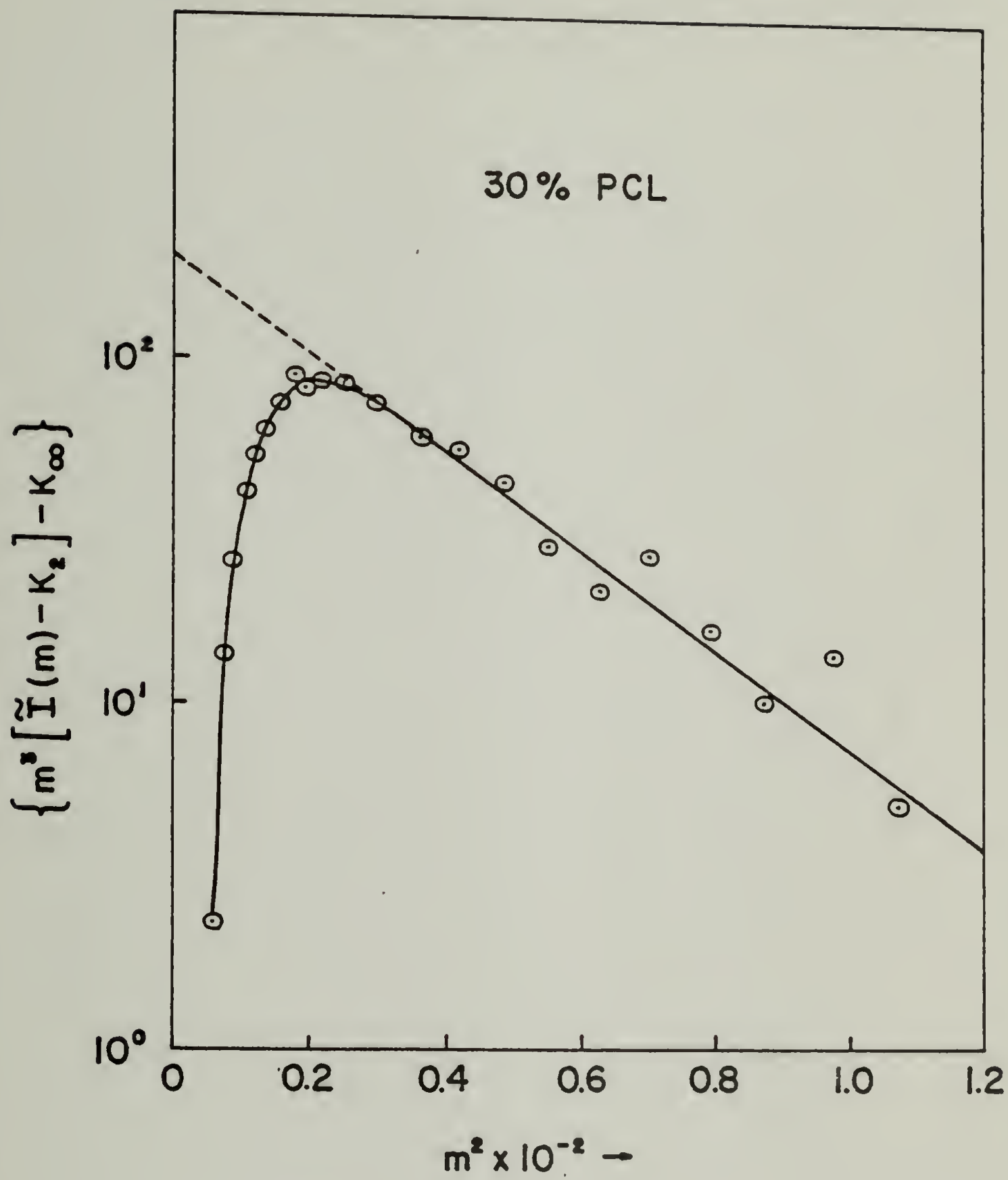


Fig. 45

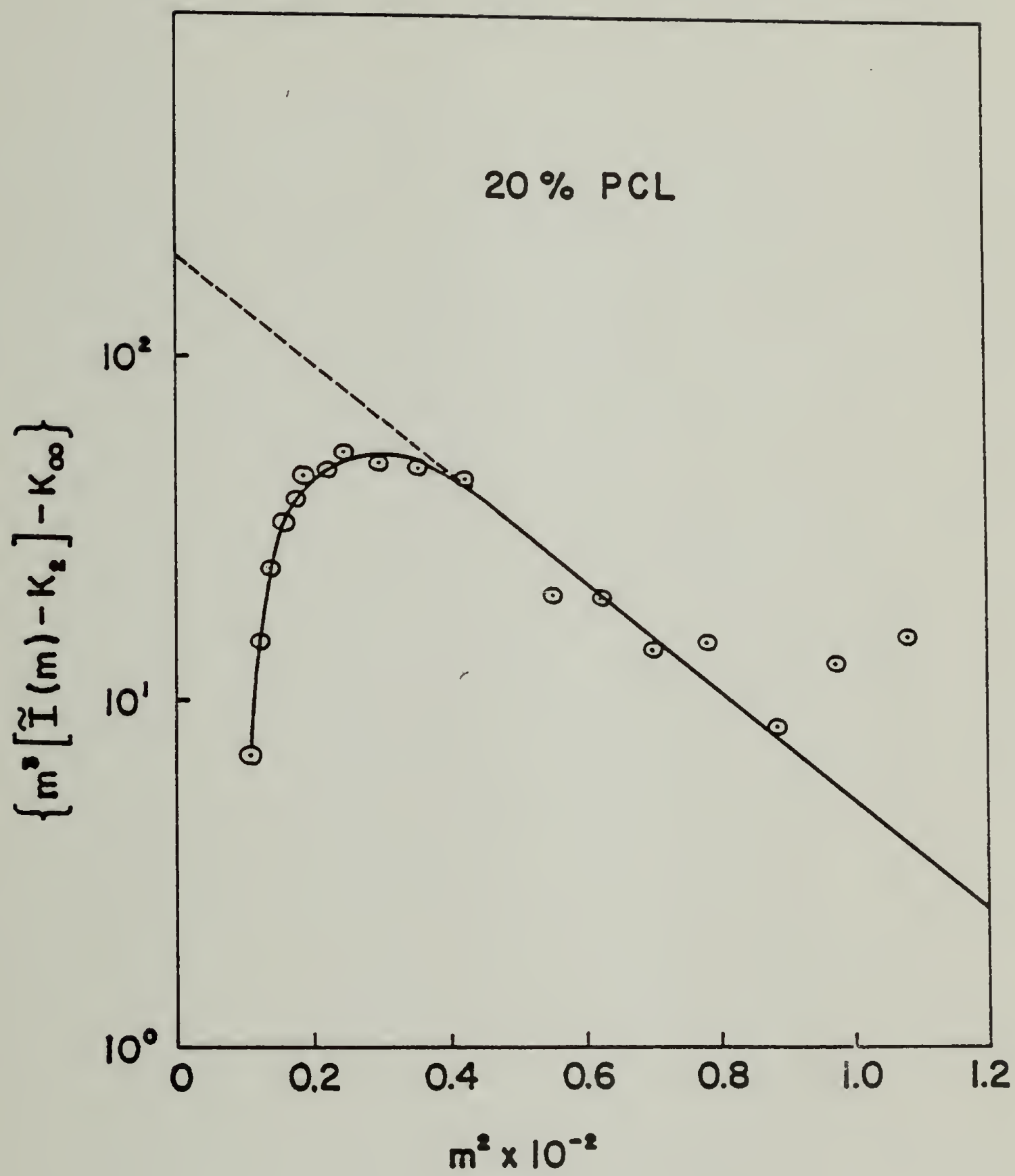


Fig. 46

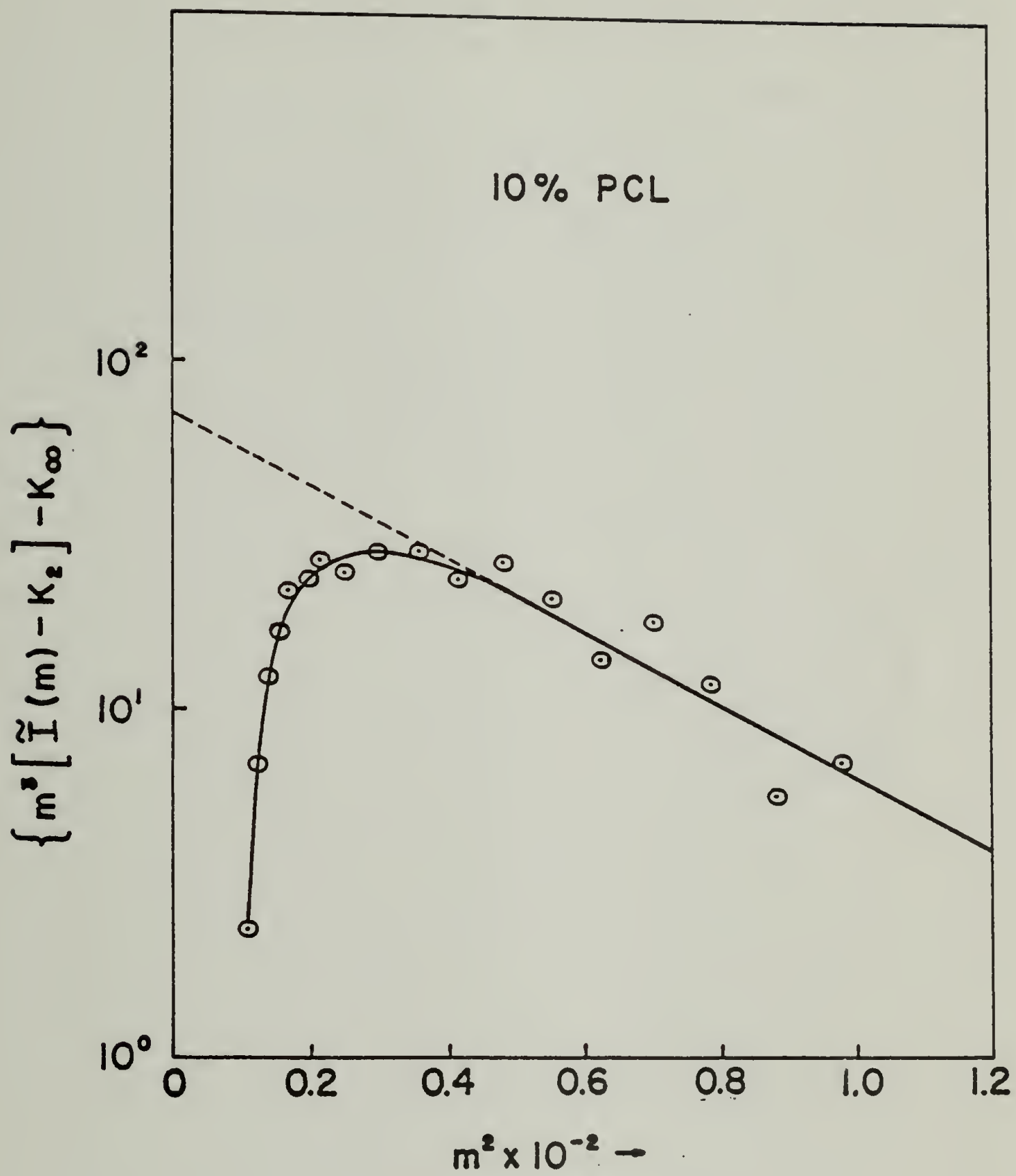


Fig. 47

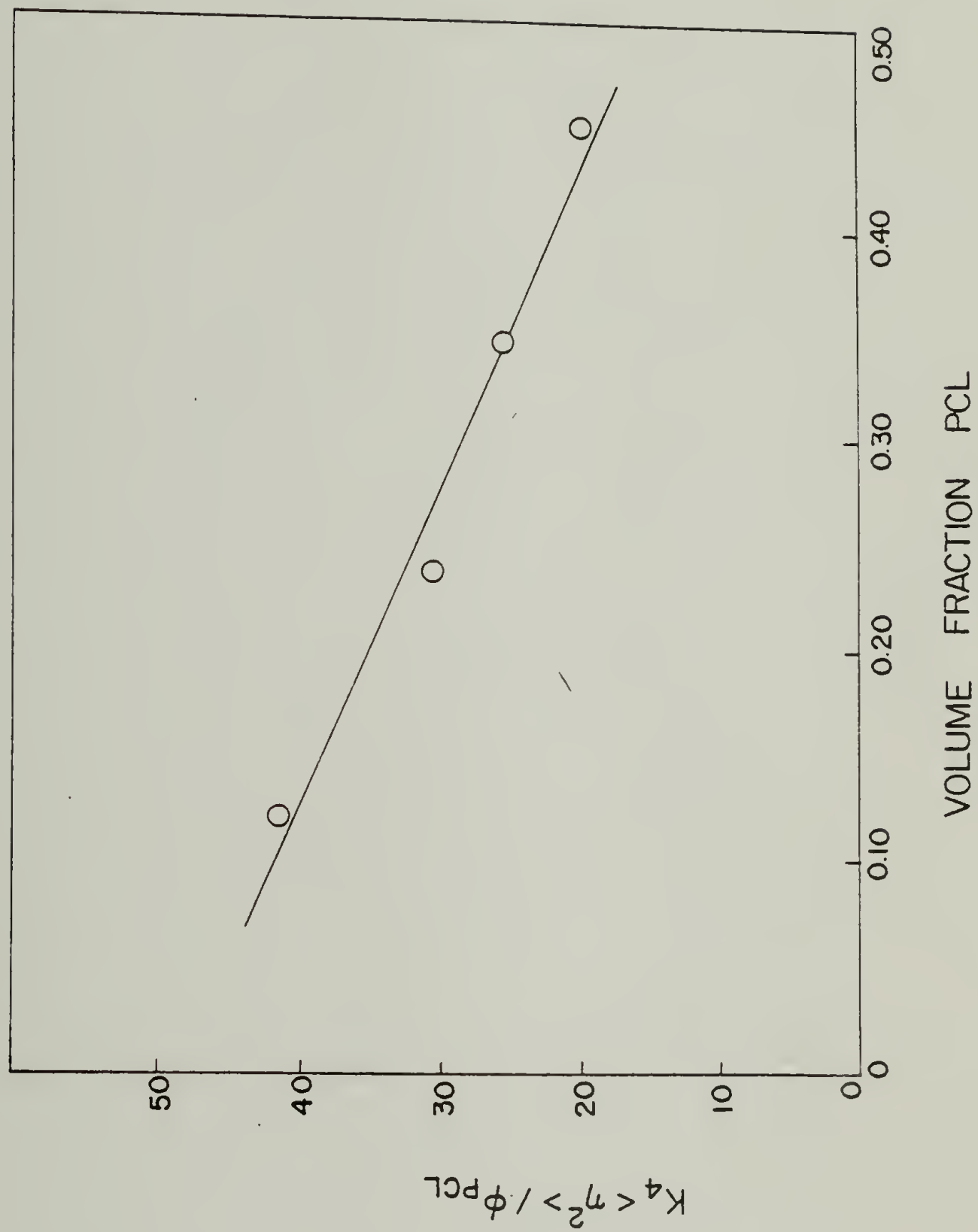


FIG. 48

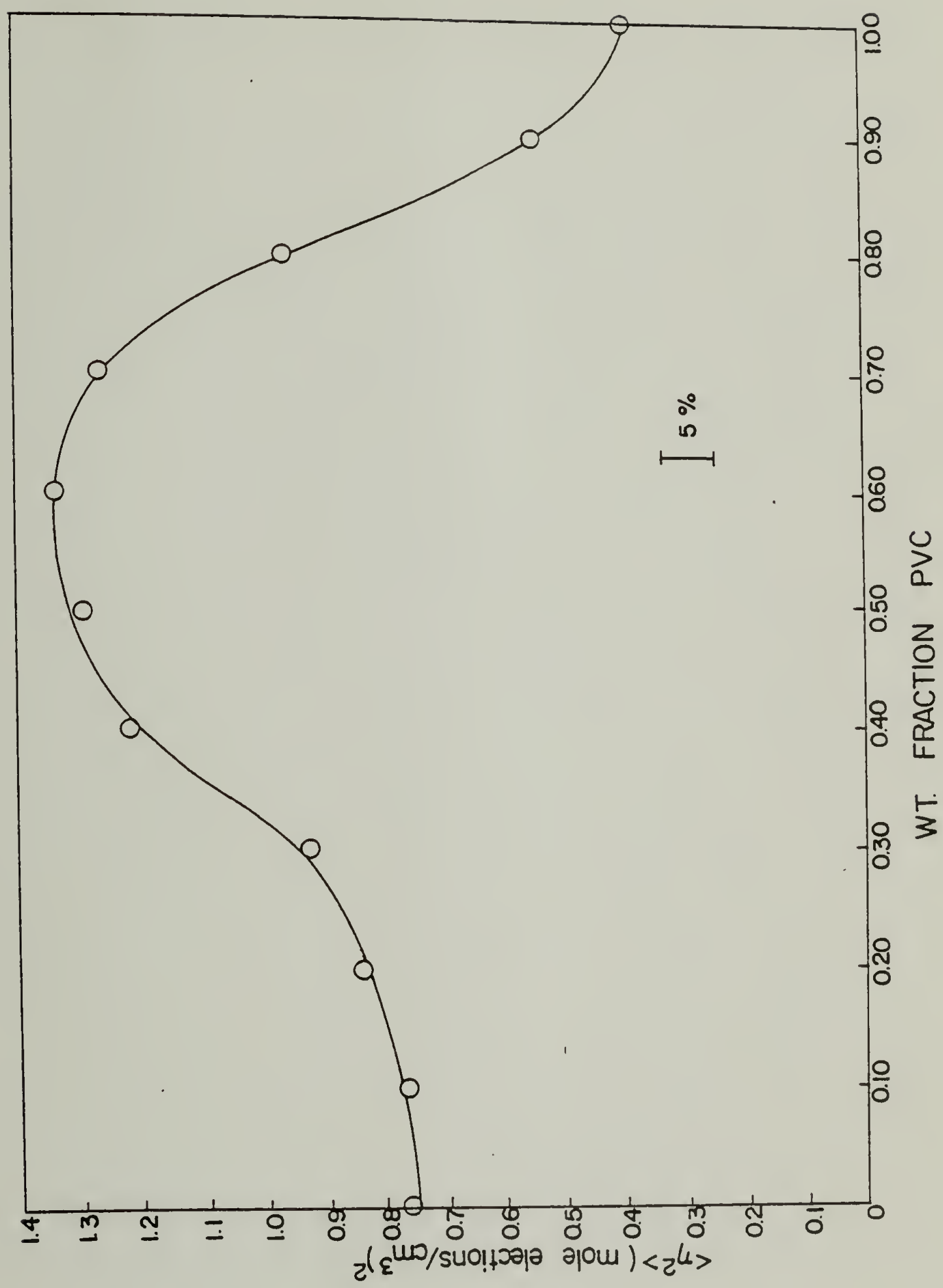
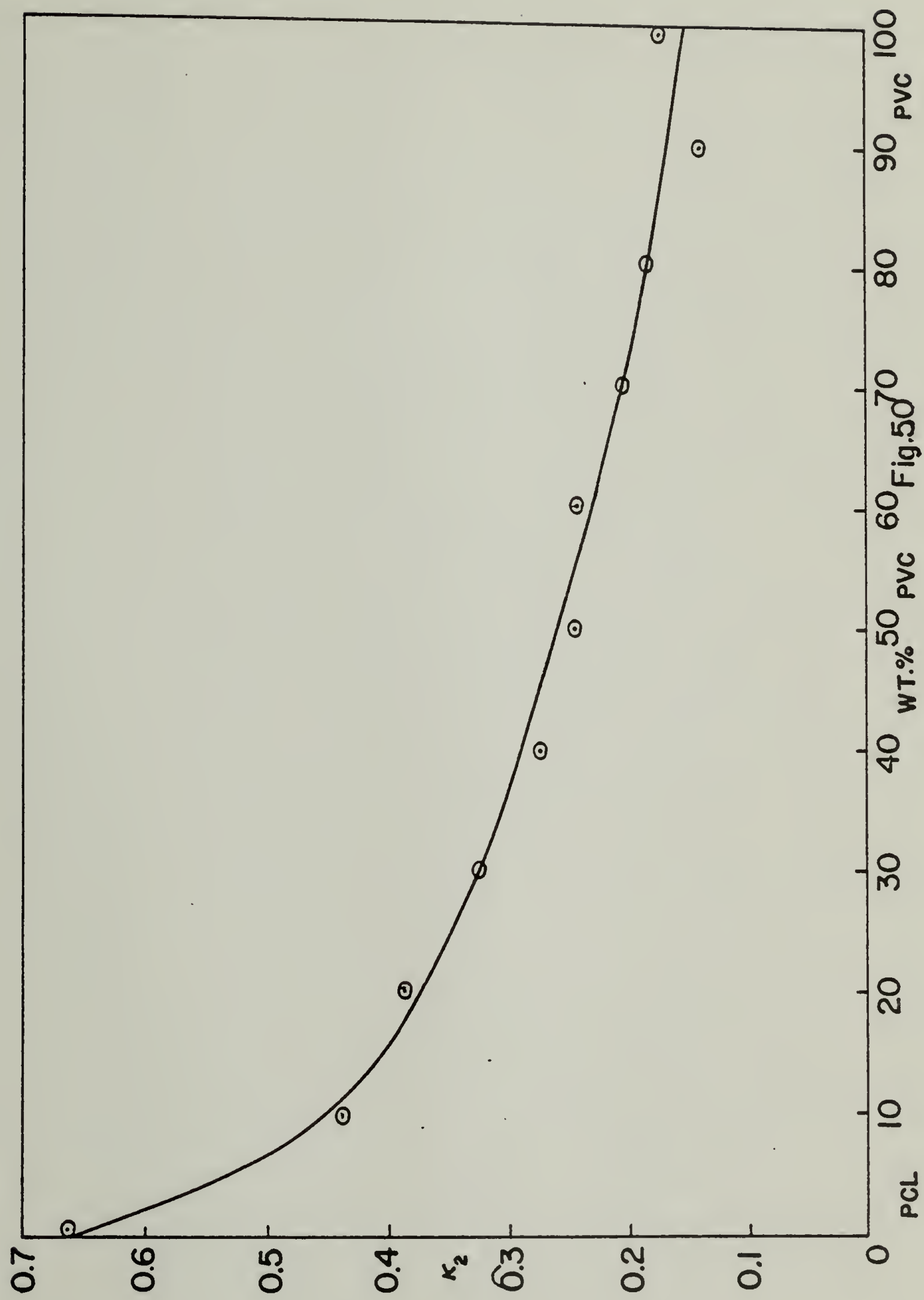


FIG. 49



LOW ANGLE LIGHT - SCATTERING OF PCL/PVC BLENDS

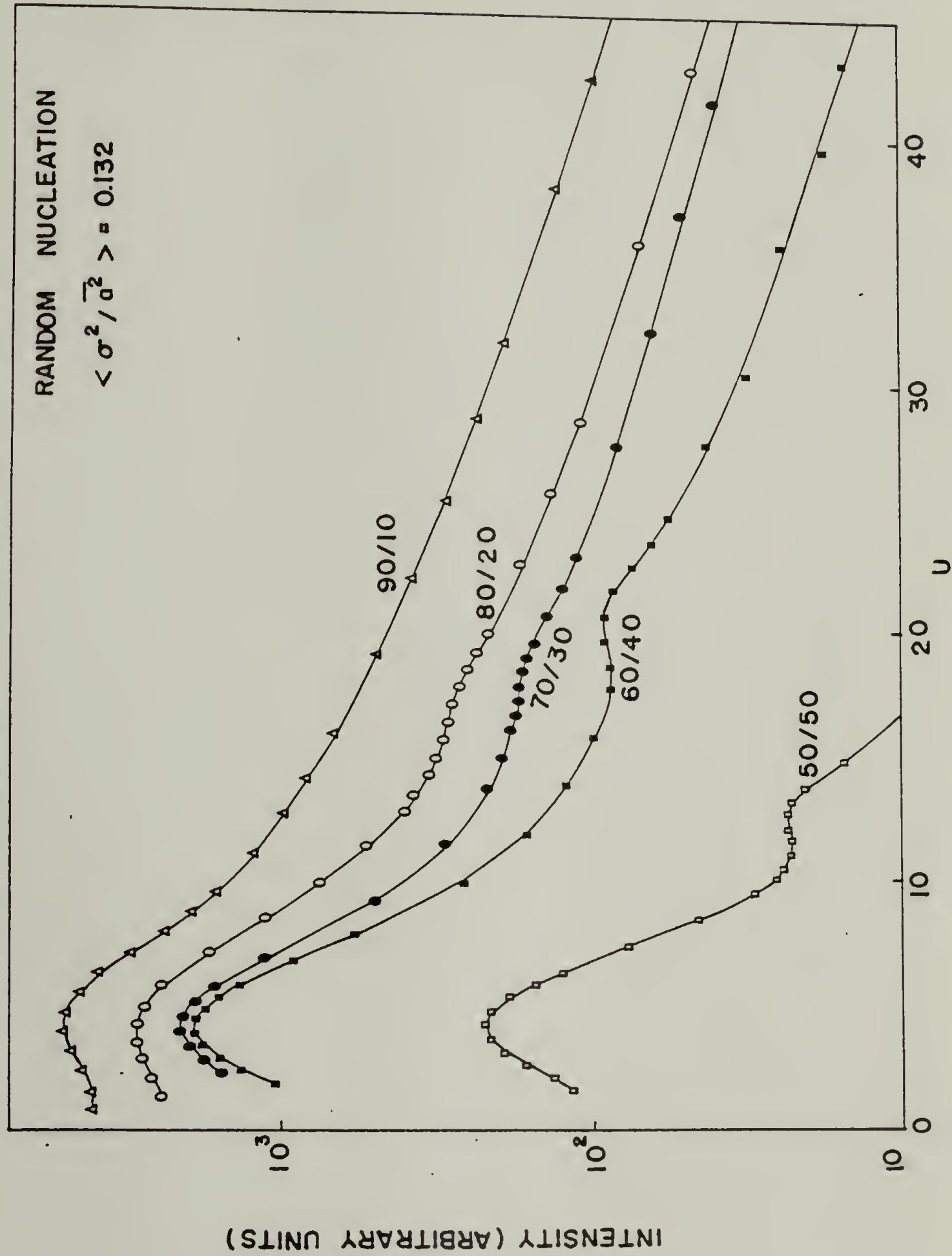


FIG. 51

